MICROWAVE IMAGING FOR SECURITY APPLICATIONS

By

Sultan Almazroui

Submitted in accordance with the requirements for the degree of

Doctor of Philosophy

THE UNIVERSITY OF SUSSEX
Department of Engineering and Informatics

March 2015

Contents

List of Figures

List of Tables

List of Abbreviations

AIT	Advanced Imaging Technology
AS&E	American Science and Engineering
ASK	Available Seat Kilometres
ATR	Automated Target Recognition
CAT	Computed Axial Tomography
CCTV	Closed Circuit Television
CPSF	Coherent Point Spread Function
CT	Computed Tomography
CWD	Concealed Weapon Detection
DAS	Delay-And-Sum
DBIM	Distorted Born Iterative Method
DNA	Deoxyribonucleic Acid
ED	Eigenvalue Decomposition
EDS	Explosive Detection Systems
EMR	Electromagnetic Resonance
FAA	Federal Aviation Authority
FDTD	Finite-Difference Time-Domain
IATA	International Air Transport Association
ICAO	International Civil Aviation Organization
INL	Idaho National Laboratory
IR	Infra-Red
IRA	Irish Republic Army
IT	Information Technology
KV	Kilo Volt
MAMI	Multistatic Adaptive Microwave Imaging
MEMS	Micro Electro Mechanical system
MIMO	Multiple-Input-Multiple-Output
MMW	Millimetre Wave
MR-CSI	Multiplicative Regularized Contrast Source Inversion
MRI	Magnetic Resonance Imaging
MRM	Multistatic Response Matrix

ORT	Object Recognition Tool
PETN	Pentaerythrite Tetranitrate
PLF	Passenger Load Factor
RAF	Red Army Faction
RPK	Revenue Passenger Kilometres
SAR	Synthetic Aperture Radar
SVD	Singular value Decomposition
TIP	Threat Image Protection
TNT	Trinitrotoluene
TR-MUSIC	Time Reversal Multistatic Signal Classification
TSA	Transportation Security Administration
UDHR	Universal Declaration of Human Right
UK	United Kingdom
USA	United States of America
USFDA	United States Food and Drug Administration
UWD	Ultra Wide Band
VIP	Very Important Persons
VNA	Virtual Network Analyser

Acknowledgements

First of all I would like to thank my main supervisor, Dr William Wang, who always supported me throughout the journey of my PhD. His office always welcomed me, at any time, for discussion about my project. He always supported me with new ideas and creative methods to continue my research. His personality and excellent management skills will always be remembered. Also I would like to thank Professor Chris Chatwin for his excellent discussions about security management where he was expert in such a field. I also owe a tremendous debt of gratitude to the Visiting Scholar, Dr Guangfu Zhang, who was always strong in the field of microwave engineering and supported me with his knowledge in the field. I also want to thank my collegue, Xiaolin Zhang, who was always available to answer questions related to the research field. I would also like to thank Dr Phill Birch and other University research reviewers who reviewed my work every year and gave their opinions about my project.

This project was funded by the United Arab Emirates Embassy where I send my thanks to all the team for their excellent coordination with me and the University of Sussex. Finally, I would like to thank my family and my parents for their continued motivation to succeed in my PhD work.

Special Thanks also goes to Janet Snow from SPRU who helped proofreading my thesis.

There is no way that I could ever express my gratitude to all of the above mentioned people, including my friends. Their support was priceless.

Abstract

Microwave imaging technologies have been widely researched in the biomedical field where they rely on the imaging of dielectric properties of tissues. Healthy and malignant tissue have different dielectric properties in the microwave frequency region, therefore, the dielectric properties of a human body's tissues are generally different from other contraband materials. Consequently, dielectric data analysis techniques using microwave signals can be used to distinguish between different types of materials that could be hidden in the human body, such as explosives or drugs. Other concerns raised about these particular imaging systems were how to build them cost effectively, with less radiation emissions, and to overcome the disadvantages of X-ray imaging systems. The key challenge in security applications using microwave imaging is the image reconstruction methods adopted in order to gain a clear image of illuminated objects inside the human body or underneath clothing.

This thesis will discuss in detail how microwave tomography scanning could overcome the challenge of imaging objects concealed in the human body, and prove the concept of imaging inside a human body using image reconstruction algorithms such as Radon transformation image reconstruction.

Also, this thesis presents subspace based TR-MUSIC algorithms for point targets and extended targets. The algorithm is based on the collection of the dominant response matrix reflected by targets at the transducers in homogenous backgrounds, and uses the MUSIC function to image it. Lumerical FDTD solution is used to model the transducers and the objects to process its response matrix data in Matlab. Clear images of metal dielectric properties have been clearly detected. Security management understanding in airports is also discussed to use new scanning technologies such as microwave imaging

in the future.The main contribution of this reseach is that microwave was proved to be able to image and detect illegal objects embedded or implanted inside human body.

Key Words

Microwave Tomography, Security Imaging, Dielectric properties, Human Body Tissues, Image reconstruction, Simulation, Microwave imaging, Subspace based TR-MUSIC, security management, aviation security, body scanners, privacy.

Chapter 1: **Microwave Imaging for Security and Medical Applications**

1.1 INTRODUCTION

This chapter will walk the reader through the journey of microwave imaging since it started up to the most recent developments. It will introduce the reader to microwave capabilities in biomedical and security applications, and what has been done to date in this area. The motivation of this research into microwave imaging is that microwave waves are less harmful than X-rays and could be produced at a lower cost than any other imaging system. Also microwaves have advantages in the collection of dielectric properties of tissues. However, they also have disadvantages in image quality and these challenges have been studied in this research.

In the medical field, X-ray mammography has shown the best results in detecting human breast tumours. However, it has disadvantages such as compressing the breast of women during the test for image quality, stability of the breast during the test, painful test procedure for women, false negative rates of missing the cancer of between 4% and 34% [1], ionizing X-ray.

Ultrasound imaging could be used for further investigation after the mammogram test for masses discovered in the breasts. MRI is used to enable more image information to be collected before surgery or any suspected discovery after the mammogram. This concludes that there have always been many systems and procedures for detection investigation, which leads to an increase in the cost of imaging. Consequently microwave imaging can be seen to use non-ionized rays to obtain the dielectric properties of tissues, and is more comfortable for the women being tested. Image quality

has been extensively researched when using microwaves by a trade-off between resolution and tissue penetration depth. Resolution is one of the most important factors to consider when it comes to designing a microwave imaging system.

Resolution has been explained in terms of wavelength, but the penetration depth of the microwave system could also be limited when using different frequencies. The human body is considered to be a high degree loss if using a microwave imaging system. The penetration depth of microwaves into human tissues was studied in [2]; it was concluded that at 3GHz the penetration depth for muscle and fat tissue is 1.2 and 9cm, respectively. The penetration depth for normal and cancerous breast tissue are 4.4 and 2.3cm. This confirms that material with water and liquid content absorbs more microwaves and could be penetrated better than any other materials.

A comparison study in [3] between continuous microwave wave radiation and pulsed microwave wave radiation to calculate the penetration depth for tissue media has concluded that lower frequency pulsed microwave radiation can travel deeper in tissue media than higher frequency; this takes into account their conductivities and permittivity. This research concentrates more on lower microwave frequencies than higher frequencies, between 1-10GHz. A study in [4] showed different microwave frequencies for different tissues, and showed that the higher the frequency, the less penetration depth for biological tissue.

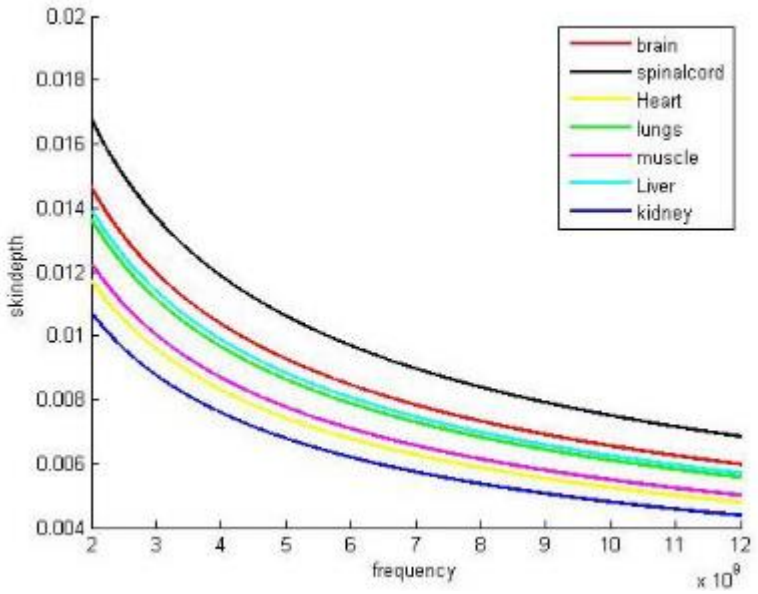

Figure 1.1: Adapted from [4] penetration depth of microwave for different tissues of human body

From [5] and all the above reviews about the relationship between resolution, frequency and penetration depth, we came to the conclusion that the higher the frequency the more details of the object could be achieved with pulsed microwave radiation. At the same time, however, there would be less penetration through the complex layers of tissue in the human body. We would, therefore, lose imaging in the objects that microwaves cannot reach at higher frequency radiation; at the same time at a lower frequency higher penetration could be achieved but with a lower imaging quality. Therefore a trade-off between the choice of frequency and penetration depth should be considered to obtain moderate imaging resolutions. This research has chosen a microwave pulse radiation between 1GHz and 10GHz to obtain the best imaging results.

X-ray tomography and microwave tomography have the same method of illuminating the object to be tested or seen, but the final image reconstruction for the X-ray relies on the density of the tissues, whereas the microwave relies on the dielectric information of the tissues. The wavelength in X-rays is less than the size of the object that can show the

image easily, but the microwave wavelength is always larger than the object size and causes large diffraction around the object; this cannot be ignored.

1.2 MICROWAVES IN MEDICAL FIELD DEVELOPMENT

Microwaves have the properties of being able to travel through an opacity medium, which makes them a non-invasive agent for imaging, testing or taking measurements. An opacity medium could be a human body, and its organs. Therefore the microwave sensors have been manufactured according to the factors that affect microwave rays such as water and temperature. Three approaches have been developed using microwave imaging for breast cancer; these approaches are passive, dual and active approaches. Passive microwaves are when radiometers are used to measure the temperature level caused by malignant tissues compared to other healthy tissues when applying microwave signals; these are then later assisted by the use of mammograms [6]. When dual microwave-acoustics are used to illuminate the breast, they show a tumour expanding and creating a pressure wave resulting from higher conductivity, energy deposited, or heat rise in the tumour region [7].

Active microwave imaging involves the use of microwave transducers by illuminating the object and obtaining the scattered field data to be calculated for image reconstruction, as discussed later in this thesis. Previous research attempted to reconstruct an optical image from the microwave range of frequency, but this research has not shown any good results [8]. Microwave imaging in the field of medicine has been investigated since the 1980s [9]. In addition, the first tomographic images of microwave tomography have shown good results, as shown in [10].

Part of knowing that microwave techniques are suitable for imaging difficult areas is how to reconstruct the images from the data obtained by experiments or any simulated

data. Later in this thesis research, two different types of imaging algorithms that support the use of microwave imaging will be shown. The first one is the use of available X-ray CT tomography algorithms that have been developed using the popular Fast Fourier Transform Algorithm to show different proposed images and models. The second one took into consideration the scattering mechanism of the microwave rays when they are projected on the object models such as a human body or metallic materials.

The use of microwave imaging to detect foreign objects within the human body has proven to be sensitive, non-invasive, non-ionized and low cost [11]. Also, the use of microwave imaging has been extended to the field of security to see concealed objects underneath passenger's clothing using millimetre waves [12].

Microwave imaging attracted huge attention in medical areas for cancer imaging research because of the electrical properties, permittivity and conductivity of the malignant tissue that differs from normal healthy tissue [13]. Also microwave frequencies are non-ionizing and could travel through human body tissues with a moderate resolution. The experimented research of microwave antennae were transducers (receivers and transmitters) of scattered rays from the illuminated object and has proven to be able to detect a small size of tumours of between 5-10mm [14]. One of the clinical systems that have been used for research was carried out at Dartmouth College by Meaney. This system used monopoles antennae to excite microwave rays from 3MHz- 3GHz. It showed some good results, as shown in [15]. Another clinical system has also been developed by the University of Bristol. They used ultra wideband microwave imaging from 4.5-10GHz excited by cavity-backed patch antennae; these showed better results as shown in [16].

As discussed above the research into microwaves in the medical field has been extensively undertaken, especially the antennae of microwaves such as dipole, MEMS-steerable antennae, Horn antennae, Vivaldi antennae, slot antennae, patch antennae and dielectric antennae [17]–[25]. The system in microwave imaging was always how to obtain the best data that could be measured from the transducer of microwaves, and then this data has to be calculated by reconstructing the image using a different type of imaging algorithm. The two main imaging algorithms have been achieved by 1) microwave tomography [15], [26]–[29] and 2) radar-based imaging[30]–[37].

All of the above state-of-the-art imaging algorithms tried extensively to visualize the image of the tumour by drawing shapes of that tumour. This is done by collecting information about the object illuminated and its dielectric properties to reconstruct the shape of the tumour, as seen from [38], [39]. To shed light on the clinical prototype for cancer detection developed by Dartmouth College, the United States developed a 16 circular monopole antennae array. Its frequency was between 0.5-3GHz and its continuous wave was able to reconstruct a 2D image; this system was later upgraded to reconstruct a 3D image using the Gauss-Newton iterative strategy. Clinical results showed that normal and abnormal breast tissue images contrasted on average between 150% to 200%, with an accuracy of between 80% to 90%. The minimum size of the object detected was between 2-3mm; with a typical resolution of 5-10mm. Figure 1.2 shows a test bed system.

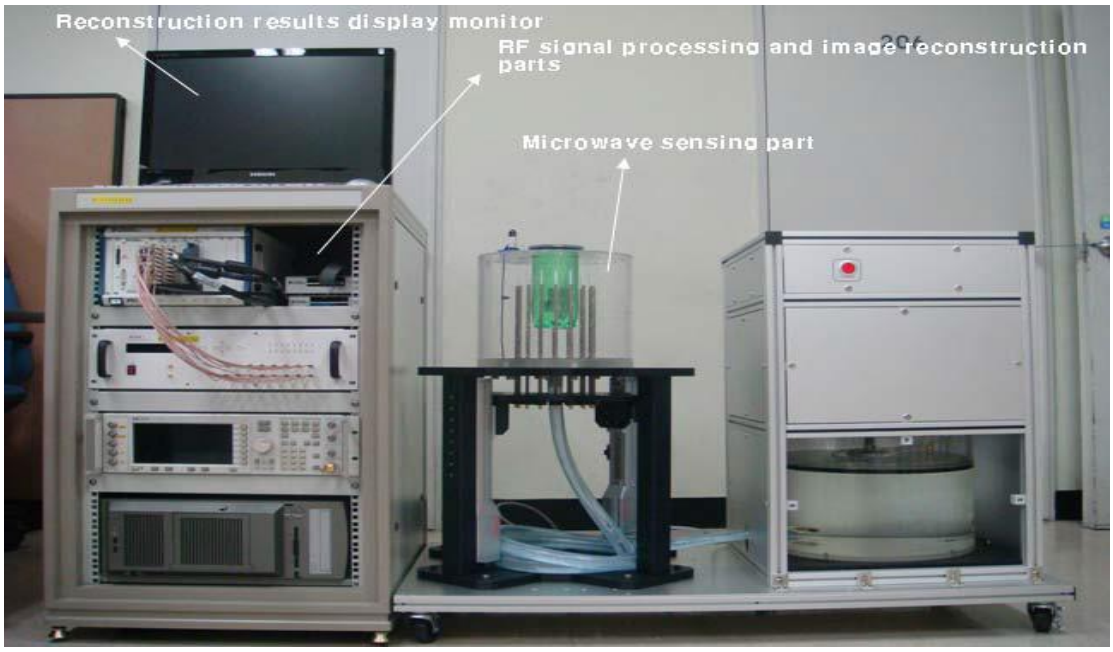

Figure 1.2: Microwave Tomography Prototype Test Bed System at Dartmouth College

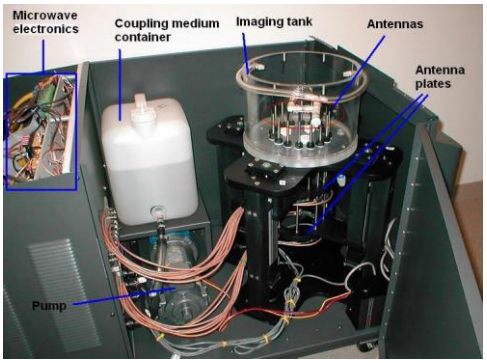

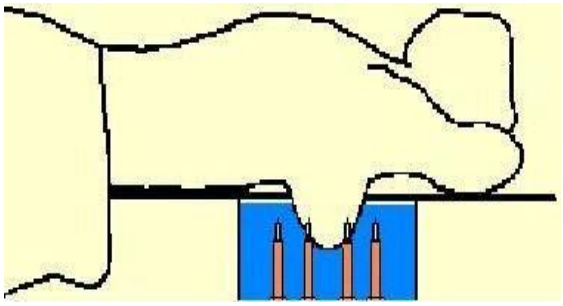

Figure 1.3: Microwave Imaging System at Dartmouth College

The University of Bristol team has developed an ultra wideband radar-based microwave imaging system using a hemispherical patch antenna array operating at a frequency range from 4-9GHz. The number of antennae was gradually developed from 16

antennae to 60 antennae for better results. Their imaging system was based on the radar approach used for military and ground penetration applications, which was proposed in 1996 and 1998 by Benjamin and Hagness respectively [36]-[38]. Their imaging algorithm was based on the first algorithm, standard delay-and-sum (DAS) focusing, used for underground mining [43], [44], and the multistatic adaptive microwave imaging method (MAMI) for early breast cancer detection [11].

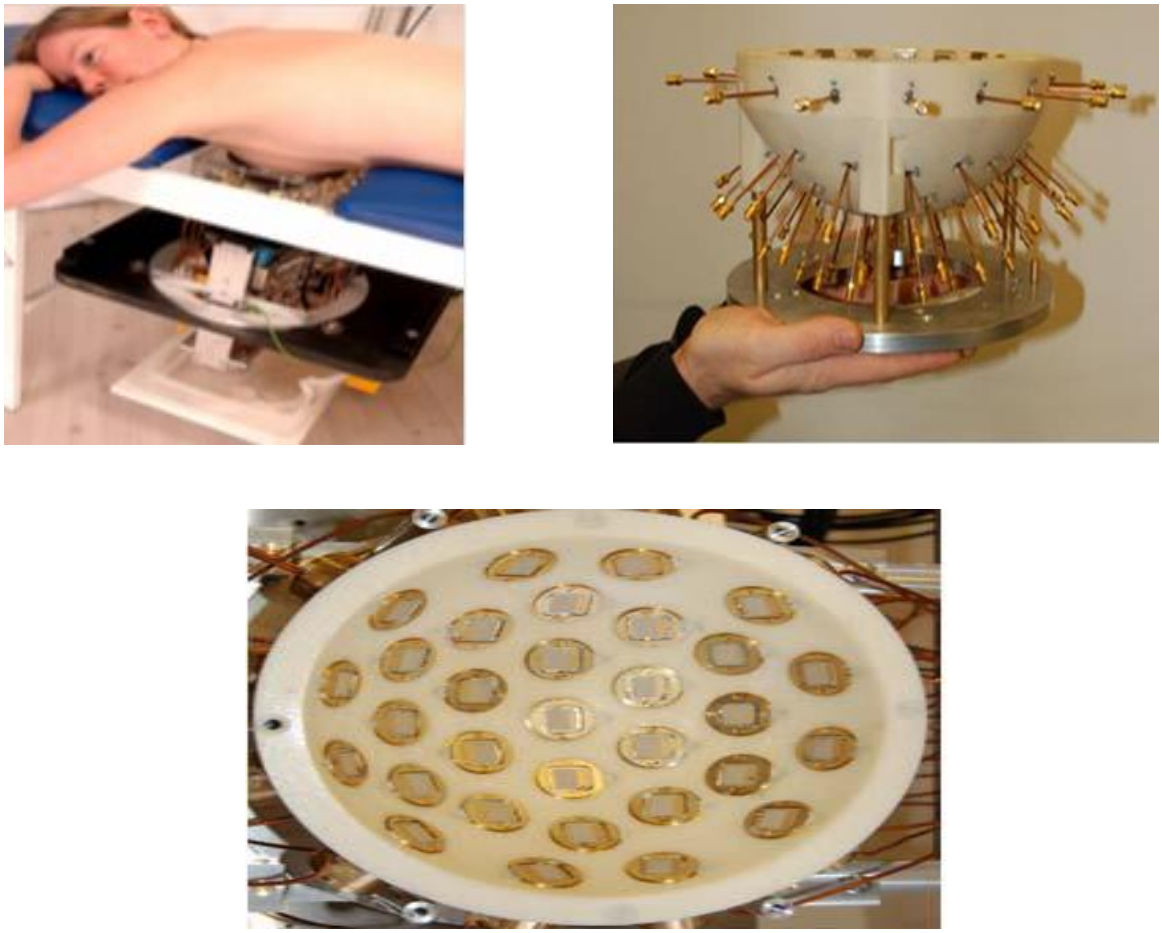

Figure 1.4: University of Bristol Ultra Wide Band Radar Based Microwave Imaging System

Another microwave imaging system has been developed in the University of Manitoba in Canada using a Vivaldi antenna to excite frequencies from the range between 3-6GHz. Their imaging algorithm used was an enhanced version of the distorted born terative method (DBIM), and the multiplicative regularized contrast source inversion (MR-CSI) method [45].

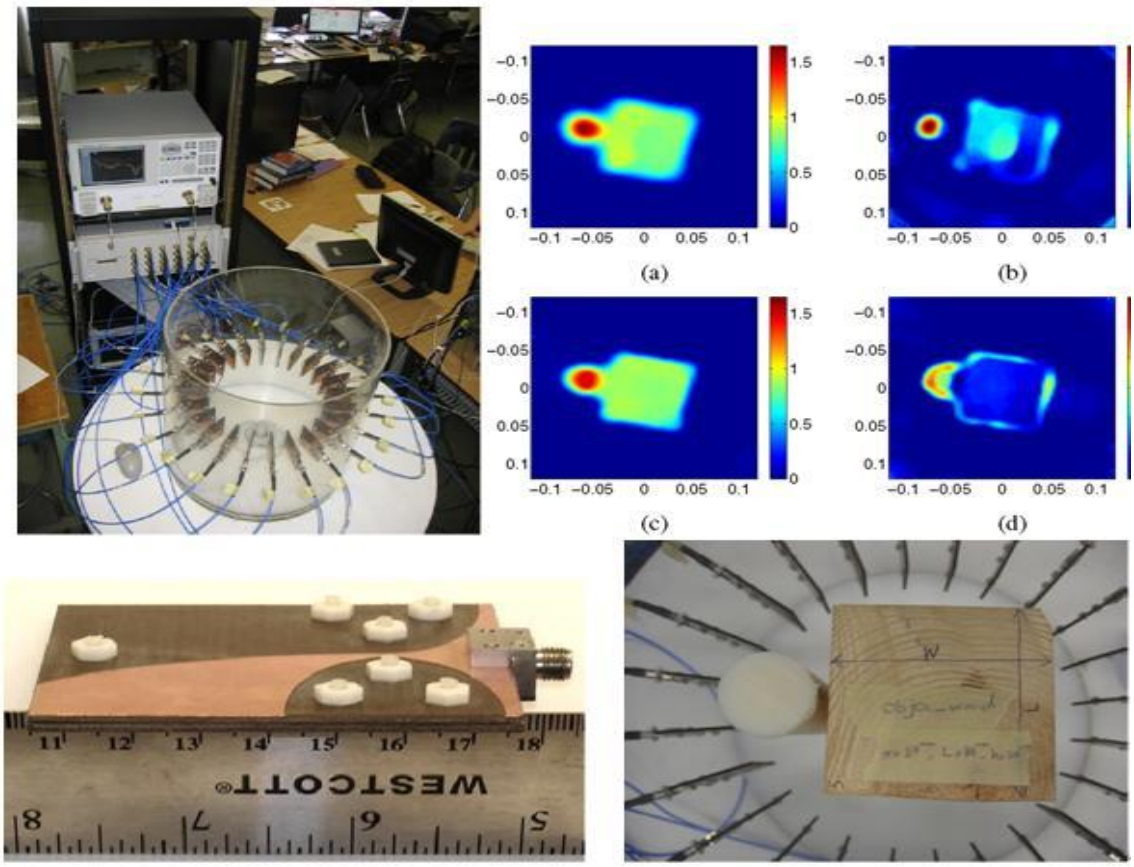

Figure 1.5: Microwave Imaging System by the University of Manitoba, Canada

In addition, a team at the University of Denmark has developed a hardware system that consists of 32 coaxial probe antennae, with operating frequency between 0.3-3GHz, to produce a 3D image using the single frequency Newton iteration method. The reconstruction image took between 90 and 130 minutes to be produced [46].

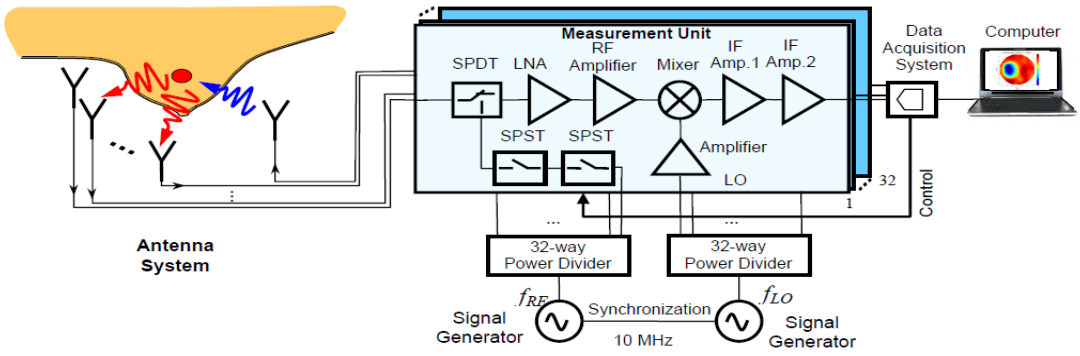

Figure 1.6: Microwave Imaging System Architecture for the University of Denmark

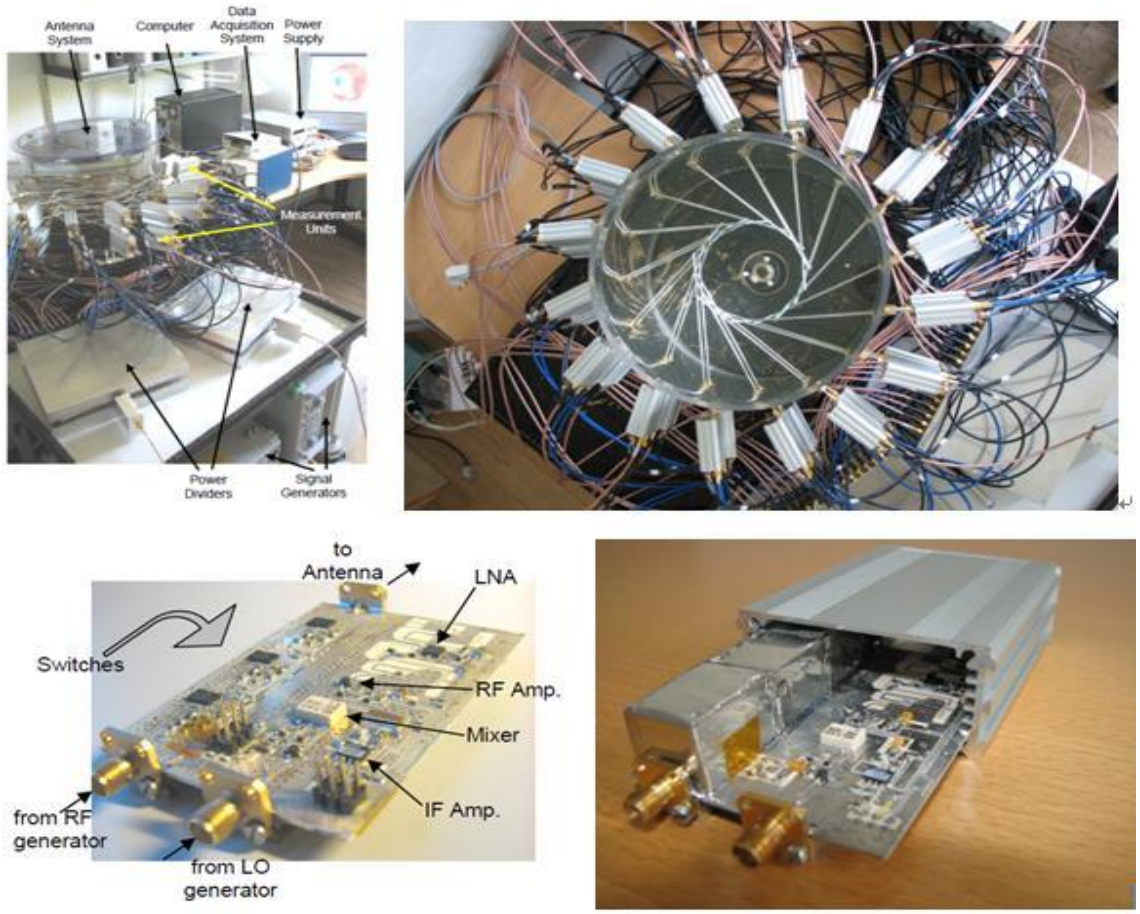

Figure 1.7: The University of Denmark Microwave Hardware System, Measurement Unit and the Antennae

The Chungbuk University in South Korea has built a microwave imaging system with a 16 circular monopole antennae array, with operating frequencies of between 0.5-3GHz. The resulting image was in 2D using the iteration plus FDTD method [47].

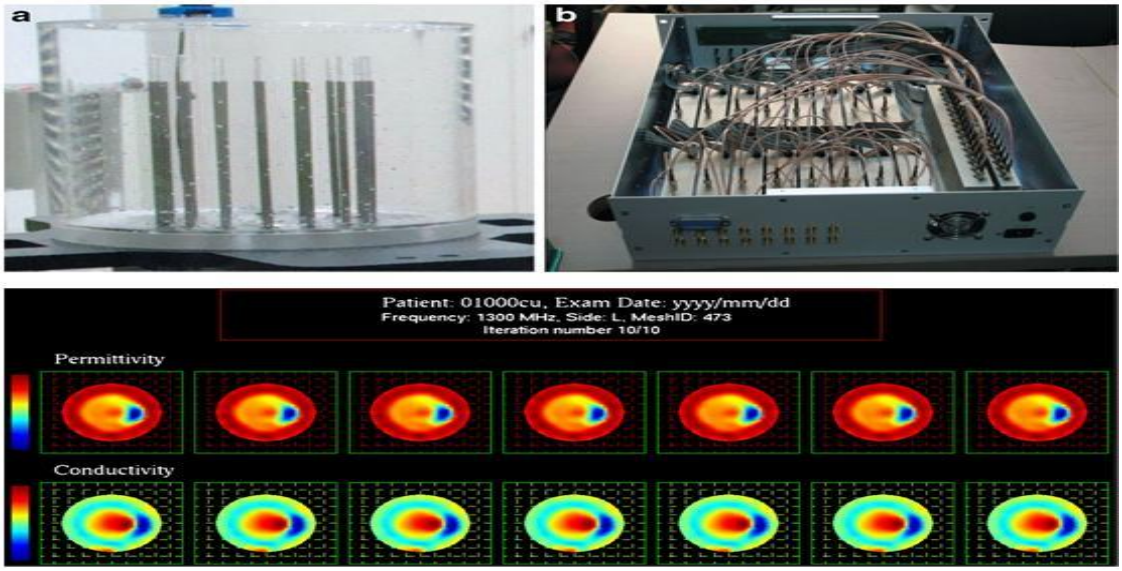

Figure 1.8: Chungbuk University Microwave Imaging System

The Australian IT and Electronic Engineering College developed an ultra-wide band imaging system consisting of a circular 12 Tapered Slot Antennae (TSAs) array, with an operating frequency of between 3-11 GHz. Their imaging algorithm is time domain or frequency domain with a 2D imaging result [33].

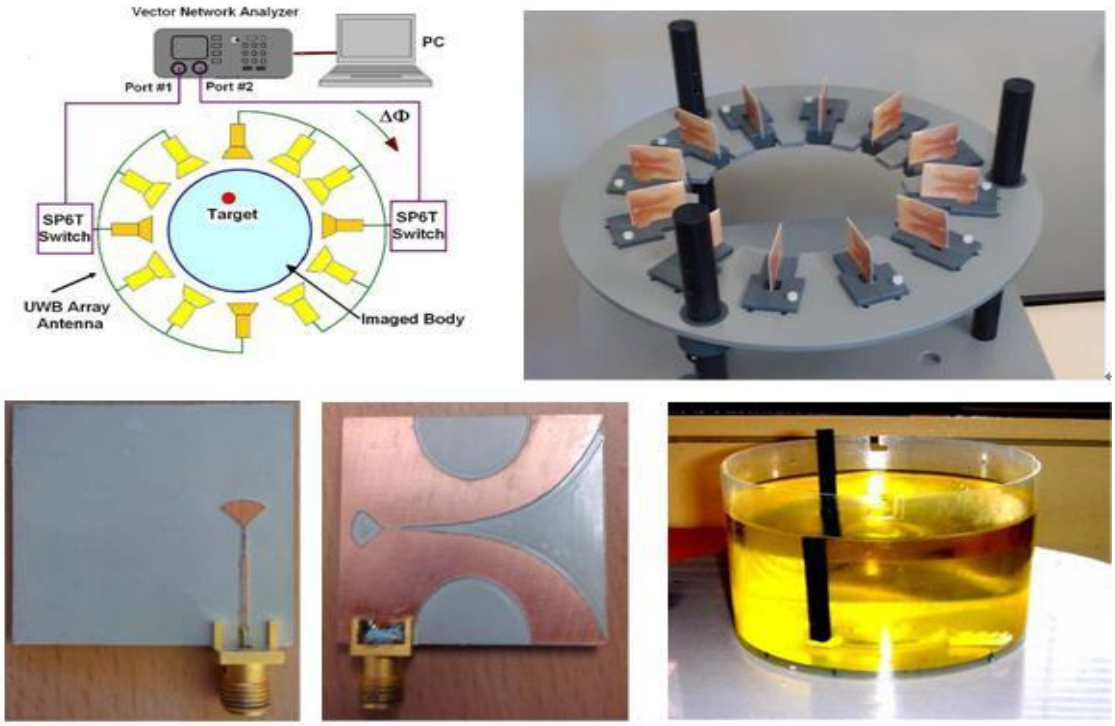

Figure 1.9: Australian IT and Electronic Engineering College Microwave System

It has been seen from the above review of microwaves in medical research that this is a promising technology. However, there are still many challenges to overcome, such as acquiring a high resolution when imaging objects are to be detected. Improving the resolution should be a trade-off between the penetration depth of the wavelength and the frequency chosen; this should not to be high or more than 10 GHz. In practice the microwave imaging system should take into consideration some factors such as:

1) Overall system planning and irradiation program simulation and evaluation;
2) The antenna array cell design and integration;
3) The scattering data acquisition and storage;
4) Image reconstruction algorithm;
5) System control and conversion software systems; and
6) System testing and performance evaluation.

A proposed experiment has been constructed to do this research: this will be discussed in Chapter 6.The above review of microwave imaging used in the medical scanning applications could be transferred to serve the field of security scanning technology which is the purpose of this research.

1.3 MICROWAVE TECHNOLOGIES IN SECURITY FIELD DEVELOPMENT

The microwave range lies between 300MHz and 30GHz, corresponding to a wave length of between 1mm and 1 metre. The one used for the security check in this thesis will be between 1-10GHz to have better penetration to the human body. Microwaves are used extensively in communication devices such as mobile phones, medical and security applications.

In biomedical and security applications, the challenge for using microwaves was how to image objects using dielectric materials information, even though it has a long wavelength, in order to penetrate media such as living tissues, plastic, clothing, ceramic, soil, fog, etc. Detecting contraband materials and weapons underneath human clothing or within their bodies is a vital concern in the field of security for transportation, events and VIP buildings. Microwaves, as seen in the medical review, could be adapted to suit security applications. Here microwave technology will be discussed and reviewed up to the current situation in the field of security imaging.

Microwave imaging has been used in the security application field, such as imaging through walls to counter terrorism [44]-[46], and detecting concealed weapons [47]-[49].

As discussed previously, microwave frequency has been chosen depending on the trade-off between depth of penetration and resolution. A lower frequency is needed for medical research to penetrate deep inside the human body, but a higher frequency is needed for applications that are limited by diffraction. The microwave wave systems approach could be divided into four categories:

1. Using a short pulse of frequency from each antenna to the targets to be illuminated; then all these scattered waves from the target have been measured at each antenna to form an image. This technique is called Broadband/Noise Pulse Microwave Imager.
2. When two beams of electromagnetic wave have been aimed at the target and then interfere to calculate the amplitude and the phase. This is called microwave holography[54], [55].

3. Similar to the pulse microwave imager, but this depends on the illuminated object sending information or intensity to be calculated for image reconstruction. This is called a Passive Millimeterwave Imager [56], [57].
4. When a frequency modulated continuous wave has been aimed on a moving target to obtain distance information and then a reflected wave is calculated based on a frequency shift. This is called a Microwave/Radar Imager.

An ultra-wide band system has been developed using multiple-input-multiple-output (MIMO) and synthetic aperture radar (SAR). A combination of a digital beam forming in the MIMO array with SAR in the orthogonal direction has shown a 3D volumetric image, as shown in Figure1.10 [58].

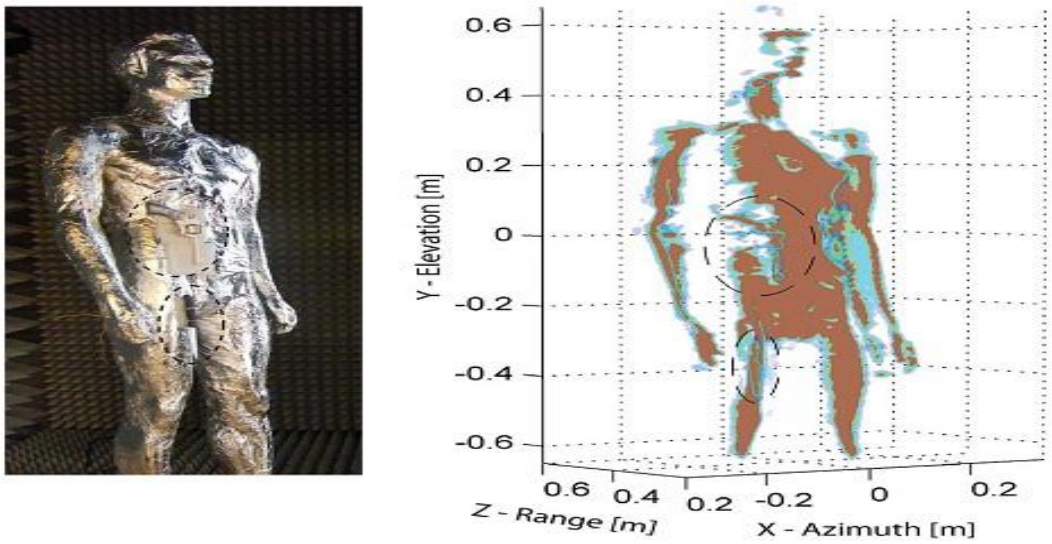

Figure 1.10: 3D Volumetric Image Adapted from [58]

An additional microwave imaging research range of between 576-600GHz to detect concealed weapons from a distance of 4-25 metres using a radar-based imaging system has shown decent imaging results. Less than 1cm resolution at a distance of 4 metres has been obtained [59]. MMW for concealed object detection could be active and passive, as it is portable and transportable. In addition, a stand-off position has been achieved.

1.4 EXISTING TECHNOLOGIES FOR CONCEALED OBJECT DETECTION

A number of existing technologies are used for the detection of concealed objects; they will be discussed here and their limitations explained. The security technology illustrated will focus on imaging technology because of its relationship to this thesis. Explosive detection systems could include screening and other methods such as tracing detection systems.

Screening technologies are used to check passengers and their baggage, and should match the criteria of national laws when implemented in sensitive locations such as airports. The aviation authorities always have requirements for the use of scanning technology to be deployed in airports. Some of these requirements are, for example, the type of material hidden, its shape image, location of the targets, total resolution and the quantity that could be detected. At the same time, the technology should be suitable for the management side such as throughput, fast and reliable. Scanning equipment for baggage cannot be deployed to scan humans, and this is because of the danger of these scanning technologies affecting human health. This factor will be discussed in detail in later chapters.

The most trusted technique in airports is a physical search method such as pat-down searches. The downside of this method that it cannot detect any thing implanted inside the human body. Therefore searches using imaging technology are becoming more widespread. Imaging technologies can see an image of the human body and interpret the image. These technologies will be discussed here, and will include X-rays and millimetre wave systems, etc.

This research focusses on the image reconstruction collected from microwave techniques. For baggage scanning in aviation security this is called bulk detection. Bulk detection uses technologies such as X-rays, gamma rays, millimetre waves and electromagnetic fields.

Explosives components have their own characteristics; the main components of explosives are oxygen, nitrogen, hydrogen and carbon. Each of these components has their own dielectric properties; these will be discussed in Chapter 2 for their microwave detection. Explosive devices consist of an explosive agent and a detonating agent. An explosive agent consists of inorganic nitrate and carbonaceous fuels, and the detonator agent consists of metal tubes and shells with an igniting explosive. Plastic explosive can detonate by itself [60]. The new threat from terrorism is that they can implant explosives inside their bodies [57]-[59]. To view explosives or drugs in a person or luggage scan, it is important to analyse the geometry of the metal or the shape of the object. Material density is also important for detection. Drugs, including narcotics such as heroin or cocaine, have chloride. Narcotics have low nitrogen and oxygen, but they have high carbon and hydrogen.

1.4.1 Acoustic and ultrasonic detection

The acoustic method relies on the acoustic reflectivity of objects hidden underneath clothing. The image of this technology depends on the rigidity of the object such as metal or hard plastics. The limitation of this method is that it does not differentiate between different types of material such as weapons or non-weapon objects. For example, if the passenger is carrying a phone or weapon the system cannot tell the difference between them. Also leather jackets can cause large acoustic reflections that will prevent any detection of hidden weapons. Nevertheless a combination of acoustic and ultrasonic methods has been investigated to detect concealed weapons in [64].

Their approach was to be able to locate a zone with ultrasonic and then non-linear interaction by generating a lower acoustic wave frequency to penetrate clothing better than traditional direct ultrasonic. The advantage of this technology is that it is harmless to the human body; however, it does have its limitations as previously mentioned.

1.4.2 Metal detection and earth magnetic field distortion

These devices include walk through gates and portable devices for concealed weapon detection. They depend on the passive sampling of the distortion of the Earth's magnetic field. The detectors of these devices are called Gradiometer Metal Detectors. This type of detector will sound an alarm if a person goes through the gates and is carrying metal. This technology is a new application to the existing technology of magnetometer. This database where magnetic signatures for different types of weapons are stored and are used to differentiate them from different types of non-weapon metallic. These different metals are easily detected by using an advanced signal processing algorithm. Recently a new Joint Time Frequency Analysis digital signal processing has been developed that reduces false alarms [65].

This technology is passive so it will not affect any medical device, which is an advantage. However, because this technology requires the object to be ferromagnetic, objects such as aluminium, copper or stainless steel cannot be detected. Also the detection quality depends on the number of the gradiometer: the higher number of gradiometer, the better the detection, but at the same time the cost is also higher.

Figure 1.11: Adopted from INL Portal for CWD

1.4.3 Inductive magnetic field method

This concealed weapon detection technology uses a passive electromagnetic inductive technique. The device is a walk through gate that contains two coils: one is the transmitter coil and the second one is a receiver coil. A pulsed current with a frequency of between 5 kHz to 5MHz is fed into the transmitter coil, which results in a time varying magnetic field received by the receiver. If there is a conductive material between those two coils then a secondary magnetic field will be produced and interfered

by the transmitter coil to produce a current, called an eddy current, to flow to the detector or receiver coil. An eddy current is affected by the shape and size of the conductive material; therefore it could carry unique information for that material. A database has been stored if that type of metal is considered to be threat to the rest of the material detected.

Figure 1.12: Adapted from [66]

This technology suffers from sensitivity problems, and it cannot detect non-metallic objects. Also small objects cannot be detected because the signals detected from the human body are larger than the signal detected from the small sized objects. Objects could be detected without its location in this technology where the passenger or the suspect has to go through a physical pat-down search.

1.4.4 Electromagnetic resonance based on radar sweep detection

This technology depends on an active sweep of radar frequency between 200MHz-2GHz and, in addition, uses electromagnetic resonance as a signature to recognize weapons and contraband materials. The target can be illuminated by a sweep of frequency or pulses then reflected signals from the object in the target space give the object a unique electromagnetic signature (EM resonance). This is then compared with other EM resonance signatures for other materials in order to know if the object is a threat or not. In addition, a neural network has been used to distinguish a weapon's signature and other material's signatures [67]. Although this technology is simple, it faces a high rate of false alarms. The signature of a person carrying a weapon is very similar to one not carrying a weapon.

1.4.5 Millimetre wave

Millimetre waves use radiation longer than infrared (IR), from 1-10mm wavelength, which is shorter than radio waves and microwaves. Millimetre waves have been studied extensively to provide better imaging for contraband material. Millimetre waves systems have already been deployed in airports in America, the UK and Europe [64]-[67]. Figure 1.13 shows an example of a current millimetre wave scanner [72, p. 10]. Millimetre waves are in the range from 30GHz-300GHz. Millimetre wave imaging has been investigated by many researchers for concealed weapons' detection. A novel approach of a millimetre wave has been developed using millimetre waves of between

26-40GHz to detect concealed weapons: hidden weapons have been discovered by studying their unique electromagnetic characteristics [73].

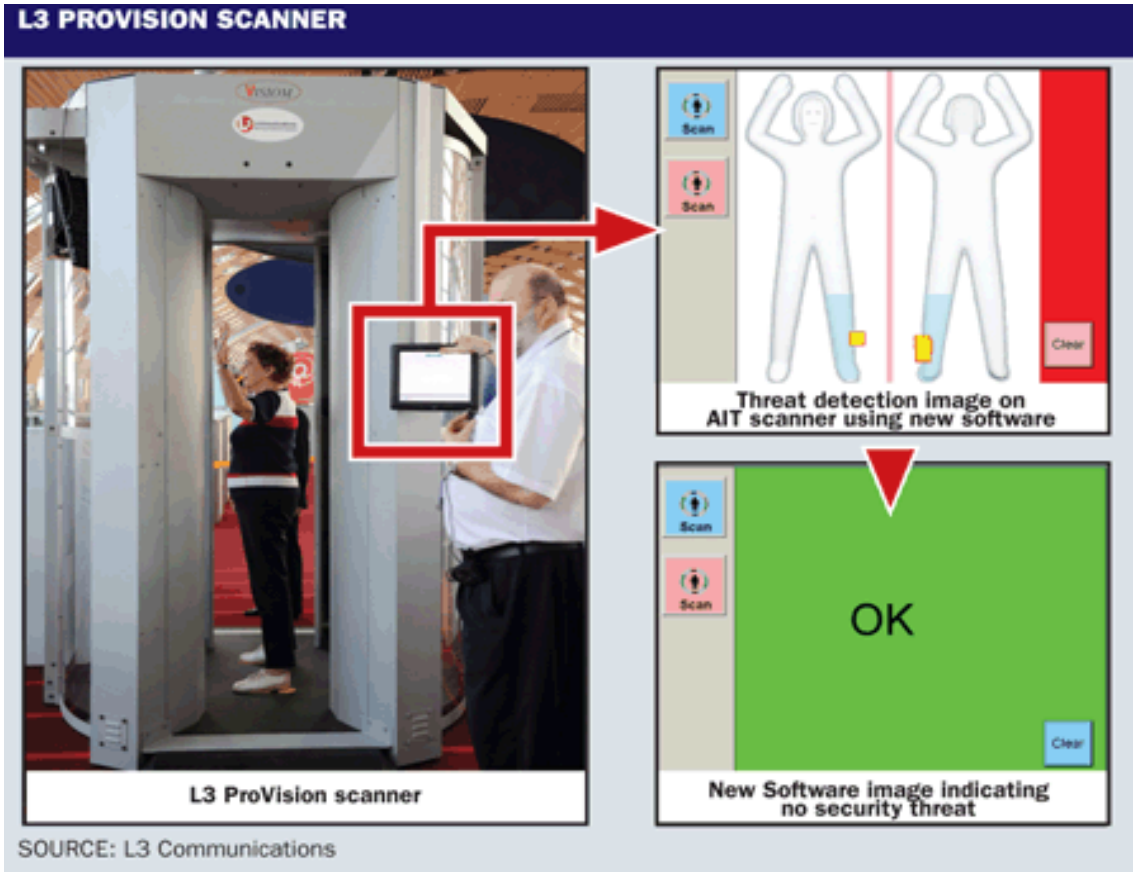

Figure 1.13: Millimetre Wave Scanner Adapted from [74]

1.4.6 THz imaging

THertz imaging operates on the 0.1-1mm wavelength, which are sometimes called sub-millimetre waves. Concealed objects, such as metallic guns, plastic or chemical explosives, have special characteristics towards the THz spectrum range. Metallic guns block the THz completely; other less metallic weapons will partially reflect the THz frequency. However, human skin will absorb the THz because of its high water content. The use of THz scanning for human bodies is useful because it can show the reflection of metallic or non-metallic objects, but content with water, such as the human body, will be shown completely dark [75].

The advantage of this technology is that it is non-ionized, safe to the human body, and has a wide spectra of THz and high resolution. However, because the human body absorbs THz radiation it cannot be used to detect inside the human body, which is the main objective of this thesis. Another disadvantage is that THz requires a special output power to generate THz at standoff detection. This will be limited and affected by the atmospheric conditions, which also leads to higher cost of equipment [75].

Figure 1.14: Terahertz Imaging Adapted from [76]

Thruvision produces a state of THz scanners, TS4 [indoor] and TS5 [outdoor], but even though it uses non-ionized radiation there are still concerns about the power used. For their product characteristics they use a passive system that delivers a robust detection of concealed materials at standoff distances. They use passive heterodyne systems that employ a mixer as the main component to receive the blackbody radiation transmitted

by the object. It has a 250GHz received radio frequency downgraded and converted by local oscillator to a few Gigahertz of intermediate frequency.

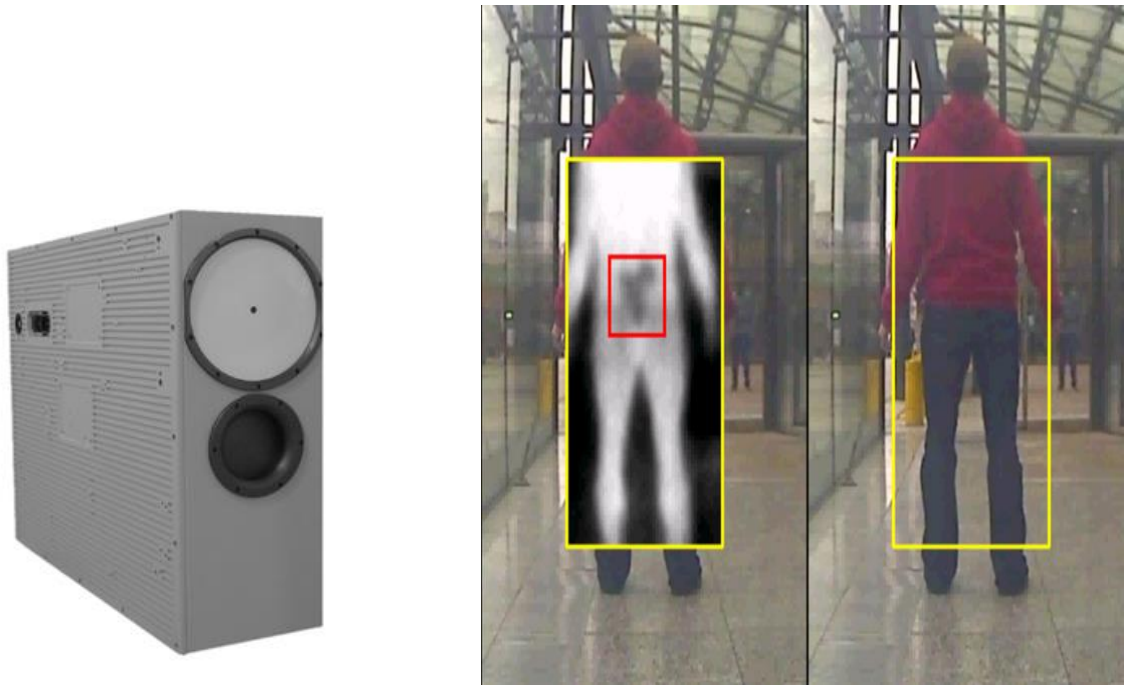

Figure 1.15: TS4 and the Imaging Results Adapted from [77]

Figure 1.16: TS4 and the Imaging Results Adapted from [78]

Researchers have been questioning the safety of Terahertz by arguing that a set of terahertz emission exposures could distress the normal dynamics of DNA, and consequently affect the gene expression and DNA replication [79].

The privacy issue is a concern for THz because of its ability to penetrate clothes at a wavelength of 1.2mm.

1.4.7 Infrared imager

Infrared is usually used for night vision to show the temperature of objects in the dark, such as human bodies [80]. Therefore, this technology has also been developed to see concealed weapons hidden underneath clothing. The approach in this technology is that the human body will emit infrared radiation, which will be absorbed by clothing first and will then be received by infrared detectors to analyse the results of possible targets within a human body. However, the resulting infrared images will be poor if the clothing of that person was loose; this is because the infrared radiation emitted will be spread over a wider area of clothing, which will limit the purpose of imaging of such a technology.

Iscon has developed a state-of-the-art infrared imaging scanner that will scan a full body in 30 seconds. Their technology combines infrared and heat transfer methods. The infrared camera shows the objects heated by heat transfer, therefore no radiation has been emitted [81]. Figure 1.17 shows human body images scanned, and Figure 1.18 shows a human body scanner from Iscon.

Also the purpose of this study is to image contraband materials in the human body, and if there is material embedded inside a human body for a long time, its temperature will

be similar to the human body. Therefore detection will be difficult for those concealed objects.

Figure 1.17: Images Shown from Iscon Whole Body Scanner

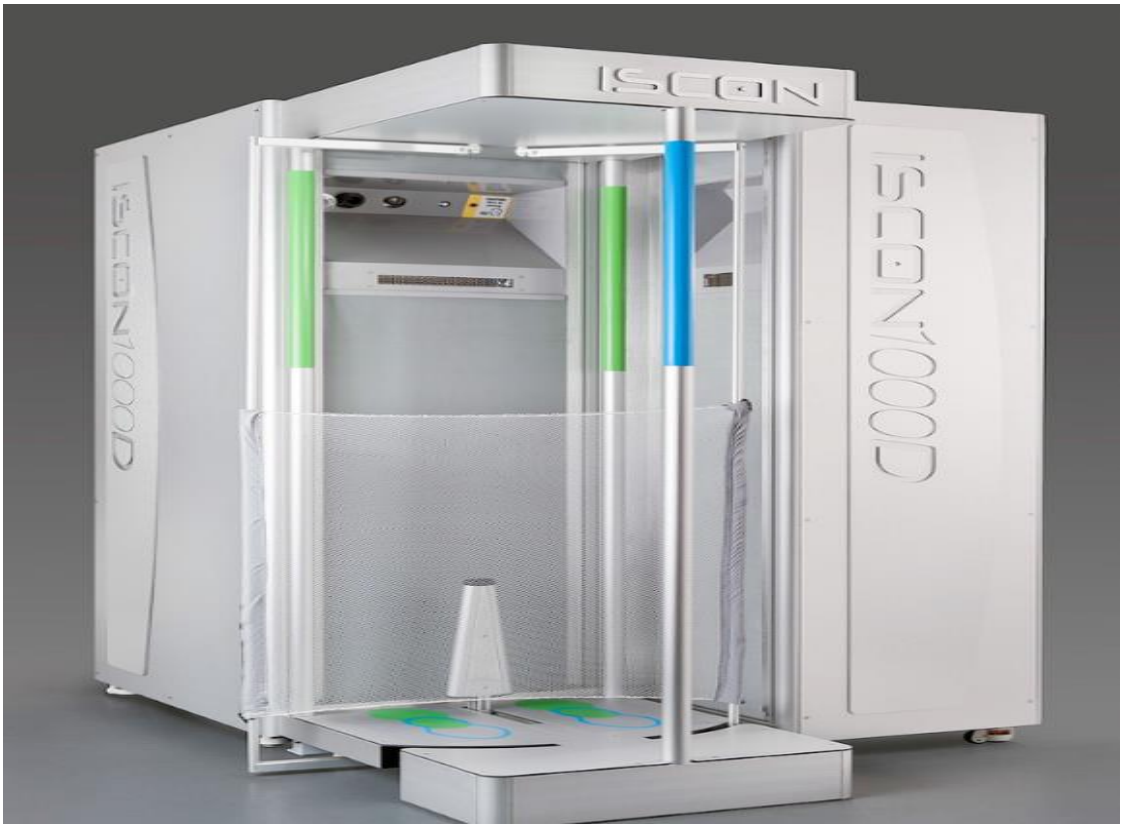

Figure 1.18: Iscon Body Scanners Adapted from [81]

1.4.8 X-ray imager

X-ray penetration is high, which makes it suitable to inspect containers, suitcases and dense boxes. X-ray sources used in X-ray machines emit energy from 1,000 to 1,000,000 electron volts ($10^{-4} - 10^{-7} \mu m$). This amount of energy passing through objects is absorbed by some of the objects to be imaged. The amount of X-ray photons in the X-ray stream of light is calculated by a number of factors such as the absorption of the photoelectric, electronic production and antielectron and inelastic scattering of a photon, known as Compton scattering [82]. The calculation of an attenuation coefficient will be based on the amount of energy passed through the object and the active atomic number of the object. A brief description of different types of method will be explained here.

Single energy X-ray system

This system emits 120 keV. It can detect targets made of metals clearly, and can detect explosive devices such as explosive wires, detonators and batteries. The disadvantage of this system is that it cannot see behind or within high atomic number targets. Moreover it cannot detect explosive materials.

Dual energy X-ray system

The dual energy system is considered to have a better resolution than the single energy X-ray. It can image both dense materials such as metals and less dense materials such as clothing and food. This means that it can differentiate between high atomic number materials and low atomic number materials. Moreover it can send information about the location, shape and density of the materials.

Computer tomography (CT)

CT is a diagnostic technique that uses extraordinary X-ray equipment to generate cross-sectional images of the human body. In order to get this image, the cross-section has to project the X-ray at several angles around the human cross-section. The resolution of the CT scans depends on the spatial and contrasts of the object. The X-ray detectors collect a number of photons, and then these data are processed using an image algorithm to reconstruct the image. This process is occasionally named spiral, volume, or three-dimensional CT scanning. There is no CT scan employed for human scans in airports because it takes a long time to scan a person.

Backscattering

Backscatter X-ray systems irradiate the scanned objects with low dose X-rays, from 0.01 to 10nm wavelengths. Compton scattering has been identified where it has been calculated from the incident photon on the objects and its scattering angle. It is specialized in detecting materials with lower atomic numbers, such as explosive powders and drugs. There are different types of scattering X-ray systems, one which has been developed by a leading company in the market, American Science and Engineering (AS&E). They have created a Z-backscatter imaging system by employing a low energy 50KV X-ray that can only show the surface of the human body, which means it can also show behind clothing. The person is scanned vertically by a pencil beam, and then the image is transported horizontally by scattered radiation detected at the detectors beside the X-ray tube. Figure 1.19 shows an image of a human hiding pistols and knives [83]. Figure 1.20 shows a later development of AS&E personal scanners.

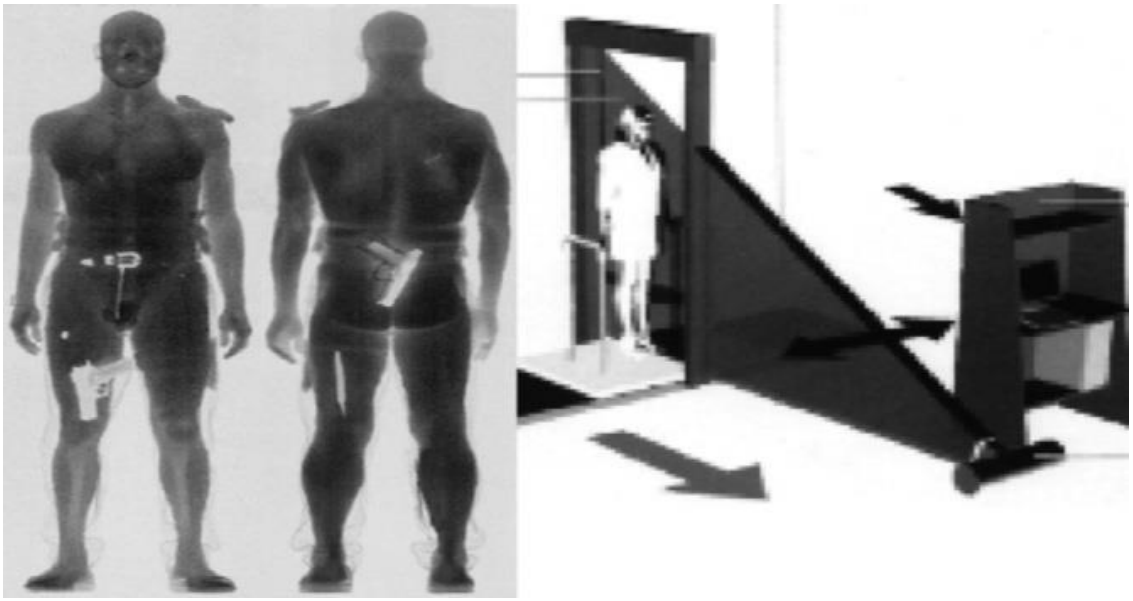

Figure 1.19: Adapted from [83] **Backscatter Imaging of Humans**

Figure 1.20: AS&E Smart Check System Adapted from [84]

Of course, for better penetration of passengers' baggage a higher energy X-ray emission is needed to detect detailed objects. Direct X-ray imaging technique can be used in medical applications, but it cannot be used for security scans because of its high dose. Nevertheless, backscatter X-rays are used in security applications, as illustrated above.

This is an X-ray technology that reconstructs images from inside a passenger's body by the reflection of low dosage X-rays emitted at the body. After the reflection a 2D image is shown on a computer screen to show if there are any hidden contraband materials. It is fast and reliable but cannot see through heavy materials, as seen from experience. It is used as a secondary scan machine if the passenger has been selected for further screening.

Although this system scans quickly, it raises concerns over privacy and health issues. In addition, in order to scan a human body a total of four scans per person are required, front, back and sides. Backscatter penetration is limited; therefore anything hidden in a human body will not be detected. Rapiscan have developed a backscatter system that has been employed in some airports.

Figure 1.21: Rapiscan System Secure 1000 Adapted from [85]

The most recently developed system by Tek84 Engineering Group LLC is called AIT84; this system can detect guns, knives and plastic weapons underneath passengers' clothing or hidden in private/groin areas and on the sides of the body. It is only 5ft wide and has been implemented in Israeli airports where security is critical in that region of the world [86]. Figure 1.22 shows the AIT84 system. The disadvantage of these systems is privacy intrusion because it shows anatomical information about the passenger. There are also health issues because of its radiation: no matter how low the radiation is, the risk is still there. The United States Food and Drug Administration (USFDA) did not state officially that it is 100% safe for human bodies [87].

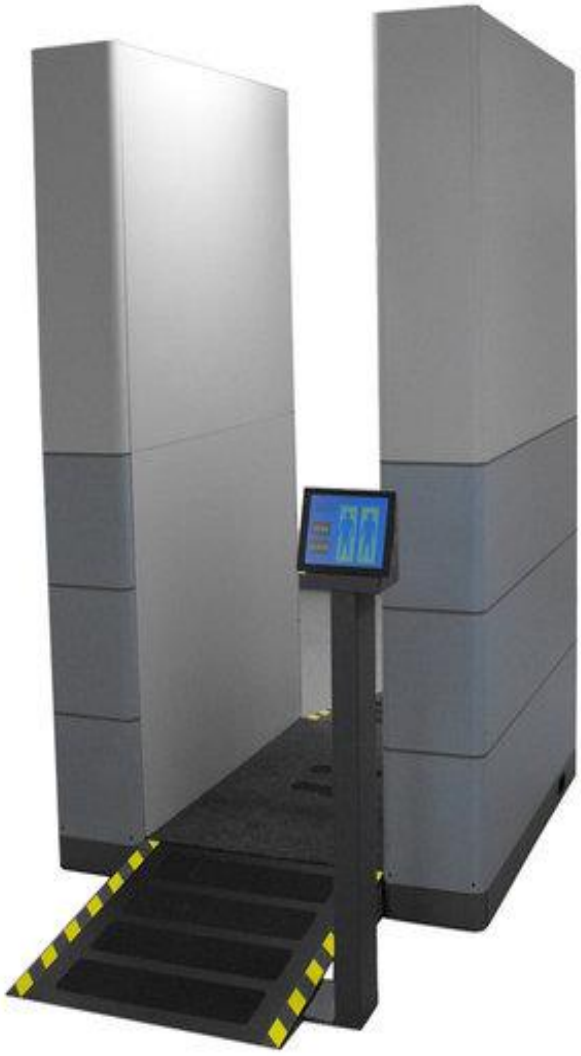

Figure 1.22: AIT84 System Adapted from [88]

X-rays are seen by the public as unsafe systems because of its radiation. Even though the dosage used is almost equivalent to two minutes of high altitude flight or 1/2500 as per the American College of Radiology [89]. Nevertheless the risk is still there for people who already have skin cancer, gene mutations damage and young children [90].

In addition to the radiation, the public were also concerned over privacy issues. As a result of such issues, in 2013 TSA planned to remove X-ray backscatter from American airports and use other technologies such as millimetre waves: this has Automated Target Recognition (ATR) that hides passenger details. The X-ray backscatter manufacturer Rapiscan has failed to deliver software that hides passenger details when scanning.

1.5 MOTIVATION

From all the above techniques, it is clear that no single method meets the requirements of security and detecting concealed objects within the human body. The requirement of security imaging is to be able to image inside human body taking in consideration the resolution and penetration depth. Millimetre waves have been researched widely and there are actually systems in airports using millimetre wave imaging. As discussed before, microwave imaging can detect dielectric properties of material embedded inside the human body, is non-invasive, and can detect metallic or non-metallic material. Therefore this is the area that will interest security applications in the near future.

Existing human body security imaging systems in airports are X-ray machines or metal detectors. Millimetre waves have been used for detecting concealed weapons under passenger clothing. Microwave through wall imaging has been used recently in law enforcement operations and differentiating between terrorists and their hostages if they are behind walls.

All the other problems of how to find dangerous objects if passengers are carrying them in their bags have been solved by different security imaging systems such as X-ray machines, CT explosive scanners and other types of imaging systems such as backscatters for liquid and powder detectors. Also chemical sniffers were used in airports with the help of dogs. However, the challenge of the detection of materials such as drugs or explosives if a human has planted anything in his body remains. These should be detected directly without involving dangerous X-ray radiation on human bodies. An X-ray is an ionized radiation that affects both the security personal and suspected criminals.

1.6 OBJECTIVES

It can be seen from the above review that a lot of research has been done on all the security imaging techniques, but not much in microwave imaging for security systems. Although microwave holography has been researched, their imaging results are not robust. The essential part of this research in microwave imaging is to understand how microwaves interact with human body organs or other materials, such as explosives or drugs that could be surgically implanted in the bodies of smugglers and terrorists. When understanding microwave interaction it will be easier to construct experiments to add human tissues dielectric properties to our models in the next chapter's numerical simulations. Also the imaging process of microwaves plays a vital role in how to reconstruct an image out of microwave rays. There are a number of image reconstruction algorithms that have been researched before and used for microwave holography, such as synthetic aperture radar (SAR).

New imaging algorithms will be suggested and tried in this research to differentiate between human organs and contraband materials. The target should be constructed as a

cross-section of the human body and foreign materials embedded inside them. Cross-sections of the human body will be layers of skin and other human organs with different dielectric properties. Simulated target points will be tested to see how effective the resolution achieved using a state-of-the-art imaging reconstruction algorithm called TR-MUSIC.

The aim of this thesis is to investigate whether microwave imaging is the future for security applications, and to study the management side of this research when new scanning technology is installed in places to be secured, such as airports, shopping malls, events and VIP buildings.

1.7 CHAPTER SUMMARY

The above chapter has reviewed the use of microwave imaging in both medical and security applications. This chapter started with the introduction of microwave radiation and its advantage over X-ray radiation, and explained the motivation behind microwave radiation as a safe, non-ionised radiation suitable for human body scanning technology. Microwave imaging has been researched extensively in the field of medical applications, where it is used in the detection of tumours using the dielectric properties of materials. This indicates that dielectric properties of materials are an essential part of microwave imaging; this will be discussed in the next chapter.

Microwave imaging research has been carried out by a number of universities, including Dartmouth College in the USA, The University of Bristol in the UK, and the University of Manitoba in Canada, University of Denmark, The Chungbuk University in South Korea, and The Australian IT and Electronic Engineering College. We observed that the imaging resolution should be a trade-off between the frequency chosen and the penetration depth of the wavelength; this should not be too high or more than 10GHz.

The chapter showed the up-to-date technologies used for scanning human bodies for the detection of concealed objects. Microwaves have been used for security applications, such as imaging through walls to counter terrorism and detecting concealed weapons. It explained the method of tomography used for microwave and X-ray systems. All security applications for contraband material detection have been discussed in this chapter. These have mainly been in airport security check points where this research is included in airport scanning technology.

The motivation of this research in microwave imaging is the challenge of imaging inside human bodies using dielectric properties of tissues, to detect if terrorists or smugglers surgically or manually implant illegal objects inside their bodies. The objectives are summarised by way of understanding the effect of microwaves on human body tissues or other contraband material (which will be discussed in the next chapter), using different imaging algorithms for reconstructing the image, modelling target and contraband materials embedded in modelled human body cross-sections, to investigate whether microwave imaging is the future for security applications, and to study the management side when installed in places needing to be secure, such as airports, shopping malls, events and VIP buildings.

Finally this chapter explained the purpose of this research and gave an idea of how interesting microwave imaging is.

Chapter 2: **Dielectric properties of materials on microwave**

Understanding an electromagnetic field interaction with human tissues is important for the calculation of the dielectric properties of tissues [87]-[92]. The study of dielectric properties of biological material and its polarization mechanism was started by Herman P. Schwan, whose name has been linked with many key findings in the area over the past 50 years. Further analysis and studies have been undertaken by Pethig, 1979 [92], Stuchly, 1979 [92], Schwan and Foster, 1980 [97], Pethig and Kell, 1987 [96], and Foster and Schwan, 1989 [93].

2.1 PERMEABILITY, PERMITTIVITY AND CONDUCTIVITY

There are differences in the definition between permeability, permittivity and conductivity of tissue medium; the easy definition between them all is as follows:

- permeability denotes the capability of a tissue medium to allow magnetic fields to pass through it;
- permittivity characterises similar for electric fields; and
- Conductivity signifies the ability of a material to allow a stream of electrical or heat current to travel through it; this is because of the free electrons generated.

As explained previously, when it comes to scanning technology that involves microwave radiation, the scanned human body is considered by the cell membrane and its conductive intercellular watery tissues. The dielectric properties of the human body, including permeability, permittivity and conductivity, are not well known and are always dependent on the person's activity. These dielectric properties from 10Hz to 10GHz have been researched extensively by Gabriel for more than 50 years[98]. Human body tissues always contain water; therefore they will not act as conductor or dielectric.

The best way of describing this is as a frequency-dependant dielectric with losses. The lower the frequency the deeper the electromagnetic wave can travel through the skin resulting in high penetration depth. The higher the frequency the lower penetration depth that wave length could travel through the skin.

Also from [99], the dielectric properties of biological tissue change according to the level of water inside these tissues, and the frequency creating a loss factor as well. Figure 2.1 shows different dielectric properties for three tissues from the range between 10 KHz to 1GHz. These tissues are blood, which has a very high water contents muscle, which has a medium level of water, and fat, which has a low level of water. It shows that the higher the frequency the less the relative permittivity for the highest water content. This means that the higher water content of tissues the more lossy it is, but on the other hand the drier the tissues the less lossy it is. The magnetic permeability inside biological tissues is considered to be similar to that in a vacuum[100].

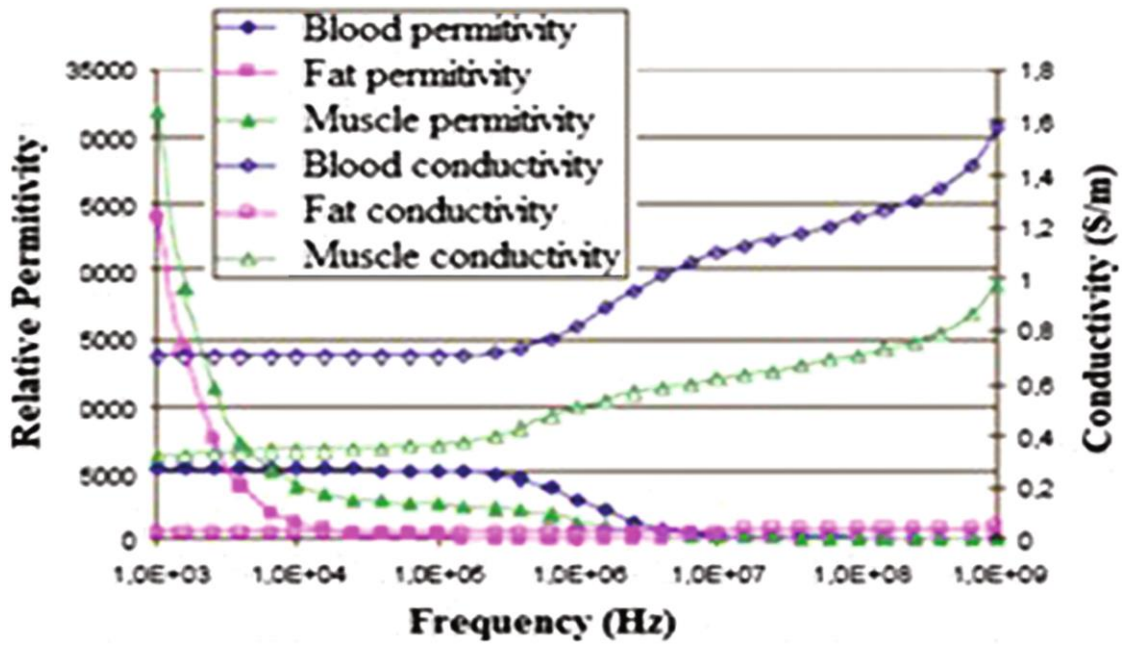

Figure 2.1: Blood, Muscle and Fat dielectric properties for different frequencies adapted from[99]**.**

2.2 DIELECTRIC PROPERTY THEORY

Historically, dielectric properties were observed by Faraday as the change in capacity of an empty capacitor when a material was positioned inside this capacitor. Faraday used the term 'specific inductive capacity' to explain the ratio of the capacities of the filled and unfilled capacitors, and then this ratio measure was given the term permittivityε. The electrical properties for any material positioned between a two plate capacitor with an area A and distance d between the plates of the capacitor can be calculated using the following Equations:

Conductance: $$G = A\sigma/d \; Units \; Farad \quad (1)$$

Electrical capacitance: $C = A\varepsilon\varepsilon_0/d$ units Ohm" or Siemens (2)

The conductivity σ is a measure of how easily the delocalized charge carriers can travel through the material when an electric field is applied, and is a proportional factor between the electric field and the electric current density. In biological material, the conductivity is the measure of the ability of its atomic and molecular charge to be transported throughout its volume. The factor ε_0 is the dielectric permittivity of free space, and has the value $8.854X10^{-12}$ "F m", whereas ε_r is the permittivity of the material relative to that of free space: ε is referred to as the dielectric constant. Pethig and Kell, 1978 in [96] gave a simple example, see Figure 2.2, of how an electric dipole has been shaped around a globular protein and at the surface of a membrane.

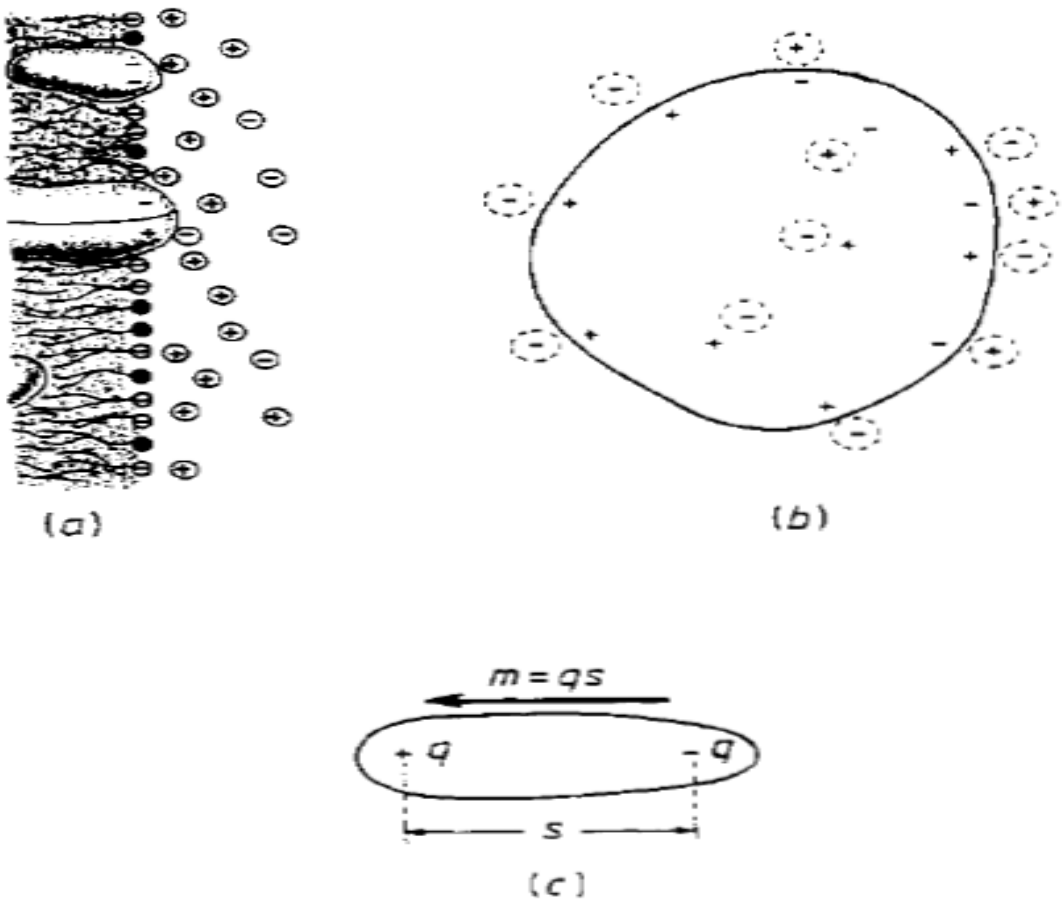

Figure2.2: Adapted from [96]

This is a diagram of the electrical double layers moulded at the surface of a charged biological membrane (a), and around a charged, aqueous globular protein (b). A simple polar molecule (c), containing in this case of a pair of opposite unit charges +q and -q, detached by a distance S and possessing a dipole moment of m = qs C m.

It consists of two magnitudes of a q negative and q positive charge separated by a vector distance. Therefore the molecular dipole moment $m = qs$ has a unit of Cm. From this example the dielectric property of tissues depends on the molecular size, structure and its content to calculate their relative permittivity, which can be written as a complex function from [101]:

$$\varepsilon^*(\omega) = \varepsilon_\infty + (\varepsilon_s - \varepsilon_\infty)/(1 + i\omega\tau) \quad (3)$$

in which ε_∞ is the measure of the permittivity when the polarized material is incapable to respond to the electric field, ε_s is the static permittivity where polarization is fully observed sometimes at low frequency, ω is the angular frequency of the sinusoidal electrical field (in Rad s^{-1}), i is $(-1)^{1/2}$ and τ is the relaxation time. The real and imaginary part of complex permittivity may also be x form:

$$\varepsilon^* = \varepsilon' - j\varepsilon'' \quad (4)$$

Where the real part isε', which is defined as the measure of charge displacement and consequence of energy stored in the material, and equivalent to the permittivity defined in (3). It is given by:

$$\varepsilon'(\omega) = \varepsilon_\infty + (\varepsilon_s - \varepsilon_\infty)/(1 + \omega^2\tau^2) \quad (5)$$

The imaginary partε'', of the above complex permittivity is called the loss factor, which is the measure of electrical energy dissipated when associated with the movement of polarizable charges in phase with the electric field. This is given by:

$$\varepsilon''(\omega) = (\varepsilon_s - \varepsilon_\infty)(\omega\tau)/(1 + \omega^2\tau^2) \quad (6)$$

It could also be defined in terms of frequency dependent conductivity as

$$\varepsilon'' = \sigma(\omega)/\ \varepsilon_0\omega = (\sigma_0 + \sigma_d(\omega))/\omega\varepsilon_0 \quad (7)$$

Where σ_0 is the steady state conductivity caused by the mobility of ions when the external field is excited, and $\sigma_d(\omega)$ is the frequency dependant conductivity caused by dielectric polarization.

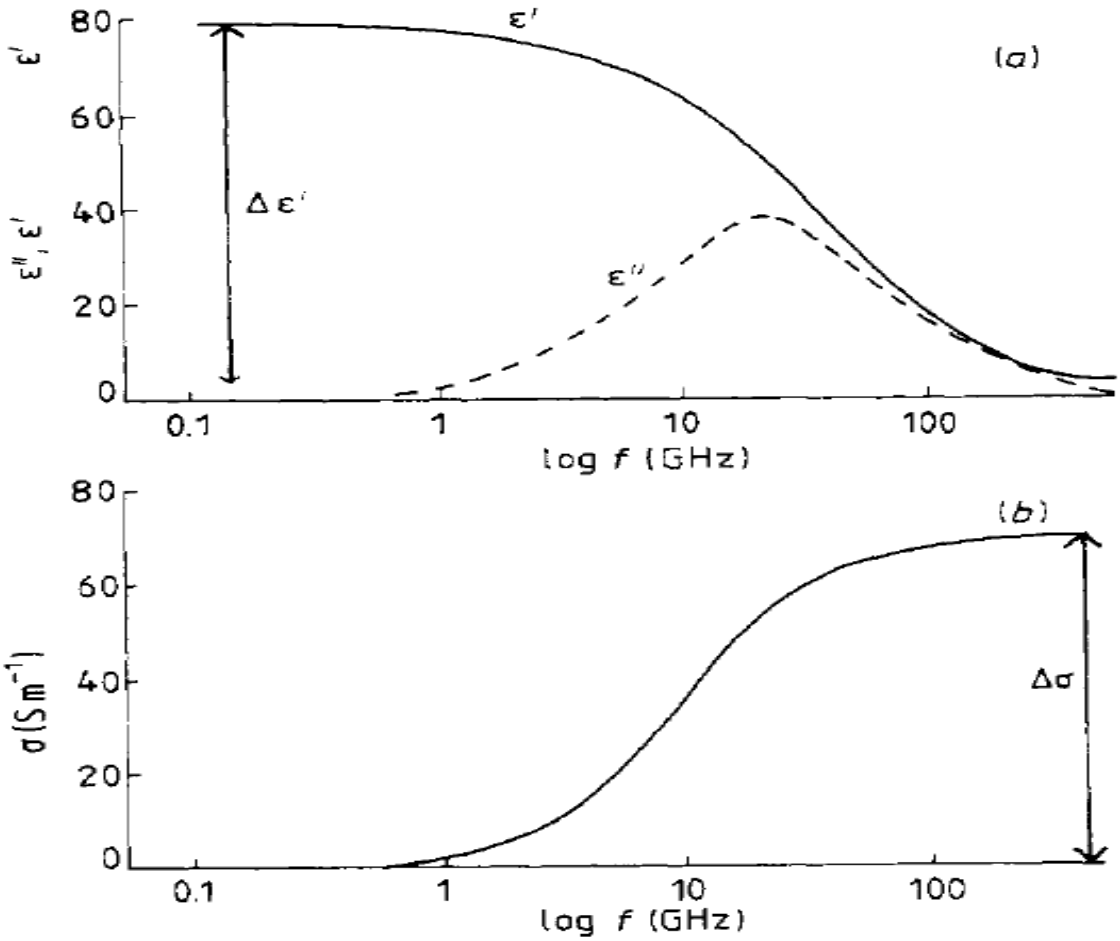

Figure 2.3: Adapted from [96]**.**

The dielectric dispersion displayed by pure water at 20°C, shown in terms of the change in (a) the real (ε') and imaginary (ε "**;** dielectric loss) parts of the permittivity, and (b) the frequency dependence of the conductivity. The low-frequency conductivity at neutral pH, because of the existence of H+ and OH^-ions, has electrical conductivity value of some $5\mu Sm^{-1}$.

We can outline the magnitude of dielectric dispersion in Figure 2.3 (a) as

$$\Delta\varepsilon' = \varepsilon'_s - \varepsilon'_\infty \qquad (8)$$

By combining Equation (5) and (6)

$$\varepsilon'(\omega) = \varepsilon'_{\infty} + \Delta\varepsilon'/[1 + \left(\frac{f}{f_c}\right)^2] \quad (9)$$

And

$$\sigma(\omega) = \sigma_s + (2\pi\varepsilon_0 f^2 \Delta\varepsilon')/f_c[1 + \left(\frac{f}{f_c}\right)^2] \quad (10)$$

Where f_c is the relaxation frequency ($f_c = 1/2\pi\tau$), the factor σ_s is the conductivity at low frequency where relaxation frequency is lower than f_c, and contains the steady state conductivity and dielectric losses associated with polarization processes. By putting $f \gg f_c$ the conductivity increment is shown in Figure 2.3 (b) and calculated by

$$\Delta\sigma = \sigma_{\infty} - \sigma_s = 2\pi f_c \varepsilon_0 \Delta\varepsilon' \quad (11)$$

From the above it shows that if the frequency has been changed across the dielectric dispersion, the change in conductivity is proportional to the change in permittivity. Therefore the total energy of the electric field is constant and it must either be stored as reflected $\varepsilon'(\omega)$ or dissipated as reflected$\varepsilon''(\omega)$. Equation (11) could be rewritten by

$$\tau = \Delta\varepsilon'\varepsilon_0/\Delta\sigma \quad (12)$$

Equations (11) and (12) only consider frequencies with single relaxation time.

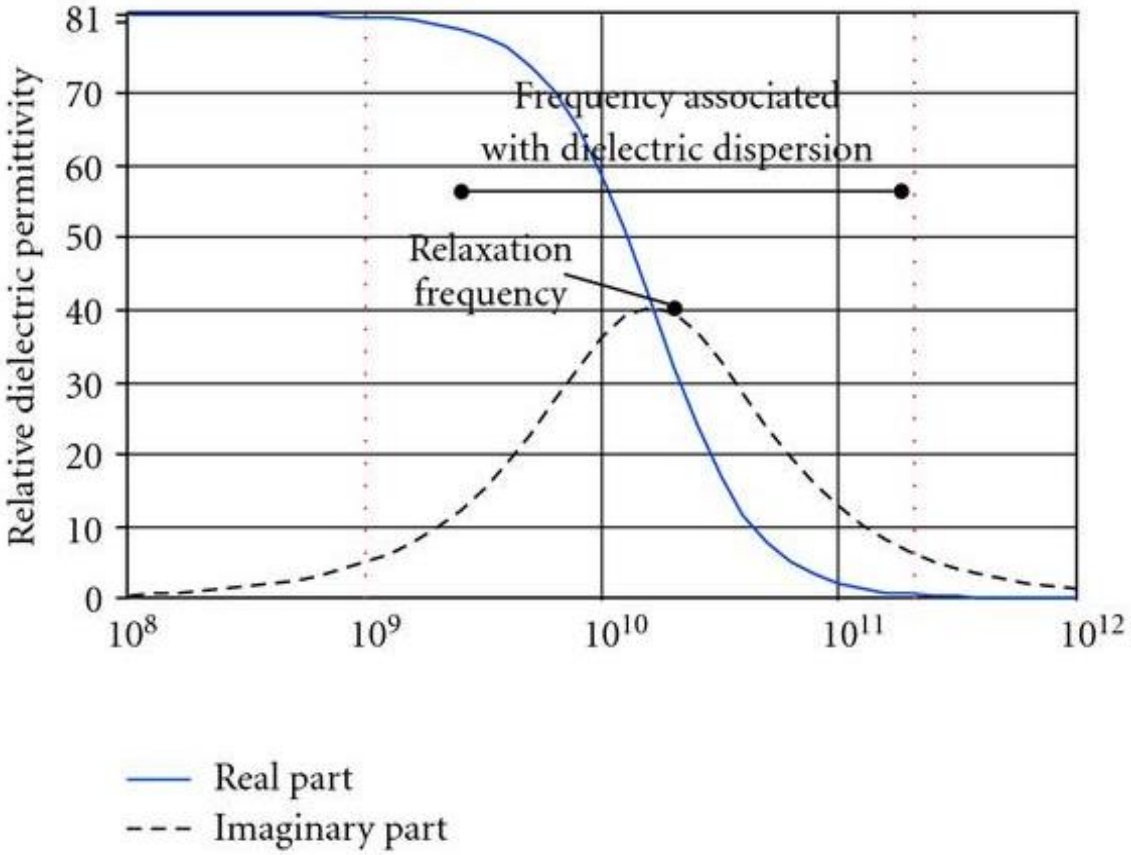

Figure 2.4: Adapted from [102]**. Graphical Presentation of Debye's Model in Liquid Water**

When frequencies are used as a parameter to calculate the complex permittivity, a plot of ε' against ε'' is obtained, a semicircle is created, and its centre lies on the abscissa which intersects ε'axis at the points $\varepsilon'_{-\infty}$and ε'_{-s} over a range of frequency. This is recognized as a Cole-Cole Circle, termed after the brothers K. S. and R. H. Cole who first derived it [103].

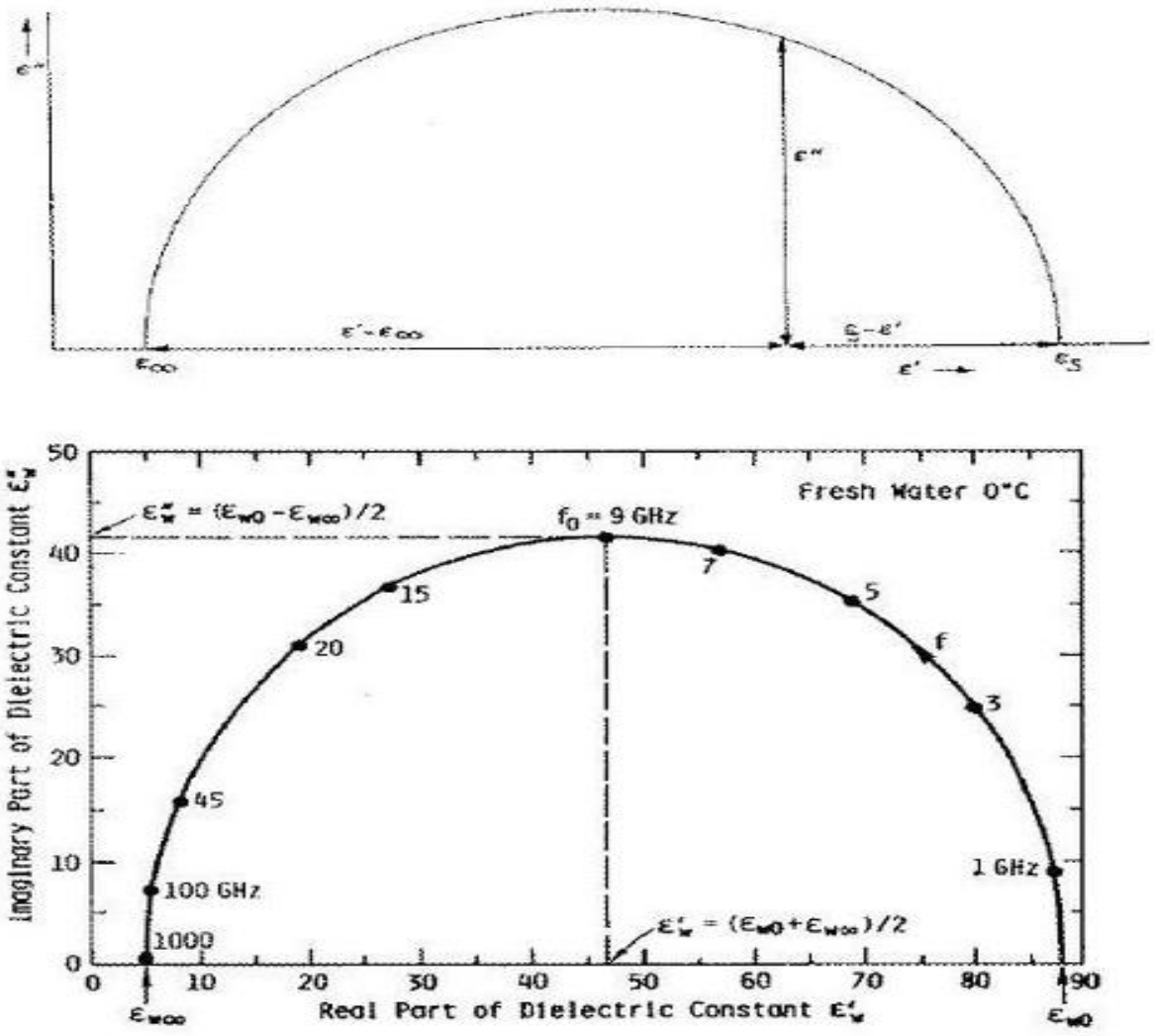

Figure 2.5: Adapted from [104]**, shows Cole-Cole Model Plot**

2.3 BIOLOGICAL TISSUES SPECTRUM

As previously stated, the dielectric properties of tissue are the measure of the interaction of the electromagnetic field with the tissue constituent at the cellular and molecular level. The polarization mechanisms of the interaction are well studied and identified theoretically and experimentally [91]. The dielectric spectrum of biological tissue specified at the [91] depends on the frequency and temperature. Therefore it consists of three main regions, known as α, β, ϒ dispersions, and is divided into low, intermediate and high frequencies from hertz to gigahertz.

The α dispersion is due to the polarization of ionic diffusion at the membrane of the cell in the range between hertz to kilohertz. The β dispersion caused by the polarization at the membrane of the cell and intracellular membranes in the region of intermediate frequencies (100 kilohertz). The ϒ dispersion is due to the polarization and relaxation of water in tissue in the region of gigahertz. From these definitions of different dispersion regions, the measurement of dielectric properties of tissue that has been investigated by [94] was between the tail of the β dispersion and the good part of the ϒ dispersion (50-20,000MHz). Measurements of dielectric properties of tissue used a Cole-Cole expression where the complex permittivity is expressed as (13):

$$\hat{\varepsilon}(\omega) = \varepsilon_{\infty} + \frac{\varepsilon_s - \varepsilon_{\infty}}{1+(j\omega\tau)^{1-\alpha}} + \frac{\sigma_l}{j\omega\varepsilon_0} \quad (13)$$

ε_{∞} Permittivity at the field frequency where $\omega\tau \gg 1$

ε_s Permittivity at the field frequency where $\omega\tau \ll 1$

σ_l Conductivity of the ionic drift and lower frequency polarization mechanisms

α Broadening of the dispersion

α Is zero for pure water but for tissue is ≥0 and negligible for body fluid. The relaxation time τ of tissue is usually longer than the one for pure water, which signifies a restriction of rotation capability of tissue with water molecules for the reason of organic environment.

2.4 DIELECTRIC PROPERTIES DATA OF HUMAN TISSUE

Dielectric properties of the human body have been discussed by several researchers. The most reliable data was produced by Gabriel, 1996 [105], under variable tests of microwave frequencies. Semenov and his group have used Federal Communication Commission tabulated values for the human body's dielectric properties in their simulation experiments [106],[107]. As we are using Matlab simulation experiments only, the dielectric properties of the human body helped to model the cross-section of the human body. This dielectric data will help to easily distinguish it from other contraband materials' dielectric properties, where it will show differences in image results after reconstruction. The First experiments in this research will be using Radon transformation technique [108] and the second experiments in this research will be using TR-MUSIC technique. The advantage here of dielectric property analysis is that the dielectric property values of explosives or drugs are lower than human body tissue, which contains blood and water. Table 1; shows different dielectric properties of human body tissues with different frequency range ,based on Gabriel's study[109].More human body tissue dielectric properties are included in Appendix D.

Table 2.2: Variable biological tissues dielectric properties for different frequencies adapted from [109]**.**

Tissue name	Frequency [Hz]	Conductivity [S/m]	Relative permittivity	Loss tangent	Wavelength [m]	Penetration depth [m]
Air	1GHz	0	1	0	0.29979	N/A
Aorta	1GHz	0.72866	44.561	0.29393	0.044442	0.049146
Bladder	1GHz	0.39663	18.85	0.37823	0.067887	0.059107
Blood	1GHz	1.5829	61.065	0.46596	0.037411	0.026875
BloodVessel	2GHz	1.1708	43.089	0.24421	0.02267	0.029982
BodyFluid	2GHz	2.1556	68.472	0.28294	0.01794	0.020578
BoneCortical	2GHz	0.31007	11.654	0.23914	0.043604	0.058856
BoneMarrow	3GHz	0.12085	5.2378	0.13824	0.043561	0.10078
BrainWhiteMatter	3GHz	1.5106	35.541	0.25467	0.01663	0.021118
BreastFat	3GHz	0.17889	5.0386	0.21273	0.044272	0.066986
Cartilage	3GHz	2.205	37.605	0.35134	0.016057	0.014983
Cerebellum	4GHz	3.2796	42.427	0.34737	0.011341	0.010697
CerebroSpinalFluid	4GHz	5.1959	63.73	0.36638	0.0092394	0.008288
Cervix	4GHz	2.9533	45.706	0.29037	0.010973	0.012278
Colon	4GHz	3.4636	51.31	0.30335	0.010347	0.011102
Cornea	4GHz	3.6521	49.229	0.33338	0.01054	0.010336
Duodenum	4GHz	3.8476	59.611	0.29006	0.0096088	0.010762
Dura	4GHz	2.7456	40.096	0.30772	0.011702	0.012384
EyeSclera	4GHz	3.4044	50.448	0.30326	0.010435	0.0112
Fat	4GHz	0.1829	5.1249	0.16038	0.033002	0.065918
GallBladder	5GHz	4.6525	54.763	0.30542	0.0080114	0.0085398
GallBladderBile	5GHz	5.9127	64.915	0.32745	0.0073465	0.0073279
Gland	5GHz	4.6614	53.342	0.31416	0.0081123	0.0084174
Heart	5GHz	4.8626	50.274	0.34772	0.0083348	0.0078538
Kidney	5GHz	4.9423	48.059	0.36971	0.0085094	0.0075686
Lens	5GHz	3.5606	41.671	0.30719	0.0091829	0.0097349
Liver	5GHz	3.8278	39.26	0.35052	0.0094296	0.0088186
LungDeflated	5GHz	3.9413	44.859	0.31587	0.0088451	0.0091305
LungInflated	5GHz	1.722	18.966	0.32641	0.013592	0.013599
Lymph	7GHz	7.4403	50.08	0.38151	0.0059482	0.0051373
MucousMembrane	7GHz	5.5823	37.146	0.38591	0.006904	0.0058993
Muscle	7GHz	6.4607	46.865	0.35401	0.006163	0.0057101
Nail	7GHz	1.4431	9.171	0.40406	0.013872	0.011357
Nerve	7GHz	3.7733	26.216	0.36961	0.0082296	0.0073216
Oesophagus	7GHz	8.1918	54.315	0.3873	0.0057088	0.0048617
Ovary	7GHz	6.5446	36.891	0.45556	0.0068831	0.0050472
Pancreas	7GHz	7.4403	50.08	0.38151	0.0059482	0.0051373
Prostate	7GHz	7.6733	50.216	0.39239	0.0059346	0.0049928
Retina	7GHz	7.0332	45.994	0.39268	0.0062008	0.0052133
SkinDry	10GHz	8.0138	31.29	0.46038	0.0052291	0.0037979
SkinWet	10GHz	8.951	33.528	0.47989	0.0050416	0.0035267
SmallIntestine	10GHz	12.687	42.03	0.54258	0.0044728	0.0028047
SpinalCord	10GHz	6.0295	23.778	0.45581	0.0060013	0.0043983
Spleen	10GHz	11.381	40.56	0.5044	0.0045721	0.0030585
Stomach	10GHz	13.314	48.923	0.48919	0.0041697	0.0028668
Tendon	10GHz	10.339	29.31	0.63406	0.005299	0.002905
Testis	10GHz	12.377	45.248	0.4917	0.0043346	0.0029665
Thymus	10GHz	12.132	45.15	0.48301	0.0043432	0.0030204
Thyroid	10GHz	12.132	45.15	0.48301	0.0043432	0.0030204
Tongue	10GHz	11.077	41.484	0.47998	0.0045325	0.00317
Tooth	10GHz	2.1359	8.1197	0.47284	0.010252	0.0072681
Trachea	10GHz	8.5368	31.09	0.49358	0.0052282	0.0035658
Uterus	10GHz	12.492	45.341	0.49526	0.0043285	0.0029432
Vacuum	10GHz	0	1	0	0.029979	N/A
VitreousHumor	10GHz	15.126	57.872	0.46982	0.0038414	0.0027391

2.5 DIELECRIC PROPERTIES OF EXPLOSIVES AND DRUGS

As discussed above, the dielectric properties of material ε' are the electrical field strength value in an empty medium to that tested material. It is indicated that the material has a dielectric constant as an insulator. When microwave energy is dissipated into the material then the energy is converted to heat; therefore this measure is called the dissipated factor. Moreover the dielectric constant of a material could refer to the density of the material.

As explained above, the dielectric properties of the human body, and explosives or drugs that could be imbedded in the human body also have its own dielectric properties. Therefore the difference between both dielectric properties could be used to detect foreign materials in the human body. For instance, plastic explosives and explosive powders have very low dielectric properties and a low dissipation factor; therefore the lower density of these materials could be observed.

The relative permittivity for most explosives is between 2.70-3.14 [110], while plastic objects are in the range of 2.08-5.04 [111]. Metals can be highly reflective materials that could reflect microwaves and be observed clearly. Table 2.2 shows some materials and their relative permittivity.

Table 2.2: Relative Permittivity of Some Material, Compiled from [101]-[103]

Material	Relative permittivity	Frequency
Comp B (explosive)	2.90	1GHz
Comp C-4 (explosive)	3.14	1GHz
RDX	3.14	1GHz
PETN(explosive)	2.72	1GHz
TNT(explosive)	2.70	1GHz
Black powder	3.3	2GHz
Pistol Powder	3.1	2GHz
Ceramic	5.60	3GHz
Glass (Pyrex)	4.82	3GHz
Plexiglass	2.60	3GHz
Styrofoam	1.03	3GHz
Teflon	2.08	10GHz
Polystyrene	2.54	10GHz
Polyethylene	2.25	10GHz
Lucite	2.56	10GHz
Cocaine and Heroin	3	Not observed

2.6 CHAPTER SUMMARY

This chapter has summarised the history and the theory behind the calculation of dielectric properties.

The dielectric properties of materials include permittivity, permeability and conductivity. Complex permittivity of materials has been calculated. The chapter shows that if the frequency has been changed across the dielectric dispersion, the change in conductivity is proportional to the change in permittivity. Therefore the total energy of the electric field is constant, and it must either be stored as reflected $\varepsilon'(\omega)$ or dissipated as reflected$\varepsilon''(\omega)$.

The Cole-Cole Circle technique was used to calculate complex permittivity of materials. The dielectric spectrum of biological tissue depends on the frequency and temperature. Therefore it consists of three main regions, known as α, β, ϒ dispersions, and are divided into low, intermediate and high frequencies from hertz to gigahertz.

The dielectric properties of the human body has been researched by Gabriel[105] with different values to each tissues, as shown in table 2.1.

The dielectric properties of contraband materials have been explained; some of the values are shown in table 2.2.

The explained dielectrics properties of different materials have helped in modelling cross-sections with embedded targets inside them containing different dielectric properties. The next chapters will use the discussed dielectric properties in this chapter to set up the experiential simulation in Matlab and FDTD software to reconstruct the images using microwave radiation.

Chapter 3: **Microwave tomography for security applications**

3.1 INTRODUCTION

Microwave imaging systems exist under different types of technologies and these technologies are found in medical imaging systems. There are already several papers that discuss the use of microwave imaging via the analysis of dielectric properties of tissues using different techniques [113], [114]. Microwave imaging is non-ionizing, non-invasive, sensitive and low-cost [11], which makes it a promising area for security applications for use in border control, such as in airports.

Although the microwave is not comparable to the X-ray in image resolution, it has the advantage of imaging physiological changes [88], [106]. The preferred microwave illumination level frequency for imaging makes it safe and non-destructive for the operator, avoiding the hazards of radiation from the X-ray systems used in airports at the moment.

This chapter will illustrate the possible application of Security Imaging Systems using microwave frequencies of between 0.9GHz to 2.36GHz, since it has been already researched in the medical field[106]. The concerns raised about this imaging system were how to construct them cost effectively and with less radiation emission. Microwaves used to face the issues of expensive hardware and insufficient computing power, but now the technologies have advanced, indicating a brighter future for microwave systems, especially with the knowledge of the interaction of electromagnetic waves between human body tissue and their dielectric properties [105], [116].

The current human body inspection systems in airports are metal detectors, which can only detect metals concealed in a person's clothing; they are ineffectual if the person is hiding other illegal materials such as plastic explosives or drugs. There is an additional machine in airports that uses high dosage X-ray radiation, but it is very harmful for both the scanned person and the operator.

This chapter discusses the possibility of microwave tomography imaging techniques for security applications, using dielectric property analysis to discuss the data of dielectric properties of the human body to be used in the simulation, describes the minimum resolution and microwave frequency to be used in the imaging for security applications, and describes the simulation results.

3.2 RADON TRANSFORMATION IMAGE RECONSTRUCTION THEORY

The Radon transformation algorithm was discovered by Johann Radon. His imaging algorithm has already been used in x-ray medical imaging and Computed tomography medical scanning. Figure 3.1 shows a basic diagram of how images constructed using a Radon transformation algorithm.

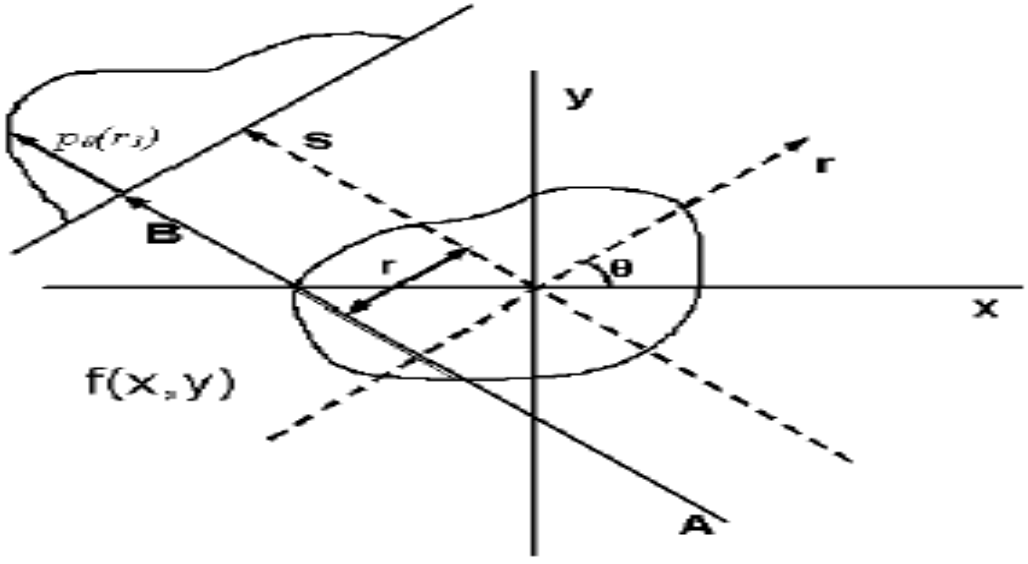

Figure 3.1: adapted from [117] **Parallel beam geometry for Radon Image reconstruction algorithm**

When it comes to image an object, a beam of waves is made of a set of line integrals at a given angle. We would like to image the object$\mu(x,y)$. This method is better explained if we consider the collection of data as a series of parallel rays across a projection at angle θ and at a position$r$. This is repeated for different angles around the object. For attenuation, the exponential of tissue is:

$$I = I_0 \exp(-\int \mu(x,y)ds) \tag{14}$$

Where $\mu(x)$ is the attenuation coefficient at position x along the wave path. Therefore the total attenuation p of a wave at a position r on the projection at angle θ is given by the line integral;

$$p(r,\theta) = int\frac{I}{I_0} - -\int \mu(x,y)ds) \tag{15}$$

As seen from the figure, r will be expressed as;

$$r = x\cos\theta + y\sin\theta \tag{16}$$

So the equation above will be

$$p(r,\theta) = \iint_{-\infty}^{\infty} f(x,y)\delta(x\cos\theta + y\sin\theta - r)dxdy \tag{17}$$

Where $f(x,y)$ represent(x,y). The above function is the Radon transformation of the 2 D object. The above projection slice theory tells us that if we could have an infinite number of one dimensional projections of an object at an infinite number of angles to reconstruct the original image$f(x,y)$, therefore if we need to find the $f(x,y)$ back from the above equation we need to find the inverse of the Radon transformation from the filtered back propagation algorithm.

$$f(x,y) = \int_0^{2\pi} p(\theta, x\cos\theta + y\sin\theta)d\theta \tag{18}$$

The above mathematical function is already a tool in Matlab that is added to the total imaging reconstruction algorithm code used for our experiment in this chapter.

3.3 RESOLUTION AND FREQUENCY FOR MICROWAVE TOMOGRAPHY

The resolution of the illuminated object by microwave tomography is affected by factors such as microwave wavelength, reconstruction algorithms, and signal-to-noise ratio adjustments in microwave tomography imaging systems, number of emitters and receivers, and dielectric properties of biological objects. The resolution of microwave tomography has been studied by Serguei Semenov [106]. Their microwave operating frequencies were between 0.9 and 2.36GHz and signal-to-noise ratio was 30dB. They concluded that a resolution of between 6.3-7.8mm was achieved at 2.36GHz. Therefore, knowing that the wavelength in water at 2.36 is equal to 1.44cm, the spatial resolution achieved was better than half of the wavelength. They also concluded that a resolution of between 7.3-9.5mm was achieved at 0.9GHz. Therefore, knowing that wavelength in a medium at 0.9GHz is equal to 3.32cm, the spatial resolution resulting experimentally was better than the quarter of the wavelength ($\lambda/4$ = 8.3mm). These have demonstrated that microwave resolution is not limited by the wavelength in medium. The smallest object that could be detected is 6.3mm; therefore, that is the minimum resolution required for microwave security applications. For security control of contraband, 6.3mm diameter or higher is the required resolution to detect any illegal object hidden in the human body.

3.4 EXPERIMENT SET UP DETAILS

In the next sections there will be a numerical simulation based on suitable assumptions when it comes to microwave tomography scanning of human body cross-sections. The dielectric properties of the selected human body tissues to be in that cross-section were in the range 0.9-2.36GHz. The dielectric properties decreased in value when the

frequency chosen increased, which explains that it has a proportional relationship. Therefore the scenario is to choose human body tissues with dielectric properties in one frequency, such as 0.9GHz, and then choose another material to be embedded in that cross-section modelled with the same 0.9GHz dielectric properties; this could be metals or any other contraband powders. In most cases illegal powders have almost similar values of dielectric properties in frequency objection, ranging from 0.9-2.36GHz. Its dielectric value would range from 1-3.5 maximum because they do not contain water or blood like human body tissues.

To ease our problem on Matlab, we started with square shaped cross-section layers of different human tissue dielectric properties values, and small objects embedded inside these layers with different dielectric properties each time. The dielectric properties data of human body tissues have been taken from websites[109], [118]. Later models will be spheres, which are closer to human body cross-sections. Again it will be similar scenario to the square model idea of layers of different human body tissue dielectric properties values. To visualise the sphere cross-section more clearly, the model will be made of a few layers with illegal objects embedded in them. These models will then be image reconstructed using a Radon transformation algorithm, as explained previously.

3.5 NUMERICAL SIMULATION FOR MICROWAVE TOMOGRAPHY USING RADON TRANSFORMATION TECHNIQUE

The microwave tomography technique is adapted here to test human body cross-sections by subjecting them to microwave rays and analysing the image created. In order to develop this program in Matlab we had to follow the flow chart below, described in Figure 3.2.

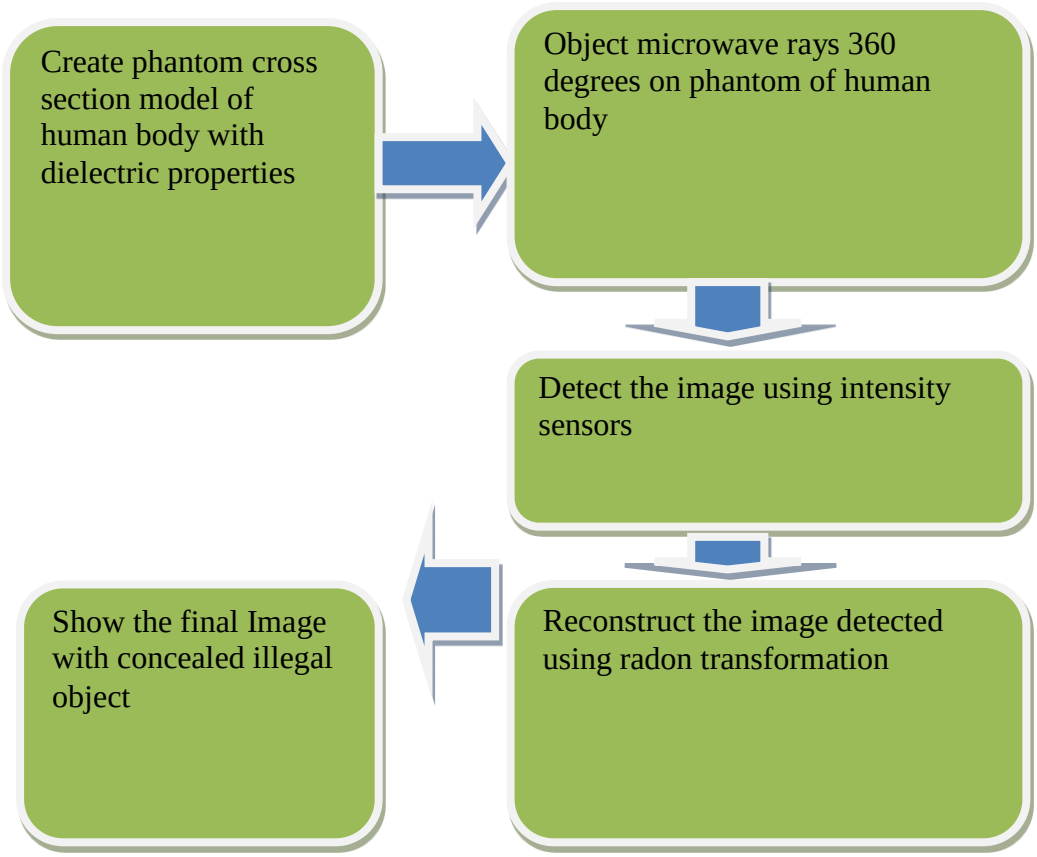

Figure 3.2: Flowchart of Microwave Tomography Simulation

The simulation was carried out to prove the concept of detecting different dielectric properties of materials inside a human body cross-section. After projecting the microwave ray onto the developed phantom of a human body cross-section there will be an image reconstruction algorithm using radon transformation to calculate the dielectric properties from the inside of the human body. If there is an extra object such as a metal gun, it should be easily observed as an object with high pixel intensity, raising suspicions and showing different dielectric property values inside the human body. The first assumption of the simulation was to treat the human body cross-section in the form of a square cross-section to ease the problem as shown in Figures 3.3and 3.4.

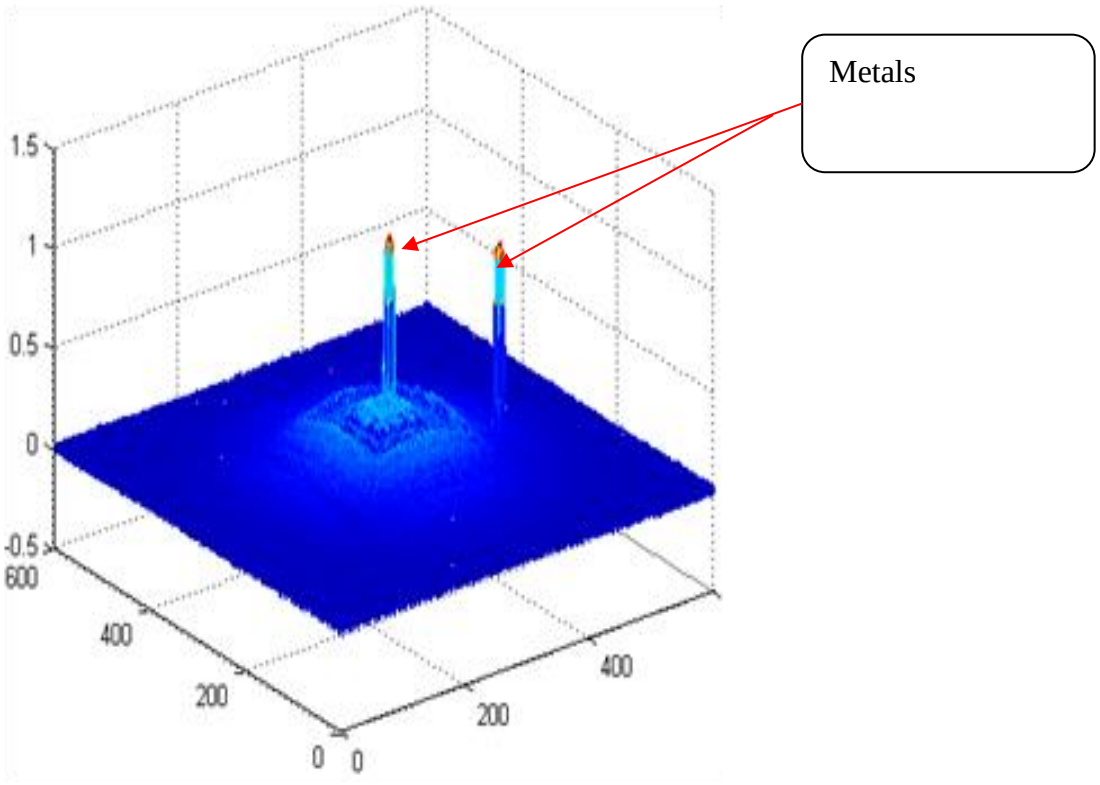

Figure 3.3: Shows Two Metal Pieces Blocking the Microwave with High Intensity

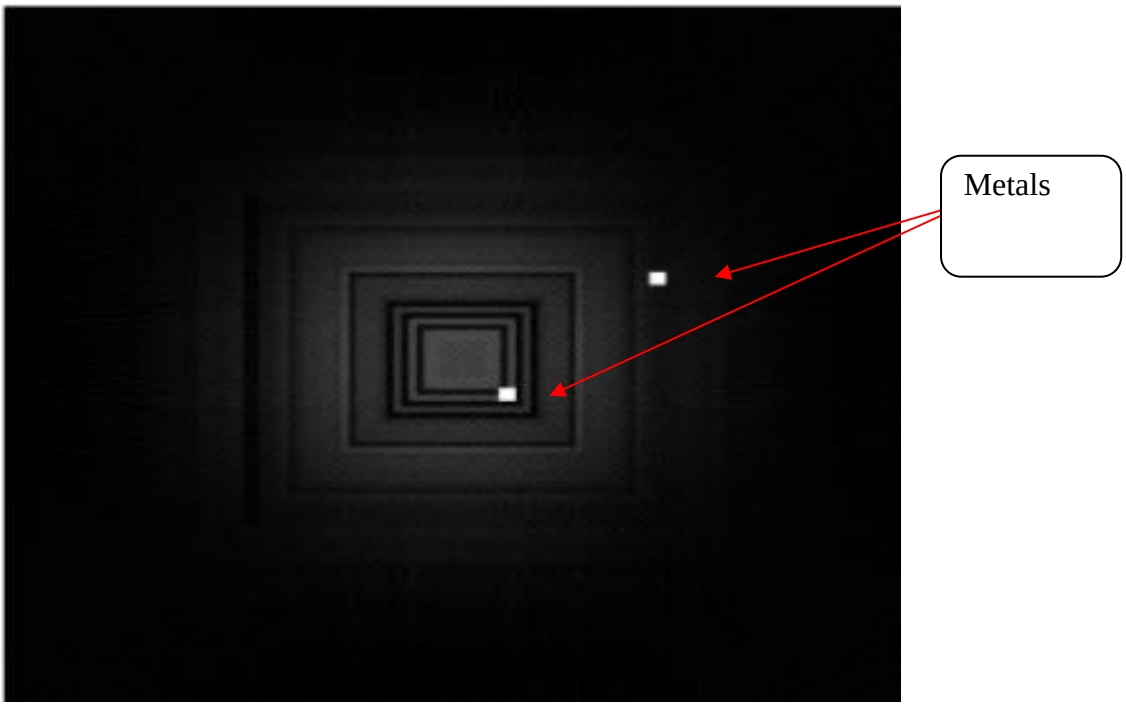

Figure 3.4: Final Image of Two Metal Pieces after Reconstruction

From Figure 3.4 the locations of the two white or high intensity points have been replaced with different dielectric properties values, which are lower than the human dielectric properties in the cross-section. The square shape is assumed to be different

layers of human cross section. Remarkably it is still detected because of its low value compared with higher values of human body tissue dielectric properties, as shown in Figures 3.5 and 3.6.

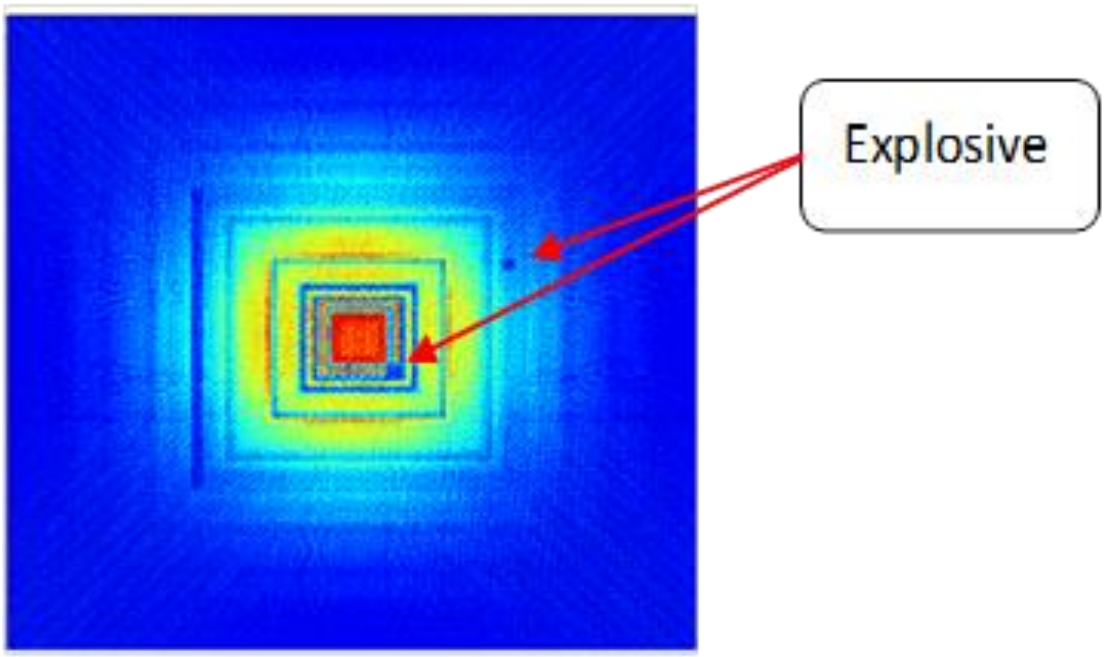

Figure 3.5: Shows Two Contraband Materials Inserted in the Cross Section

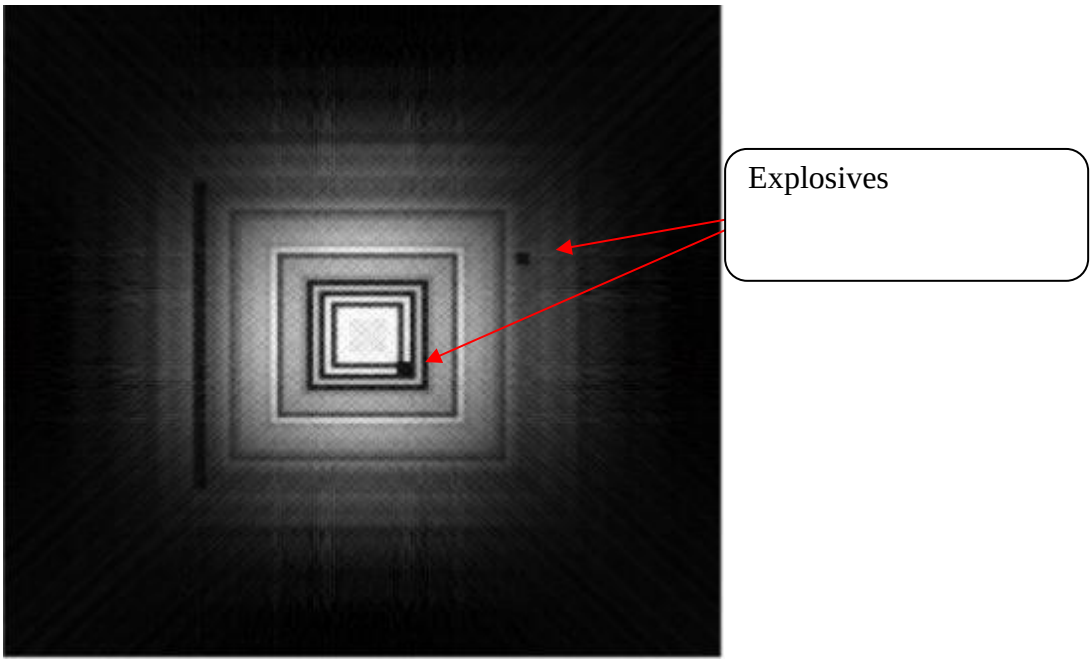

Figure 3.6: Final Image of Contraband Materials after Reconstruction

As the use of a square cross-section showed successful results, to make it more realistic another phantom sphere cross-section of the human body was developed, giving us the results in Figures 3.7 and 3.8.

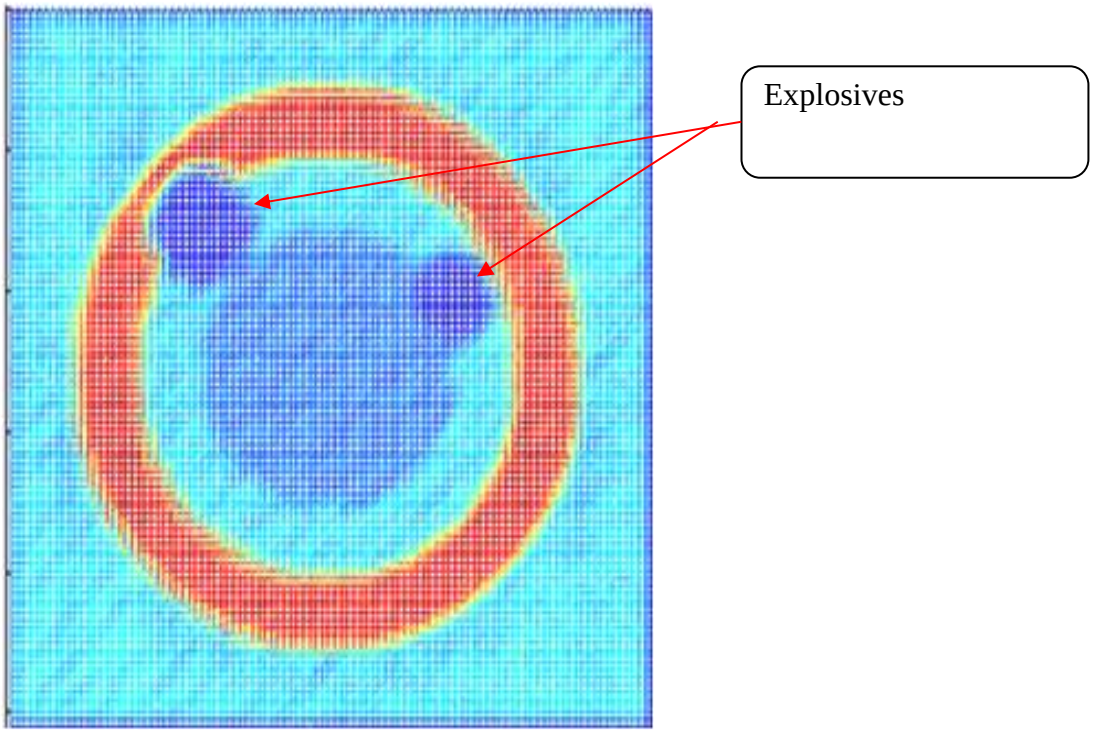

Figure 3.7: Sphere Cross-Section with Two Contrabands Overlapping the Usual Dielectric Properties of a Human Body

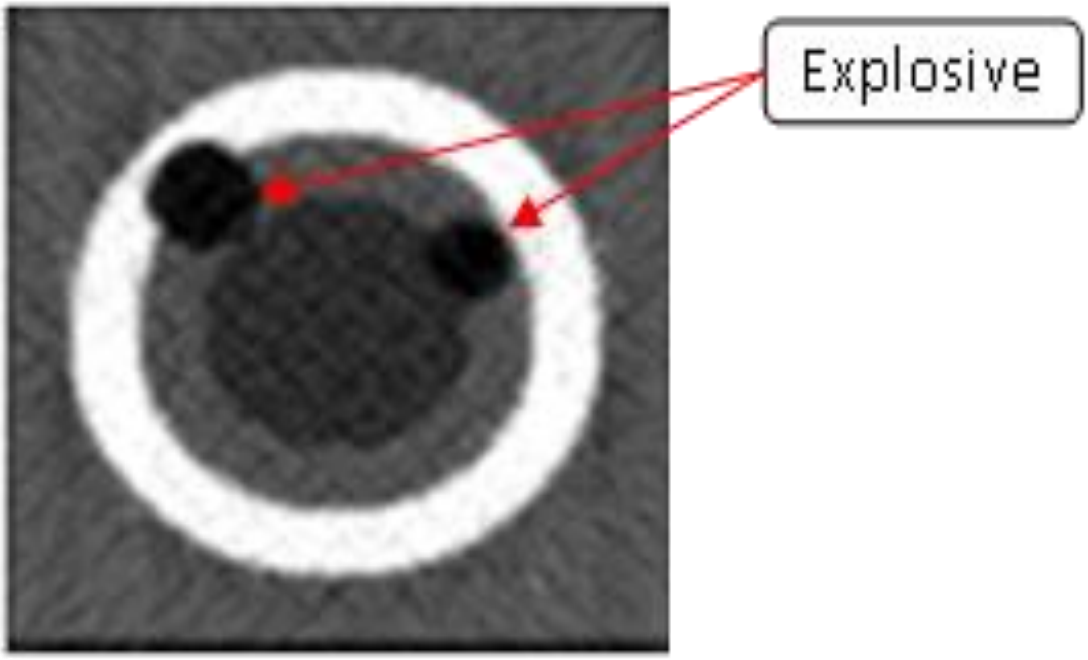

Figure 3.8: Final Image of Contraband Materials after Reconstruction

From these we can see how 8.3mm and 6.3mm resolution of a very low dielectric property microwave image can be visualized after the image reconstruction simulation.

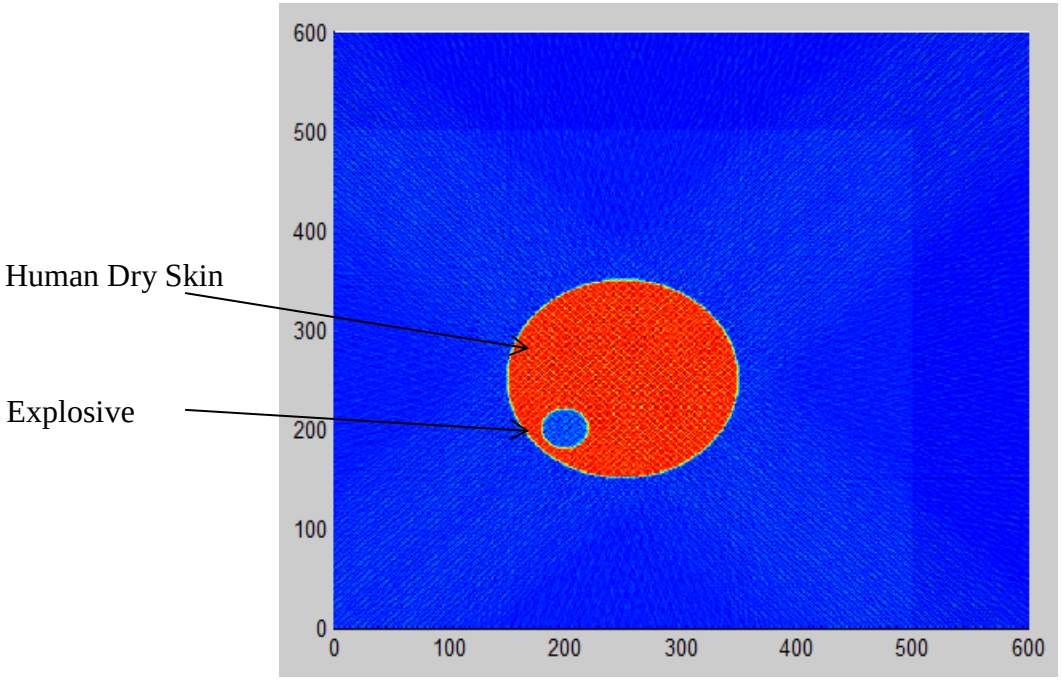

Figure 3.9:10cm radius of sphere cross-section and 2cm radius of illegal powder embedded inside it

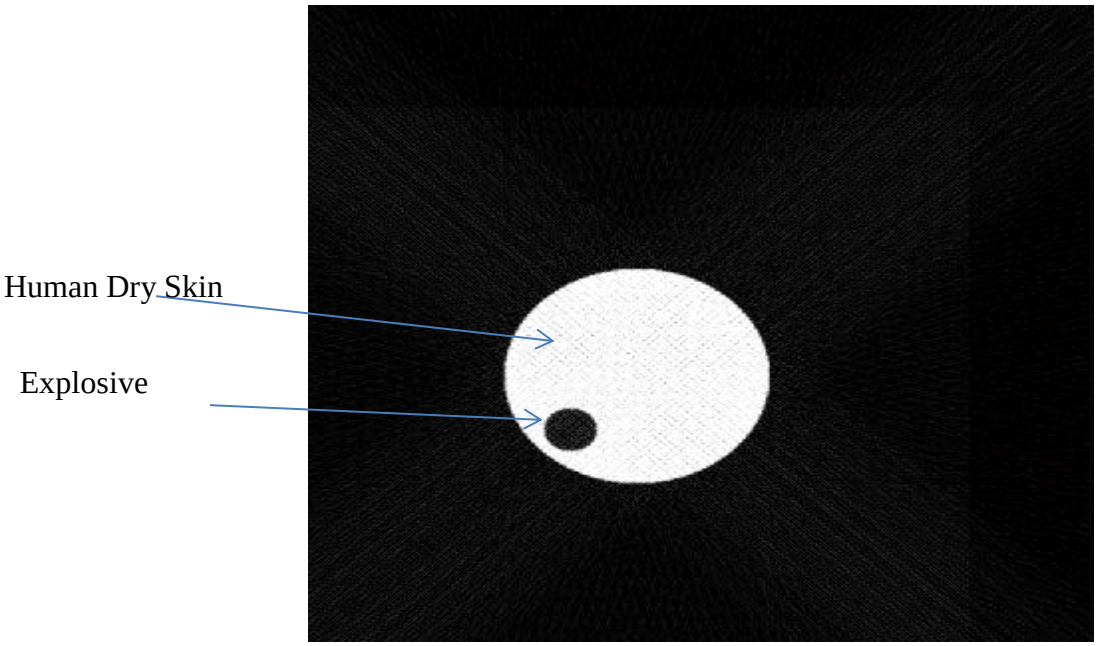

Figure 3.10: Final image of contraband materials embedded in human dry skin after reconstruction

The above simulation result shows a sphere cross-section of 10cm radius, assumed to be dry skin; its dielectric value is 36.587315 at 4GHz. There is 2cm illegal object

embedded inside it, which has a dielectric value of 3 at 4GHz microwave objection. The background of this model is air and its dielectric value assumed to be 1; because the dielectric value of the illegal object (powder) is very low it can be seen clearly. This result could be compared with the next chapter's simulations to make comparisons between Radon Transformation theory and TR MUSIC theory in image formation techniques for microwave imaging.

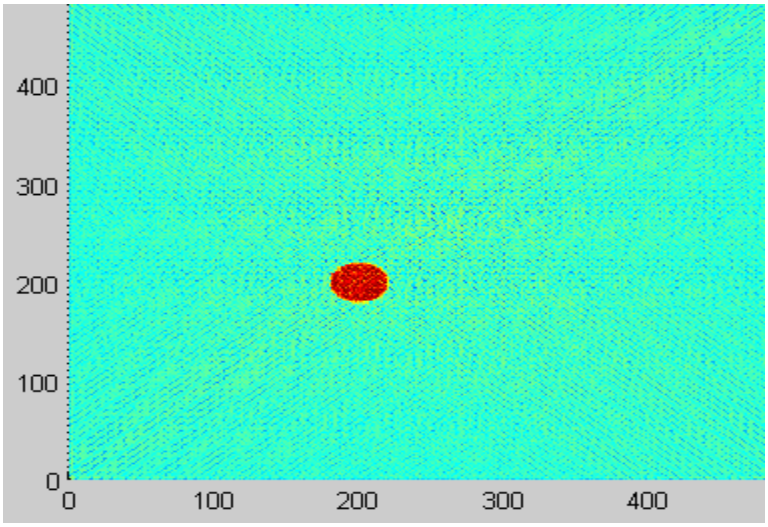

Figure 3.11: 2 cm radius of illegal powder

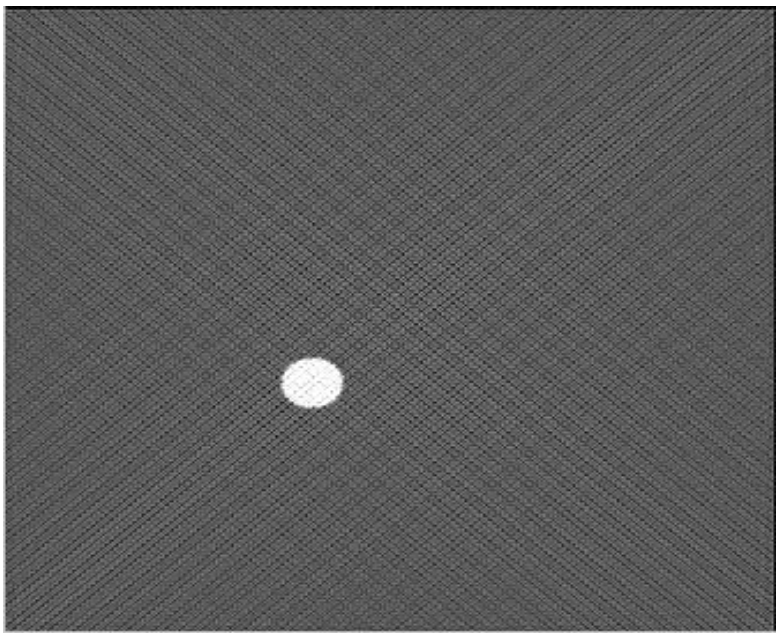

Figure 3.12: final Image of contraband materials after image reconstruction

The above simulation shows 2 cm radius of illegal powder with a defined dielectric of 3 at 4 GHz microwave objection.it has been detected clearly even that its dielectric value is closer to the background dielectric value which is Air. This scenario could be a hidden powder underneath clothes such as jackets or underwear where terrorist uses most for their operations. This simulation result could be compared later in chapter 6 with other simulation results using TR-Music Algorithm.

As seen from the simulation, we already have the data of the human body with microwave dielectric properties simulated and reconstructed using a Radon transformation technique. There were two pieces of metal (metallic explosive devices) that were blocking the microwave radiation and showed very clearly, detected as higher intensity to the projected microwave rays as shown in Figures 3.3 and 3.4. Furthermore, powdered explosives or drugs could be detected because of their lower dielectric property values compared with the human dielectric properties shown in Figures 3.5-3.7. Further development of the simulation technique could enable us to match real human bodies with real microwave images, tested in this simulated image reconstruction program.

3.6 CHAPTER SUMMARY

This chapter explained the reason for choosing microwave imaging over X-ray imaging when it comes to health factors and the complexity of technology. In this chapter, the frequency range of the experiments used for microwave imaging was between 0.9-2.36GHz; this range has been used before in medical devices. Knowing the dielectric properties of human tissues is an essential part of this research; this is because we need to be able to model the human body cross-section in Matlab. The resolution of imaging

is not limited with the wavelength for microwave imaging, as was explained in Section 3.3.

The minimum resolution required for security applications is 6.3mm, but the resolution could achieve better values in future research. The theory of the Radon transformation technique and its inverse algorithm to be used for the final image reconstruction of microwave imaging has been explained. Experiment set-up details were explained to give the reader details of how we arrived at the final image after image reconstruction. A flowchart explained the numerical simulation for the microwave tomography.

The simulation started with square layers of human tissues and illegal objects embedded inside them; it showed the illegal objects very clearly. The illegal objects used were metals and very low dielectric powders; these were shown successfully. Sphere cross-sections treated as a human body torso were modelled and illegal circular objects were embedded inside them; these were also shown very clearly. This chapter ended successfully with clear imaging results.

The next chapter will discuss a new image reconstruction theory called Time Reversal MUSIC. This will be applied for the next microwave tomography numerical simulation experiments in the later chapters.

Chapter 4: **Time Reversal MUSIC Theory**

This chapter describes the mathematical theories behind Time Reversal MUSIC (Multistatic Signal Classification) in locating and visualizing embedded targets in a homogenized or inhomogenized medium such as the human body. Super resolution imaging was formed by using singular value decomposition in the combination with time reversal MUSIC. This chapter will also investigate the relationship between the number of antennae *N* and the number of scattered targets *M*, to be illuminated where MUSIC algorithm could solve well-known vector subspace if $N > M$. In the simulation we will see the effect of the TR MUSIC algorithm in the well-known targets by specifying the number of the antennae in an arbitrary location around the targets using this Equation:

$$N \geq \frac{2\pi R f}{c} \tag{19}$$

Where *R* is the radius from the centre of the illumination area to the arbitrary location of each antenna.

4.1 TR MUSIC THEORY

Throughout this theory discussion, the Equations will be discussed in the form of frequency domain where it is originally expressed in the time domain and processed through Fourier Transforms as shown below:

$$F(x) = \frac{1}{2\pi}\int_{-\infty}^{\infty} d\omega \tilde{F}(\omega) e^{+i\omega t} \tag{20}$$

With

$$\tilde{F}(\omega) = \int_{-\infty}^{\infty} dt\, F(t) e^{-i\omega t} \tag{21}$$

Therefore in a frequency domain the time reversal signal time dependant will be phase conjugation.

Assuming an arbitrary antenna array placed evenly, or in other words regularly spaced at the positions $\xi i, \xi j$, i and j, are treated as transducers where they can transmit and receive at the same time, i and $j = 1, 2, 3, \ldots, N$. The antennae here are dipole point sources where they radiate a vector field $E_j(x, \omega)$ into the space where targets of illegal dielectric objects are imbedded. The radiated field from the jth antenna at x access is:

$$E_j(x, \omega) = G(x, \xi j) e_j(\omega) \tag{22}$$

By neglecting the multiple scattering between targets, the resulting scattered field from the jth antenna (single antenna excitation) are identical to:

$$E_j{}^S(x, \omega) = \sum_{m=1}^{M} G(x, X_m) \tau_m(\omega) G(X_m, \xi j) e_j(\omega) \tag{23}$$

Where $\tau_m(\omega)$ is the amplitude of the scattered target, X_m is the location of *mth* targets, $e_j(\omega)$ is the input voltage applied to the antennae for transmission, ω is the angular frequency, $G(x, X_m)$ is the Green function of the medium where the targets are inserted.

Once all the antennae are excited by a voltage at the source from the ith antennae, the resulting scattering field on the ith will be:

$$E_i{}^S(x, \omega) = \sum_{j=1}^{N} E_j{}^S(\xi i, \omega)$$

$$= \sum_{j=1}^{N} \sum_{m=1}^{M} G(\xi i, X_m) \tau_m(\omega) G(X_m, \xi j) e_j(\omega) \tag{24}$$

Now, by introducing the Green function column vectors, the above Equations can be interpreted into matrix representation, therefore:

$$\overrightarrow{g_m(\omega)}^0 = \{G^0\ (\xi_i, X_m)\}$$

$$= [G^o(\xi_1, X_m), G^o(\xi_2, X_m), \dots, G^o(\xi_N, X_m)]^T \quad (25)$$

The scattered field on the transducers will be a symmetrical multistatic response matrix:

$$\mathrm{H} = \left[\mathrm{h_{ij}}\right]_{\mathrm{N\times N}} = [\sum_{m=1}^{M} G(\xi i, X_m)\tau_m(\omega)G(X_m, \xi j)]$$

$$= \sum_{m=1}^{M} \tau_m \overrightarrow{g_m}^0 \overrightarrow{g_m}^{0^T} \quad (26)$$

Equation (23) can be rewritten as:

$$E_i{}^s(x, \omega) = \sum_{j=1}^{N} \mathrm{h_{ij}}\, e_j = He \quad (27)$$

Where e is the applied voltage on the antennae for excitation:

$$\mathrm{e}=\{e_j\} = [e_1, e_2, \dots, e_N]^T \quad (28)$$

The above equations can be applied to both homogeneous and inhomogeneous media where the targets will be embedded and depends entirely on the Green functions to be known and calculated.

4.1.1 Time reversal matrix

Time reversal matrices are defined as:

$$TR(\omega) = H^{\dagger}(\omega)H(\omega)$$

$$= H^{*}(\omega)H(\omega) \tag{29}$$

The superscript † indicates to the adjoint matrix, and because the multistatic response matrix is symmetric then $H^{\dagger}(\omega) = H^{*}(\omega)$ where the superscript asterisk * represents the complex conjugate.

Because of symmetry, and in terms of Green function vectors, the time reversal matrix is equal to:

$$\text{TR}=\left[\sum_{m=1}^{M}\tau_m\overrightarrow{g_m}^{0}\overrightarrow{g_m}^{0^T}\right]^{*}\left[\sum_{m'=1}^{M}\tau_{m'}\overrightarrow{g_{m'}}^{0}\overrightarrow{g_{m'}}^{0^T}\right]$$

$$= \sum_{m=1}^{M}\sum_{m'=1}^{M}\Lambda_{m,m'}\overrightarrow{g_m}^{0^*}\overrightarrow{g_{m'}}^{0^T} \tag{30}$$

Where

$$\Lambda_{m,m'} = \tau_m{}^{*}\,\tau_{m'} < \overrightarrow{g_m}^{0}, \overrightarrow{g_{m'}}^{0} > \tag{31}$$

When $\neq m'$, $\Lambda_{m,m'} = 0$

Where the angular product stands for the standard inner product inC^N, such as:

$$< \overrightarrow{g_m}^{0}, \overrightarrow{g_m}^{0} >=< \overrightarrow{g_m}^{0^*}, \overrightarrow{g_m}^{0} >$$

$$= \sum_{n=1}^{N}\overrightarrow{g_m}^{0^*}(n)\overrightarrow{g_m}^{0}(n) \tag{32}$$

4.1.2 Eigenvalues and eigenvectors of the time reversal matrix

The time reversal matrix is Hermitian, therefore it has orthogonal eigenvectors having non-negative eigenvalues. The rank of the TR will depend on the number of target *M* and number of antenna *N*. Two cases will be discussed as well as resolved scatterers or targets and non-well resolve scatterers or targets.

4.1.3 Well resolved scatterers

It is termed a well resolved target when the measure of$\Lambda_{m,m'}$. Equation (31) is approximately zero when$m \neq m'$. This occurs in the case of orthogonal Green function vectors, and the inner product between Green functions vectors are approximately zero, i.e.:

$$< \overrightarrow{g_m}^0, \overrightarrow{g_{m'}}^0 >= \sum_{n=1}^{N} \overrightarrow{g_m}^{0^*}(n)\overrightarrow{g_{m'}}^0(n)$$

$$= \sum_{n=1}^{N} G^*(\xi_n, X_m)G(\xi_n, X_{m'}) \approx 0, \quad (33)$$

For $m \neq m'$ then

$$H(x, X_{m'}) = \sum_{n=1}^{N} G^*(\xi_n, x)G(\xi_n, X_{m'}) \quad (34)$$

The above equation is called the coherent point spread function (CPSF). If$x = \xi_n, n = 1, 2, \ldots, N$, which represents the antenna emitted waves Green function into space. Therefore the inner product of Equation (33) $< \overrightarrow{g_m}^0, \overrightarrow{g_{m'}}^0 >$ is also the point spread function for the antenna array at the image point if$x = \xi_m$, and the measure of Λ can be represented in relationship of CPSF as:

$$\Lambda_{m,m'} = \tau_m{}^* \tau_{m'}, H(x, X_{m'}) \quad (35)$$

The geometry of the antennae array and the wavelength of the radiation is an essential factor for the spatial extent. Therefore if two targets, location X_m and$X_{m'}$, are separated greater than the effective spatial extent of CPSF, then $\Lambda_{m,m'}$ reduces approximately to

$$\Lambda_{m,m'} = |\tau_m|^2 \rho_m \delta_{m,m'} \tag{36}$$

Where $\delta_{m,m'}$the Kroneker delta is function and ρ_m expressed as

$$\rho_m = H(X_m, X_m) = < \overrightarrow{g_m}^0, \overrightarrow{g_m}^0 > \tag{37}$$

And this is the case of well resolved target or scatterers.

From (35) and (30) the time reversal operator become in the form

$$TR(\omega) = |\tau_m|^2 \rho_m \overrightarrow{g_m}^{0^*} \overrightarrow{g_m}^{0^T} \tag{38}$$

Which represents the projection operator of the spanned subspace by a complex conjugate vector of the Green functionsg_m.

The Green function vectors are orthogonal with norm squared equal to ρ_m In the case of the well resolved target such as;

$$< \overrightarrow{g_m}^0, \overrightarrow{g_{m'}}^0 >= \rho_m \delta_{m,m'} \tag{39}$$

Therefore in the case of a well resolved target, the eigenvectors of the time reversal matrix is the complex conjugate of the Green function vectors. Therefore $|\tau_m|^2 |\rho_m|^2$ are the eigenvalues.

$$TR\overrightarrow{g_{m_0}}^{0^*} = \sum_{m=1}^{M}|\tau_m|^2\rho_m\overrightarrow{g_m}^{0^*}\overrightarrow{g_m}^{0^T}\overrightarrow{g_{m_0}}^{0^*}$$

$$= \sum_{m=1}^{M}|\tau_m|^2\rho_m\overrightarrow{g_m}^{0^*}\rho_{m_0}\delta_{m,m_0}$$

$$= \left|\tau_{m_0}\right|^2\left|\rho_{m_0}\right|^2\overrightarrow{g_{m_0}}^{0^*} \quad (40)$$

The eigenvectors of the time reversal matrix *H* are considered to be one of the complex conjugates of the Green function vectors, and under the assumption that *M* is less than *N* antenna element the remaining *N-M* eigenvectors are equal to 0 values because of their orthogonalities on the Green Functions, such as

$$TR(\omega)\upsilon = |\tau_m|^2\rho_m\overrightarrow{g_m}^{0^*}\overrightarrow{g_m}\overrightarrow{v}^{0^T}=0 \quad (41)$$

Where υ is the orthogonal eigenvectors on the space spanned by the Green function.

Thus

$$C^N = \mathcal{S} \oplus \mathcal{N} \quad (42)$$

Where $\mathcal{S}$ is the signal subspace spanned by the Green function$\mathcal{S} = \left\{span(\overrightarrow{g_m}^{0^*}, m = 1, 2, \dots, M)\right\}$, $\mathcal{N}$ is the noise subspace, and C^N is the N-dimensional complex valued column vectors (the space of the applied voltage to the N element antenna array). The above mathematic formulae are based on the assumption of the *M* number of targets are less than the number of antennae *N*. In the case of well resolved targets, the eigenvectors of the signal space $\mathcal{S}$ are propotional to the complex conjugate of the Green function vectors:

$$\upsilon_m = \frac{\overrightarrow{g_m}^{0^*}}{\sqrt{\rho_m}}, m = 1, 2, \dots, M. \quad (43)$$

4.1.4 The case of non-resolved targets

By going back to Equation (40):

$$TR = \sum_{m=1}^{M} \sum_{m'=1}^{M} \Lambda_{m,m'} \overrightarrow{g_m}^{0^*} \overrightarrow{g_{m'}}^{0^T} \quad (44)$$

The $\Lambda_{m,m'}$ will not be the diagonal matrix, and the time reversal matrix will still be the projection operator onto the subspace spanned by the complex conjugates of the Green functions vector $\overrightarrow{g_m}^0$, identified also as the signal subspace $\mathcal{S}$. However, there will no longer be a complex conjugate Green function eigenvector for the *TR*, but rather there will be superpositions of these eigenvectors. In the case of non-resolved targets the rank of *TR*, dimension of the subspace $\mathcal{S}$ will not be equal to *M* because of target size and configuration. By representing the *TR* orthogonal set of eigenvectors by $\upsilon_m, m = 1, 2, \dots, M, M+1, \dots, N$ where the first M represents the eigenvectors with non-zero eigenvalues, which spans the signal subspace$\mathcal{S}$. The remaining N-M eigenvectors have zero eigenvalues and span the noise subspace$\mathcal{N}$;

$$TR\upsilon_m = \lambda_m \upsilon_m \, , m = 1, 2, \dots, M.$$

$$TR\upsilon_m = 0, m = M + 1 + 2, \dots, N$$

$$< \upsilon_m, \upsilon_{m'} > = \delta_{m,m'}$$

The representation of the signal and noise subspace projection operators is as follows:

$$P_{\mathcal{S}} = \sum_{m=1}^{M} \upsilon_m \upsilon_m^{\dagger} \tag{45}$$

$$P_{\mathcal{N}} = \sum_{m=M+1}^{MN} \upsilon_m \upsilon_m^{\dagger} \tag{46}$$

From Equation (42) the sum of the above operators will be the identity operator inC^N:

$$P_{\mathcal{S}} + P_{\mathcal{N}} = I \tag{47}$$

4.1.5 Time reversal eigenvectors focusing

If we consider well resolved targets, the signal space eigenvectors of the TR are proportional to the complex conjugate of the Green function vectors as in Equation (44). The wave field excited from each antenna when the input voltage is $e = \{e_j(\omega)\}$ is equal to the eigenvectors of the signal space $\upsilon_m = \{\upsilon_m(j)\}, m = 1, 2, \ldots . M$ and by using Equation (47):

$$E_j(x, \omega) = \sum_{j=1}^{N} G(x, \xi j) \upsilon_m(j) \tag{48}$$

And from Equation (44) and Equation (3):

$$\upsilon_m = \frac{\overrightarrow{g_m}^{0^*}}{\sqrt{\rho_m}}, m = 1, 2, \ldots, M$$

$$= \frac{1}{\sqrt{\rho_{\ m}}} \sum_{j=1}^{N} G^* \left(\eta, \xi_j\right) G(x, \xi_j)$$

$$= \frac{1}{\sqrt{\rho_{\ m}}} H^*(x, \eta) \tag{49}$$

Therefore from the above Equations in the case of a well resolved target, the use of Equation (49) will satisfy calculating the location of the target, which will be the maximum value of this calculated image field. The image field calculation in Equation (49) using CPSF will depend on the number of antenna element arrays, the geometry of the arrays and the wavelength, as discussed earlier.

When using Equation (47) it is necessary to know the Green function of the background medium. On the other hand, however, there is no need to know the Green function when calculating the eigenvalues and eigenvectors of the time reversal matrix. However, the above does not include the non-resolved targets where linearity of the signal space eigenvectors will lead to a linear combination of CPSFs, and each will focus on different targets with different amplitudes. This will result in image fields interfering with each other and will show poor image quality. All the above is the classical image formation process, which will be replaced later with the MUSIC (Multistate Signal Classification) subspace method to deal with both resolved and non-resolved targets.

4.1.6 MUSIC

This section will discuss the use of a MUSIC algorithm with a TR algorithm that will still require multistatic data using the FDTD method to calculate the time reversal Matrix $TR(\omega) = H^*(\omega)H(\omega)$ and the eigenvectors of this matrix. The MUSIC algorithm considers the time reversal matrix $TR(w)$ as a projection operator onto the subspace of C^N spanned by the complex conjugates of the Green function vectors (the signal subspace) $\mathcal{S}$ and that the noise subspace $\mathcal{N}$ is spanned by the eigenvectors of $TR(\omega)$ having zero eigenvalue. As a result, the complex conjugate of the Green

function vector must be orthogonal to the eigenvector of the time reversal matrix, which will be zero eigenvalue; i.e.

$$< \upsilon_{m0}, g_m^* >=< \upsilon_{m0}^*, g_m >= 0 \quad (50)$$

If $m = 1, 2, \dots, M, m0 = M + 1, \dots, N$, where υ_{m0} are the eigenvectors of the $TR(w)$ having zero eigenvalue, the pseudo-spectrum according to the algorithm:

$$B(X_p) = \frac{1}{\sum_{m0=M+1}^{N} |< \upsilon_{m0}^*, g_p >|^2} \quad (51)$$

And

$$g_p(\omega) = \{G(\xi_I, X_p)\} = \left[G(\xi_1, X_p), G(\xi_2, X_p), \dots, G(\xi_N, X_p)\right]^T \quad (52)$$

Is the Green function vector for the target located at the assumed positionX_p, and (51) is the MUSIC algorithm for the time-reversal algorithm. To implement the MUSIC algorithm the denominator of the pseudo-spectrum has been used in relation with the projection operator used, as discussed in Equations (44, 45, and 46). Therefore by using Equation (51) in particular, the denominator of the pseudo-spectrum will be

$$\sum_{M+1}^{N} |< \upsilon_{m0}^*, g_p >|^2$$

$$= \sum_{M+1}^{N} |< \upsilon_{m0} g_p^* >|^2$$

$$= \left|P_{\mathcal{N}} g_p^*\right|^2 = \left|[I - P_{\mathcal{S}}] g_p^*\right|^2 \quad (53)$$

The above MUSIC algorithm should be connected with the time reversal imaging technique, which could be expressed in the following form: $E_j(x,w)$

$$E_j\left(X_p,\omega\right)=\sum_{j=1}^{N}G(X_p,\xi_j)\upsilon_{m0}(j)=<\upsilon_{m0}^{*},g_p> \qquad (54)$$

x has been replaced byX_p, g_p is the Green function vector calculated atX_p, which is calculated in Equation (52). υ_{m0} is the $m0'$th eigenvector of $TR(w)$ having zero eigenvalue. Consequently the pseudo-spectrum in Equation (51) can be expressed in two forms, the first one as:

$$B\left(X_p\right)=\frac{1}{\sum_{M+1}^{N}\left|E_{m0}(X_p,\omega)\right|^2} \qquad (55)$$

In Equation (55) the pseudo-spectrum is inversely proportional to the sum of the intensities of the images made from the eigenvectors having zero eigenvalue. Consequently, time reversal images will be calculated from the images corresponding to zero eigenvalues. The second possible form of pseudo spectrum could be concluded from the simple form of time-reversal operator expressed as:

$$TR(\omega)=\sum_{m=1}^{M}|\tau_m|^2\rho_m\overrightarrow{g_m}^{0*}\overrightarrow{g_m}^{0T} \qquad (56)$$

And from Equations (44) and (54) to be formed as the following Equations;

$$\sum_{M+1}^{N}\left|<\upsilon_{m0}^{*},g_p>\right|^2=\left|[I-P_S]g_p^{*}\right|^2$$

$$=\left|g_p^{*}-\sum_{m=1}^{M}\upsilon_m<\upsilon_m,g_p^{*}>\right|^2$$

$$= \left|g_p\right|^2 - \sum_{m=1}^{M} \left|E_m\left(X_p, \omega\right)\right|^2 \quad (57)$$

which explains that the pseudo-spectrum is inversely proportionate to the difference amongst the intensity of the image of the steering vector and the sum of the intensities of the images shaped from the eigenvectors having a non-zero eigenvalue. Therefore the time reversal image will be calculated from the images corresponding to non-zero eigenvalues.

4.2 FINAL MATHEMATICAL MODEL BASED ON PREVIOUS THEORY

We can assume that N is the number of antennae and M is the number of targets to be illuminated at different locations$x_1, x_2, \ldots., x_m$, with reflectivity strengths of $\tau_{1,}\tau_2, \ldots., \tau_M$. $\xi i, \xi j$ is the location of the transducers and$m = the\ number\ of\ targets = 1, 2, \ldots, M$. The signal vector sent out from transducers will be represented in the below expression:

$$S(w) = [S_1(w), S_2(w), \ldots\ldots, S_N(w)]^T\ (1) \quad (58)$$

where *T* denotes to transpose.

The reflected signals received at the jth transducers will be expressed as the following Equation:

$$R_j(w) = \sum_{m=1}^{M} \sum_{i=1}^{N} G^o(\xi_j, x_m)\tau_M G^o(\xi_i, x_m)\tau_i(w) \quad (59)$$

the illumination vectors can be defined at the following expression:

$$\overrightarrow{g_m}^0 = [G^o(\xi_1, x_m), G^o(\xi_2, x_m), \ldots, G^o(\xi_N, x_m)]^T \quad (60)$$

The total wave field received at the transducer including to the number of targets and their locations will be:

$$H(w) = \sum_{m=1}^{M} \tau_m \overrightarrow{g_m^0} \overrightarrow{g_m^0}^T \tag{61}$$

And from (45) the total wave field vector received will be:

$$\vec{R}(w) = H(w)\vec{\tau}(w) \tag{62}$$

Therefore the time reversal matrix, keeping in mind the reciprocity factor, will be expressed as:

$$TR(w) = \overline{H(w)}H(w) = H^*(w)H(w) \tag{63}$$

where * denotes to adjoint. It is known that Hermitian matrices share properties with real symmetric matrices by having eigenvalues always real, therefore from (61) and (63) the Hermitian matrix of $TR(w)$ will be expressed as follows:

$$TR(w) = \sum_{m=1}^{M} \tau_m \overline{\overrightarrow{g_m^0} \overrightarrow{g_m^0}^T} \sum_{\acute{m}=1}^{M} \tau_{\acute{m}} \overrightarrow{g_{\acute{m}}^0} \overrightarrow{g_{\acute{m}}^0}^T$$

$$= \sum_{\acute{m}=1}^{M} \sum_{m=1}^{M} \Lambda_{m,\acute{m}} \overrightarrow{\overrightarrow{g_m^0}} \overrightarrow{g_{\acute{m}}^0}^T \tag{64}$$

where total reflectivities

$$\Lambda_{m,\acute{m}} = \overline{\tau_m}\tau_{\acute{m}} < \overrightarrow{g_m^0}, \overrightarrow{g_m^0} \geq \overline{\tau_m}\tau_{\acute{m}} \overline{\overrightarrow{g_m^0}}^T \overrightarrow{g_m^0} \tag{65}$$

The image of the targets could be shown from the construction of the response matrix as in (63), but if we use the MUSIC formula to create the image, which has the advantage

of defining the signal space V^S in term of Singular Value decomposition and defining theV^N, then the image function will be expressed as:

$$I(x) = \frac{1}{\left\| p_{V^N} \overrightarrow{g^0}(x) \right\|^2} \tag{66}$$

where $\overrightarrow{g^0}$the illumination is vector and H_{V^N} is the projection operator.

It could be assumed that$\overrightarrow{u_1}, \overrightarrow{u_2}, \dots, \overrightarrow{u_M}$ are the singular vectors that span signal spaceV^S, then the imaging function will be:

$$I(x) = \frac{1}{\|\vec{g}^0(x)\|^2 - \left\| P_{V^S} \vec{g}^0(x) \right\|^2} = \frac{1}{\|\vec{g}^0(x)\|^2 - \sum_{m=1}^{M} |\vec{g}^0(x) \cdot \overrightarrow{u_m}|^2} \tag{67}$$

This concludes the final theory of the proposed model. We should now consider that the array of antennae is divided in t transmitters located at $\xi_1, \dots, \xi_t$ and r receivers located at $\eta_1, \dots, \eta_k$, therefore the response matrix for the M point target positioned at $x_1, \dots, x_M$ with reflectivity strength $\tau_1, \dots, \tau_M$ referring to Equations (65) and (66),

$$H(w) = \sum_{k=1}^{M} \tau_m \, \overrightarrow{g_m{}^t} \, \overrightarrow{g_m{}^r}^T \tag{68}$$

Where

$$\overrightarrow{g_m{}^t} = [G^o(\xi_1, x_m), G^o(\xi_2, x_m), \dots, G^o(\xi_t, x_m)]^T \tag{69}$$

and

$$\overrightarrow{g_m{}^r} = [G^o(\eta_1, x_k), G^o(\eta_2, x_k), \dots, G^o(\eta_r, x_k)]^T \tag{70}$$

are the left and right illumination vectors for the transmitters and receivers array that span the column and raw of signal spaces V_C^S and V_R^S correspondingly. Therefore the imaging function for using MUSIC for both vectors will be:

$$I(x) = \frac{1}{\left\|\overrightarrow{g_t}^0(x)\right\|^2 - \left\|P_{V_C^S}\overrightarrow{g_t}^0(x)\right\|^2} + \frac{1}{\left\|\overrightarrow{g_r}^0(x)\right\|^2 - \left\|P_{V_C^S}\overrightarrow{g_r}^0(x)\right\|^2} \qquad (71)$$

The above formulation is the main concept of the well resolved target, but if the target size and numbers are more than the resolution of the array then the above formula in Equation (71) will not be enough to find the desired target. Therefore extra filtration formulae were proposed to calculate the geometry of the targets by selecting the appropriate signal space according to the resolutions of the array.

This will compute the time reversal matrix $TR = H(w)^* H(w)$ and the eigenvalues and the eigenvectors of this matrix. The MUSIC algorithm considers the time reversal matrix TR as a projection operator onto the subspace of C^N spanned by the complex conjugates of the Green function vectors (the signal subspace), and that the noise subspace N is spanned by the eigenvectors of T having zero eigenvalue. As a result the complex conjugate of the Green function vector must be orthogonal to the eigenvector of the time reversal matrix, which will be zero eigenvalue; i.e.:

$$< \mu_{m0}, g_m^* >=< \mu_{m0}^*, g_m > 0 \qquad (72)$$

If $m = 1, 2, \dots, M, m0 = M + 1, \dots, N,$ where μ_{m0} are the eigenvectors of the T having zero eigenvalue, the pseudo-spectrum according to the algorithm

$$D(X_p) = \frac{1}{\sum_{m0=M+1}^{N} |<\mu_{m0}^*, g_p>|^2} \qquad (73)$$

and

$$g_p(w) = \{G(R_I, X_p)\}$$

$$= [G(R_1, X_p), G(R_2, X_p), \dots, G(R_N, X_p)]^T \quad (74)$$

is the Green function vector for the target located at the assumed positionX_p. Equation (73) is the MUSIC algorithm for a time-reversal algorithm,

4.2.1 Non-resolved targets

To implement the MUSIC algorithm the denominator of the pseudo-spectrum has been used in relation to the projection operator in terms of the signal subspace projection operator. This has been used in the following Equations:

$$P_S = \sum_{m=1}^{M} \mu_m \mu_m^{\dagger} \quad (75)$$

$$P_N = \sum_{m=M+1}^{MN} \mu_m \mu_m^{\dagger} \quad (76)$$

$$P_N + P_S = I \quad (77)$$

4.2.2 Implementation of MUSIC

Therefore the denominator of the pseudo-spectrum will be

$$\sum_{M+1}^{N} |< \mu_{m0}^*, g_p >|^2 = \sum_{M+1}^{N} |< \mu_{m0} g_p^* >|^2$$

$$= |P_N g_p^*|^2 = |[I - P_S] g_p^*|^2 \quad (78)$$

4.2.3 Connection with classical time-reversal imaging

The above MUSIC algorithm should be connected to the time reversal imaging technique, which could be expressed in the following form:

$$\psi_{m0}(X_p, \omega) = \sum_{j=1}^{N} G(X_p, R_j)\mu_{m0}(j)$$

$$=< \mu_{m0}^{*}, g_p > \quad (79)$$

r has been replaced byX_p, g_p is the Green function vector calculated atX_p, which is calculated in Equation (76). μ_{m0} is the $m0'$th eigenvector of T having zero eigenvalue.

Consequently, the pseudo-spectrum in Equation (78) can be expressed in two forms, the first one as:

$$D(X_p) = \frac{1}{\sum_{M+1}^{N} |\psi_{m0}(X_p, \omega)|^2} \quad (80)$$

In Equation (80) the pseudo-spectrum is inversely proportional to the sum of the intensities of the images shaped from the eigenvectors having zero eigenvalue. Thus time reversal images will be calculated from the images corresponding to zero eigenvalues.

The second possible form of pseudo-spectrum could be concluded from the simple form of time-reversal operator expressed as:

$$T = \sum_{m=1}^{M} |\tau_m|^2 \rho_m g_m^{*} g_m^{T} \quad (81)$$

and from Equations (75) and (76) to be formed as the following Equations:

$$\sum_{M+1}^{N} = \left| < \mu_{m0}^{*}, g_p > \right|^2 = \left| [I - P_S] g_p^{*} \right|^2$$

$$= \left| g_p^{*} - \sum_{m=1}^{M} \mu_m < \mu_m, g_p^{*} > \right|^2$$

$$= \left| g_p \right|^2 - \sum_{m=1}^{M} \left| \psi_m(X_p, \omega) \right|^2 \qquad (82)$$

which explains that the pseudo-spectrum is inversely proportional to the difference between the intensity of the image of the steering vector and the sum of the intensities of the images made from the eigenvectors having a non-zero eigenvalue. Therefore the time reversal image will be calculated from the images corresponding to non-zero eigenvalues.

4.3 CHAPTER SUMMARY

This chapter has taken the reader through the journey of TR-Music theory discussed and explained before in [119]–[123]. The theory explained here was based on the purpose of this research, which is human body security scanning. Therefore all the terms and mathematical definitions used were purely for the purpose of security scanning. The mathematical expressions of all formulas were based on the creativity of this research only. This chapter has investigated the relationship between the number of antennae N and the number of scattered targets M, to be illuminated where the TR-MUSIC algorithm could solve well-known vector subspace if N > M. This is also true in the case of non-resolved targets when M > N, the rank of *TR matrix*. The dimension of the subspace $\mathcal{S}$ will not be equal to *M* because of target size and configuration; therefore a sum of signal and noise subspace has to be calculated to bring the real identity matrix as

in equation (77). Later the final mathematical model was created based on the original theory of TR-MUSIC.

The mathematical model explained the time reversal theory was then connected to the MUSIC theory to arrive at the final image created to be used for microwave imaging in the next chapters. The MUSIC algorithm considers the time reversal matrix, TR (w), as a projection operator onto the subspace of C^N spanned by the complex conjugates of the Green function vectors (the signal subspace) S, and that the noise subspace N is spanned by the eigenvectors of TR (w). Super resolution imaging was formed by using singular value decomposition in combination with time reversal MUSIC, as seen in equation (67). The use of a MUSIC algorithm with a TR algorithm will still require multistatic data using the FDTD method to calculate the time reversal Matrix TR. The mathematical model will use the data received at the transceivers to reconstruct the final image. Better understanding of this chapter's theory will be shown in the next chapter.

Chapter 5: **Microwave Tomography**

This chapter will discuss how the previous theory could be used as tomography to gather microwave images.

5.1 THEORETICAL DEVELOPMENT OF MICROWAVE TOMOGRAPHY

Microwave imaging systems existing under different types of technologies have been found in applications in medical imaging systems. There are already several papers discussing the use of microwave imaging via the analysis of dielectric properties of tissues using different techniques [113]. Microwave imaging has non-ionizing, non-invasive, sensitive and low-cost features [11], which makes it a promising technology for applications in security areas, such as border control in airports. Although the resolution of microwave imaging is not as high as an X-ray, it has the advantage of being capable of imaging physiological changes [115], [124]. The preferred illumination level in frequency for microwave imaging makes it safe and non-destructive for operator and customer, avoiding the hazards of X-ray radiation used in airport security.

This chapter will illustrate the possible application of Security Imaging Systems using microwave frequencies between 2GHz to 10GHz, which has already attracted research interests in the medical field [106]. In active microwave imaging methods there are two types of possible detection method for contraband materials: microwave tomography and UWB radar techniques, which have been investigated in both the medical field and security systems [109].

Microwave tomography has been successful in measuring the dielectric properties of the object to be imaged by solving non-linear inverse scattering problems [126], where the UWB techniques used to measure the targets are only from the back scattering signals

[127]. The UWB technique on its own has failed to get the best resolution needed [121], whereas the time reversal Multi-static Signal Classification (MUSIC) technique has found a gap within the UWB to gain a higher resolution.

The time reversal with electromagnetic inverse scattering imaging method has been used in many applications such as ultrasonic imaging in medical applications, detection of underground mines, and other target detection systems such as radar or sonar systems. The MUSIC algorithm is used to describe the theoretical and experimental measurement of the scattered wave received at multiple antenna arrays located in arbitrary positions around the illuminated targets. This calculates the number of signals, directions of arrivals, strength of the scattered wave, polarization and level of noise interference [128]. The key ideas behind this algorithm are (1) physical demonstration of the scattered field matrix, and (2) filtration approach constructed on the arrays resolution and the singular value decomposition of the response matrix.

The method proposed in this chapter can be used to analyse the dielectric properties of the target, using different waveforms such as plane wave or point source, and using near or far field data. This method calculates the amplitude modulation of the signals coming from the dominant scattered field and then time reverses it in conjunction with the MUSIC algorithm. The ideas of the image reconstruction algorithm is similar to the concept of the multi-static radar system, by transmitting an electromagnetic wave of single or multiple frequencies towards the targeted area and receiving a matrix of scattered field data, then being analysed and viewed as an image. This method of measuring a scattered wave field received at the transducers (receiver’s antenna) is suitable for the security application of detecting image target location and its geometry.

This approach is more straightforward and simpler than the usual approaches of an inverse problem where the whole medium is considered as unknown. Solving a non-linear inverse problem will image the targets, but it takes a long time because of the iteration method that is usually used to solve a non-linear optimization: it is also expensive, which requires a huge computation process. In a homogeneous medium with each iteration, solving the adjoint forward problem in addition to shape regularization is needed to find the shape derivative.

The subspace-based TR-MUSIC direct imaging algorithm proposed in this thesis will locate the target as well as its shape where dominant scattering wave field is detected. Moreover the target has its own dielectric properties that distinguish it from the background medium.

In heterogeneous media the detection of the target depends on two factors: (1) position of the dominated scattering event at the boundary of the target in the medium; (2) how well the Green function of the medium can be approximated.

The image reconstruction formulation is based on the Helmholtz Equation where all the transmitters send out pulses to the target, and the scattered wave, called the response matrix, is recorded at the receivers. Then an iterated time reversal procedure is used as well as the Singular Value Decomposition to extract the dominant scattered events that describe the shape information of the target. The algorithm proposed in this thesis can be used to analyse the dielectric properties of the target, use different waveforms using data near field or far field.

The concerns raised about this imaging system were how to construct them cost effectively and with lower radiation emissions. Microwave imaging was used to face the issue of expensive hardware and insufficient computing power. However, technologies

have advanced, and have indicated a brighter future for microwave systems, especially with the knowledge of the interaction of electromagnetic waves between human body tissue and their dielectric properties [106], [107]

The current human body walk-through inspection systems in airports are metal detectors, which can only detect metals concealed in the person's clothing; they are ineffective if the person is hiding other illegal materials such as plastic explosives or drugs. There are additional machines at airports that use a high dosage X-ray radiation, but it is very harmful for both the scanned person and the operator. Moreover, the goal of our research is to find contraband materials concealed within a human body. However, at this stage we have only investigated the strength of another image reconstruction method to find concealed metallic weapons within a human body, and then this algorithm will be developed to find extremely small hidden targets within the human body using dielectric properties analysis.

Compared with microwave tomography, wave front reconstruction and Delay-and-Sum algorithms, a subspace-based TR-MUSIC algorithm is supposed to feature in super-resolution, simplicity and generalizability. In this chapter, we propose a multi-static radar system to visualize concealed metallic weapons within clothing, and it will later be extended to dielectric object detection. We will also discuss the possibility of microwave imaging techniques for security applications using a Subspace-based TR-MUSIC algorithm.

5.2 RECONSTRUCTION ALGORITHM USING TR-MUSIC

In the wave Equation of lossless and stationary medium, the quadratic differential relationship between field components and time keep the invariance to the sign of time, upon which the concept of time-reversal is based. If $\mathrm{E}(\boldsymbol{x}, \mathrm{t})$ is the solution to the wave

Equation (83), $E(\boldsymbol{x}, -t)$ is also its solution, which is entitled as the time-reversal field of$E(\boldsymbol{x}, t)$.

$$\nabla^2 E(\boldsymbol{x}, t) - \mu\varepsilon \frac{\partial^2}{\partial^2 t} E(\boldsymbol{x}, t) = 0 \tag{83}$$

where $E(\boldsymbol{x}, t)$ is the electric field component at position $\boldsymbol{x}$ and time t, μ and ε are the permittivity and permeability of the medium, respectively. The wave propagation process means that the time-reverse field $E(\boldsymbol{x}, -t)$ would exactly retrace the path of the original wave$E(\boldsymbol{x}, t)$. If $E(\boldsymbol{x}, t)$ is the divergent scattered field, then $E(\boldsymbol{x}, -t)$ is the convergent wave that will focus on the source with the physical or computational TR process. In the frequency domain, the TR process can be implemented by phase conjugation, using $\overline{E(\boldsymbol{x}, \omega)}$ to replace$E(\boldsymbol{x}, \omega)$, where the superscript bar denotes complex conjugation and $E(\boldsymbol{x}, \omega)$ is the Fourier transformation of$E(\boldsymbol{x}, t)$.

5.2.1 Multi-static Response Matrix (MRM) and TR operator

For the array of N transducers in Figure 1.1, we can define the inter-element impulse response $h_{ij}(t)$ to be the signal received at the ith transducer with an impulse sent out from the jth transducer, $i, j = 1, 2, \dots, N$ the matrix.

$$H(t) = \left[h_{ij}(t)\right]_{N \times N} \tag{84}$$

is called the multi-static response matrix in time domain. Due to the space reciprocity of the static medium, the matrix $H(t)$ is symmetric, i.e. $h_{ij}(t) = h_{ji}(t)$. For a source signal distribution

$$S(t) = [s_1(t), s_2(t), \dots, s_N(t)]^T \tag{85}$$

The received signals at the array are

$$R(t) = [r_1(t), r_2(t), \dots, r_N(t)]^T = H(t) * S(t) \quad (86)$$

where the star sign $*$ denotes convolution in time domain. In the frequency domain, it becomes

$$R(\omega) = H(\omega)S(\omega) \quad (87)$$

$P(\omega)$ is called multi-static frequency response matrix at frequencyω. The Hermitian operator

$$K(\omega) = H^{\dagger}(\omega)H(\omega) \quad (88)$$

is also called the time-reversal matrix, where the superscript † denotes complex conjugation transposition. $K(\omega)S(\omega) = H^{\dagger}(\omega)H(\omega)S(\omega) = H^{\dagger}(\omega)R(\omega)$ means the received signals are back propagated after phase conjugated, according to the TR principle mentioned above, toward the source positions they come from.

There exists singular value decomposition (SVD) for matrix $H(\omega)$

$$H(\omega) = U\Sigma V^{\dagger} \quad (89)$$

with m singular values$\sigma_1 \geq \sigma_2 \geq \cdots \sigma_m \geq 0$, where $m = \text{rank}(H)$, U and V are left singular vectors and right singular vectors, respectively. The first m columns and the last $N - m$ columns of V span the row space and nullspace of $H(\omega)$, respectively, and the first m columns of U span the column space of $H(\omega)$, the last $N - m$ columns of U span the nullspace of $H^T(\omega)$, respectively. It can be shown that the orthonormal columns of U and V are eigenvectors of $H(\omega)H^{\dagger}(\omega)$ and$H^{\dagger}(\omega)H(\omega)$, respectively, and the eigenvectors of the TR matrix $K(\omega)$ can be shown to correspond to different targets in a one-to-one manner. So the singular vectors of $H(\omega)$ play the same role as the

eigenvectors of$\mathrm{K}(\omega)$. That is the reason why the subspace-based MUSIC method is also called TR-MUSIC method. Mathematically and practically, SVD of $\mathrm{H}(\omega)$ is preferred compared to the eigenvalue decomposition (ED) of $\mathrm{K}(\omega)$, because: (1) SVD uses orthonormal bases whereas ED uses a basis that generally is not orthonormal; (2) all matrices (even rectangular ones) have a SVD and not all matrices (even square ones) have an ED.

5.2.2 MRM matrix structure for point targets in electromagnetic scattering problems

Electromagnetic wave propagation is dominated by the Green function $\mathrm{g}^0(\boldsymbol{x}_1,\boldsymbol{x}_2)$ of the background medium, where $\boldsymbol{x}_1$ denotes the field point and $\boldsymbol{x}_2$ the source point. Due to the spatial reciprocity of the homogenous background, the $\boldsymbol{x}_1$and$\boldsymbol{x}_2$can be exchanged, that is$\mathrm{g}^0(\boldsymbol{x}_1,\boldsymbol{x}_2) = \mathrm{g}^0(\boldsymbol{x}_2,\boldsymbol{x}_1)$.

Assume that there are M point scatterers placed at $\boldsymbol{x}_1,\boldsymbol{x}_2,\cdots,\boldsymbol{x}_\mathrm{M}$in the imaging region with isotropic reflectivity 1, and the array element antenna locates at$\boldsymbol{\xi}_1,\boldsymbol{\xi}_2,\cdots,\boldsymbol{\xi}_\mathrm{N}$, respectively. If Born approximation is applied, i.e. neglecting the multiple scattering effect, $\mathrm{H}(\omega)$ can be written

$$\mathrm{H}(\omega) = \sum_{\mathrm{m}=1}^{\mathrm{M}} \mathrm{G}^0(\boldsymbol{x}_\mathrm{m})\mathrm{G}^0(\boldsymbol{x}_\mathrm{m})^\mathrm{T} =$$

$$\begin{bmatrix} \sum_{\mathrm{m}=1}^{\mathrm{M}} \mathrm{g}^0(\boldsymbol{\xi}_1,\boldsymbol{x}_\mathrm{m})\mathrm{g}^0(\boldsymbol{x}_\mathrm{m},\boldsymbol{\xi}_1) & \cdots & \sum_{\mathrm{m}=1}^{\mathrm{M}} \mathrm{g}^0(\boldsymbol{\xi}_1,\boldsymbol{x}_\mathrm{m})\mathrm{g}^0(\boldsymbol{x}_\mathrm{m},\boldsymbol{\xi}_\mathrm{N}) \\ \vdots & \ddots & \vdots \\ \sum_{\mathrm{m}=1}^{\mathrm{M}} \mathrm{g}^0(\boldsymbol{\xi}_\mathrm{N},\boldsymbol{x}_\mathrm{m})\mathrm{g}^0(\boldsymbol{x}_\mathrm{m},\boldsymbol{\xi}_1) & \cdots & \sum_{\mathrm{m}=1}^{\mathrm{M}} \mathrm{g}^0(\boldsymbol{\xi}_\mathrm{N},\boldsymbol{x}_\mathrm{m})\mathrm{g}^0(\boldsymbol{x}_\mathrm{m},\boldsymbol{\xi}_\mathrm{N}) \end{bmatrix} \quad (90)$$

Where $\mathrm{G}^0(\boldsymbol{x}_\mathrm{m})$ is called illumination vector for$\boldsymbol{x}_\mathrm{m}$, defined by

$$\mathrm{G}^0(\boldsymbol{x}_\mathrm{m}) = \left[\mathrm{g}^0\left(\boldsymbol{\xi}_{1,}\boldsymbol{x}_\mathrm{m}\right), \mathrm{g}^0\left(\boldsymbol{\xi}_{2,}\boldsymbol{x}_\mathrm{m}\right), \cdots, \mathrm{g}^0\left(\boldsymbol{\xi}_{\mathrm{N},}\boldsymbol{x}_\mathrm{m}\right)\right]^\mathrm{T} \qquad (91)$$

According to (91), it is clear that $\mathrm{H}(\omega)$ is a linear combination of M illumination vectors$\mathrm{G}^0(\boldsymbol{x}_1), \mathrm{G}^0(\boldsymbol{x}_2), \cdots,$ and$\mathrm{G}^0(\boldsymbol{x}_\mathrm{M})$, and furthermore,$\mathrm{rank}(\mathrm{H}) = \min(\mathrm{M}, \mathrm{N})$.

5.2.3 Subspace-based MUSIC algorithm

In the MUSIC algorithm, for $\mathrm{M} < N$ case, since$\mathrm{rank}(\mathrm{H}) = \mathrm{M}$. The first M columns of U span the column space of $\mathrm{H}(\omega)$ in terms of SVD theory, which is defined as the signal spaceV^S, and the last $\mathrm{N} - \mathrm{M}$ columns of V span the nullspace of$\mathrm{H}(\omega)$, defined as the noise spaceV^N, which is the orthogonal complement ofV^S. For an arbitrary search point $\boldsymbol{x}$ in the imaging region, its illumination vector is$\mathrm{G}^0(\boldsymbol{x})$, if it collocates with any point among$\boldsymbol{x}_1, \boldsymbol{x}_2, \cdots, \boldsymbol{x}_\mathrm{M}$, then $\mathrm{G}^0(\boldsymbol{x})$ belongs to V^S and its projection to V^N equals to zero, otherwise the projection of $\mathrm{G}^0(\boldsymbol{x})$ to V^N is finite. According to this finding, a pseudo-spectral imaging function can be constructed as

$$\mathrm{I}(\boldsymbol{x}) = \frac{1}{\left\|\mathrm{P}_{\mathrm{V}^\mathrm{N}}\mathrm{G}^0(\boldsymbol{x})\right\|^2} = \frac{1}{\sum_{\mathrm{k}=\mathrm{M}+1}^{\mathrm{N}}|\mathrm{v}_\mathrm{k}\cdot\mathrm{G}^0(\boldsymbol{x})|^2} \qquad (92)$$

where v_k is the kth column vector of$\mathrm{V}$. This imaging function will peak greatly at the positions of point targets, and super-resolution characteristics can be expected.

5.2.4 TR-MUSIC algorithm for extended targets

It can be assumed that when there is noise in measurement or an extended target, the performance of the TR-MUSIC algorithm is degraded, but it can be applied in these circumstances. The key issue is how to decide the optimal M value to obtain the best imaging results if the array element number is big enough. For extended targets, the peaks of the imaging function no longer correspond to the point targets one-by-one, and may exist on the target boundary or inside the object due to the physical resonance and

dielectric property of the objects. In this scenario, TR-MUSIC can be used to sketch the shape of extended targets, which is demonstrated in the following simulation examples.

5.3 CHAPTER SUMMARY

This chapter has taken the reader through a quick history of microwave imaging and its advantages, where different types of technologies have been found in applications in medical and security imaging systems. Microwave tomography has been successful in measuring the dielectric properties of the object to be imaged by solving non-linear inverse scattering problems [126], where the UWB techniques used to measure the targets are only from the back scattering signals [127]. It has been found that a Time reversal multistatic classification (MUSIC) technique has achieved higher resolution when combined with UWB technique [119].

For comparisons between microwave tomography, wave front reconstruction and delay-and-sum algorithms, a subspace-based TR-MUSIC algorithm is supposed to be a better algorithm in terms of simplicity, generality and resolutions. The key ideas behind the Time reversal multistatic classification (MUSIC) algorithm are (1) a physical demonstration of the scattered field matrix, and (2) a filtration approach constructed on the arrays resolution and the singular value decomposition of the response matrix. It explained the scenario of how the data was transmitted and received, collected and processed to form Images through the TR-MUSIC mathematical Model. The Maxwell wave equation was used to calculate the electric field received at the transceivers with the consideration of the medium's permittivity and permeability. The wave propagation Time reversal process illustrates that the time-reverse field $\mathrm{E}(\boldsymbol{x}, -\mathrm{t})$ would exactly retrace the path of the original wave $\mathrm{E}(\boldsymbol{x}, \mathrm{t})$ in equation (88).

The above chapter showed how to drive the mathematical model to image microwave images based on the previous chapter of TR MUSIC theory. The resulting images based on the above mathematics will be shown in the next chapter.

The following flowchart explains the process of the mathematical model used in the next chapter's simulation to be more visible when it comes to Target Image Reconstructions.

.

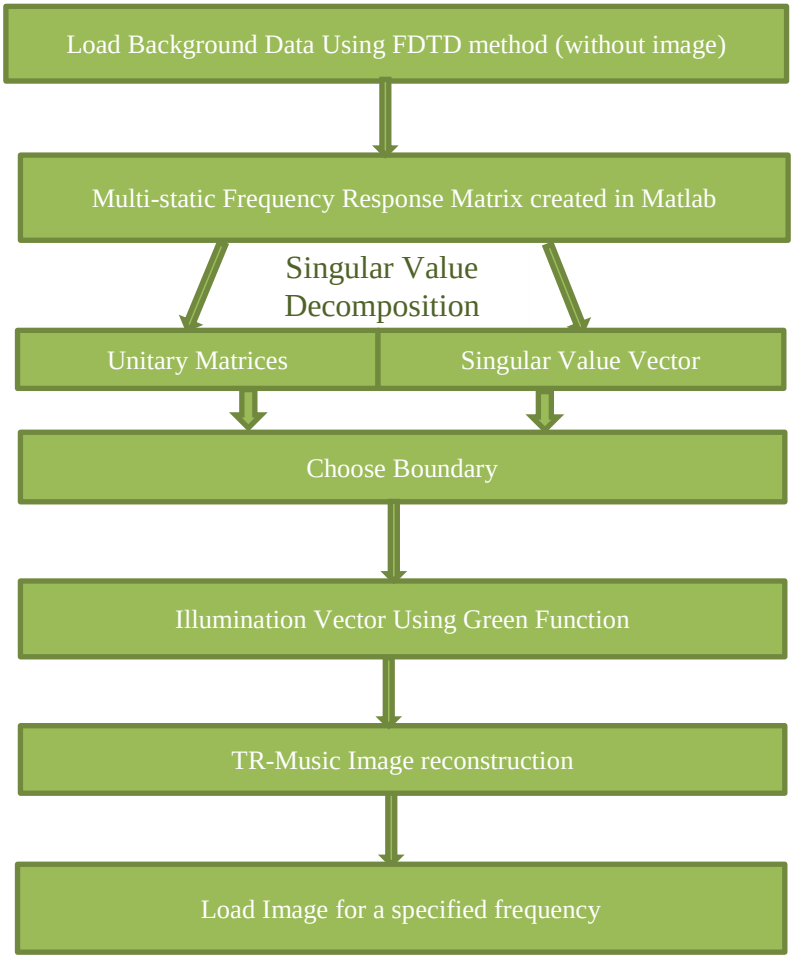

Figure 5.1: Flow chart of TR-MUSIC Algorithm

The above flow chart has been constructed in this research only and its code has been created and shown in appendix C .The data of scattered field objects were created using Lumerical FDTD after spending long training period of time on the software and then these data were applied to the Matlab code created.

Chapter 6: **2D simulation for security object detection**

To show results from microwave objection the choice was to go for simulation for both the scattered data and the reconstruction of the image using TR-MUSIC algorithm in Matlab. An experiment is explained below, which was proposed but not approved by the university to carry out due to a lack of equipment. To carry out an experiment in the lab it is proposed that the target will be modelled using different types of materials such as crude paraffin wax phantom and a small sphere of higher or lower dielectric material inside the paraffin wax as a contraband material. As shown below in Figure 6.1, for the microwave imaging system the experiment set up would be;

1. N number of UWB antennae such as Micro-strip TEM-type antennae;
2. Vector Network Analyser such as Agilent 87050A Option K24 Multiport Mechanical Switching Test Set, or other similar switch array device;
3. a controller is used to switch signal channels between transducers, and frequency change is completed by VNA;
4. coaxial used to connect from antennae to (VNA);
5. Connections between VNA and computer, where the computer can read directly measured data from the VNA and transfer it through special cables such as cable, net or USB.

The procedure for the experiment could be as follows:

1. distance from the source to target is computed;
2. analogue to digital converter from the received data;
3. computer to process the raw data received using TR Music Algorithm;
4. Display of the image for the operator.

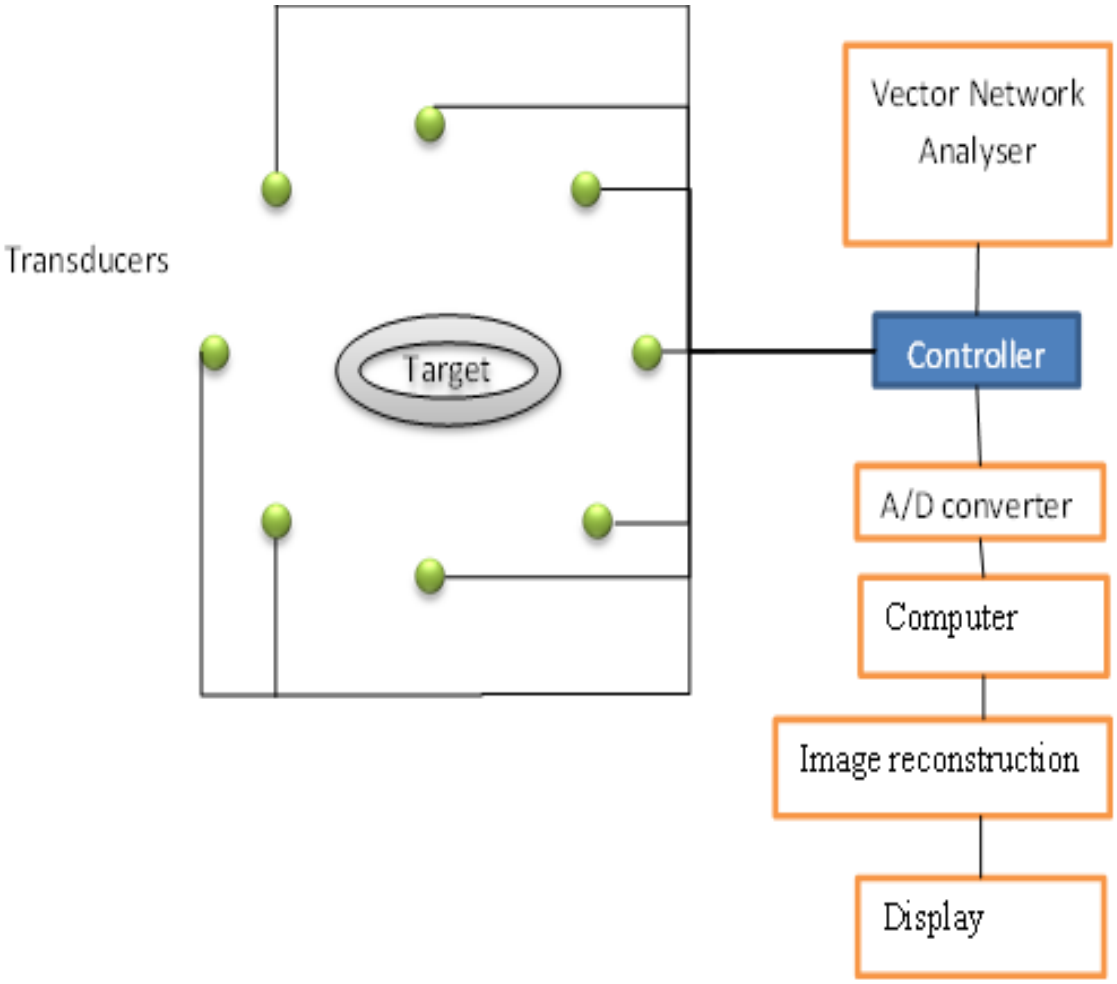

Figure 6.1: Experiment set up for Microwave Imaging System

The above experiment is mentioned here to give an understanding for the reader of how to set up a real experiment in the future.

6.1 ANTENNA AND RECEIVERS CONFIGURATION

The imaging geometry and configuration is demonstrated in Figure 6.2. The object is surrounded by a circular N-element array with radius R, and inside is the imaging region with length L and width W. Each element antenna transmits an electromagnetic wave towards the imaging region in turn, and all the elements receive all-directional wave front scattered by the object. This means that each antenna is a transducer. The

obtained scattering data are then processed to reconstruct the position and shape of the object.

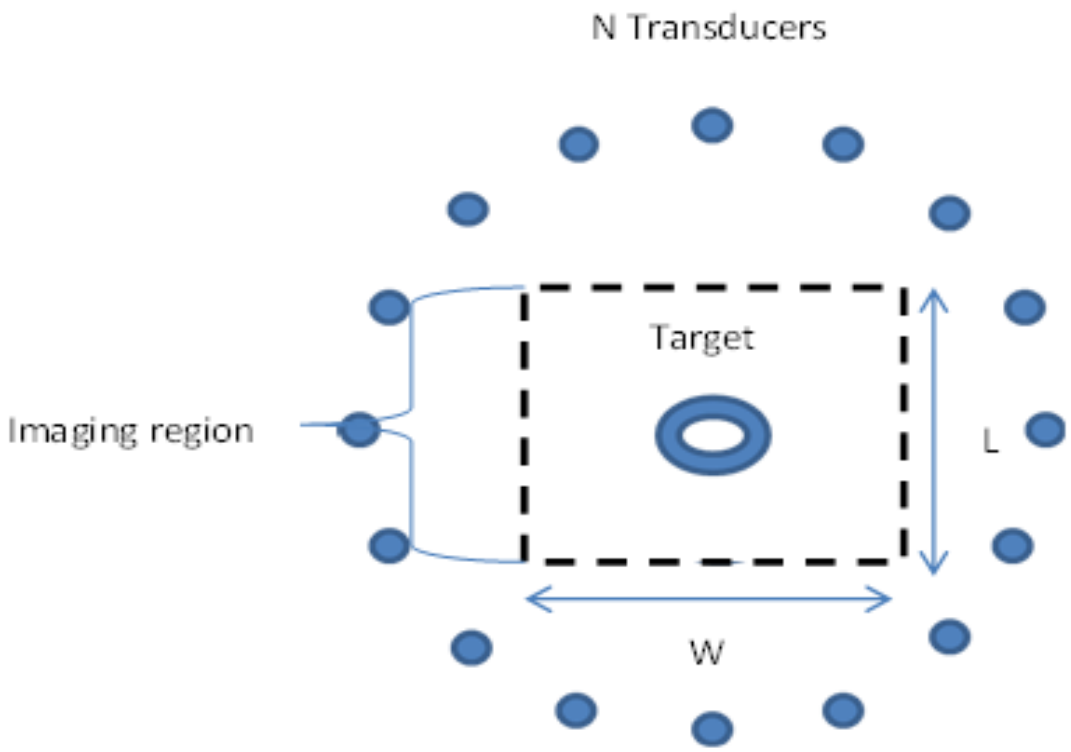

Figure 6.2: Imaging Geometry and Configuration

The above configuration was set up in lumerical FDTD solution. The FDTD solution is used to collect scattered data on each transducer. These data are then processed in Matlab with a TR MUSIC algorithm to reconstruct the image. Figure 6.3 shows how such a system was configured in lumerical FDTD solution. The shown target in Figure 6.3 could be changed at any time to any shape required.

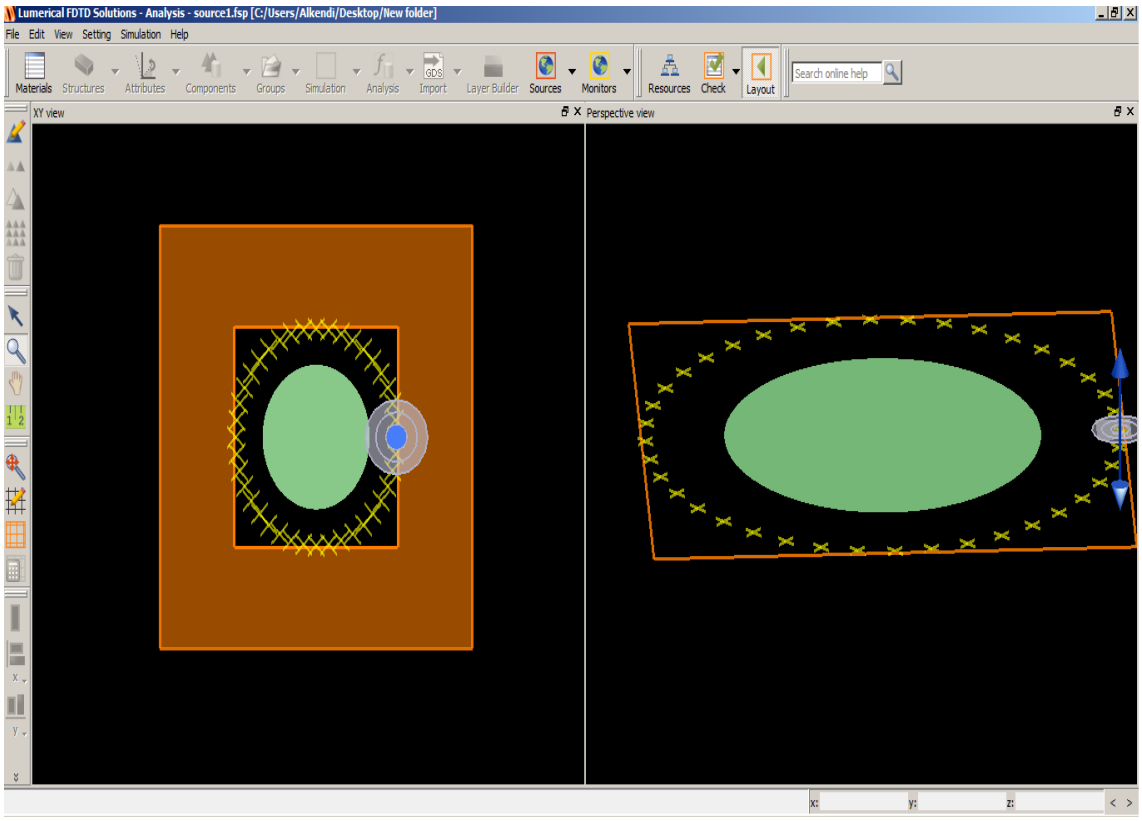

Figure 6.3: Shows Experiment set up in Lumerical FDTD Solution

6.2 SIMULATION RESULTS

The microwave imaging technique is adapted here to test 2D objects by subjecting them to multi-static single frequency excitation of microwave rays from an arbitrary antennae array around the object and analysing the image created: this program has been developed in Matlab. The simulation was carried out to prove the concept of detecting different objects in a homogenized background such as air.

After projecting the microwave ray onto the developed models of objects using the FDTD method, there will be an image reconstruction algorithm using subspace-based TR-MUSIC to calculate the scattered field absorbed by the arbitrary antenna array. To demonstrate the usage of the TR-MUSIC algorithm in microwave imaging applications, the 2D scattered fields are calculated by the FDTD method to get the MRM $H(\omega)$ to be

processed. The zero-order Hankel function of 2nd kind $\mathcal{H}_0^{(2)}(k_0\rho)$ in 2D free space is used as the Green function $g^0(\boldsymbol{x}_1,\boldsymbol{x}_2)$ in the illumination vector$G^0(\boldsymbol{x})$, where $k_0 = 2\pi/\lambda$ is the wave number and ρ is the distance between the field point and source point. The probing array consists of $N = 14$ isotropic point transducers equally distributed on the circumference of radius$R = 30\text{cm}$. The frequency of the electromagnetic wave is 3GHz and the wavelength$\lambda = 10\text{cm}$. The imaging region is$30\text{cm} \times 30\text{cm}$. Some typical imaging results are listed in the Figures 6.4-6.7.

6.3 MULTIPLE POINT TARGETS

In a numerical experiment for point targets imaging, the MRM $H(\omega)$ is calculated directly by the Hankel function but not the FDTD method. The five point targets are located at the coordinates of (-10, 0), (-1, 0), (1, 0), (-10, -10) and (0, -10), and their units of measurement are centimetres. The imaging result is shown in Figure 6.4 using 2D and 3D views. It should be noted that the vertical axis is linear scaled in the 2D view, but logarithmic scaled in the 3D view: all the following figures are the same. It can be observed that the TR-MUSIC algorithm can resolve them completely, even from the smallest distance, which is only 2cm less than$\lambda/4$. This super-resolution is obtained only from the single frequency scattering information; better resolution can be expected for multiple frequency or wide-band data.

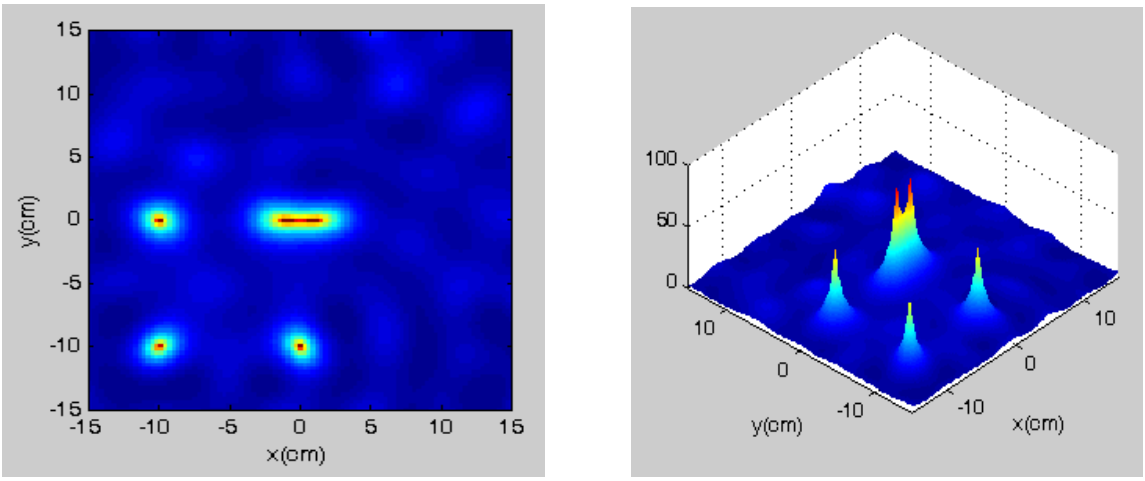

Figure 6.4: Multiple Point Targets Imaging: (Left) 2D View; (Right) 3D View

6.3.1 Small metal cylinder

In the second numerical experiment, it is assumed that the target could be a metallic gun underneath a terrorist's clothing. Therefore a small metal cylinder was created in 2D FDTD with radius R = 2cm and reconstructed by a TR-MUSIC algorithm. In Figure 6.5, the cylinder is located at the coordinate of (0, 0): it can be seen that the small cylinder looks like a point target due to radial symmetry. When the cylinder is moved to (0, 6) in Figure 6.6, it looks like a point target as before but there is a negligible virtual point at the y-axis imagery position, which may be caused by calculation error in Lumerical FDTD software. When the same two cylinders coexist in Figure 6.7, the image becomes a little complicated because of multiple scattering between them, although they can be still distinguished clearly from each other.

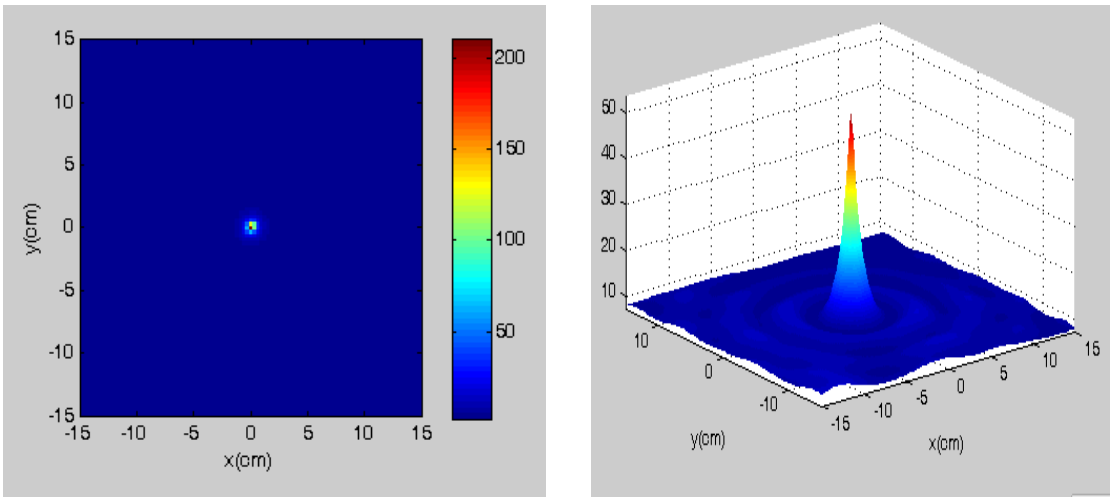

Figure 6.5: Small Metal Cylinder Located (0, 0)

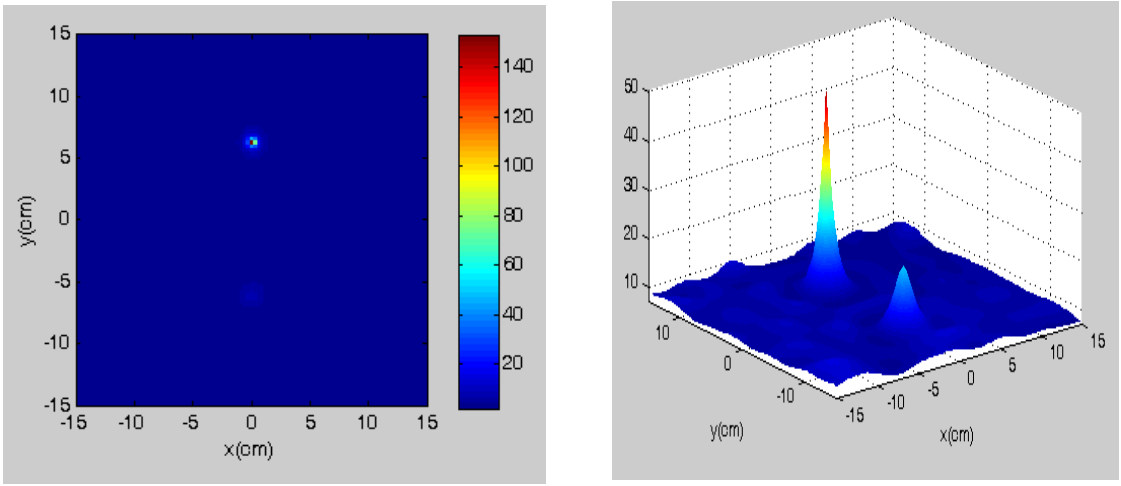

Figure 6.6: Small Metal Cylinder Located (0, 6)

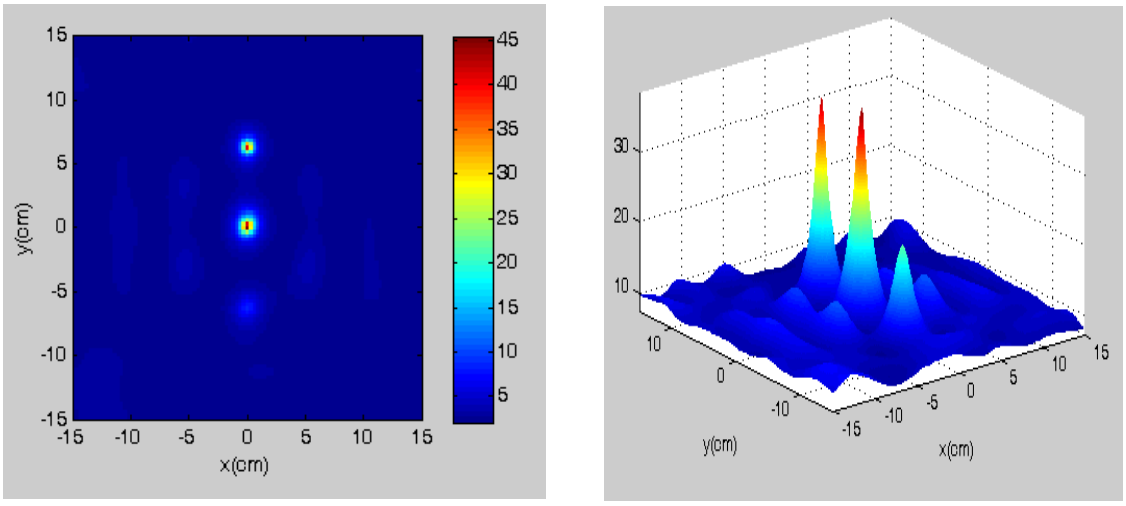

Figure 6.7: Two Small Metal Cylinders Located (0, 0) and (0, 6)

6.3.2 Extended target

Extended target means that target sizes are bigger than the wavelength object; therefore the imaging results can give their shape details. Figure 6.8 shows another metal cylinder with R=20cm and Figure 6.9 is for a metal rectangle whose dimension is 20cm×10cm, respectively. These two objects are extended targets compared to the wavelength. It can be seen that the image peaks or spotlights located on the boundary and inside the metal, the TR-MUSIC images sketch the shape for the illuminated objects, which conclude that the "large" targets can be represented by their main scattering centres as radar target characteristics.

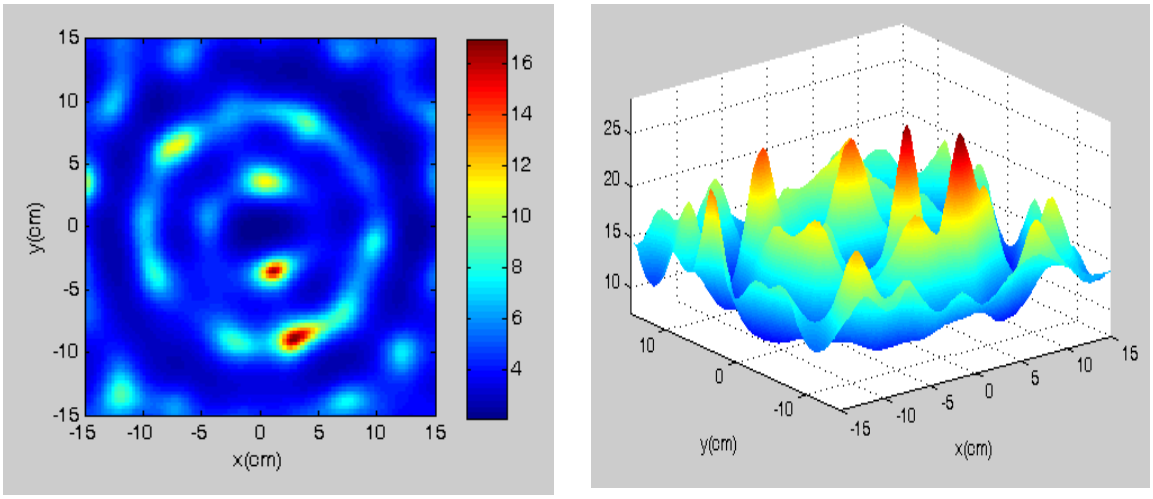

Figure 6.8: Big Metal Cylinder with R=20cm

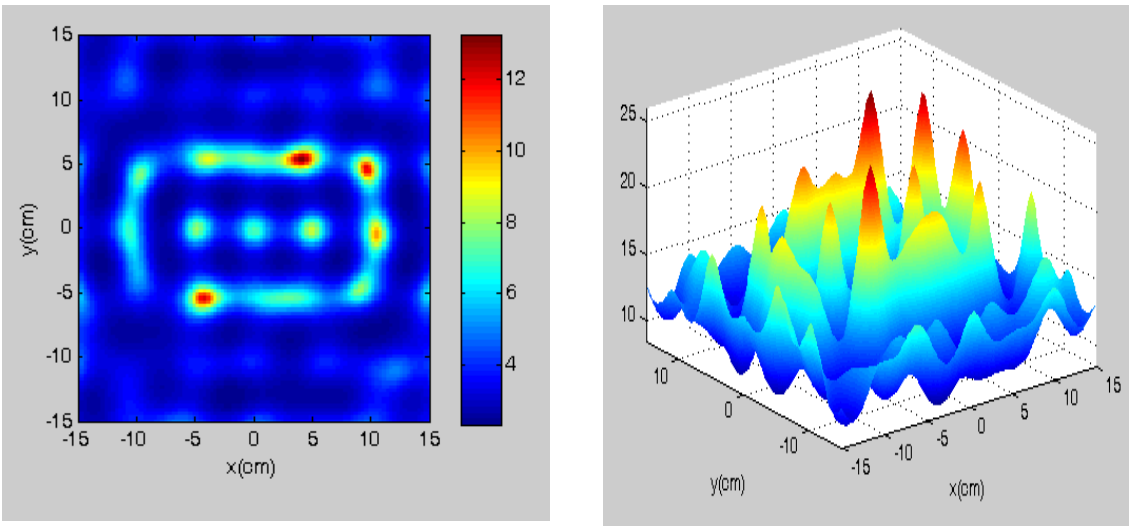

Figure 6.9: Metal Rectangle with 20cm×10cm

It can be seen from the simulation that this method (subspace-based TR-MUSIC) for image reconstruction showed a very clear point target as well as the boundary and inside of the metal objects. It is a direct algorithm, simple and does not need forward solution or iteration. The goal of this algorithm is to locate and visualize a strong scattering field that has been generated by a target's response matrix, and use Singular Value Decomposition to collect its information and generate the final image. Choosing the best M values for different types of models and shapes emitted by different frequencies of microwave will help for better TR-MUSIC imaging results of extended targets.

The simulation assumed here was for single frequency excitation; with multiple frequency excitations the result will be far superior. Consequently it could not be denied that this algorithm method will not construct the image of a metallic gun if concealed underneath clothing. Therefore the later research work will focus on the same scenarios as in Figures 6.8 and 6.9, and use more array elements to resolve them to gain a robust and clear image. Also the test of this algorithm will continue to try and build different models of different material properties and different frequency range to match the contraband materials that terrorists could use for threats.

6.4 SIMULATION RESULTS FOR RISKY OBJECTS (EXTENDED OR NON EXTENDED) WITH DIFFERENT TARGETS MODEL AND DIFFERENT FREQUENCIES

6.4.1 2GHZ

Square Model

To give the reader an idea of how we construct different type of models to be imaged using microwave the Lumerical FDTD software tool shown in Figure 6.10 shows how the square has been placed to be imaged.

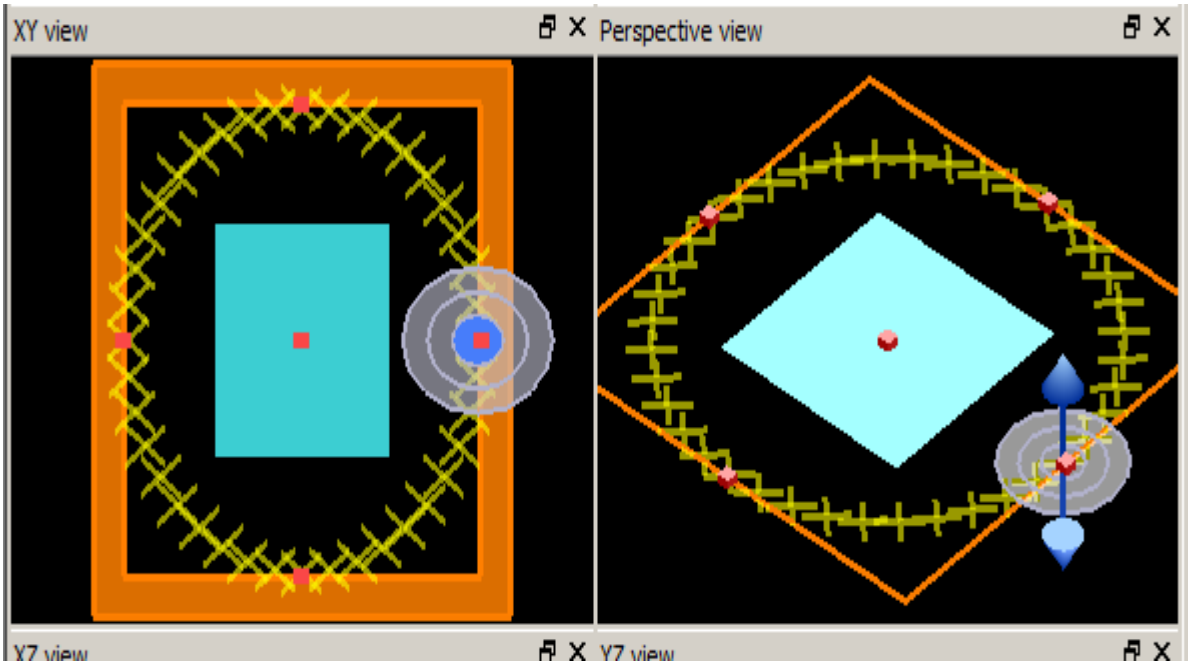

Figure 6.10: Square Shape Model in Lumerical FDTD software

All the other shapes and models will be constructed in different sizes and different materials: this will show us the value of utilizing this fascinating imaging technology. The common models will be squares, polygons, triangles, rectangles, spheres and embedded objects. Every model will be constructed with different frequencies objection, and then the data will be collected and imported in Matlab to run the TR-

MUSIC mathematical model. This will reconstruct the image caused by this microwave antenna seen around the square, or around any other object later in this discussion.

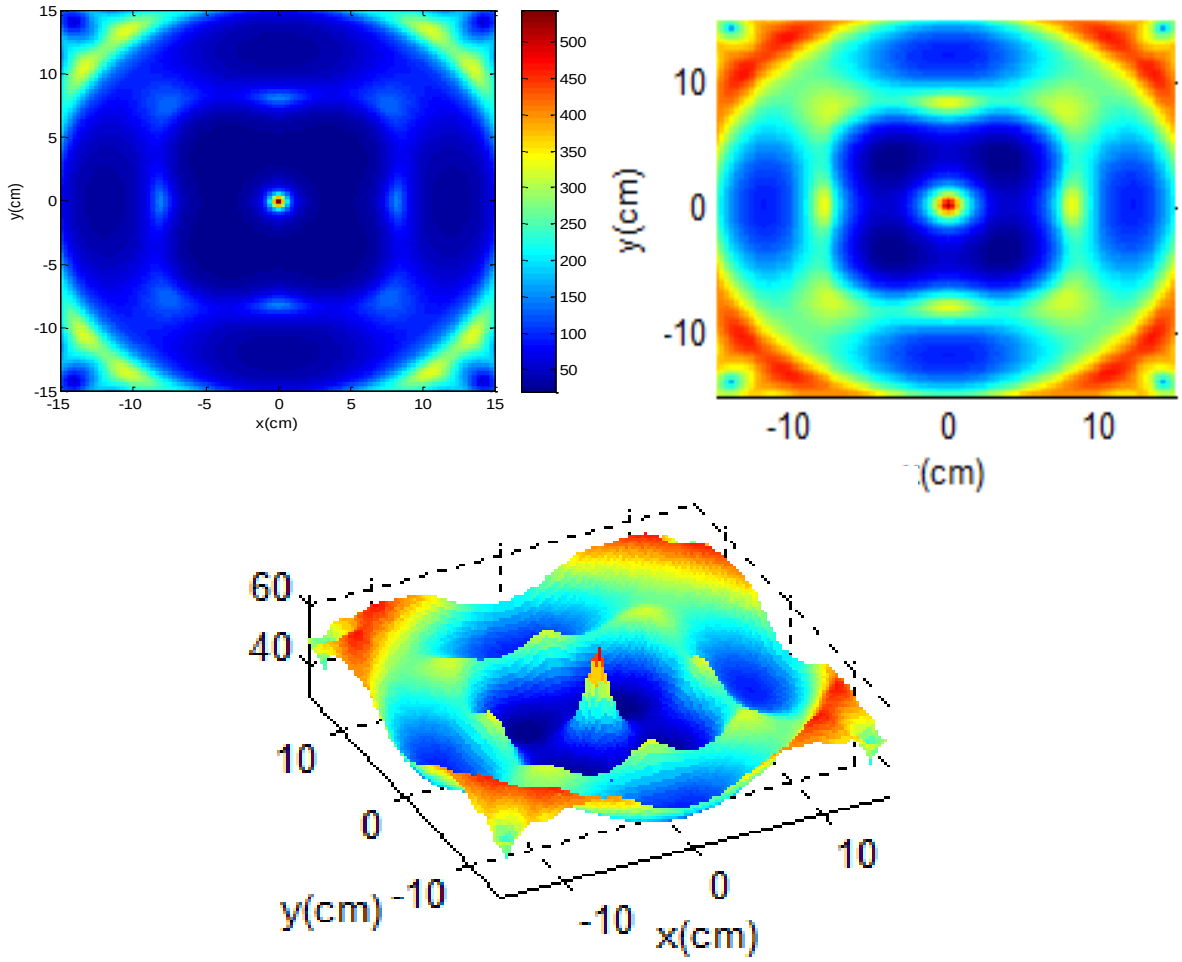

Figure 6.11: Lower Dielectric Square Shape Model Using 2GHz Objection

Figure 6.11 above illustrates the shape of a 15cm x 15cm square being imaged using 2GHz. The square has a relative dielectric of 1.4.

Polygon model

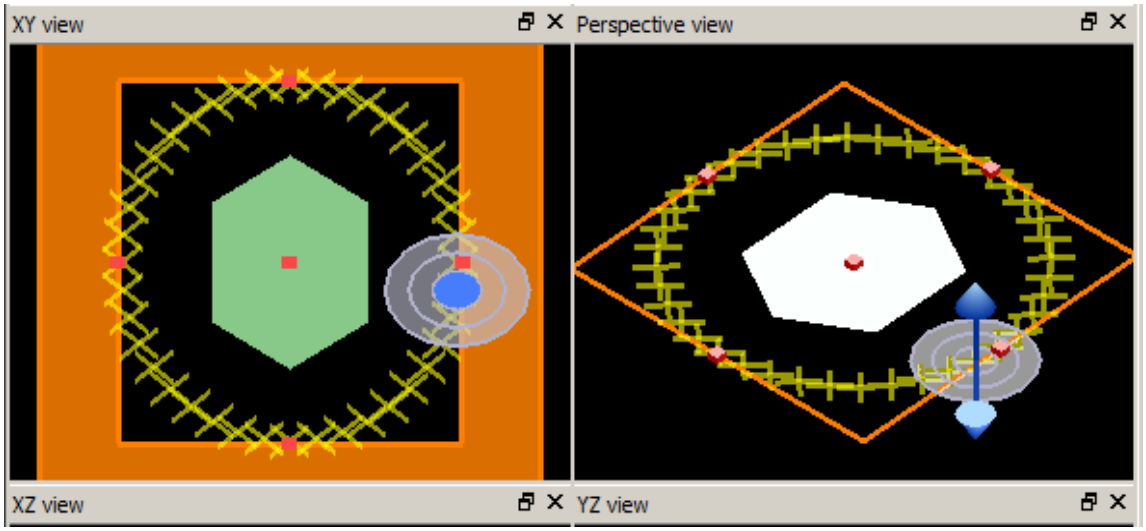

Figure 6.12: Polygon Shape Model in Lumerical FDTD Software

The above polygon points are (X,Y); (0-9), (7,-5), (7,5), (0,9), (-7,5) and (-7,-5).

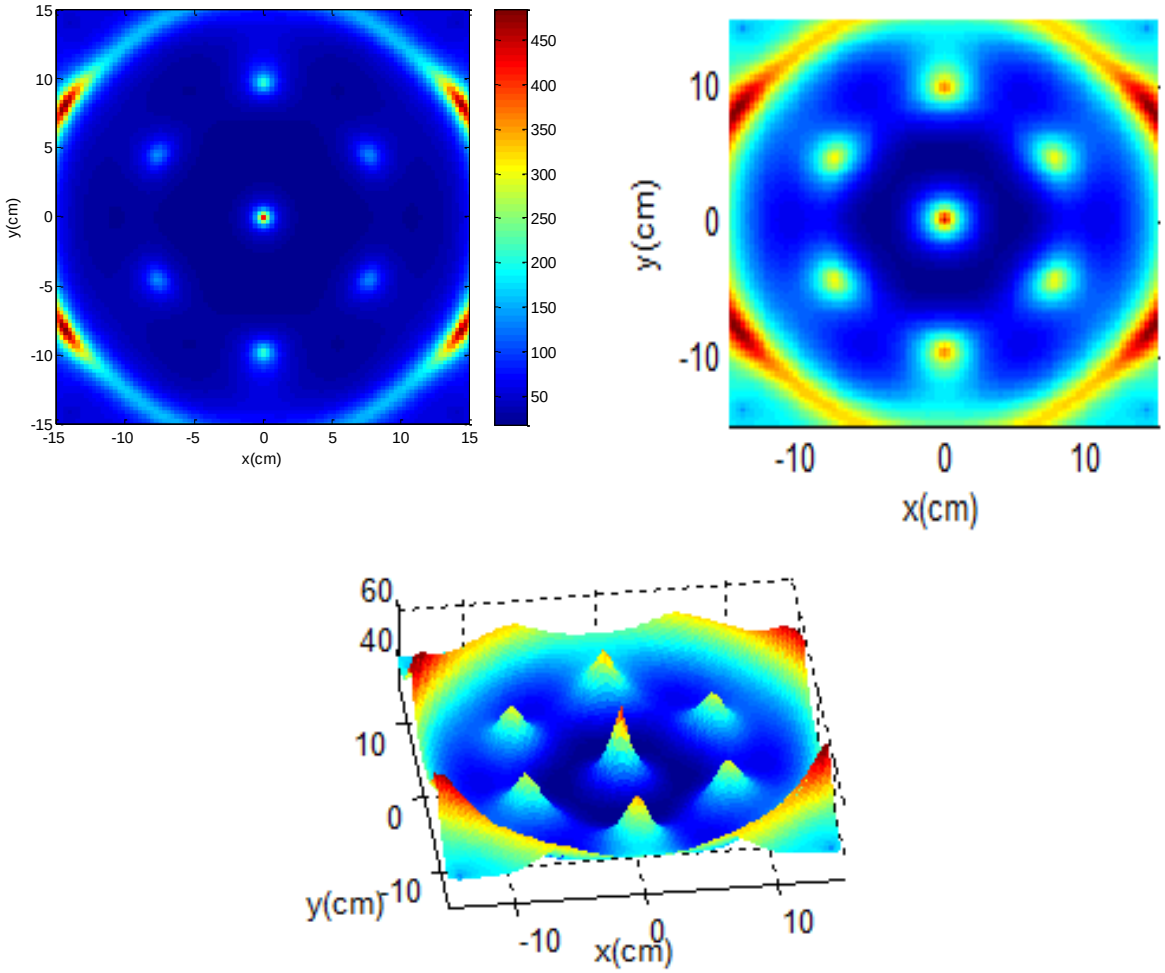

Figure 6.13: Lower Dielectric Polygon Shape Model Using 2GHz Objection

The above figure shows a polygon shape, if all the peak points were connected, which has been generated by a TR-MUSIC algorithm. The above figure shows peaks or spotlights that exist both on the boundary of the polygon object and inside it.

6.4.2 3GHz

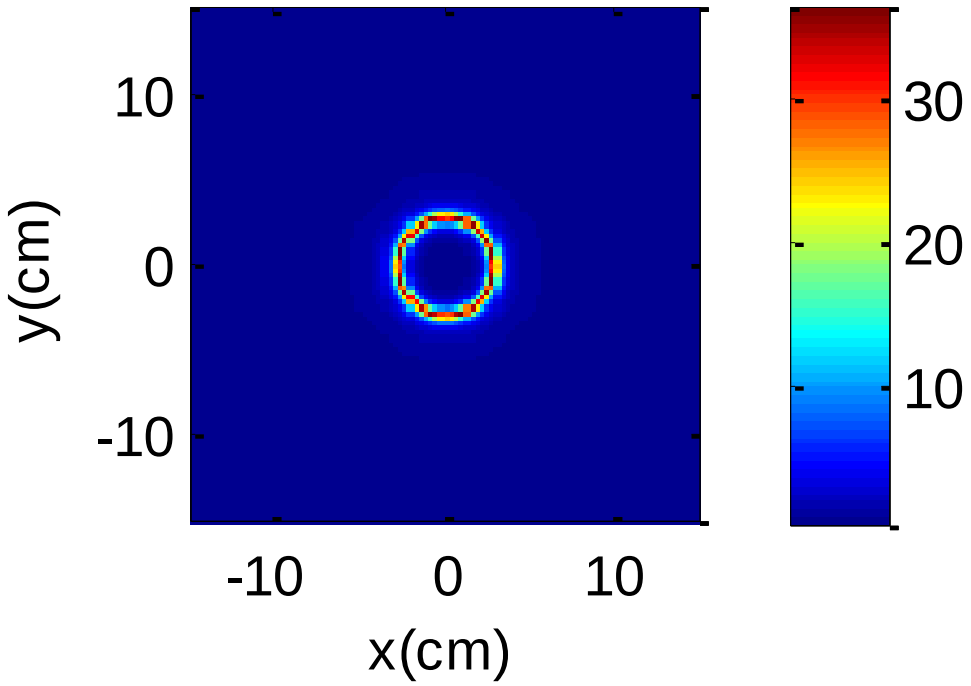

Figure 6.14: Cylinder of 5cm Radius Using 3 GHz Objections

The above illustration shows a cylinder of 5cm radius with defined relative dielectric of 2.4. It shows the very clear shape of such a cylinder because of its extended size related to the 3GHz wavelength and the imaging region 30x30. The above scenario could be any metal or material hidden underneath passengers' clothes.

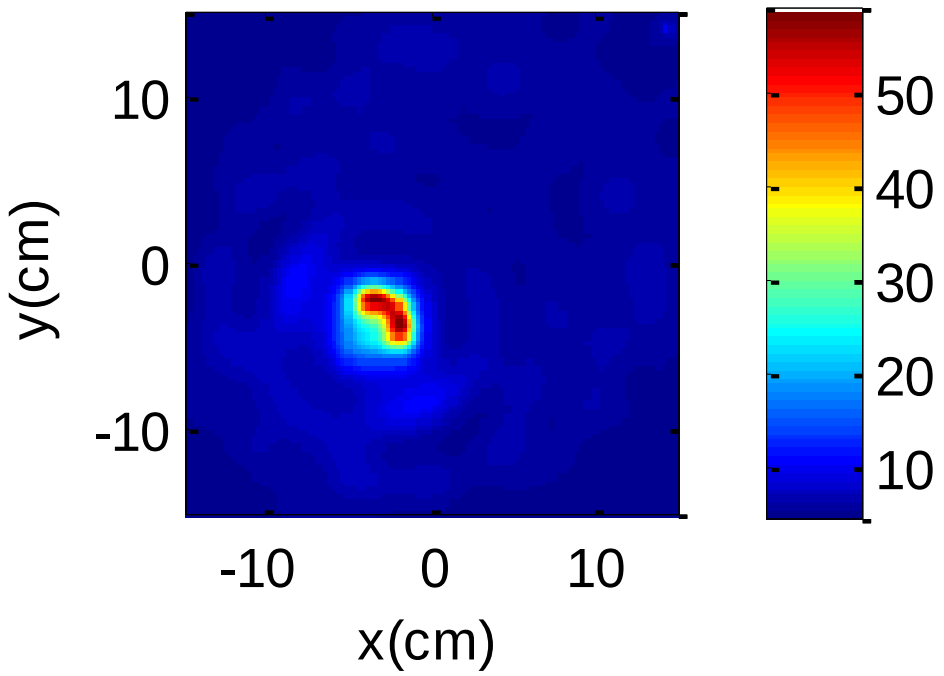

Figure 6.15: Cylinder of 3cm Radius Using 3 GHz Objections

The above figure shows a cylinder target that has a radius of 3cm and defined relative dielectric of 5. It shows part of the cylinder shape because it is not fully extended, or it could be shown clearly if we change the number of the M value. The M value is the number of the boundary between the signal subspace and noise subspace. Also this could be very small contraband materials hidden within the human body. This result makes the possibility of small targets being shown clearly very promising.

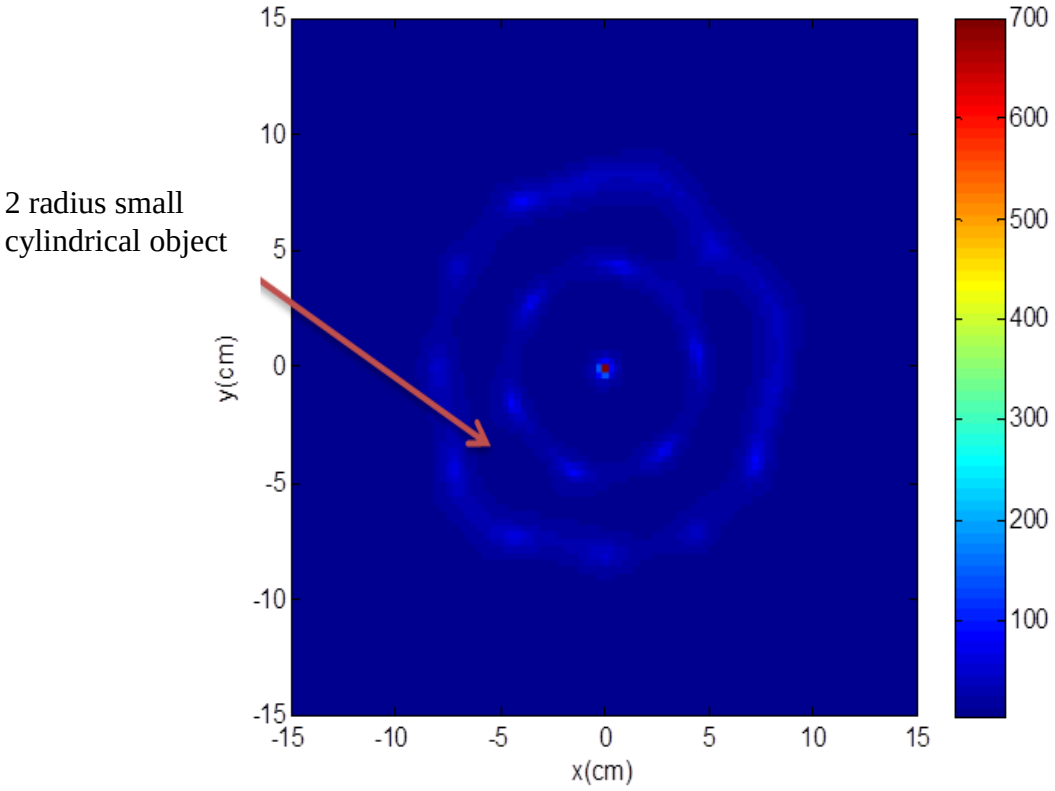

Figure 6.16: 10cm Human Body Cross Section with 2cm Object Hidden Inside

The above figure shows a human body cross-section of 10cm radius with a defined dielectric of 5. A small size of contraband material of 2cm radius is embedded within this human body cross-section and defined relative dielectric of 6.5. The above figure shows both a human body and the small contraband material embedded within this human body; which could alert the operator of the possibility of illegal items being hidden within this passenger.

6.4.3 4GHz

Triangle Model

The Lumerical FDTD software tool shown in Figure 6.17 displays how a triangle has been placed to be imaged.

Figure 6.17 below shows how to build a triangle model in FDTD using 4GHz. The transceivers' data around the triangle are then collected and implemented in Matlab code to show the imaging results

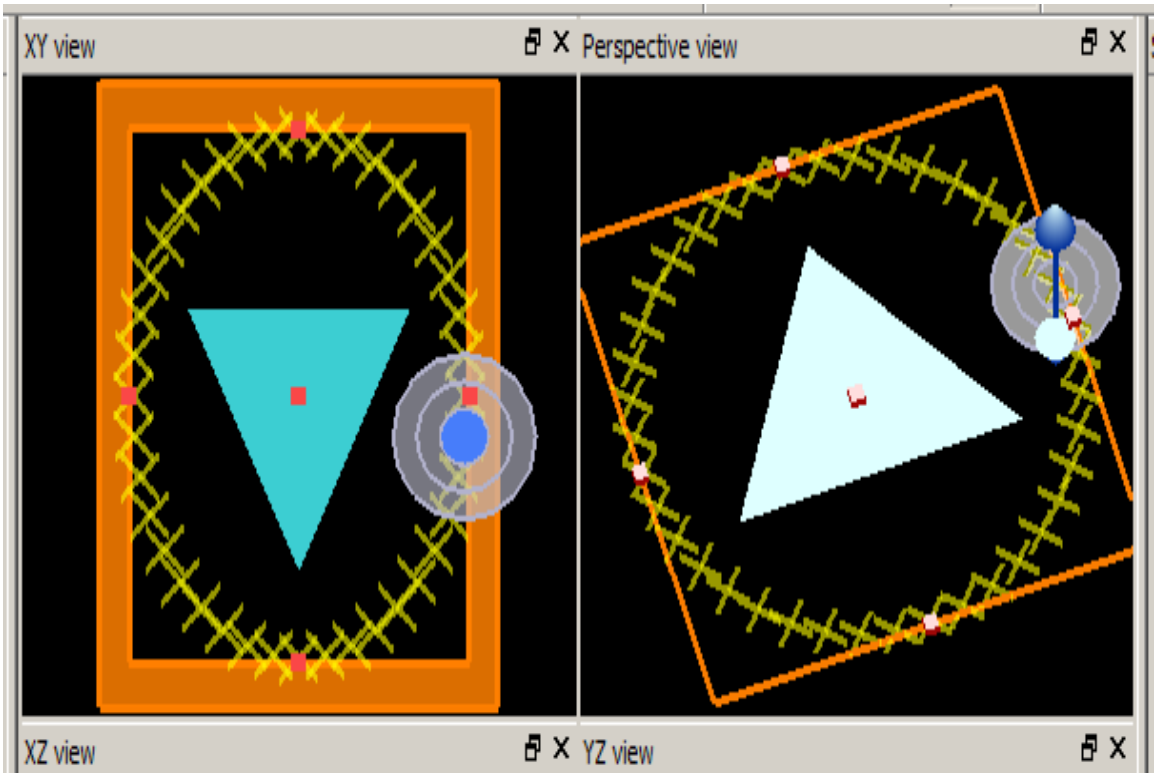

Figure 6.17: Triangle Shape Model in Lumerical FDTD Software

The above figure is a triangle shape with a relative dielectric of 1.4; the dimensions are (-10,5), (10,5) and (0,-10). As can be seen from this figure, the shape has been shown clearly: there is intensity or more details in the middle of the shape that has been shown.

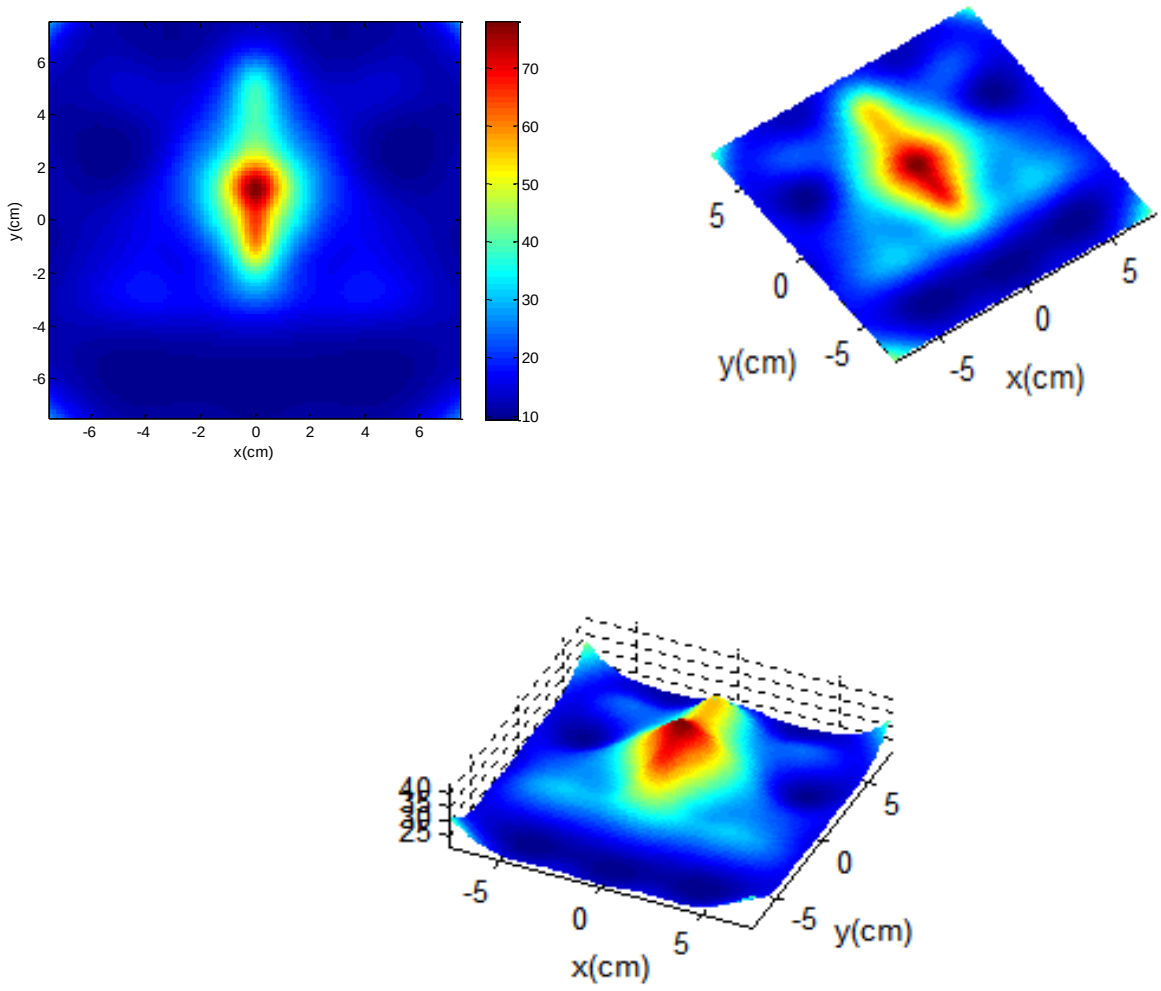

Figure 6.18: Lower Dielectric Triangle Shape Model Using 4GHz Objection

As you can see from the above figure the image of the triangle has been detected clearly. A concentrated spot light is shown in the middle of the triangle.

Polygon Model

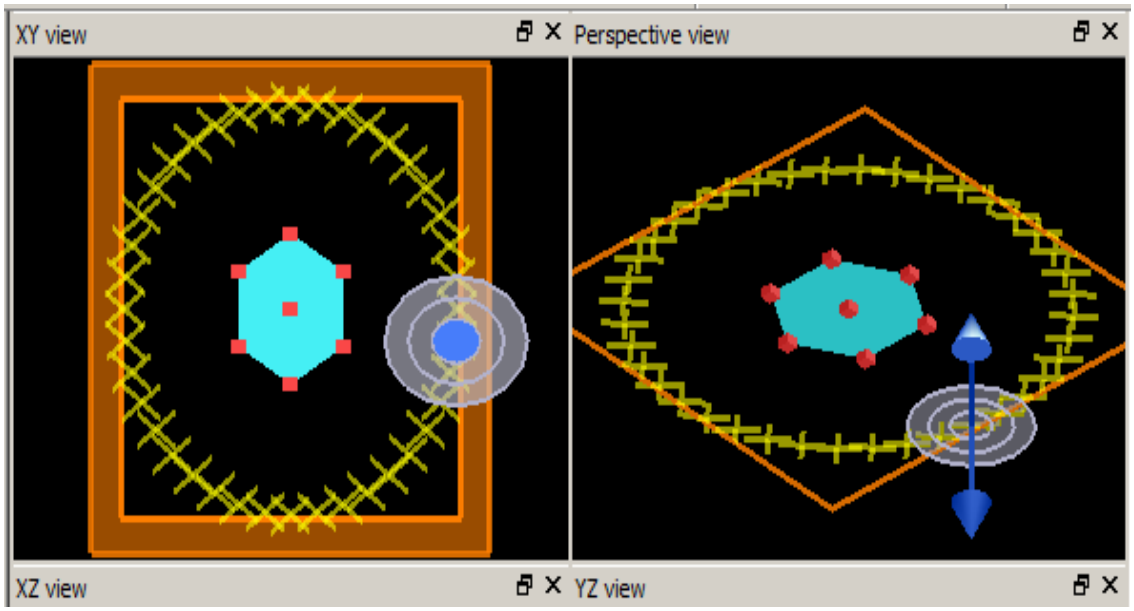

Figure 6.19: Polygon Shape Model in Lumerical FDTD Software

The above figure shows how to model a polygon shape with a relative dielectric of 1.4, using 4GHz frequency. The dimensions are (X, Y), (0,-5, 49), (4.75448,-2.745), (4.75448, 2.745), (6.723e-16, 5.49), (-4.75448, 2.745), (-4.75448,-2.745).

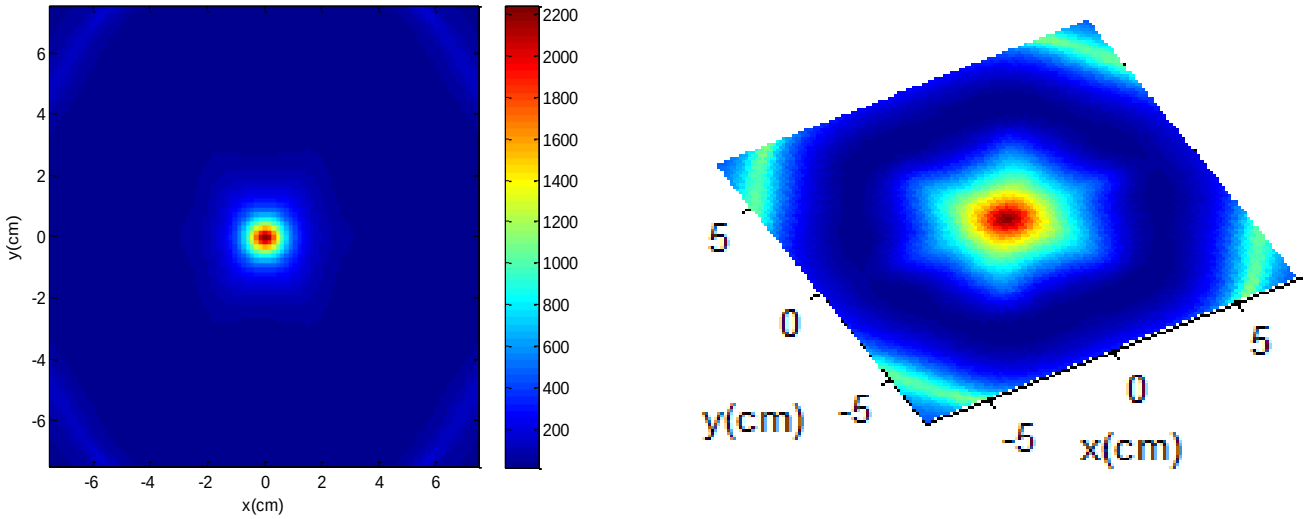

Figure 6.20: Lower dielectric polygon shape model using 4GHz objection

Figure 6.20 shows a clear image of Polygon even the dielectric of its material is low. If the material of the polygon has been changed from lower dielectric properties to metal, a perfect electric conductor, then this will cause the simulation results shown in Figure 6.21.

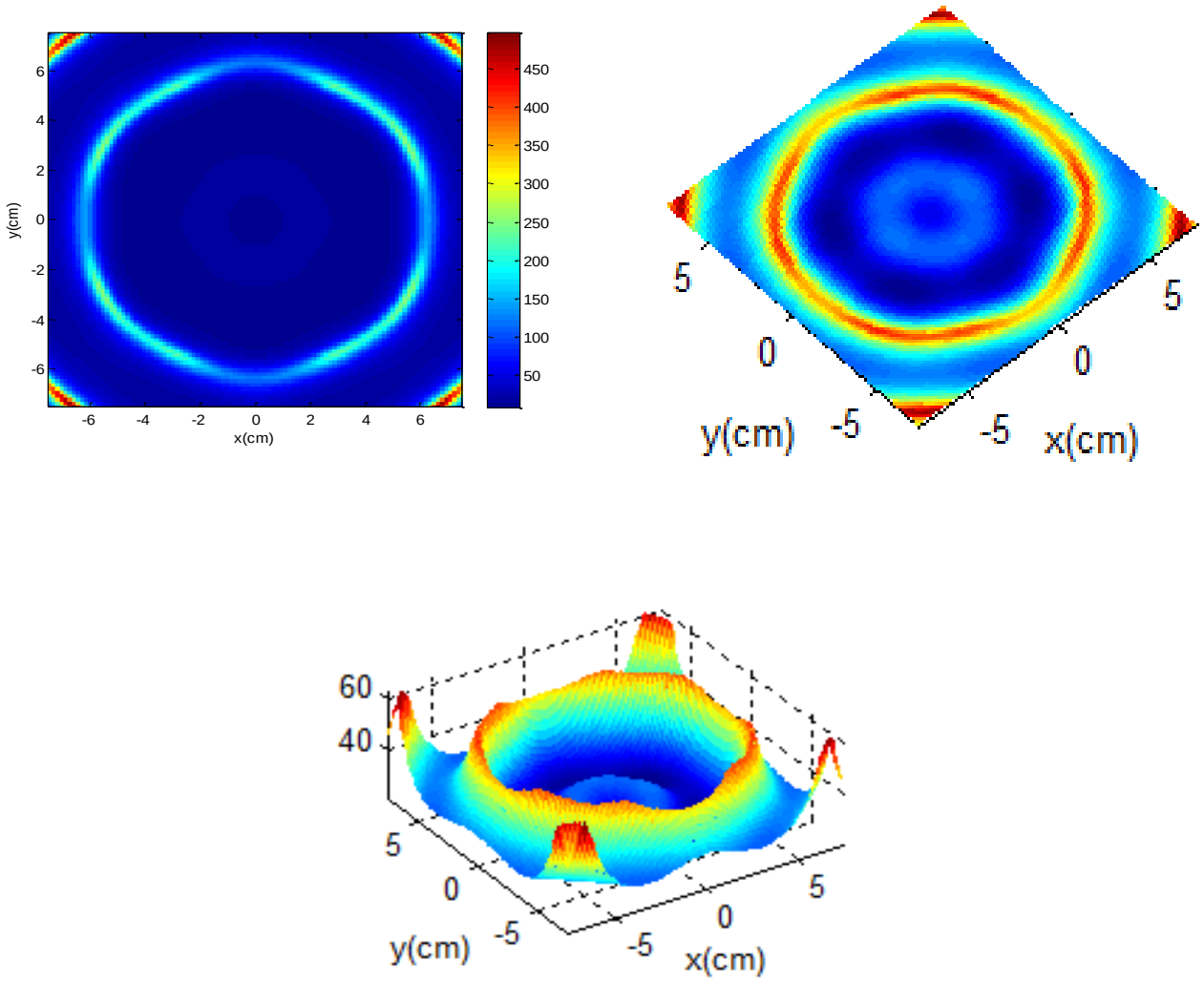

Figure 6.21: Metallic Polygon Shape Model and Different Angle of View Using 4GHz Objection

According to the above figure, a 4GHz frequency objection on the metal polygon shows the boundary of the metallic polygon clearly.

Square model

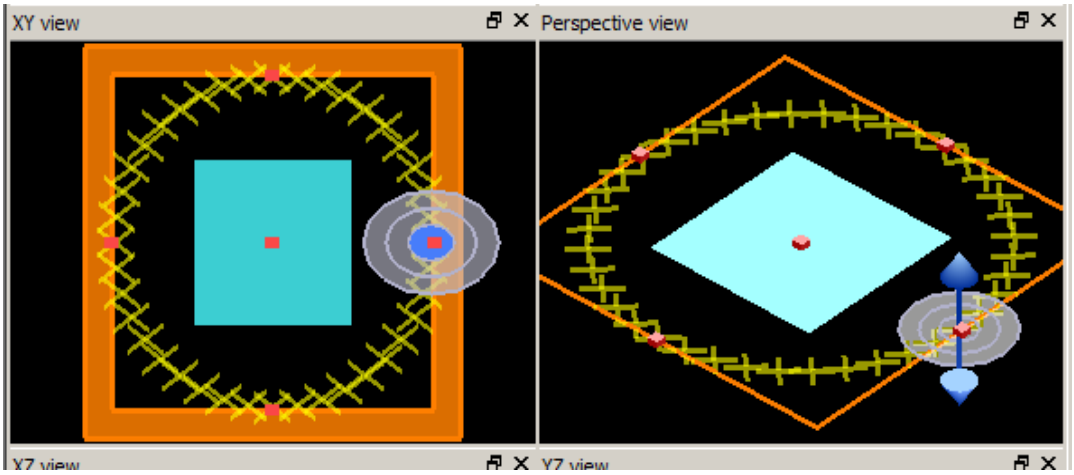

Figure 6.22: Square Shape Model in Lumerical FDTD Software

Figure 6.22 above shows the construction of the square model in FDTD containing relative dielectric of 1.4. The dimensions of the square are 15cm x 15cm. The results of the Matlab simulations are shown in the figure below.

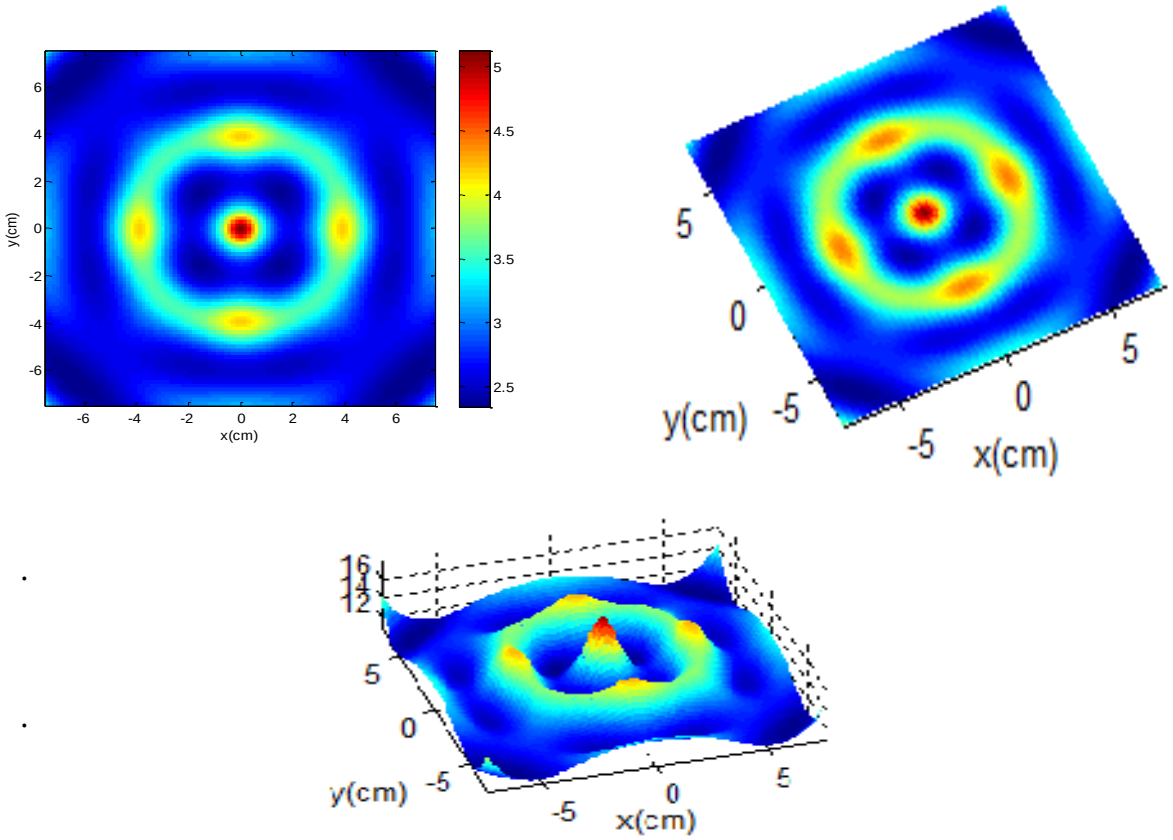

Figure 6.23: Lower Dielectric Square Shape Model and Different Angle of View

The above figures show a very clear square shape boundary, with the middle of the square showing peak spotlights.

When changing the dielectric properties of the square with dimensions of 15cm x 15cm to metal (PEC), the following results will appear:

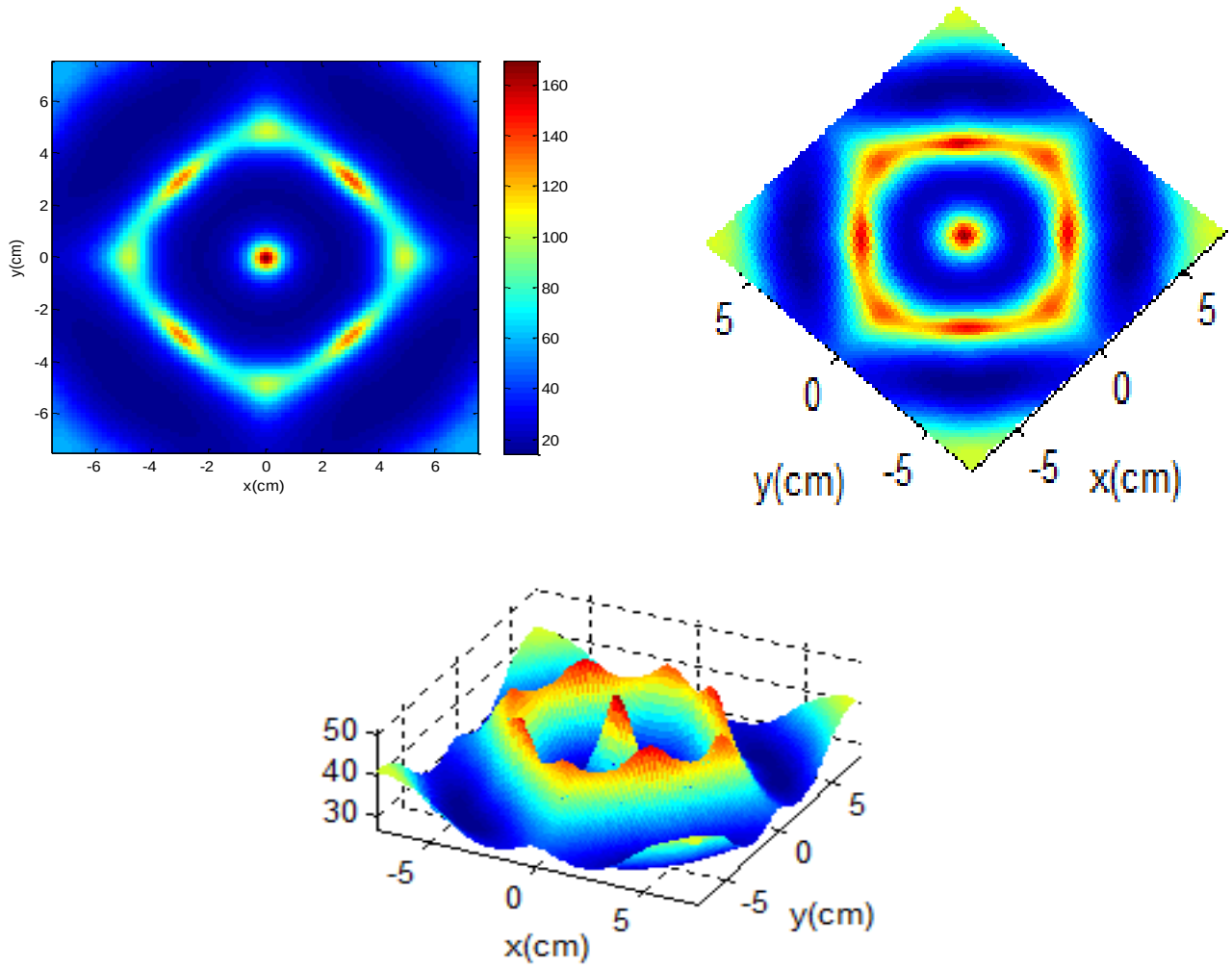

Figure 6.24: Metallic Square Shape Model and Different Angle of View

As we can see from the models above, the detail inside the models has been shown; these have directed the viewer to similar shapes projected earlier using 40 antennae.

Cylinder model object

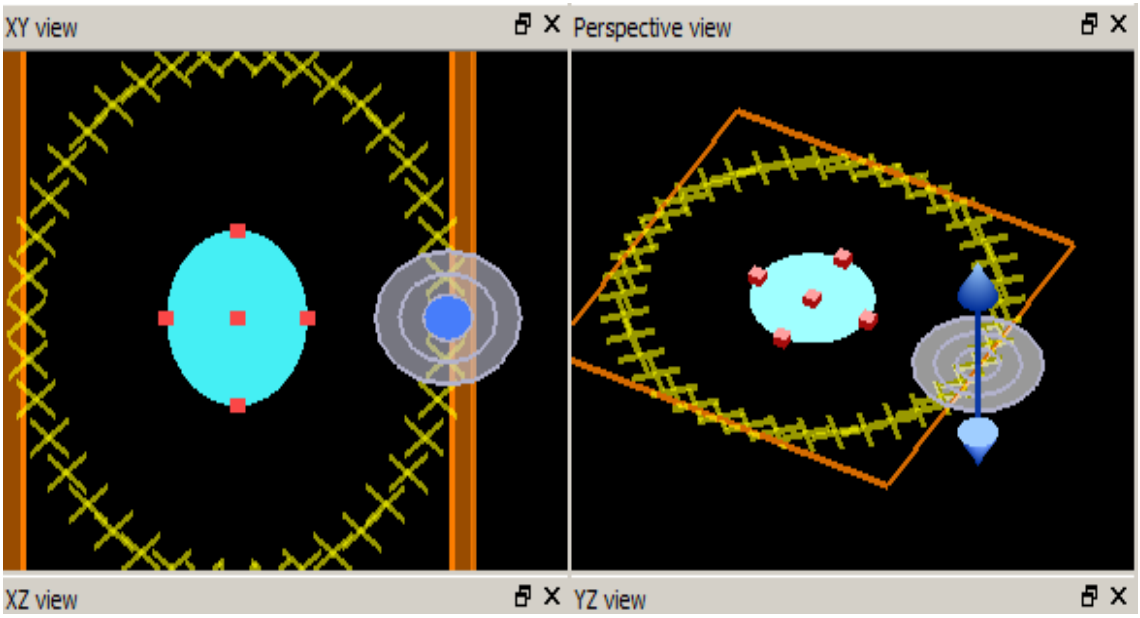

Figure 6.25: Cylinder Model With 5cm Radius

Figure 6.26 below shows a cylinder with a radius of 5cm and defined relative dielectric of 1.4. It shows a very clear image of this type of cylinder, even though the dielectric value of this material is low.

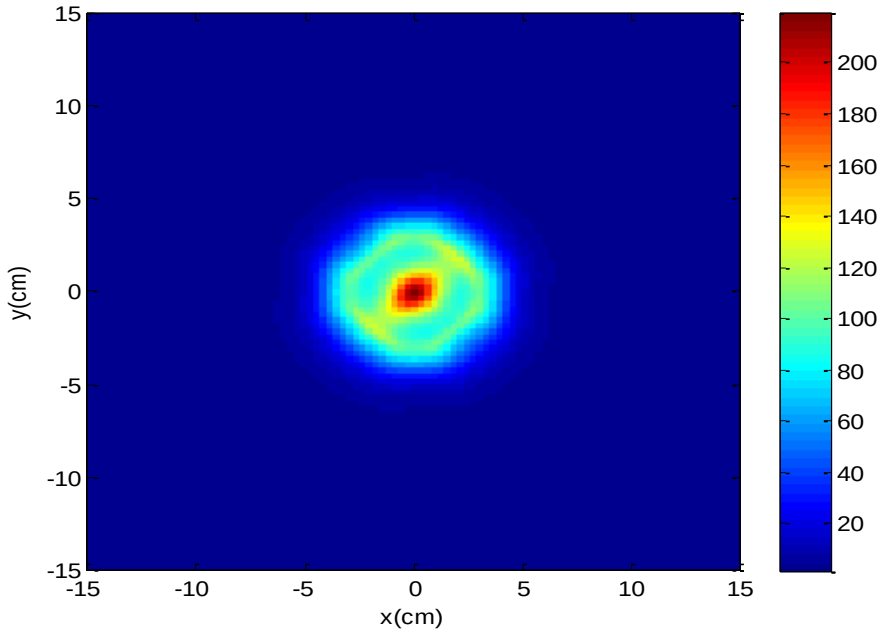

Figure 6.26: 5cm Cylinder Using 4GHz Objection

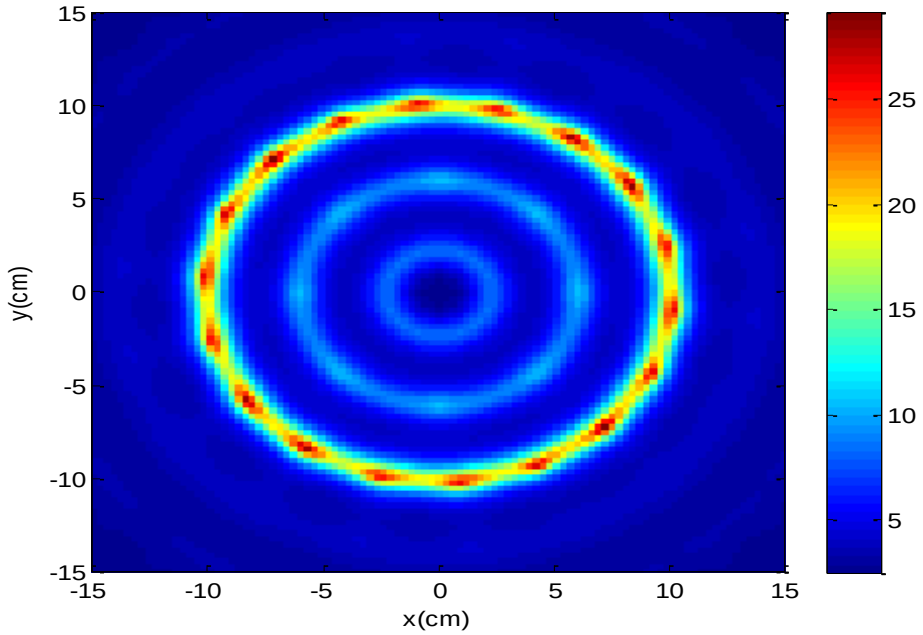

Figure 6.27: Cylinder of 10cm Using 4GHz

The above figure shows an extended target of a cylinder with a radius of 10cm and the index is a perfect electric conductor; this is considered to be metal in the simulation. There is a very nice shape as this cylinder has been achieved by 4GHz microwave objection.

Hidden Object

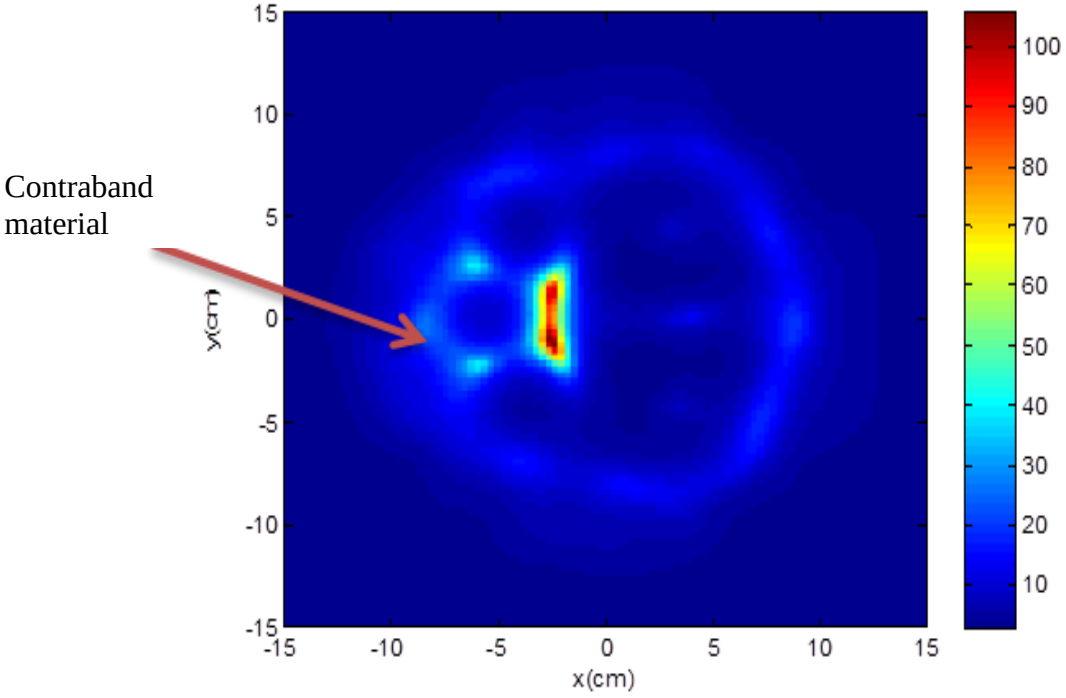

Figure 6.28: 2cm Hidden Target

The above figure shows how a 4GHz pulse can image contraband material of 2cm radius, with defined relative dielectric value of 1.4 imbedded inside a box of 15cm x 15cm dimension and dielectric value of 3. The box is assumed to be the human body medium.

6.4.4 5GHz

Square Model

A square shape model has been constructed similar to Figure 6.23 above, and the results of the image reconstruction are shown in the figures below.

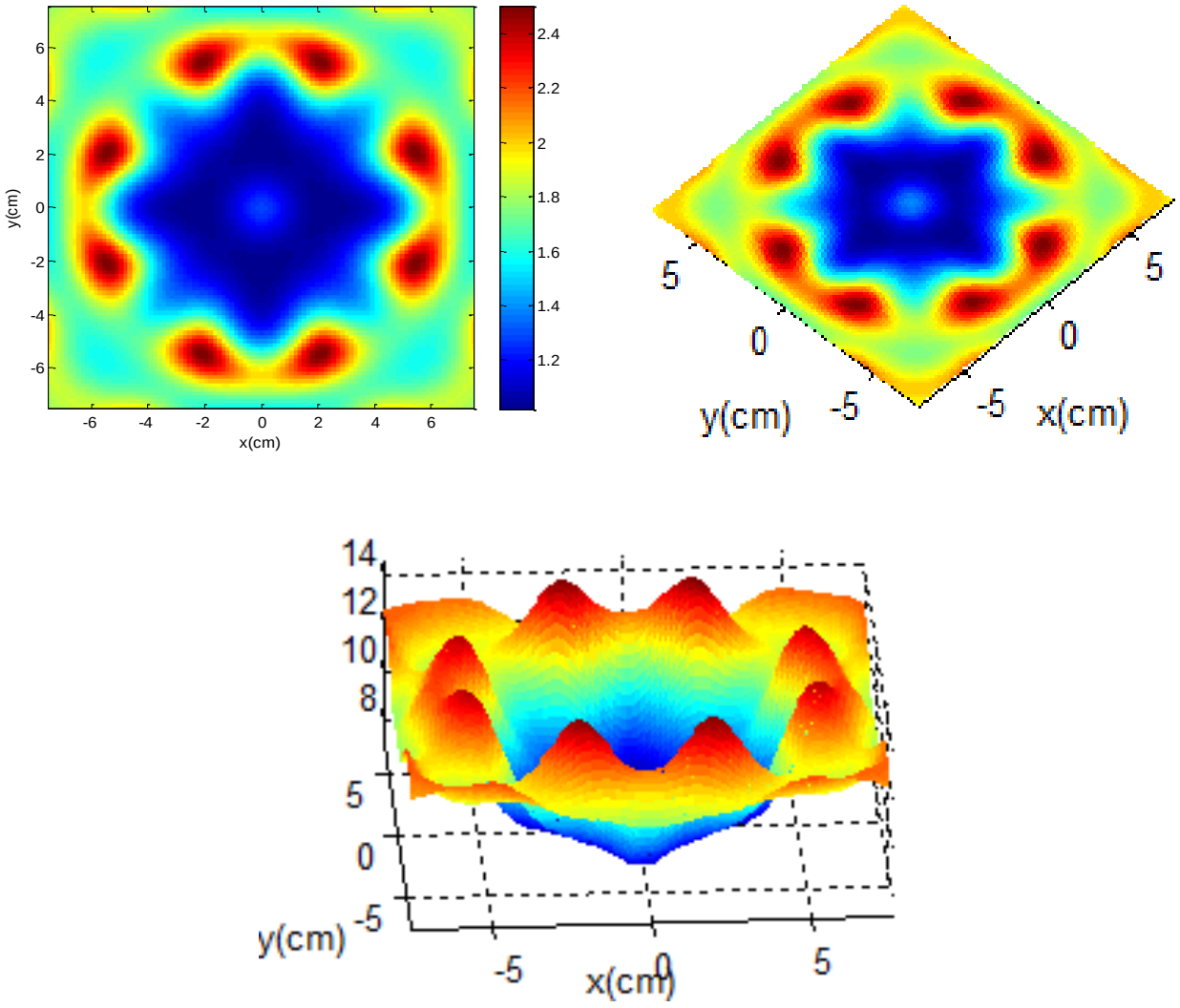

Figure 6.29: Lower Dielectric Square Shape Model, Dimension 15cm x 15cm and Different Angle of View Using 5GHz Objection

The above figure shows that the shape of square has been detected when applying 5GHz. The dielectric of the square was 1.4, and the dimensions of the square model are 15cm x 15cm.

Now, when the material of the square changes to metal, then the results would show the following:

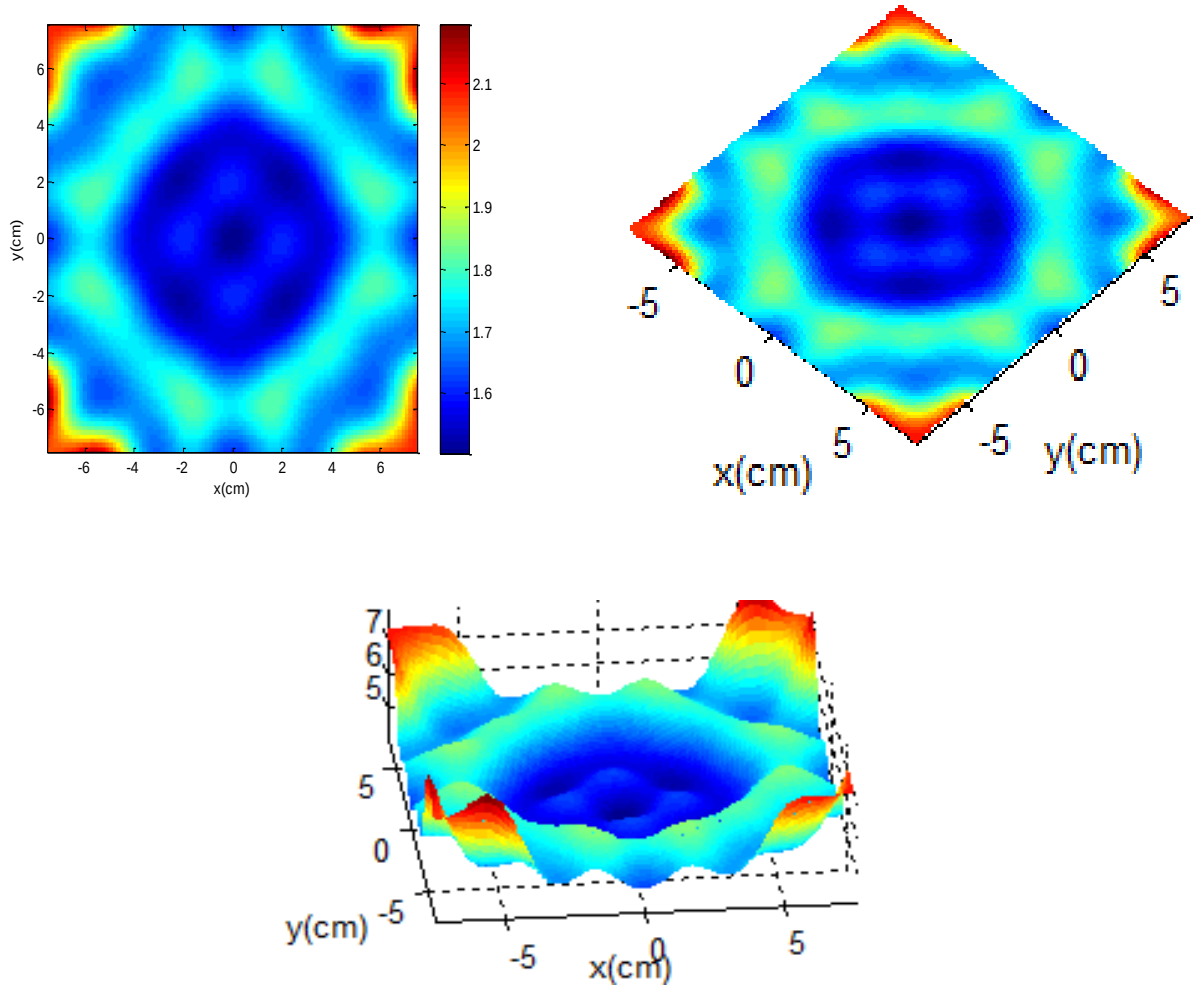

Figure 6.30: Metallic Square Shape Model Using 5GHz

The above figure shows that clear boundary lines of the square have been detected after image reconstruction.

6.4.5 7GHz

Square Model

A 7GHz projection on a square shape shows the shape of a square very clearly, as shown in Figure 6.31 below. The square has a dielectric of a perfect electric conductor or metal. The dimensions are 15cm x 15cm.

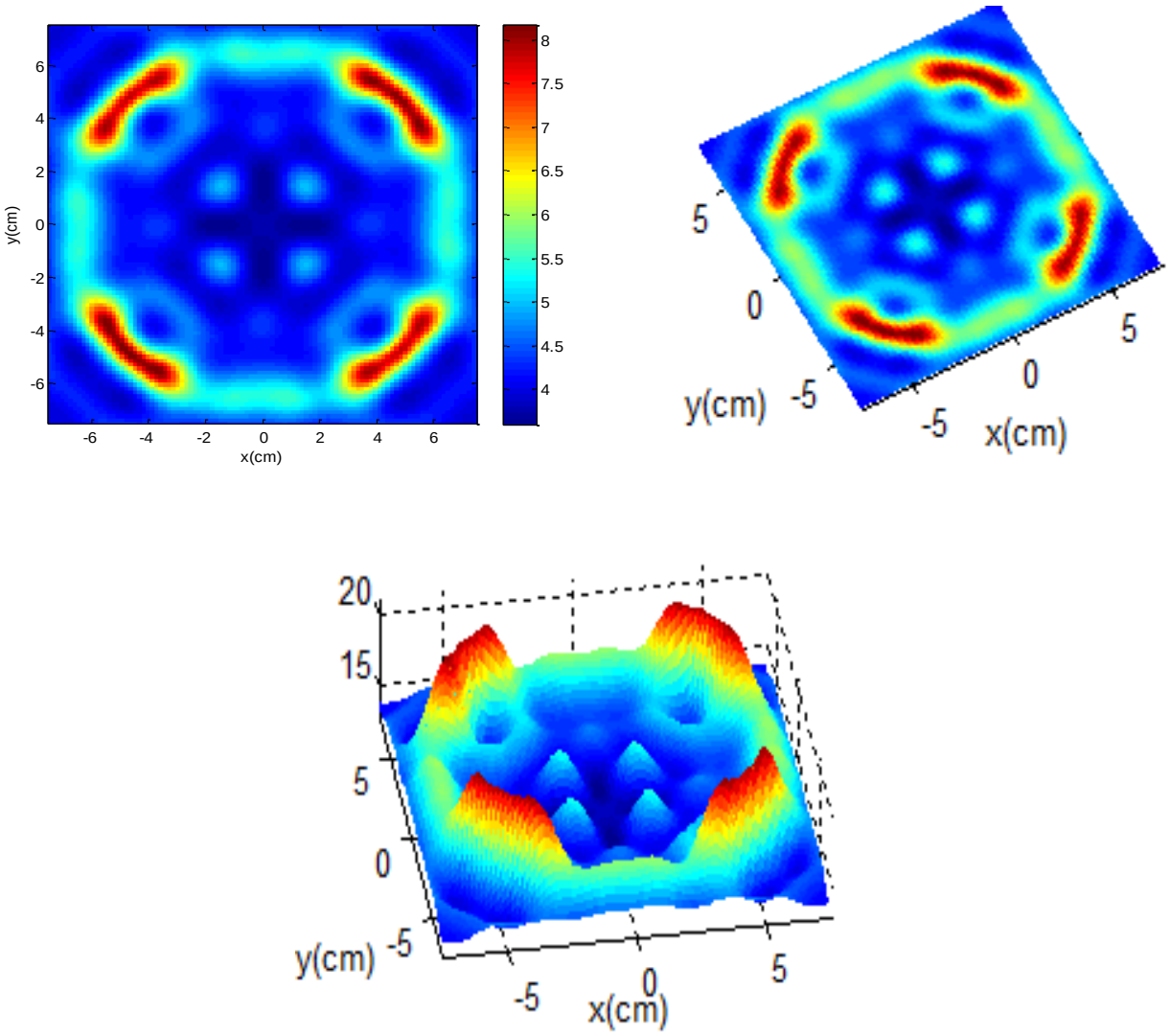

Figure 6.31: Metallic Square Shape Model Using 7GHz Objection

Now, if we change the material of the square to a lower dielectric property such as 1.4, the result would be as follows:

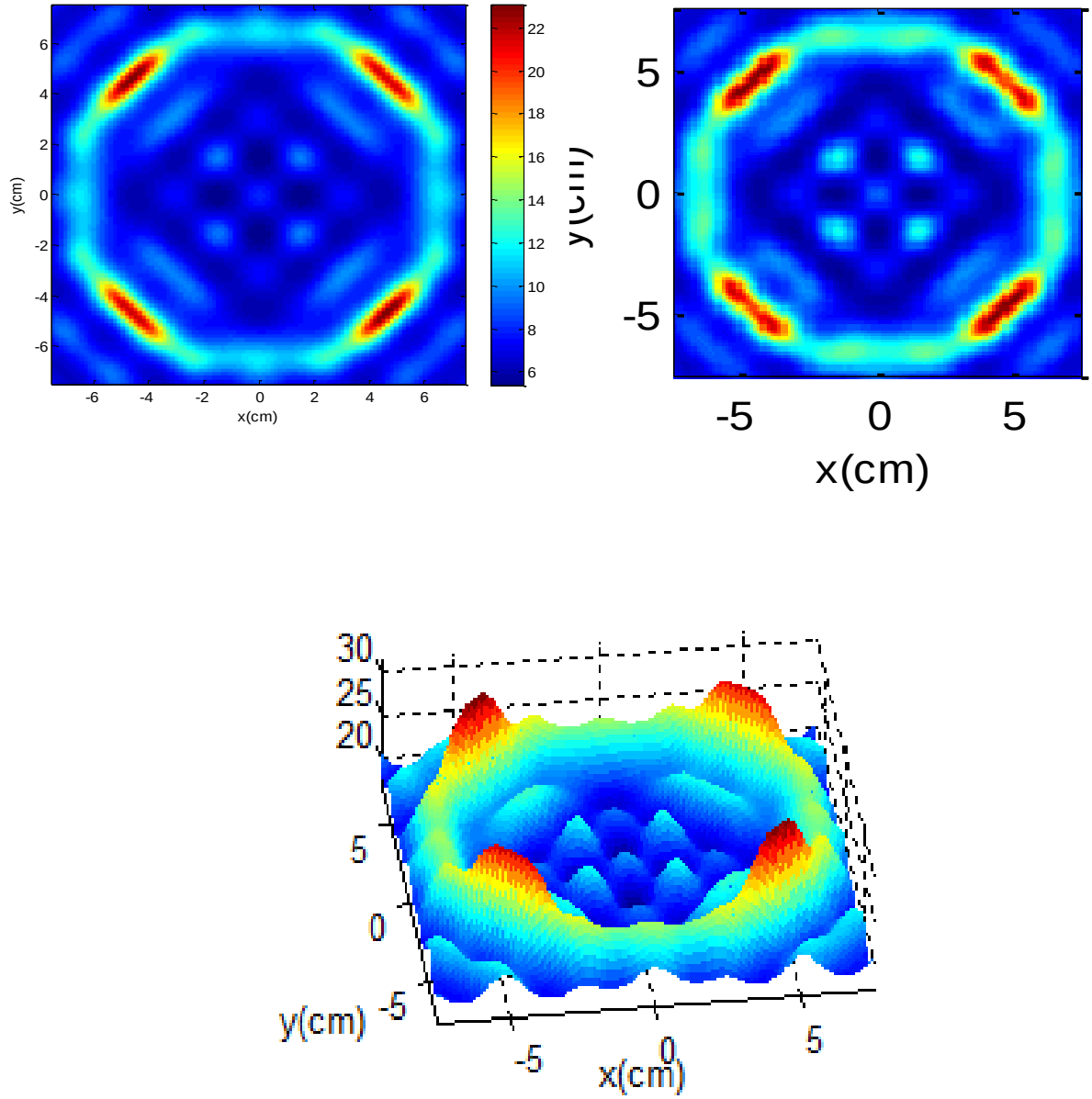

Figure 6.32: Lower Dielectric Square Shape Model Using 7GHz Objection

The above figure shows a similar but slightly different shape to the previous figure. The four boundary edges of the square show a high peak of spotlight.

Polygon Model

A polygon model shape dielectric of 1.4, constructed the same as Figure 6.19 above in FDTD, showed very clear peak points of all six edges of the polygon after image reconstruction in Matlab. This is shown in Figure 6.33 below.

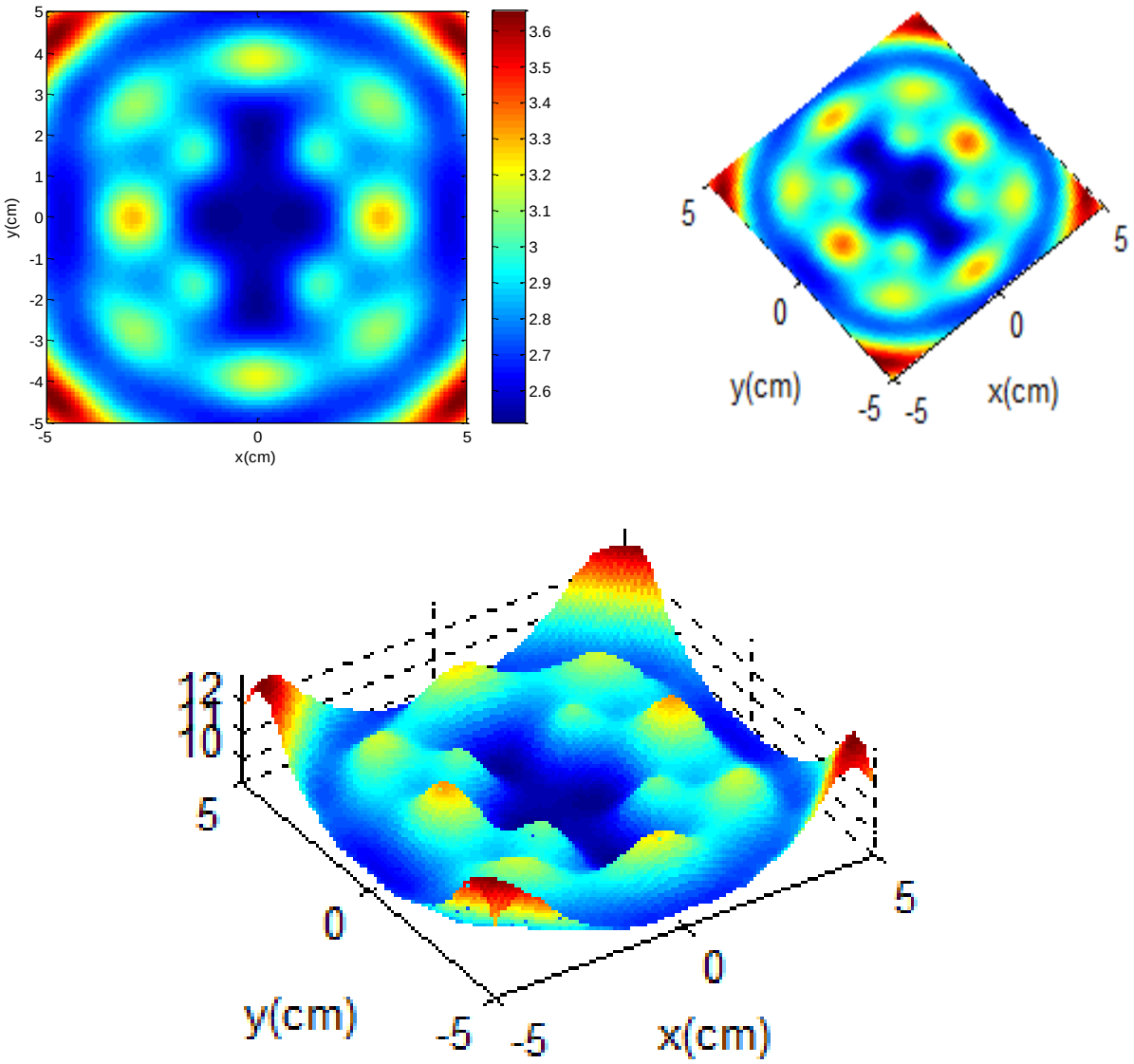

Figure 6.33: Lower Dielectric Polygon Shape Model Using 7GHz Objection

Now if we change the material of the polygon to metal (PEC) then the results would be as shown in Figure 6.34.

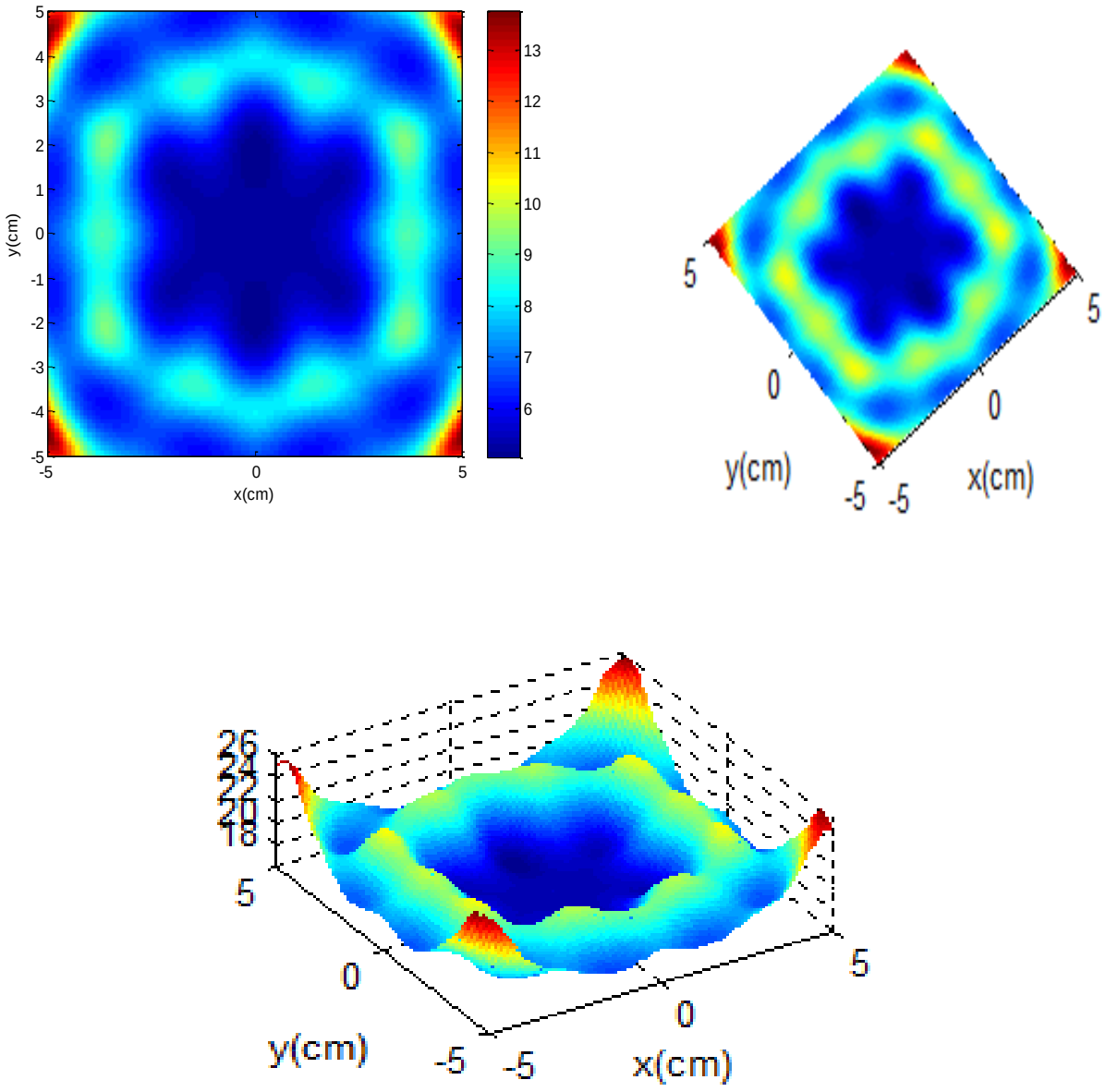

Figure 6.34: Metallic Polygon Shape Model Using 7GHz Objection

As seen from above figure, clear polygon boundary lines have been detected after image reconstruction on Matlab.

Sphere shape

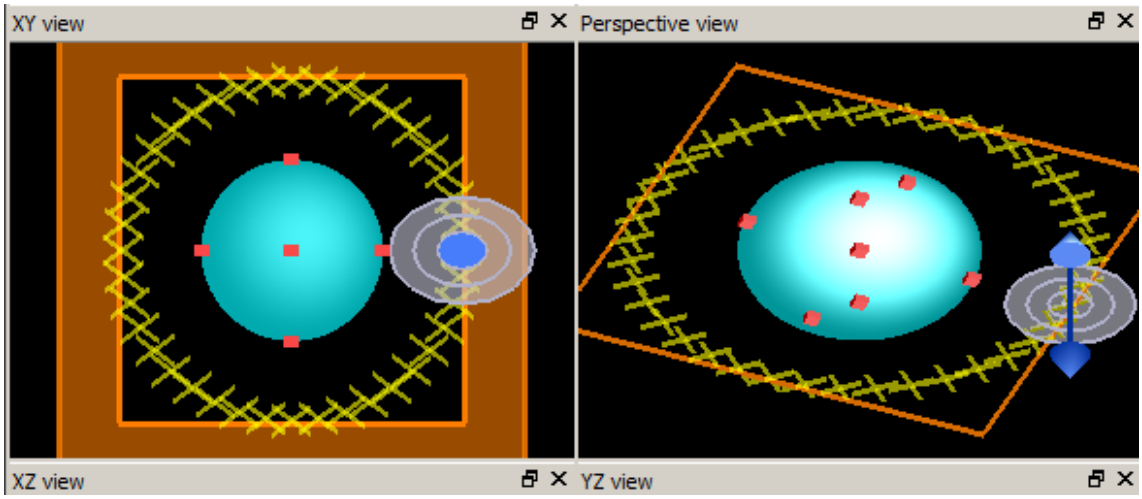

Figure 6.35: Sphere Shape Model in Lumerical FDTD Software

The above figure shows the construction of a sphere model with a radius of 8cm.

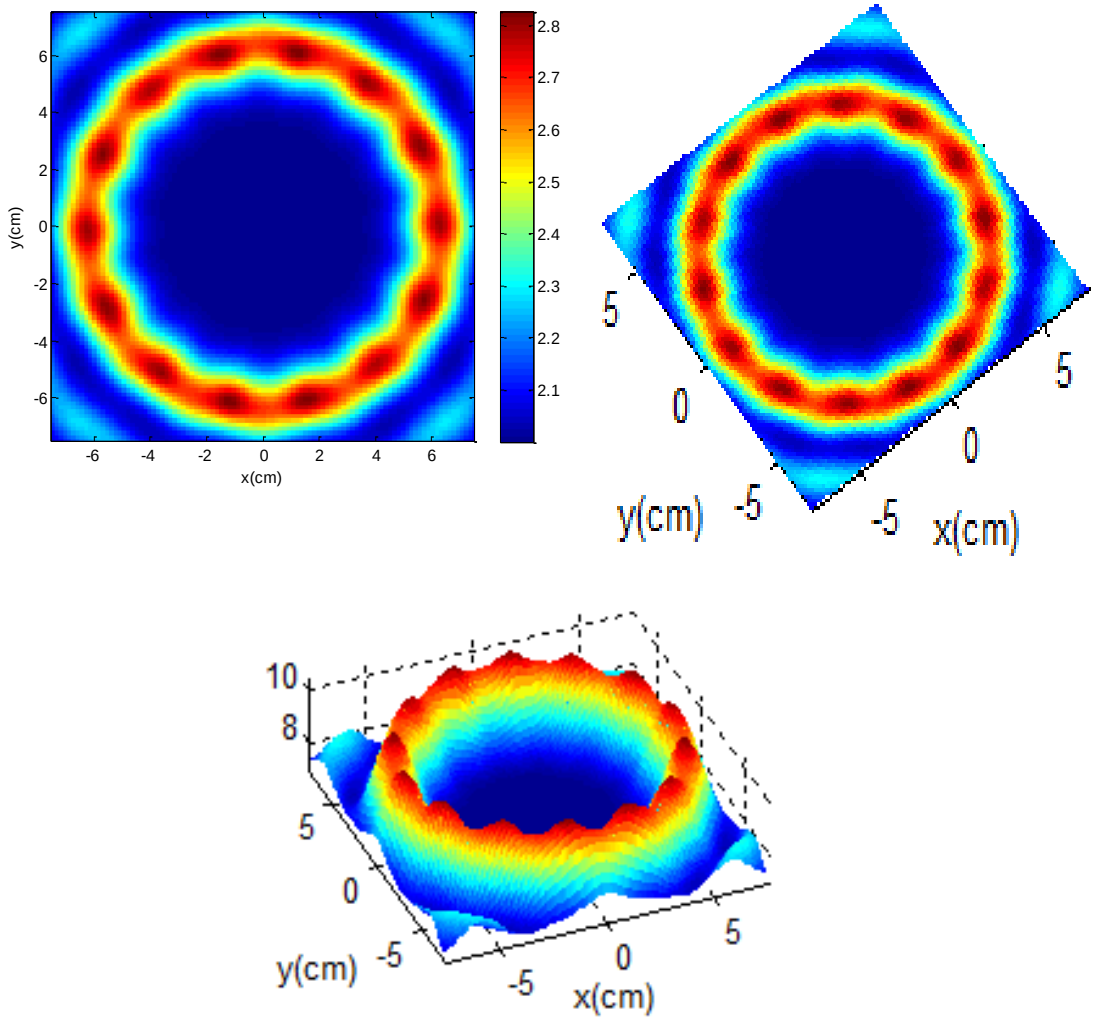

Figure 6.36: Sphere Shape Model Using 7GHz Objection

Figures 6.35 and 6.36 above show a sphere shape with a radius of 8cm and relative dielectric of 1.4. After simulation in MatLab, very clear boundary lines of the sphere shape can be seen.

Now, metal in the shape of a polygon has been embedded inside the sphere to test the imaging results. This shows if it is possible to differentiate between two materials or if hidden material can be shown. Figure 6.37 shows how to construct this in FDTD.

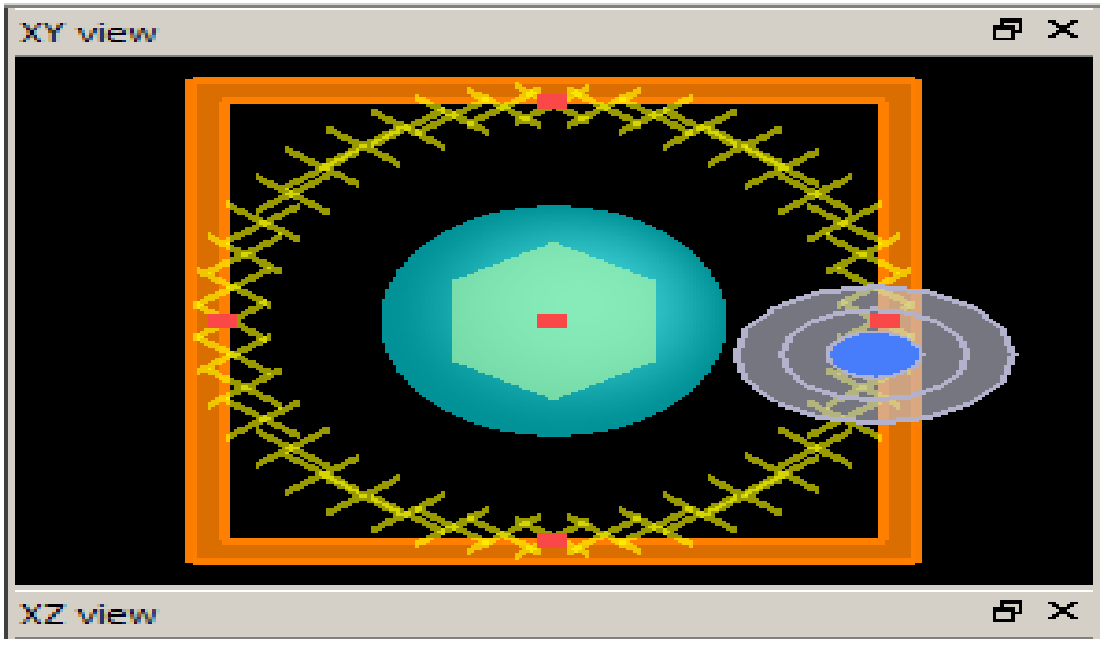

Figure 6.37: Metallic Polygon Inside Sphere Model

The idea of the illustration shown above in Figure 6.37 comes from the possibility of a metallic gun being hidden underneath human clothing. Normally the guns and knives used for terrorist acts are metallic.

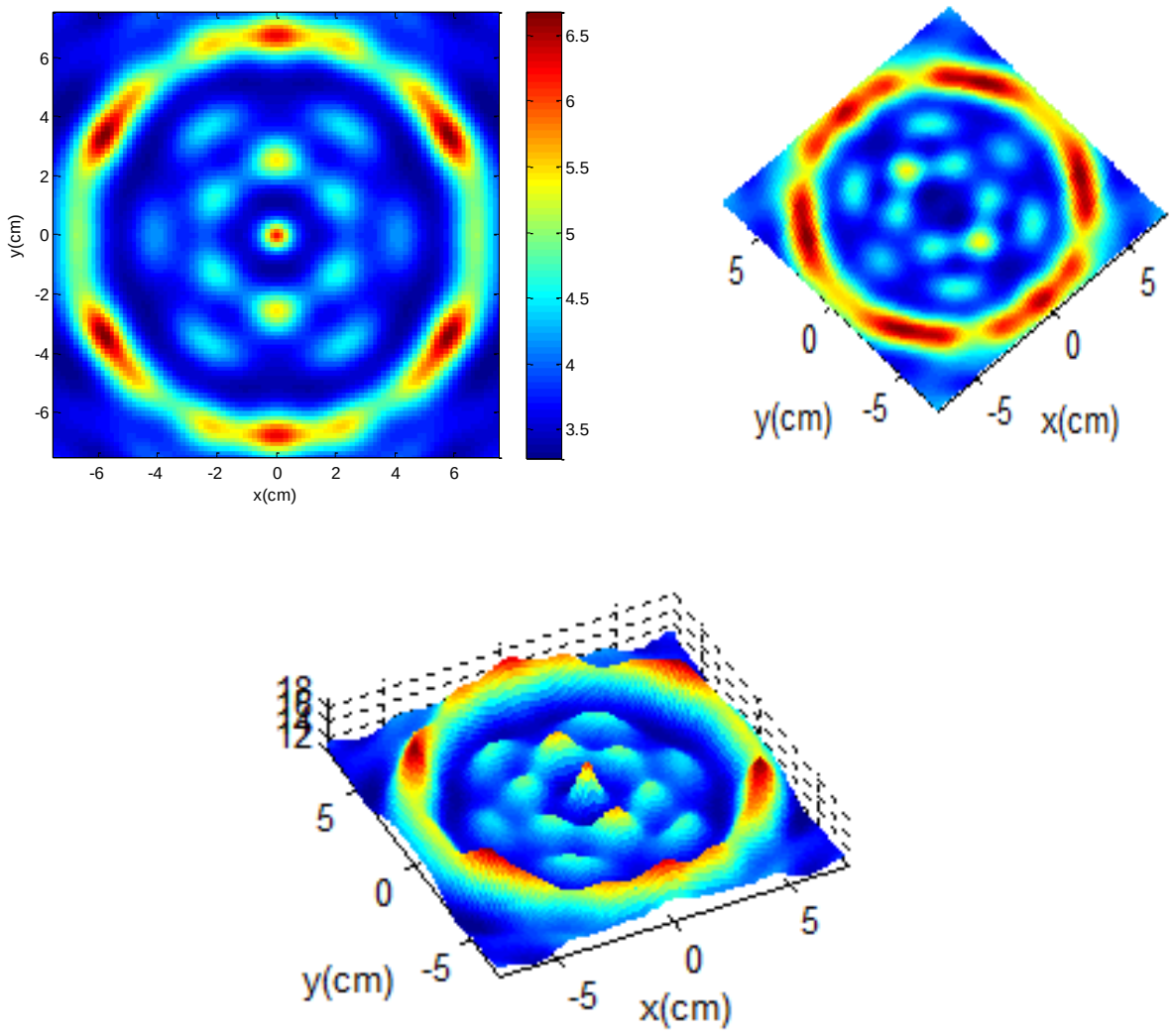

Figure 6.38: Metallic polygon hidden inside sphere

Figure 6.38 shows details of a polygon inside a sphere, and shows the sphere also. The polygon is PEC and the sphere is 1.4 dielectric.

Now if the material of both models is shown the other way round, i.e., metal for the sphere and 1.4 for the polygon, then the results will be as shown in Figure 6.39 below. A lower dielectric polygon that could be hidden in any metallic object; this might be how terrorists or smugglers smuggle their illegal materials in metallic objects. Comparing figures [6.39, 6.38] with figure 6.39 we can see how the image is different when there are no materials or objects embedded in figure 6.36.

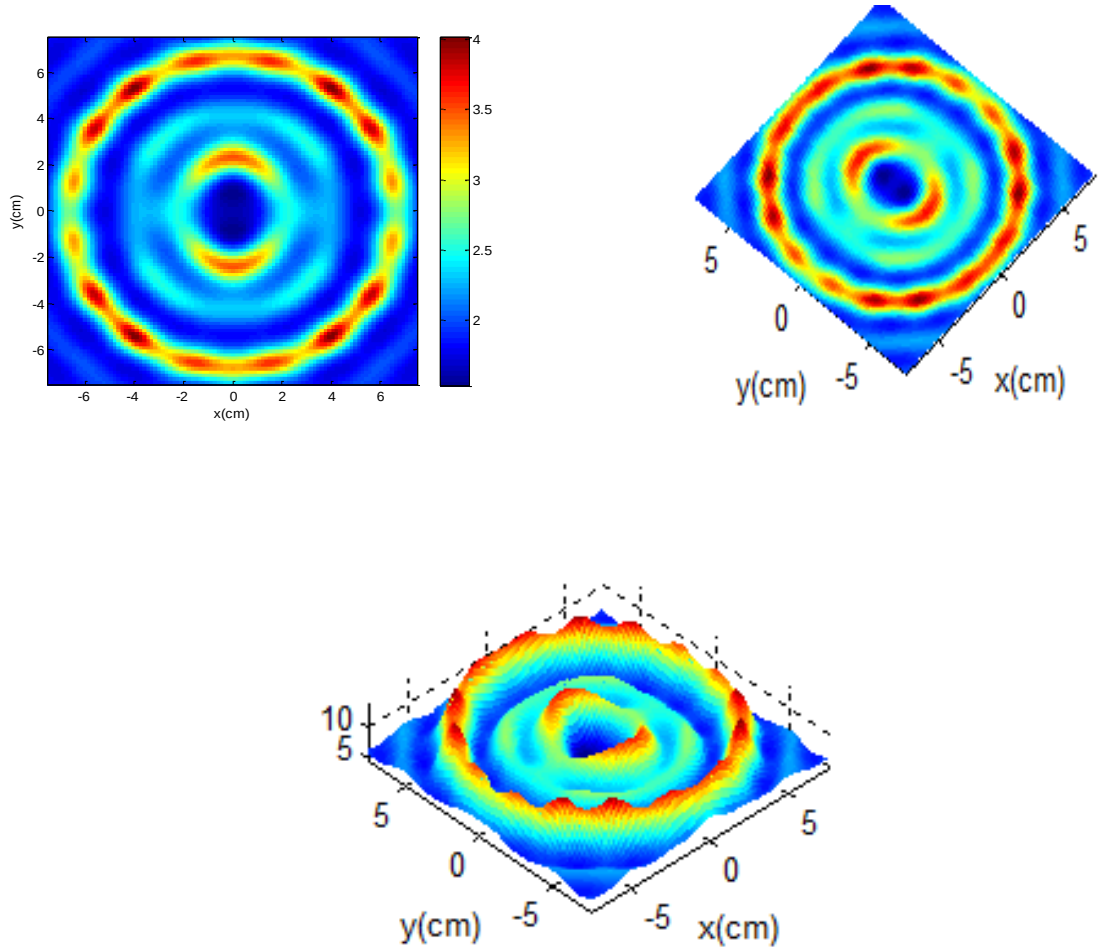

Figure 6.39: Lower Dielectric Polygon Model Inside Metallic Sphere

Figure 6.39 above clearly shows how easy it is to detect materials imbedded in other material. This is an example such as when a terrorist implants objects in their baggage. It shows the boundary of the polygon and, inside it, also the boundary of the sphere.

As you can see from the above figures, the models have been shown clearly with low or higher dielectric properties.

It can be seen from all the above results that 7GHz can show very clear images.

Cylinder or human torso cross-section using 7 GHz

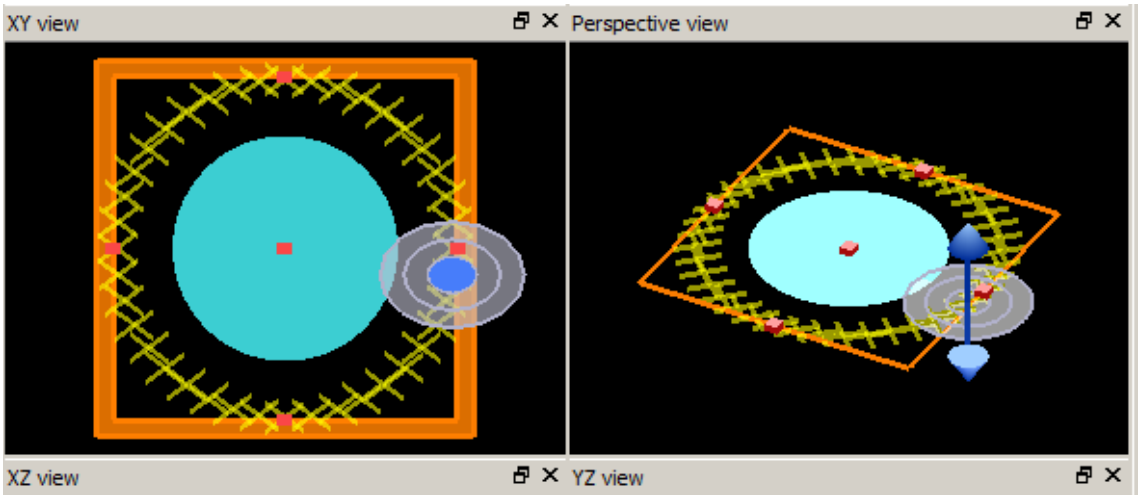

Figure 6.40: Circle Model, Assumed to be Human Torso

The above figure shows how to construct a 10cm radius of a cross-section shape model, assuming it could be a human torso.

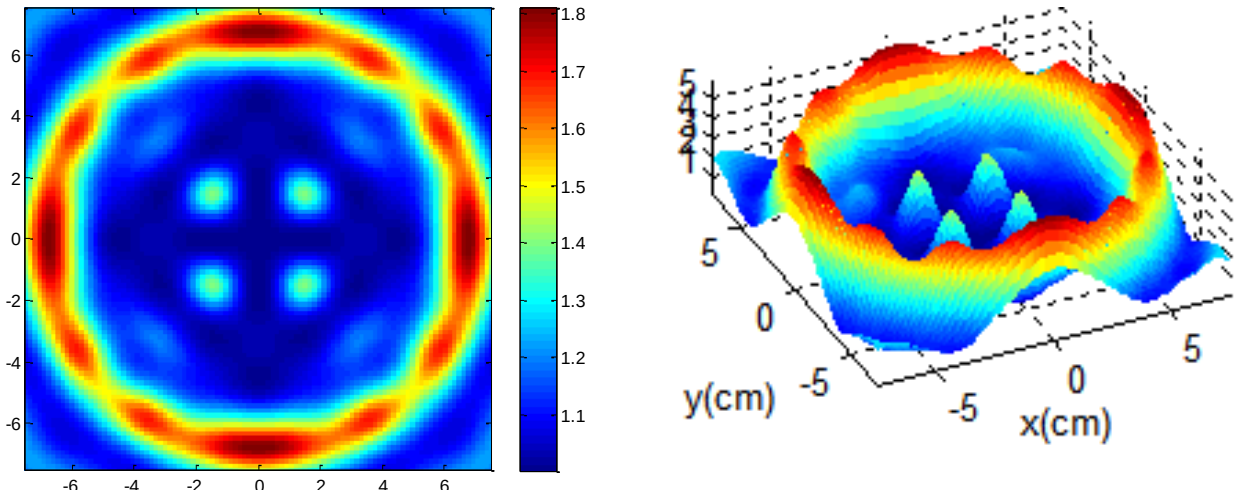

Figure 6.41: 10cm Radius Object, Assumed to be Human Torso using 7GHz Objection

As you can see from the above figure, a 10cm radius circle that could be related to the human body cross-section is shown very clearly. The dielectric of the torso was 6 in this

simulation. There is a good peak of spotlights around the cross-section that helps the viewer to visualise this model without any confusion.

6.4.6 10GHz

Square Model

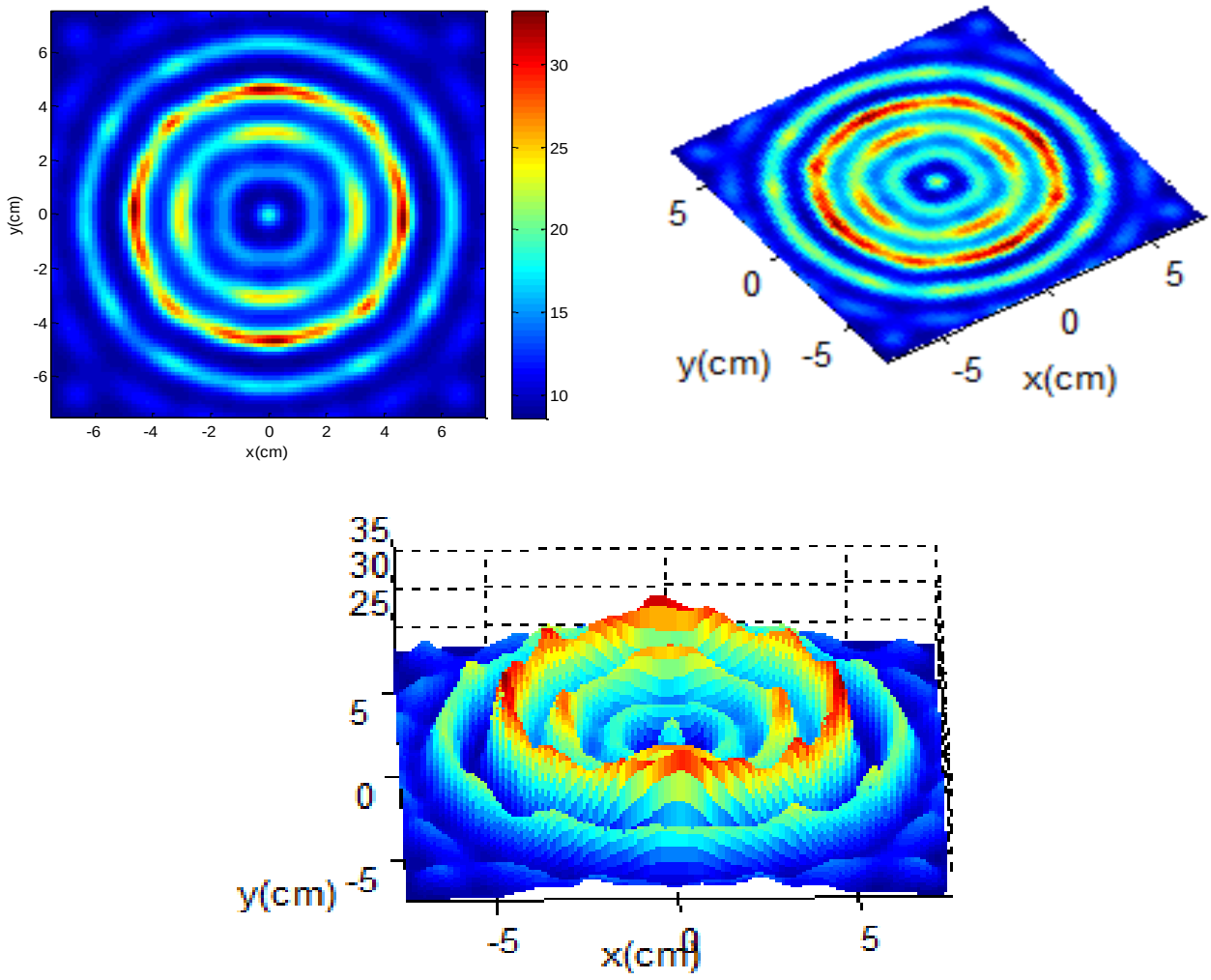

Figure 6.42: Metallic square Shape Model Using 10GHz Objection

The above figure shows shape details that could lead the viewer to a square shape. More detail is shown at 10GHz, which means the higher the frequency the better the image. On the other hand, the smaller the wave length the higher the resolution that this robust TR-MUSIC algorithm could generate.

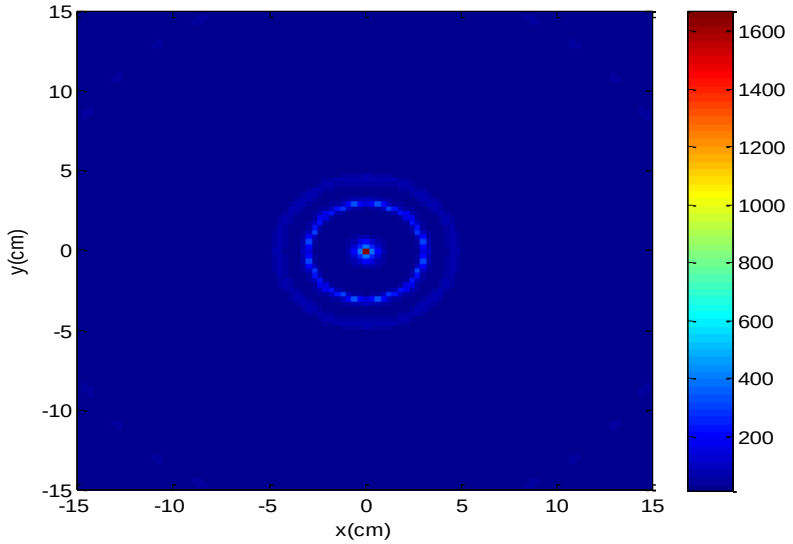

Figure 6.43: 10cm Radius Object

Figure 6.43 shows the result from omitting a 10GHz microwave and shows a circle of 10cm radius that can been seen perfectly clearly; the inner shape of the material is also shown very clearly. This concludes that the higher the frequency the clearer the image.

The simulation results in Chapter 6 approve the use of TR-MUSIC. The simulation results are much clearer than other research groups using a TR-MUSIC algorithm to reconstruct their images. Different models and shapes were tested and showed both the boundary of these models and inside them.

This research concentrated on the frequency range between 0.9 and up to 10GHz, which showed better results. Other researchers used a range of microwave frequency between 30GHz and 300GHz such as the millimetre wave where they faced loss problems [129], [130]. This research concentrated on a lower frequency range to have a better trade-off between resolution and penetration depth. In addition this simulation had tested different objects embedded inside human body tissue, and brought the reader to visualise how terrorist and smugglers could use their bodies to implant illegal objects.

Successful imaging results were obtained when it comes to different objects being embedded inside tissues, using both a Radon Transformation algorithm and a TR-MUSIC algorithm. TR-MUSIC has been used before in ground penetration detection but not in security applications. In this application it gave this research the advantage of being the first to use a TR-MUSIC algorithm in microwave imaging.

This research has investigated the 2D images for its entire algorithm, which actually gave very clear results. Some of the X-ray backscatter machines are using 2D images to find illegal objects when bags are scanned[131]. Therefore this technology could depend only on 2D rather than 3D images. If the future required 3D images, then it would only require a different layer of cross-section to be added to form the 3D image. For example, a human body cross-section could be sliced to a different number of layers and then all these slices could be summed to form a 3D image.

6.5 CHAPTER SUMMARY

This chapter aimed to show the simulation results after the microwave imaging system was set up in Lumerical FDTD and Matlab. It started with an explanation of the real microwave imaging system set up to enable the reader to visualize it in the simulation process, and to carry out a real experiment in the future. The antennae were arbitrarily but evenly located around the target in Lumerical FDTD solution to collect the Multi Static Response Data Matrix. These data were later loaded and processed in Matlab code using a TR-MUSIC algorithm. Figure 6.4 showed multiple point targets using TR-MUSIC very clearly. Figures 6.5, 6.6, and 6.7 showed a clear metallic cylinder, which could be assumed to be metallic guns hidden underneath human clothing. Figures 6.8, 6.9 showed how powerful TR-MUSIC is in showing the boundary and shape of an extended metal target. This proves that this algorithm is simple, direct and does not need forward solution and iteration for image reconstructions.

Previous successful imaging results led the research to be developed further to see the effect of different frequencies with different target models. At 2GHz the results of square and polygon models showed high peaks or spotlights that exist both on the boundary of the object and inside it. At 3GH Figure 6.14 and 6.15 showed clear cylinders of 5cm and 3cm radii in different locations, which indicates that microwave imaging can image small contraband objects. Also at 3GHz, a successful image of a 2cm radius object embedded inside a human body cross-section model was shown, which could alert the scanning officer to suspected materials within this passenger.

At 4GHz, models such as a triangle, polygon, square and cylinder have all been imaged successfully with metallic or lower defined dielectrics. An extended cylinder target with a radius of 10cm was imaged clearly at 4GHz microwave objection. Additionally a hidden object with a radius of 2cm also has been detected using 4GHz. At 5GHz a square model was imaged successfully, both metallic and lower defined dielectric. At 7GHz, models including a square, polygon and sphere were detected clearly in metallic and lower defined dielectric.

Comparing Figure 6.36 with Figures 6.38 and 6.39 shows a clear hidden object inside a sphere model. This scenario experiment comes from the possibility of metallic or plastic guns, explosive powder and drugs being hidden underneath human clothing. At 10GHz a square and cylinder model have been shown clearly.

Going back to chapter 3 figures 3.9 and 3.10 and compare it with figure 6.28 in this chapter, it shows that TR-MUSIC algorithm similar was successful in detecting 2cm radius object hidden in human body cross section. In addition if we compare also figures 3.11 and 3.12 in chapter 3 with figure 6.15 in this chapter, it shows that TR-MUSIC can detect 2 cm radiuses object or smaller objects. Image reconstruction of Radon Transformation algorithm and TR-MUSIC were slightly different for the viewer

but they all lead to the same purpose of this research which is detecting different sizes of contraband objects embedded inside human body cross sections. Images were reconstructed based on each algorithm criteria.

From the above discussion of results, it cannot be denied that the TR-MUSIC algorithm can detect any material with any dielectric property; it also concludes that, up to 10GHz, the higher the frequency the better the imaging results.

This chapter has concluded and proved that microwaves can be used in imaging for security systems, as shown from the simulation results. It has also proved that TR-MUSIC is a perfect algorithm to process data collected from circular arrays of antennae to give robust imaging results. It has also been proven that the higher the frequency the clearer the image and that different materials dielectric embedded in other materials can be shown clearly.

The next chapter will discuss the history of terrorism, the importance of aviation security, and security scanning technology management, including factors that could be considered when new imaging technology is introduced to airports.

Chapter 7: **Aviation industry and security**

7.1 HISTORY

Terrorist acts have been carried out over a long period. For example, two well-known groups are the Irish Republican Army (IRA) who carried out attacks on the British police and army in the 1970s, 80s and 90s, and Germany's Red Army Faction (RAF): both organized a series of bombings and assassinations. In 1988 there was the Lockerbie bombing disaster when flight Pan Am 103 exploded shortly after take-off from Heathrow airport. The 9/11 attack on the World Trade Centre in New York and the Pentagon in Washington D.C. in 2001. In 2004 a bomb was placed on a train in Madrid and killed more than 190 people [132]. In 2005 more than 200 people were killed and injured on the underground and buses in the London bombings.

The head of the Federal Service for Supervision of Transport in Russia announced recently that terrorist attacks on the Russia transport system have doubled between 2009 and 2010 [133]. In addition, on 25 December 2009, Umar Abdulmutallab managed to go through all security body scanners, including a millimetre wave scanner, with a hidden plastic explosive in his underwear to detonate a bomb on flight 253 from Amsterdam to Detroit.

Figure 7.1: 'Underwear Bomber': Umar Farouk Abdulmutallab is Arrested. Photo by Jasper Shuringa/New York Post [134]

In 2011, there was a bomb explosion at Moscow's busiest airport Domodedovo [135]. In August 2009 Abdullah Hassan Tali Al-Asiri, an Al-Qaeda suicide bomber, inserted half a kilo of explosive inside himself and detonated it at a meeting with Prince Nayef bin Abdulaziz Al Saud, killing himself and causing minor injuries to the prince [136]. There have also been recent attacks on Peshawar airport in Pakistan in 2012, and Kabul international airport in 2013 [137], [138]. The most recent attack on the Westgate mall in Kenya left 72 dead [139].

In addition, by looking at the open source Internet Worldwide Incident tracking system, attacks on the aviation and transport industry have increased despite the increase in security control after 9/11 [140].

Terrorism is not a tactical war that comes back every day and you respond to it: terrorism is planned for a long time and hits countries at unknown times. Therefore a plan for such terrorism has to be robustly planned to manage it when it occurs, or detect it before it happens. Therefore, securing airports, train stations and shopping malls and ports is vital to save human lives and sustain the economy.

7.2 INTRODUCTION

Any terrorist act on the aviation or transport industry will result in the loss of hundreds of lives and loss of infrastructure and equipment worth of millions of pounds; such acts will therefore have a significant impact on the economy and the travel industry. Security of airports, or any other sensitive places, starts at key locations, such as the entrance or check-in points where a terrorist could take advantage to start his terrorist act. A current security technology for scanning passengers has been discussed in Chapter 1.

The question has always been asked about how to secure the supply chain such as airports, ports, canals and shopping malls from man-made threats such as terrorism or piracy. What is the best way to guarantee security using advanced technology? Ninety per cent of global trade flows through 39 bottleneck regions [123]. Security management is to manage the attack incidents before any crisis happens.

Body scanners, such as microwave scanners for explosive detection in the human body, are useful, but they will be useless if security personnel are not very well trained in how to use them. Passengers in modern airports would like to see modern advanced technology to serve them well and secure their journey. Terrorist attacks in a country can damage its economy as a direct cost, and damage the tourism industry. They can target logistic hubs and gateways. For instance more than 14.5% of world airfreight traffic travels through Hong Kong-Shenzhen, and any attack there could have a huge impact on the global economy. Security in general costs a lot of money to make sure that people are safe.

Also there is a concern that, for example, if more security has been implemented in airports, then this will mean longer queueing times for passengers and therefore higher transport costs, which will slow the movement in airports. Although this thesis

discusses implementing advanced technology in body scanners, concerns about cyber-attacks should be taken into account when integrating this new body scanner with other security checks at airports. As discussed later, existing technologies are the solution at the moment, but every technology has limitations, although microwave technology showed a promising imaging technology for security applications.

The decision to invest in more body scanner technologies should be taken into account when planning any security investment strategy. Maybe implementing these higher end technology body scanners in international airports only, or where airports that could be a target for terrorist attacks. The transport security companies and logistics should take the lead in developing high end security technologies, i.e., body scanners, and the government should only set security regulations. At the end of the day, both the security companies and the government should collaborate together to be more effective and efficient.

7.3 SIGNIFICANCE OF AVIATION SECURITY

Aviation security is constructed around the defences established in the 1970s to fight hijackers and on approvals completed by the Commission on Aviation Security and Terrorism, which were considered in the wake of the explosion aboard Pan Am 103 over Lockerbie, Scotland. Developments in aviation security have been complex for the reason that government administrations and industry frequently found themselves at odds, not capable of resolving arguments over funding, efficiency, technology, and possible influences on processes and passengers [142].

Throughout history, terrorists, criminals and smugglers have always found aviation an easy target to access and exercise their illegal actions. Aviation is considered a strong arm for countries' economies, and if aviation is not run very well because of terrorism

or other factors, people will use different technologies in order not to travel, such as video conferencing and other telecommunication technologies. If business people find alternative ways to travelling by air, airline companies could raise their ticket prices, which will deter frequent travellers from travelling. In addition, other industries will be affected such as hotels, tourism, rentals and export or import industries.

Aviation includes airline operations and airports. Airports consist of commercial, general, private and military aviation services. Anyone who has the responsibility of securing aviation should be the most updated in strategies and new technologies to tackle new threats: screening officers should always be well trained in new screening technology. Strategies such as passenger profiling should be updated, and intelligence agencies should try to infiltrate terrorist groups to understand their intentions and plans for their next target. Aeroplanes and airports have always been high priority targets for terrorists. Aviation security is costly, tragic and lasts. It is one of the targets where terrorists can affect such enormous numbers of a country's population.

Aviation security is required to be cooperative work between different organizations, which include international and national organizations, airport ground staff operators, airline staff and government teams such as police and intelligence agencies. All have one goal, of providing safe and secure services for travellers to travel without any difficulties to strengthen the economy of the country. In airports the airline staff are obliged to check in the passengers' baggage and screen them; some airlines hire private screening companies to do this job. The airport ground staffs are responsible for the airport's general policy for internal and external security. The screening officers are sometimes hired by the government or by the airport itself: this depends on each country's policies. For example, Dubai airport only hires locals for the screening.

Governments control the security covering who comes in and who goes out through immigration and other police departments. Also they provide intelligence information to the airport to block or catch terrorists or criminals. Governments correspondingly support the research of new policies to be implemented, and technology research to enhance security such as security screening.

Since the start of civil aviation security, its programme has always been designed around detecting, preventing, or mitigating terrorist threats in relation to trivial amounts of explosives and personal weapons. Also it has been based on a number of principles, as argued in [143]. The key aspects of these principles are divided into:

1. Terrorist intrusion of civil aviation premises should be completely prevented, and that is the role of intelligence including police and government intelligence.
2. A strict policy or procedure combined with technological detection systems to prevent any terrorist from breaching the front line of security at the aviation premises.
3. Damage control procedure: if the terrorist succeeded in breaching step two of the security line, then the aircraft system and structure must be robust enough to minimize the damage.

From the illustrated security breached history of aviation security, it was important to invest in scanning equipment research and development. Following the 11 September attack the US Committee of Commerce, later Transportation, and USA Senate has formed to discuss: 1) computer aided systems used for aviation security; 2) access control of airports; 3) screening of passengers and their baggage, and how US systems are different from other countries.

In 2000, the committee identified that the key aspect of the problem is the weakness of the screeners. This is because of the huge, unbearable amount of work to check every bag by the screeners. There is a high turnover in screening staff, mainly because of limited benefits, low salaries and a boring repetitive style of work.

This concludes that there will always be a problem with human factors when screening passengers, and, in the USA, the Federal Aviation Authority (FAA) proposed the use of threat projection software deployed in the X-ray screening machine to keep the screener on alert if illegal objects were detected. Moreover this software monitors the screener's performance and actually certifies the screener for employment in the screening employment.

All the previous discussion confirms that screening is a vital issue to enhance security against terrorism and smuggling. The recent terrorist attacks have strengthened the research in finding new technologies to image inside human bodies and to detect illegal materials carried with passengers.

7.3.1 Importance of airport security

Airports are vibrant parts of the 21st century framework, demonstrating current growth and the existing procedures of globalization.

In 2013, the aviation industry opens up the UK to the worldwide tourism market, with incoming tourists putting almost £19bn into the UK economy [144].

The airline industry is a major industry that employs around 8.3 million people, and supports 15.1 million jobs worldwide [145]. Airports are an essential infrastructure of the transportation industry, where passengers use them daily. In Geneva, as an example of the growth in passenger numbers, the International Air Transport Association (IATA)

has released a report showing a strong growth of 6% year on year growth. Tables 7.1 and 7.2 show such growth compared with 2012 in detail.

Table 7.1: Passenger Growth Analysis

June 2013 vs. June 2012	RPK Growth	ASK Growth	PLF
International	5.9%	5.7%	81.4
Domestic	6.1%	5.2%	82.0
Total Market	6.0%	5.6%	81.7

Table 7.3: Passenger Growth Analysis

YTD 2013 vs. YTD 2012	RPK Growth	ASK Growth	PLF
International	4.8%	4.0%	78.5
Domestic	4.6%	3.7%	79.7
Total Market	4.8%	3.9%	79.0

RPK: Revenue Passenger Kilometres measures actual passenger traffic;
ASK: Available Seat Kilometres measures available passenger capacity;
PLF: Passenger Load Factor is % of ASKs used

Source: The International Air Transport Association (IATA)

With the growing number of travellers throughout the world, airports are critical targets for terrorist groups. Therefore technologies in the field of security are racing to overcome such attacks to manage the terrorist events before they happen; this is called critical security management. Passengers are using airports on a daily basis, which makes it a critical source of wealth to the country and improving the economy by increasing employment for people.

Passengers take the luxury, benefit and easy operations of these substantial and progressively complicated facilities for granted. However, modern passengers would also like to see no queues or delays in airports. Both security and delays in airports could have an impact on the country economically and politically. Following the 9/11 terrorist acts, all security regulations and laws and technologies in airports have been changed. These changes include 100% of passenger's baggage being screened through

explosive detection systems [128]. Sophisticated safety and security programmes have to be constructed to meet the highest level of security.

7.4 SUMMARY OF CURRENT AIRPORT SECURITY CHECKS WORLD WIDE

Most airports currently have several layers of security screening. It starts when the traveller comes to the check-in area where identification is required. They then answer some security questions from the check-in desks, such as the contents of their bags and if someone else has touched their bags. Once the passenger leaves his luggage at the check-in area he is allowed to take a certain weight of any hand luggage, including not more than 50ml of liquids. After this he goes through a checkpoint where, in some domestic European airports such as the UK and Ireland, a photograph is taken of the passenger before they reach the metal detection gate. There are several lanes containing metal detection gates and X-ray scanners to view the passengers' carry-on baggage. Liquids and laptops are taken from the carry-on baggage and screened separately for better visualization by the X-ray scanners. These X-ray scanners view a 2D image and, if the screener has suspicions about the carry-on baggage, then this baggage only will be checked manually by another officer. After this the traveller goes through the metal detector; if there is an alarm then he will be further checked by a pat-down search. If the traveller is suspected of carrying anything dangerous he goes through another human X-ray scanner to view the location of the detected alarm and further investigation. If not, then the passenger takes his screened carry-on baggage to the duty free and then to the plane.

Recently millimetre wave gates have been implemented in some UK airports, such as Gatwick. These are behind the walk through metal detector and are used for external

checks, as shown in Figure 7.2. These new millimetre wave systems require an extra person to check the screen of the system to see if there is contraband material held by the traveller: this is an extra cost for the airports.

Figure 7.2: Millimetre Wave System Used in Gatwick Airport

The baggage left by the passenger at the check-in area after weight allowance control then goes through an Explosive Detection System (EDS), which uses computed axial tomography (CAT). The image resulting from the scanned baggage is then sent to a human screener for final review and analysis before loading in the aeroplane. If there is something suspicious in the baggage then another security officer has to search the bag or deal with the baggage depending on the analysis of the images.

7.4.1 Screening of baggage

The European Parliament and council regulations for civil aviation security require all travellers and their luggage to be screened using available security screening machines [129].

Almost all European airports operate dual-energy X-ray systems to screen baggage that is held by passengers or left at the check-in area. The operator is able to visualize the images by these X-ray systems using a pseudo colour technique to differentiate between different material colours. Computed tomography (CT) machines are also implemented in some parts of European airports; these show the baggage in 3-D and can be rotated through 360 degrees. The hand luggage is screened using dual-view or multi-view.

All existing dual-view and multi-view X-ray systems, and CT show the cutting edge of such technology. These systems are equipped with very useful software such as an Image Enhancement Function (IEFs), image storage and Threat Image Protection (TIP). All this state-of-the-art software can be turned on or off while screening. IEFs are used to recognize and analyse the image more carefully, such as edge-enhancement, colour inversion, organic only and metal only, etc. Nevertheless, some researchers question the effectiveness of such software because the best recognition of the image is the original image [148], [149]. Image storing functions are used for the benefit of data storage and are to be used when necessary. Every nation has their own national law for data storage; therefore the operation of such software differs from nation to nation.

TIP has been seen to be the best function to help operators in their decisions on selecting bags with threats. TIP depends on using stored threat images to cross-check passengers' baggage, both cabin and hold bags. Fictional Threat Images (FTIs) are selected by computer to be immersed in the passenger's cabin bag image. For the hold

bags, the computer selects Combined Threat Images (CTIs) and Combined Non-Threat Images (CNTIs); these are also immersed in the real images of the hold bags.

TIP can increase the prevalence to decrease the miss rate done by the screeners. In signal detection expressions, the prevalence can be described as a measure of alteration and not an adjustment in sensitivity. A system of short-term retraining times with high prevalence and full evaluation grants the screeners the ability to embrace a good measure during times of low prevalence with no evaluation [150]. Where low prevalence in the case of cabin bags is limited because screeners can correct their mistakes and catch it, in the case of hold bags it is not possible for the screener to catch their mistakes [151]. It is also known that vigilance is described as observance, physical readiness to respond or react during visual searches decreases over time [152], [153]. TIP also shows messages of how efficient all screeners are in the screening process.

Even though X-ray imaging technology has been established for more than 41 years, it still has its limitations in penetrating high density machines. Modern passengers travel these days with their mobile phones, mp3 players, or iPad, and all these come with their cables and chargers that show more complex images to the operator. Research shows that if a laptop remains in a passenger’s bag it could prevent other items from being clear to the security officer, and it showed that laptops being screened separately provided screening officers the greatest screening practice [154]. All these electronic devices and their batteries could be similar to an improvised explosive device, therefore the operator at this point has to open the baggage manually to make sure it is not a contraband device or material.

At the moment X-ray machines were invented for the purpose of speeding up the security check process. However, the speed of any security check also depends on these

machines' belt movements and the time taken by the security officers to analyse the image. Therefore the issue here with current X-ray machines depends on human interaction with such a technology or any other new developed technology.

7.4.2 Passenger screening

As discussed earlier in the current solutions of airport screenings, there are two types of human body scanners: ionizing radiation such as X-ray systems or non-ionizing radiation systems such as terahertz and millimetre waves. They are active and passive systems. An active system emits radiation to screen the passengers and a passive system receives radiation from the passengers to visualize their bodies. However, there are privacy and health concerns from using these body scanners on human bodies. In America it is routine to use these scanners, but in Europe the law is still strict on using these scanners on passengers.

Ionizing scanners have been proven to use a very low radiation dosage, which is less than 1% of the dose a flyer will receive from exposure to cosmic rays at elevated altitudes. Therefore there is no threat of radiation from the scans according to [155]. Consequently there is no risk at all from a non-ionizing system, similar to millimetre waves, or my developed system in the earlier chapters. The process in human body screening using ionizing technology such as X-rays is to view an image of the screened person by the screener who actually interprets it to see if that person is carrying something illegal. This is thought to be revoking people's right to privacy as stated by the European Union and other privacy protection groups.

Recently new European Union regulations have been amended to allow non-ionizing body scanners to be used in European airports [147]. Millimetre wave scanners using non-ionizing technologies have solved the privacy problem by developing ATR

(Automated Target Recognition) such as millimetre waves. The body of the passenger does not appear, only a dummy photo with the location of targets, if there are any. On the screen of the imaging of mmw, if the passenger has no suspicious material concealed within his body the screen shows OK with no image. However, if there is anything it will be highlighted in the pictogram and a pat-down search will be carried out by the security officer. Figure 7.3 shows the resulting image from a millimetre wave scanner.

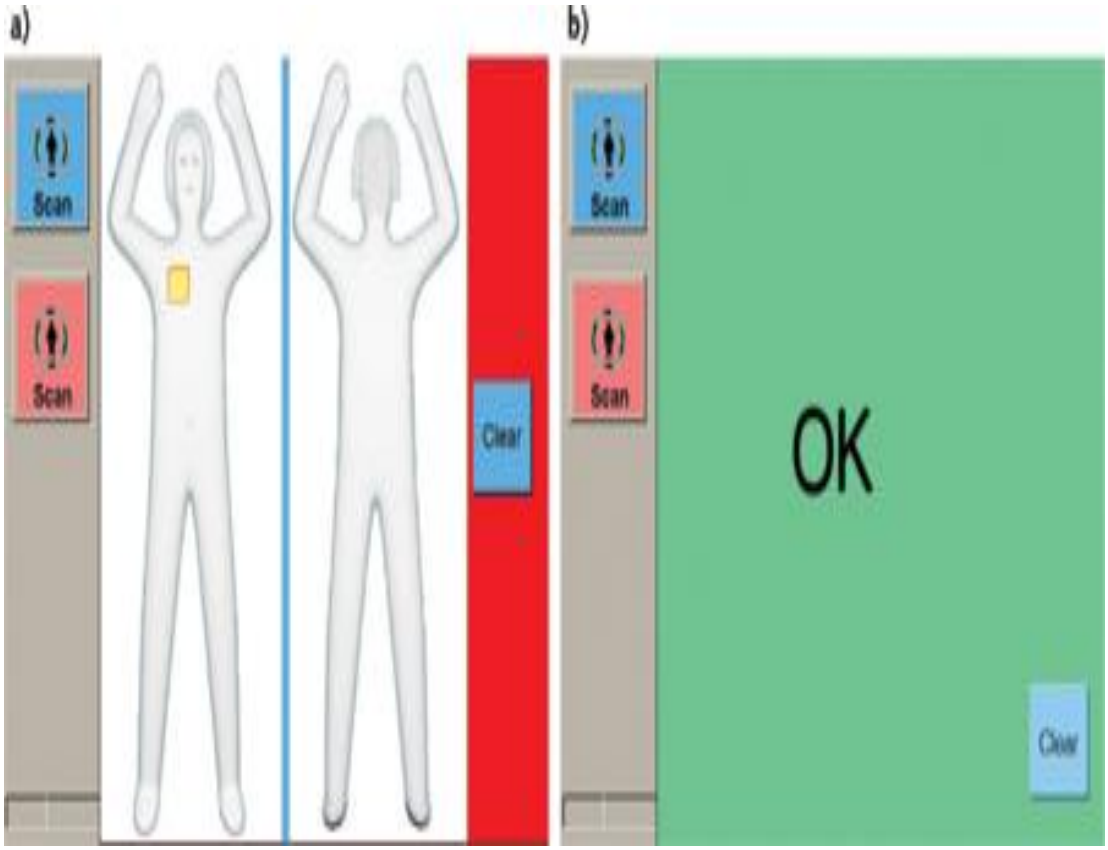

Figure 7.3: a) Shows the Location of a Possible Threat using Millimetre Wave, b) is Showing OK Sign to the Operator

However, using non-ionizing technology with ATR alone will not solve privacy concerns unless there is some kind of policy implementation within both technological and operational procedures.

As seen from the above discussion, one of the main concerns to people is privacy; the second concern is the radiation. However non-ionizing systems are no risk to passengers; in addition, the ionizing X-ray body scanners used for people in airports are also safe, but extra care has to be taken when children and pregnant women are scanned [155], [156].

Privacy concerns have been initiated and argued by the public and European Union since the first generation of X-ray systems, which show the full image of the person being scanned and interpreted by the screener. The image of a scanned person viewed by the screener in detail to look for contraband material in the image formed faced a complete rejection by the European Union. Research has been undertaken to see the balance between security and privacy invasion to people. Air travellers would like to travel safe from any terrorism; at the same time their privacy and health should be considered. Some religions have to be taken into account regarding the privacy issue.

Studies show that security officials, such as Transport Security Administration (TSA), should provide air travellers with an educational campaign about the privacy and health issues with new scanning machines [157], [158]. The balance of security and other issues could be discussed and agreed depending on the time and the circumstance for using ionized scanners.

As explained above, millimetre wave scanners have solved the issue of privacy, however, they do not store the images scanned [159]. In general, all of the above discussed scanners have their own advantages and disadvantages. The advantage of ionizing scanners is that they can provide a better resolution than non-ionizing scanners. The disadvantages of the ionizing scanner are privacy concerns, health concerns from radiation emitted, and the comprehensive training required for the security officers to

interpret the images formed. The advantage of non-ionizing scanners is that they are safe for health, there is no privacy intrusion as discussed, and less training is needed for the screeners. On the other hand, the disadvantage is lower resolution, which could miss contraband material that could be implanted in the human body. Finally security scanners have a substantial effect on humans (air travellers and screeners), security, throughput, process (policy and pat-down) and cost.

7.5 FACTORS AFFECTING SECURITY SYSTEMS

No matter how the technology has been developed, there are factors that can affect the process of security control. State-of-the-art technology can always help in the detection of contraband objects carried within people, and minimize the effect of other factors such as external factors and internal factors. External factors can always affect the security control, such as seasonal variety for airport security. For example, passengers will travel with heavier clothes in winter and carry more baggage with them; this results in more security checks or poor image quality of screened objects and will be more challenging for security operators to analyse. Internal factors that affect the security control will be the human factors both as a security operator or passenger's interaction with new technologies.

To shed light on the human factors in security control, there is the story of the TSA undercover bomber who succeeded in going through two security check points at Newark Airport USA, even though the undercover bomber carried an improvised explosive device stuffed down his pants: he also went through a pat-down search [41]. In addition, privacy and health issues were one of the main issues to be considered as factors to new security technologies.

From the above history and reviews of airport security systems, the problem still exists if any terrorist is hiding contraband materials inside his body. Moreover, although changes in security regulations and technologies have been accomplished and enhanced to be effective in detecting any terrorist act, even the consequences of this are complicated, such as delays and spending more time inspecting passengers in the airports [30]. One of the main problems that aviation security faces over a long period is detecting dangerous objects planted within a human body with clear images. Technology alone cannot do this, without security screening personnel who received the blame for poor performance. This is because of poor training and low salaries for the screeners [31]. Technologies in security could be anything from cyber security, biometric and screening technology. Our main focus in this thesis is screening technology, which has the following issues;

1. health issues;
2. privacy issues;
3. space issues due to machine size;
4. human interaction with new technologies;
5. traffic issues caused by delays in screening;
6. New technologies integration with existing technologies.

7.5.1 Human issues in scanning technology

Human factors should be included and considered in the design of scanning machines. For instance, there is a problem with detection by some screeners and this is due to image based factor view difficulty as illustrated in [160]. Viewing luggage and its contents, as well as the X-ray machines are the main factors for these difficulties. This could be solved with more computer-based training. In addition, the new X-ray

machines or any other systems with a multiview function could reduce the detection problem.

A dark alarm system has been implemented in X-ray machines to warn the screener if a dense area in the bag has exceeded limits, and a manual search has to be done at that point. The visual ability of the person is one of the factors that can affect the detection problem, but this could be solved by better training on computer-based object recognition [161]. Knowledge of the contraband materials and how they could look is also a factor. Visual ability is stable but knowledge ability is built up with time. Therefore more training is needed to keep the screeners more efficient and updated [143]-[145].

However, assessing the screener's visual ability is required before employment, and some research has demonstrated that it is important for the manager to asses screeners before they employ them using an object recognition test tool (ORT) in X-ray systems [164]. After assessing the screener, there is also a national standard test that has to be taken, as well as computer-based training as identified in [165]. Moreover, some European countries carry out a competency assessment test annually to certify the screeners, to make sure that they are capable of interpreting images from X-ray machines [166].

Although this cutting edge technology has been extensively developed and innovated, research today has moved towards whole system performance, management and leadership, operational factors and motivation of the screeners. The human factor with security was always the weakest link in today's security process, therefore training is needed in leadership awareness and team work for any security control process. There are already studies focused on the training and competency aspects [167]. Also covert

testing in security control is shown to be effective in enhancing security measures in the field of airport security. Covert testing is part of the training to the security personnel to deal with dangerous situations and give them the ultimate preparation if there are real threats [168].

7.5.2 Privacy

Privacy is seen as a vital human right. There is no specific definition of privacy, but it normally includes the right of an individual to keep his private sphere, such as body, home, property, and identity. A person has the right to be left alone [169]. The protection of privacy is seen as how far outsiders, such as the government or any other society body, can interfere in someone's private property.

In airports, security scanners can reveal sensitive information about the scanned passengers. This could be medical details or any other private areas within the body that could cause embarrassment to the scanned person. Researchers still argue whether a physical pat-down search or 3D full body image is violating the privacy of the person. It seems that a full body image that could be transferred or saved on the web invades the person's privacy more than physical touching during a search [170].

New screening technologies used in security applications ensure safety for passengers and increase security. However, questions are always being raised about their clear images that violate the privacy of human bodies. Full naked body images produced by these technologies invade the privacy and the physical integrity of our bodies, which results in an invasion of our human rights and dignity. Body scanners, such as millimetre waves and backscatter X-rays, use the most advanced and least invasive technology, and seem to be quicker for passenger inspections. However, they have

always been criticized, and concerns have been raised by privacy advocates, data protection authorities and different parliaments.

The approach detailed in this thesis in imaging the human body using microwave technology would be similar to the approach using millimetre wave technologies, but with a different frequency range. Therefore it is worth illuminating the issues arising from these advanced technologies and look at the possible solutions to minimize the threat to individual privacy.

The security of the aviation industry is set by an agency called the International Civil Aviation Organization (ICAO), but they do not give any guidance about body scanning technology. They are aware of privacy and other issues that conflict with society's interests when using body scanners. From the legal side, by using these scanners an image has already been captured, processed and stored, which breaches both data protection rights and the human rights convention, such as the Universal Declaration of Human Right 1948 (UDHR).

If a passenger chooses not to go through these body scanners then he has to face the consequences such as not flying, further questioning or a different method of passenger search such as a pat-down, which controls the freedom of the passengers. In Article 13 of the UDHR, every person has the right to freedom of movement and residence within the borders of each state. Everyone has the right to leave any country, including his or her own, and to return to his or her country [171]. In Dubai airports authorities did not agree to the deployment of these scanners and they are against these advanced body scanners. This is because, according to Arab culture and tradition, these advanced scanners show the whole body, which is a violation of human rights and sanctity. In addition the effect of these body scanners on human health is not yet known, although

they say the scanners use very low dosage radiation, a person has the right to fear unknown effects on his health.

In the end, no matter how these technologies can save lives of passengers and crews, a person has to consider whether his right to life and freedom will not conflict with his right to dignity and privacy. One example occurred in Nigerian airports on 21 September 2010 when security officers who were trained on the 3D body scanner abused the use of the scanners to see female images [172].

A person has the right not to be exposed to these scanners, but if that happened in the USA the passenger would be searched through a pat-down search and metal detection walk through gate.

In the UK, passengers have the right to opt out from these scanners, but they have to agree to a manual search or they will not be able to fly [173]. In the UK, ministers are facing pressure to legislate that children under the age of 18 do not have to be scanned as scanning is against child pornography laws. However, at the same time consequences might lead to terrorists recruiting children for their operations. In Europe there is no alternative search method if a passenger refuses to go through body scanners installed at that airport.

Passengers are also questioning why 3D body scanners are not deployed in all ICAO member states but only some of them. Also the effectiveness of these scanners was questioned since Hassan Ali Al-siri planted in himself half a kilo of explosive, which he then detonated while sitting negotiating with Prince Nayef of Saudi Arabia. Also the underwear bomber, Umar Abdualmutallab, flew from Amsterdam to Detroit with a hidden plastic bomb in his underwear: Schiphol airport had 15 body scanners at that time.

The following paragraph will discuss how to overcome the privacy issue. Some companies such as TSA have used Advanced Imaging Technologies (AIT) to search passengers at an airport; some of these AITs are backscatter X-rays and millimetre wave systems. Millimetre waves are currently equipped with privacy software called automated target recognition based on the types of the target concealed under clothing of humans. Backscatter systems are not equipped with this software; this is why backscatter X-ray systems have been removed from most American airports until privacy software has been developed.

Microwave body scanners could follow the same steps by integrating filter software to avoid privacy concerns. Millimetre wave technology has ATR (Automated Target Recognition): the body of the passenger does not appear, only a dummy photo with the location of targets if there are any. In the screen of the mmw image, if the passenger has no suspicious material concealed within his body the screen shows OK with no image. However, using AIT systems with ATR alone will not solve privacy concerns, unless there is some kind of policy implemented in both technologies and operational procedures. Policies on the AIT systems could be such as disabling the data storage on the same screening units, remote imaging location so the screener cannot see the image of the passengers. TSA also prevents its screening personnel from taking any recording devices with them. A clever privacy filter installed in the AIT units blurs facial features or provides a less detailed image of the human body; this will help to reduce privacy concerns.

Despite taking all the above cautions, still there were complaints that some passengers had been screened repeatedly, and TSA replied in its policy not to screen any passenger twice. Above all 100% security cannot be achieved, even if the machines neglect the role of privacy.

Body scanners can do the job of security, but future developments of screening systems should include an intelligent system to study the behaviour of the passengers as soon as they enter the airport, and make a probability calculation to detect and screen people who might be a terrorist. At the same time, this intelligent behaviour system could be used to alert security officers and train staff to easily target only suspicious passengers for further screening. Another way of reducing mass screening of all passengers is to profile check passengers, but this will raise concerns of fewer people being searched. From 4 December 2013, TSA created a pre-check program to passengers in most American airports. Pre-approved passengers or low risk travellers will be allowed to move through faster lanes where they do not need to take off their shoes or belts, or any laptops or gels from their bags [174]. Most passengers around the world will see this as a good approach to avoid strict screening or waiting for long periods in queues.

There is still no good answer about whether these technologies can really ensure the safety of passengers against losing their right to privacy and dignity. Therefore it is also very difficult for privacy advocates to win this argument in favour of security standards. Until now governments have failed to create a body scanner policy that takes care of the privacy law. Future policies for body scanner technology should include legal policy and technical measures to regulate scanning, and control the scanners. The expectation of the new technologies should take into account privacy issues and data protection, or develop alternative solutions to tackle the privacy problems.

Passengers should be fully notified with the information about scanning machine technology so that they can determine their right to privacy. Before deploying new scanning machines in airports a review from authorized companies, government bodies and individuals should be made available for the public to read and be informed. The manufacturer or the creator of scanning machines should be aware of the legal issues

associated with privacy that could be raised by law. These legal measures include image capture, storage, copyright, system encryption, password and complex identification/authentication mechanisms. Furthermore, the ICAOs could take body scanning measures seriously and start to link them with a human's right to privacy.

7.5.3 Traffic management or basic queueing notation

More security developments in airports have created long queues. Tight security has also caused increases in the cost and time wasted on screening non-threatening passengers, and passengers get frustrated from longer screening times. To manage such complex queues a trade-off and balance between maximum security and screening times has to be achieved. There are a number of strategies to achieve effective security and timing, such as selection of technologies or combination of technologies when it comes to screening technologies selection [175]. Moreover there are strategies developed where passengers will be screened depending on a passenger pre-screening process [176].

A multiple level of screening has been examined and proposed according to passengers' risk levels [159]-[163]. The literature provided an overview of queueing models that have focused on minimizing the number of passengers, and minimizing the time a customer spends on each security system [164]-[169]. A reasonable approach to tackle this issue could be a study by Harrison and Wein where they separate passengers as type A to go through one station alone, while other passengers, type B, goes through two stations. They classify passengers as they arrive to be chosen to be screened differently according to their dynamic policy: this minimizes the number of customers per system [188]. Moreover, research by Schwartz shows that a freedom lane selection by passengers could work better than any conventional way. That led them to develop a

static model to calculate the number of passengers and length of time at each lane depending on the class of passenger [189].

Recent research has developed a static simulation framework that makes use of the selected passenger lane depending on the neighbourhood search procedure, which succeeded in the selection of 4% probability of true alarm than the usual passenger selection lane programme [190]. The key problem when it comes to aviation security is time and security efficiency; therefore Lee and Jacobson have solved such a problem by modelling a number of policies and programmes. These are:

1. a queueing program for multilevel check point security systems in the airport made from specialized screening devices;
2. obtaining a steady state policy to minimize the time passengers spent on security systems;
3. developing a dynamic policy that analyses the balance between true alarm probability and the amount of time spent on security systems;
4. The classification of security systems into two classes, instead of the conventional primary and secondary level of screening. The two class system has proved a high throughput of passengers screened with less time for each passenger in the security system [191].

Future queueing strategy has to take into consideration the special processes to tackle time length and queueing length depending on the security levels of screened passengers. For instance, a true alarm passenger has to go through a different security class for strict screening and investigation, while lower risk passengers can go through a different security class, then it will take less time for all overall passenger security screening.

7.5.4 Hazards of microwaves

The above research has investigated whole body scanner technology, which they operate in a type of frequency such that their energy per photons is not sufficient to ionise molecules or atoms: this is non-ionised radiation. This scanner technology can image inside the human body and clothing for any hidden contraband materials.

In general, whole body scanners would be X-ray backscatterers and millimetre wave scanners. The above microwave technology research has investigated lower frequencies than millimetre wave scanners, where millimetre wave uses frequencies from 30-300GHz. Millimetre waves are so called because their wavelengths are 3-10mm in air and they take 2-5 seconds to complete a multi-directional scan. To educate ourselves more on such allowable effects on human bodies, a good reference of this statement is available on the International Commission on Non-Ionising Radiation Protection (ICNIRP) [192] and IEEE standards [193]. It is known in radio frequency that the absorption of RF measured as Specific Absorption Rate (SAR) within a given tissue mass. Therefore SAR is a quantity to measure the dose of RF in human bodies. The radiation quantity of SAR exceeding 4W/Kg is required to harm human tissues in the range between 1MHz and 10GHz. The microwave scanners are a pulsed operated mode, which will generate a low level of power density. For example the power densities for millimetre wave scanners are 1kW per metre square, which is almost one-tenth of the acclaimed guidelines for the general public.

To conclude the above subject, to date there are no known health effects from pulsed microwave scanners or millimetre wave scanners according to the Food and Drug Administration in the USA

7.5.5 Security and efficiency enhancements in airports

Firm security in scanning systems means an image of forbidden materials carried out with passengers from boarding to an aircraft or even allowed to travel. Effective efficiency means imaging the baggage of passengers using imaging systems without using a manual search method for faster operation. In order to do this, a cutting edge technology should be developed to achieve firm security and effective efficiency.

X-ray systems at the moment are developed to view baggage without human interaction unless necessary. However, even with these technologies available there are still challenges to meet high security and high efficiency. The demonstrated microwave imaging system could enhance both aspects. These technologies are in the hands of security officers who image passengers to ensure that the security is fast, not missed and producing fewer false alarms. Also there is stress caused by passengers needing to catch their flights.

To achieve security and efficiency in airports, the scanning needs to be accurate and fast in order to achieve a smooth operation and achieve passenger satisfaction. A study proposed that screeners should work on a single goal or dual goals such as speed and accurate security. It seems that when screeners work on one goal, they achieve it in favour of the other factor. For instance, if they focus on speed scanning there are errors in the scan. But if they focus on dual goals such as speed scanning and security accuracy, that slowed down the scanning operation and made the security more robust. Therefore both goals have to be managed together, as long as both goals do not affect their mental or emotional levels [194]. This means that there is a balance between speed and security accuracy that should be taken into account to reach both goals.

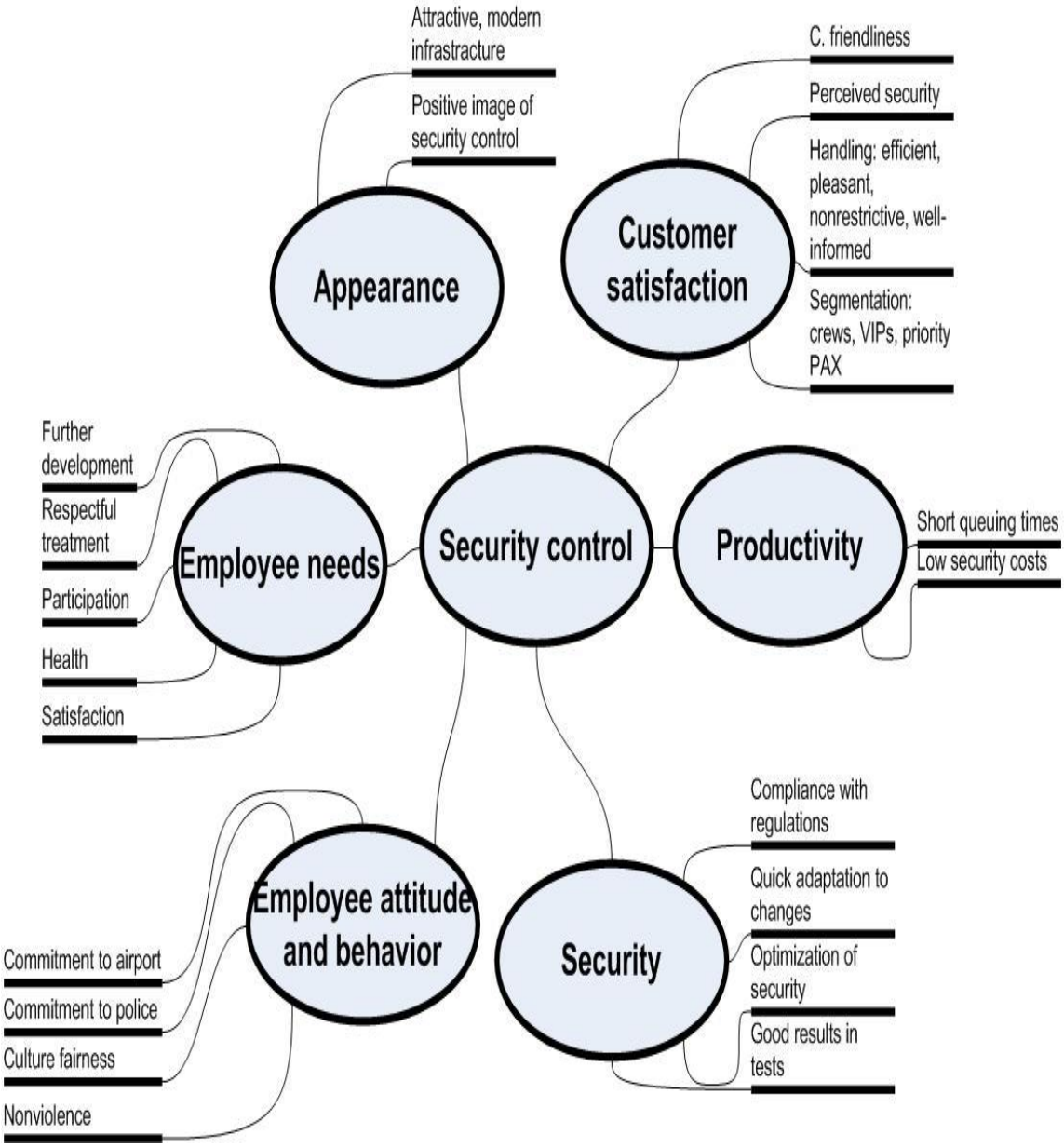

Figure 7.4: Adapted from [195]**. Displays the Six Goal Domains and the 21 Objectives Agreed by Airport Managers**

Accordingly, the legal constructions of an airport should consider the balance of security, safety, costs, operation and privacy to manage a complicated operation overall. It has become a nationwide priority that measuring productivity of an organization should come before improving it. Therefore, to measure the balance of an airport's complex operations, a system called Productivity Measurement and Enhancement System (ProMES) could be implemented [195], [196]. ProMES can be an excellent

method of setting up system performance management and security control enhancement.

Managers of airports should rely on a holistic approach to decide on investing in new security scanning technology. This approach carries out a laboratory test, field test and stress test as demonstrated in [197]. The earlier proposed microwave research should refer to this approach for future development.

7.5.6 Future imaging security in airports

Future imaging security such as X-rays and CT scanning machines could be developed to have higher resolution, be reliably fast and cost effective. This is why this thesis discusses the latest techniques in image reconstruction algorithms using microwave techniques. Automation research is gradually increasing in imaging scan technology. It is already executed in the hold baggage scan, and soon possibly it will be implemented in the scanning of cabin baggage.

CSIRO and Nuctech Company Limited developed automated systems to detect the shape of contraband materials such as chemical materials, explosives, narcotics and other organic threat materials smuggled through cargos. They looked for future development on the system to be faster in scanning for larger volumes of cargo and improved image resolution [198]. Figure 7.5 shows the prototype of the system. Automated detection is a useful function in the system, but the detection should always executed by a human. Machines could always give a false alarm and therefore screeners will not trust the machine; on the other hand, sometimes screeners will think real threats are false alarms and that could have tragic consequences.

New European laws urge researchers to find ways to detect gels or liquids. X-rays and CT scanners can visualize this easily without the need for automation, but it is a helpful

function to differentiate different types of materials from each other, such as contraband materials. Deploying new scanning technologies will change the job requirement of the screeners, or sometimes new technologies will not need screeners to sit beside the device itself. This is called remote screening where one officer can control all the images passed through scanning devices in one control room somewhere in the airport. This has been already deployed for hold baggage and in the future it could be executed for cabin baggage. This remote image control can save time, is cost effective, and has an advantage of focus for the screeners to have a quiet and pleasant environment to focus in their image analysis. The only disadvantage of this innovative method that is the screeners will be far away from the passengers and the baggage to be scanned, which will make it hard for the screeners to call the passengers if there is a real threat or even have access to the baggage.

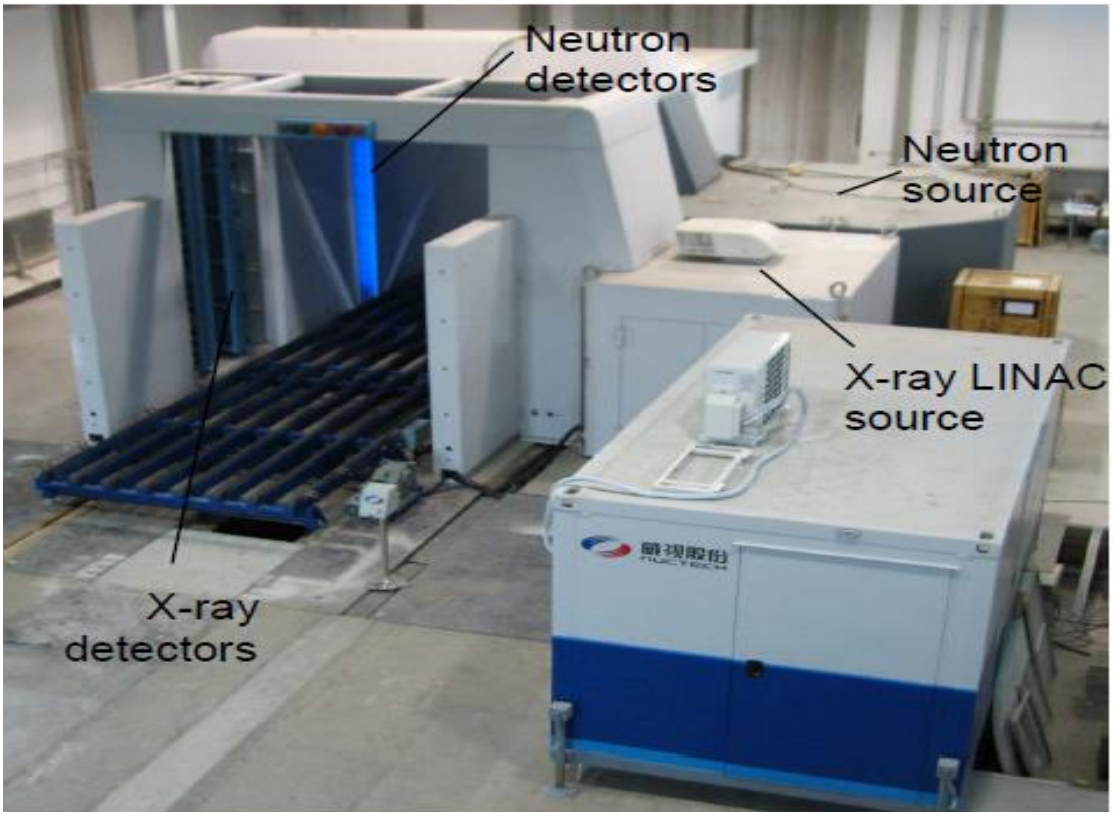

Figure 7.5: AC6015XN Air Cargo Scanner Developed by CSIRO and Nuctech Company Limited

7.5.7 Security systems integration

Airport security systems have been integrated in different ways internationally depending on the size of the airport and the country those airports are. The airports in the USA were equipped with high end technologies because of the threats received after 9/11. The regulations and rules have been changed since then, and much research has been carried out to develop airports in a smarter and more cost efficient way.

An example of exact data has been taken from the website of TSA (Transportation Security Administration). This states that they operate and manage more than 781 check points across US airports, with more than 43,000 transportation security officers [199]. This means a high cost for the TSA of approximately US$3 billion a year. Although this is a high cost of security spending at the checkpoints, an undercover test made by TSA officers at Los Angeles international airport and Chicago O'Hare International Airport, showed failure to detect contraband materials of between 60% and 75% [200].

From the above facts, the outstanding problem is still how to integrate all security screening technologies and methods with the existing airport systems to deliver better control of security with reduced current operational cost. Therefore screening in airports should be integrated with other security systems to have an effective tool for the better detection of suspected terrorists or smugglers. Pre-screening checks should be integrated with the screening systems to decide on who to screen and which baggage to concentrate screening on. Screening results should be integrated with the main security control officers for analysis and be integrated with other security systems such as facial recognition, CCTV in airports, and behaviour analysis systems.

Chapter 8: **Conclusions**

8.1 CONCLUSIONS

This thesis took the race into the development of microwave imaging in the field of the security systems. The research purpose was to image contraband materials hidden or implanted within human bodies. To this end it was proven that microwaves can image inside a human body using a state-of-the-art imaging algorithm called Time Reversal Multistatic Signal Classifications. It was important to carry out research on a technology that is less harmful and human friendly to be used in scanning people in airports, or securing VIP sites from any terrorist acts or smuggling.

The research in Chapter 1 conducted a comprehensive literature review of microwave imaging use in the field of medical and security applications. Then an understanding of microwave interaction with human bodies in Chapter 2 gave the opportunity to image different dielectric properties that could be hidden in the human body. A lumerical FDTD solution was used to gather scattered field data from objected microwaves in different type of targets. Choosing a TR-MUSIC algorithm as an imaging reconstruction method to reconstruct images from scattered fields of microwave rays objections on the target was explained in Chapter 4. A simulation showed successful imaging results in a simulated cross-section using microwave rays by both a radon transformation algorithm and TR-Music algorithm.

The above research was conducted by simulation using lumerical FDTD solutions to gather the data and then processed through a state-of-the-art TR-MUSIC algorithm using Matlab code. A simulated cross-section with an object inside them assumed to be

a human torso cross-section with different dielectric properties. In TR MUSIC it seems that the higher the frequency the better the resolution, as shown in Chapter 6.

As simulation showed successful results, a possible experiment explained in Chapter 6 could be set up in the future to gather the right results to be investigated. Also a prototype of such a system could be implemented. The limitation of my successful results showed that a real prototype should be built and implemented to gather real data rather than simulation. A real experiment in the future will prove the concept of microwave imaging. Practical experiments in this field would always be suitable to show practical evidence that microwave imaging is happening, and will give a strong reason to commercialize the system and build it in the future.

As technology proved to be successful in imaging, particularly in scanning systems, Chapter 7 therefore discussed the scanning security system management used in airports and how new technologies could be managed by airport management and operators. Most current scanning systems suffer from privacy and health concerns for passengers. All these aspects have been discussed to give the reader experience on how security is handled in airports, and how to manage security from any terrorist act or risk that could cause countries to have a major economic crisis.

Finally, this thesis proved that microwaves could be used to image inside the human body, and that this technology could be developed in a real system in the future to be used for security applications. This technology has been discussed to be suitable for a scanning system to replace X-ray systems used in airports. Microwave systems are non-ionized, safe, protect passenger’s privacy, and provide clear images of objects inside human bodies.

8.2 RECOMMENDATIONS

It is recommended in the future to execute the experiment set up in Chapter 6 to collect real data on modelled targets. Practical results will then be available to provide robust and accurate information to lead to the development of a real prototype.

It is recommended that a real prototype system should be developed to enhance this type of research area. It is also recommended that microwave imaging techniques discussed in this thesis could be combined with other technologies for better imaging results, as seen from [201]. Combined images from different technologies plus microwaves in one system will lead to a more informative image that will help the operator to obtain a better analysis.

After successful prototype development, extra software for privacy protection could also be developed to be integrated with the prototype to show attractive solutions for airport body scanning systems.

It is recommended also to develop a video-based system to be added to the current system to enhance the security imaging.

It is recommended that this system could be integrated with other security systems in the airport for better security management.

References

[1] P. T. Huynh, A. M. Jarolimek, and S. Daye, “The false-negative mammogram,” *Radiogr. Rev. Publ. Radiol. Soc. N. Am. Inc*, vol. 18, no. 5, pp. 1137–1154; quiz 1243–1244, Oct. 1998.

[2] G. Ku and L. V. Wang, “Scanning microwave-induced thermoacoustic tomography: Signal, resolution, and contrast,” *Med. Phys.*, vol. 28, no. 1, p. 4, 2001.

[3] J. Kieliszek and R. Kubacki, “Analysis of Penetration Depth of Carrier Frequency and Harmonics of Pulse Modulated Microwaves in Biological Structures,” in *International Conference on Microwaves, Radar Wireless Communications, 2006. MIKON 2006*, 2006, pp. 287–290.

[4] S. Kumari and S. Raghavan, “Biological effects of microwave,” in *Information Communication and Embedded Systems (ICICES), 2014 International Conference on*, 2014, pp. 1–6.

[5] M. Jirousek, M. Peichl, and H. Suess, “A new microwave aperture synthesis radiometer for spectral imaging,” in *Microwave Conference, 2007. European*, 2007, pp. 606–609.

[6] C. H. Jones, “Methods of breast imaging,” *Phys. Med. Biol.*, vol. 27, no. 4, pp. 463–499, Apr. 1982.

[7] R. A. Kruger, K. D. Miller, H. E. Reynolds, W. L. Kiser, D. R. Reinecke, and G. A. Kruger, “Breast cancer in vivo: contrast enhancement with thermoacoustic CT at 434 MHz-feasibility study,” *Radiology*, vol. 216, no. 1, pp. 279–283, Jul. 2000.

[8] G. Tricoles and N. H. Farhat, “Microwave holography: Applications and techniques,” *Proc. IEEE*, vol. 65, no. 1, pp. 108–121, Jan. 1977.

[9] J. Jacobi, L. E. Larsen, and C. T. Hast, “Water-Immersed Microwave Antennas and Their Application to Microwave Interrogation of Biological Targets,” *IEEE Trans. Microw. Theory Tech.*, vol. 27, no. 1, pp. 70–78, Jan. 1979.

[10] L. E. Larsen and J. H. Jacobi, “The Use of Orthogonal Polarizations in Microwave Imagery of Isolated Canine Kidney,” *IEEE Trans. Nucl. Sci.*, vol. 27, no. 3, pp. 1183–1191, Jun. 1980.

[11] Y. Xie, B. Guo, J. Li, and P. Stoica, “Novel Multistatic Adaptive Microwave Imaging Methods for Early Breast Cancer Detection,” *EURASIP J. Adv. Signal Process.*, vol. 2006, no. 1, p. 091961, Apr. 2006.

[12] R. N. Anderton, R. Appleby, P. R. Coward, P. J. Kent, S. Price, G. N. Sinclair, and M. R. M. Wasley, “Security scanning at 35 GHz,” 2001, vol. 4373, pp. 16–23.

[13] E. C. Fear, S. C. Hagness, P. M. Meaney, M. Okoniewski, and M. . Stuchly, “Enhancing breast tumor detection with near-field imaging,” *IEEE Microw. Mag.*, vol. 3, no. 1, pp. 48–56, Mar. 2002.

[14] S. P. Poplack, T. D. Tosteson, W. A. Wells, B. W. Pogue, P. M. Meaney, A. Hartov, C. A. Kogel, S. K. Soho, J. J. Gibson, and K. D. Paulsen, “Electromagnetic Breast Imaging: Results of a Pilot Study in Women with Abnormal Mammograms,” *Radiology*, vol. 243, no. 2, pp. 350–359, May 2007.

[15] P. M. Meaney, M. W. Fanning, D. Li, S. P. Poplack, and K. D. Paulsen, “A clinical prototype for active microwave imaging of the breast,” *Microw. Theory Tech. IEEE Trans. On*, vol. 48, no. 11, pp. 1841–1853, 2000.

[16] M. Klemm, I. J. Craddock, J. A. Leendertz, A. Preece, and R. Benjamin, “Radar-Based Breast Cancer Detection Using a Hemispherical Antenna Array

#x2014;Experimental Results," *Antennas Propag. IEEE Trans. On*, vol. 57, no. 6, pp. 1692 –1704, Jun. 2009.

[17] C. Yu, M. Yuan, J. Stang, E. Bresslour, R. T. George, G. . Ybarra, W. T. Joines, and Q.-H. Liu, "Active Microwave Imaging II: 3-D System Prototype and Image Reconstruction From Experimental Data," *IEEE Trans. Microw. Theory Tech.*, vol. 56, no. 4, pp. 991–1000, Apr. 2008.

[18] D. . Woten, M. El-Shenawee, and S. Tung, "Planar broadband dual-linearly polarized MEMS steerable antenna," in *IEEE Antennas and Propagation Society International Symposium, 2009. APSURSI '09*, 2009, pp. 1–4.

[19] D. . Hutchings and M. El-Shenawee, "Fabrication of broadband MEMS antennas and application to target detection," in *2010 IEEE Antennas and Propagation Society International Symposium (APSURSI)*, 2010, pp. 1–4.

[20] R. K Amineh, A. Trehan, and N. K. Nikolova, "TEM horn antenna for ultra-wide band microwave breast imaging," *Prog. Electromagn. Res. B*, vol. 13, pp. 59–74, 2009.

[21] X. Li, S. C. Hagness, M. K. Choi, and D. W. van der Weide, "Numerical and experimental investigation of an ultrawideband ridged pyramidal horn antenna with curved launching plane for pulse radiation," *IEEE Antennas Wirel. Propag. Lett.*, vol. 2, no. 1, pp. 259–262, 2003.

[22] J. Bourqui, M. Okoniewski, and E. C. Fear, "Balanced Antipodal Vivaldi Antenna With Dielectric Director for Near-Field Microwave Imaging," *IEEE Trans. Antennas Propag.*, vol. 58, no. 7, pp. 2318–2326, Jul. 2010.

[23] D. Gibbins, M. Klemm, I. Craddock, J. . Leendertz, A. Preece, and R. Benjamin, "A Comparison of a Wide-Slot and a Stacked Patch Antenna for the Purpose of Breast Cancer Detection," *IEEE Trans. Antennas Propag.*, vol. 58, no. 3, pp. 665–674, Mar. 2010.

[24] M. . Al-Joumayly, S. M. Aguilar, N. Behdad, and S. C. Hagness, "Dual-Band Miniaturized Patch Antennas for Microwave Breast Imaging," *IEEE Antennas Wirel. Propag. Lett.*, vol. 9, pp. 268–271, 2010.

[25] W. Huang and A. Kishk, "Compact dielectric resonator antenna for microwave breast cancer detection," *IET Microw. Antennas Propag.*, vol. 3, no. 4, pp. 638–644, Jun. 2009.

[26] A. Abubakar, S. Semenov, V. G. Posukh, and P. M. van den Berg, "Application of the multiplicative regularized contrast source inversion method to real biological data," in *Microwave Symposium Digest, 2005 IEEE MTT-S International*, 2005, p. 4 pp.–.

[27] A. E. Bulyshev, A. E. Souvorov, S. Y. Semenov, V. G. Posukh, and Y. E. Sizov, "Three-dimensional vector microwave tomography: theory and computational experiments," *Inverse Probl.*, vol. 20, no. 4, p. 1239, Aug. 2004.

[28] Q. Fang, P. M. Meaney, S. D. Geimer, A. Streltsov, and K. D. Paulsen, "Microwave image reconstruction from 3-D fields coupled to 2-D parameter estimation," *IEEE Trans. Med. Imaging*, vol. 23, no. 4, pp. 475–484, Apr. 2004.

[29] Z. Q. Zhang and Q. H. Liu, "Three-dimensional nonlinear image reconstruction for microwave biomedical imaging," *IEEE Trans. Biomed. Eng.*, vol. 51, no. 3, pp. 544–548, Mar. 2004.

[30] E. C. Fear and M. . Stuchly, "Microwave detection of breast cancer," *IEEE Trans. Microw. Theory Tech.*, vol. 48, no. 11, pp. 1854–1863, Nov. 2000.

[31] E. C. Fear, X. Li, S. C. Hagness, and M. . Stuchly, "Confocal microwave imaging for breast cancer detection: localization of tumors in three dimensions," *IEEE Trans. Biomed. Eng.*, vol. 49, no. 8, pp. 812–822, Aug. 2002.

[32] P. Kosmas and C. M. Rappaport, “Time reversal with the FDTD method for microwave breast cancer detection,” *IEEE Trans. Microw. Theory Tech.*, vol. 53, no. 7, pp. 2317–2323, Jul. 2005.
[33] S. K. Davis, H. Tandradinata, S. C. Hagness, and B. D. Van Veen, “Ultrawideband microwave breast cancer detection: a detection-theoretic approach using the generalized likelihood ratio test,” *IEEE Trans. Biomed. Eng.*, vol. 52, no. 7, pp. 1237–1250, Jul. 2005.
[34] X. L. E. J. Bond, “Microwave imaging via space-time beamforming for early detection of breast cancer,” *Antennas Propag. IEEE Trans. On*, no. 8, pp. 1690 – 1705, 2003.
[35] “Microwave Imaging via Space–Time Beamforming.pdf.” .
[36] X. Li, S. K. Davis, S. C. Hagness, D. W. van der Weide, and B. D. Van Veen, “Microwave imaging via space-time beamforming: experimental investigation of tumor detection in multilayer breast phantoms,” *IEEE Trans. Microw. Theory Tech.*, vol. 52, no. 8, pp. 1856–1865, Aug. 2004.
[37] X. Li and S. C. Hagness, “A confocal microwave imaging algorithm for breast cancer detection,” *IEEE Microw. Wirel. Compon. Lett.*, vol. 11, no. 3, pp. 130–132, Mar. 2001.
[38] M. El-Shenawee, O. Dorn, and M. Moscoso, “An Adjoint-Field Technique for Shape Reconstruction of 3-D Penetrable Object Immersed in Lossy Medium,” *IEEE Trans. Antennas Propag.*, vol. 57, no. 2, pp. 520–534, Feb. 2009.
[39] M. El-Shenawee, “Resonant spectra of malignant breast cancer tumors using the three-dimensional electromagnetic fast multipole model,” *IEEE Trans. Biomed. Eng.*, vol. 51, no. 1, pp. 35–44, Jan. 2004.
[40] R. Benjamin, “Near-field spot-focused microwave sensing for the detection of buried land-mines,” in *The Detection of Abandoned Land Mines: A Humanitarian Imperative Seeking a Technical Solution, EUREL International Conference on (Conf. Publ. No. 431)*, 1996, pp. 128–132.
[41] R. Benjamin, “Synthetic, post-reception focusing in near-field radar,” in *The Detection of Abandoned Land Mines: A Humanitarian Imperative Seeking a Technical Solution, EUREL International Conference on (Conf. Publ. No. 431)*, 1996, pp. 133–137.
[42] S. C. Hagness, A. Taflove, and J. E. Bridges, “Two-dimensional FDTD analysis of a pulsed microwave confocal system for breast cancer detection: fixed-focus and antenna-array sensors,” *IEEE Trans. Biomed. Eng.*, vol. 45, no. 12, pp. 1470–1479, Dec. 1998.
[43] R. Benjamin, I. J. Craddock, G. S. Hilton, S. Litobarski, E. McCutcheon, R. Nilavalan, and G. N. Crisp, “Microwave detection of buried mines using non-contact, synthetic near-field focusing,” *Radar Sonar Navig. IEE Proc.* -, vol. 148, no. 4, pp. 233–240, Aug. 2001.
[44] R. Benjamin, G. Hilton, S. Litobarski, E. McCutcheon, and R. Nilavalan, “Post-detection synthetic near field focusing in radar or sonar,” *Electron. Lett.*, vol. 35, no. 8, p. 664, 1999.
[45] C. Gilmore, P. Mojabi, A. Zakaria, M. Ostadrahimi, C. Kaye, S. Noghanian, L. Shafai, S. Pistorius, and J. LoVetri, “A Wideband Microwave Tomography System With a Novel Frequency Selection Procedure,” *IEEE Trans. Biomed. Eng.*, vol. 57, no. 4, pp. 894–904, Apr. 2010.
[46] V. Zhurbenko, T. Rubæk, V. Krozer, and P. Meincke, “Design and realisation of a microwave three-dimensional imaging system with application to breast-cancer

detection," *IET Microw. Antennas Propag.*, vol. 4, no. 12, pp. 2200–2211, Dec. 2010.

[47] K.-C. Kwon, Y.-T. Lim, C.-H. Kim, N. Kim, C. Park, K.-H. Yoo, S.-H. Son, and S.-I. Jeon, "Microwave Tomography Analysis System for Breast Tumor Detection," *J. Med. Syst.*, vol. 36, no. 3, pp. 1757–1767, Jun. 2012.

[48] W. Zhang, A. Hoorfar, and L. Li, "THROUGH-THE-WALL TARGET LOCALIZATION WITH TIME REVERSAL MUSIC METHOD," *Prog. Electromagn. Res.*, vol. 106, pp. 75–89, 2010.

[49] F. Soldovieri and R. Solimene, "Through-Wall Imaging via a Linear Inverse Scattering Algorithm," *IEEE Geosci. Remote Sens. Lett.*, vol. 4, no. 4, pp. 513–517, Oct. 2007.

[50] Lin-Ping Song, Chun Yu, and Qing Huo Liu, "Through-wall imaging (TWI) by radar: 2-D tomographic results and analyses," *IEEE Trans. Geosci. Remote Sens.*, vol. 43, no. 12, pp. 2793–2798, Dec. 2005.

[51] R. Appleby and H. B. Wallace, "Standoff Detection of Weapons and Contraband in the 100 GHz to 1 THz Region," *IEEE Trans. Antennas Propag.*, vol. 55, no. 11, pp. 2944–2956, Nov. 2007.

[52] D. O. Korneev, L. Y. Bogdanov, and A. V. Nalivkin, "Passive millimeter wave imaging system with white noise illumination for concealed weapons detection," in *Conference Digest of the 2004 Joint 29th International Conference on Infrared and Millimeter Waves, 2004 and 12th International Conference on Terahertz Electronics, 2004.*, 2004, pp. 741–742.

[53] D. M. Sheen, D. L. McMakin, and T. E. Hall, "Three-dimensional millimeter-wave imaging for concealed weapon detection," *IEEE Trans. Microw. Theory Tech.*, vol. 49, no. 9, pp. 1581–1592, Sep. 2001.

[54] A. Zhuravlev, A. Bugaev, S. Ivashov, V. Razevig, and I. Vasiliev, "Microwave holography in detection of hidden objects under the surface and beneath clothes," in *General Assembly and Scientific Symposium, 2011 XXXth URSI*, 2011, pp. 1–4.

[55] O. Yurduseven, "Indirect Microwave Holographic Imaging of Concealed Ordnance for Airport Security Imaging Systems," *Prog. Electromagn. Res.*, vol. 146, pp. 7–13, 2014.

[56] V. M. Patel and J. N. Mait, "Passive millimeter-wave imaging with extended depth of field and sparse data," in *Acoustics, Speech and Signal Processing (ICASSP), 2012 IEEE International Conference on*, 2012, pp. 2521–2524.

[57] M. Peichl, S. Dill, M. Jirousek, and H. Suess, "Passive microwave remote sensing for security applications," in *Radar Conference, 2007. EuRAD 2007. European*, 2007, pp. 32–35.

[58] X. Zhuge and A. Yarovoy, "A Sparse Aperture MIMO-SAR-Based UWB Imaging System for Concealed Weapon Detection," *IEEE Trans. Geosci. Remote Sens.*, vol. 49, no. 1, pp. 509–518, Jan. 2011.

[59] K. B. Cooper, R. J. Dengler, N. Llombart, T. Bryllert, G. Chattopadhyay, E. Schlecht, J. Gill, C. Lee, A. Skalare, I. Mehdi, and P. H. Siegel, "Penetrating 3-D Imaging at 4- and 25-m Range Using a Submillimeter-Wave Radar," *IEEE Trans. Microw. Theory Tech.*, vol. 56, no. 12, pp. 2771–2778, Dec. 2008.

[60] "Explosive material," *Wikipedia, the free encyclopedia*. 04-Aug-2014.

[61] "Is al Qaeda planning to surgically implant bombs inside Western suicide bombers? | News.com.au." [Online]. Available: http://www.news.com.au/world/is-al-qaeda-planning-to-surgically-implant-bombs-inside-western-suicide-bombers/story-fndir2ev-1226977295414. [Accessed: 06-Aug-2014].

[62] “Nightmare of terrorists with bombs surgically implanted INSIDE their bodies,” *Mail Online*. [Online]. Available: http://www.dailymail.co.uk/news/article-2387332/Nightmare-terrorists-bombs-surgically-implanted-INSIDE-bodies.html. [Accessed: 06-Aug-2014].
[63] “Surgically implanted explosive device,” *Wikipedia, the free encyclopedia*. 30-Jul-2014.
[64] A. Achanta, M. Mckenna, and J. Heyman, “Nonlinear acoustic concealed weapons detection,” in *Applied Imagery and Pattern Recognition Workshop, 2005. Proceedings. 34th*, 2005, p. 7 pp.–27.
[65] D. K. Kotter, L. G. Roybal, and R. E. Polk, “Detection and classification of concealed weapons using a magnetometer-based portal,” 2002, vol. 4708, pp. 145–155.
[66] “Sell Flat Walk tradenote.net.” [Online]. Available: http://www.tradenote.net/hot_selloffers.php/page/3/keyword/walk/?type=sell. [Accessed: 08-Aug-2014].
[67] A. R. Hunt, R. D. Hogg, and W. Foreman, “Concealed weapons detection using electromagnetic resonances,” 1998, vol. 3575, pp. 62–67.
[68] “Advanced Imaging Technology (AIT),” *Transportation Security Administration*. [Online]. Available: /traveler-information/advanced-imaging-technology-ait. [Accessed: 18-Jul-2014].
[69] “Airport body scanners: Are they hazardous?,” *EDN*. [Online]. Available: http://www.edn.com/design/analog/4417389/3/Airport-body-scanners--Are-they-hazardous-. [Accessed: 18-Jul-2014].
[70] “Manchester Airport : Body Scanners.” [Online]. Available: http://www.manchesterairport.co.uk/manweb.nsf/Content/X-Ray-Scanners-Public-Information. [Accessed: 18-Jul-2014].
[71] “Millimetre Wave.” [Online]. Available: http://www.smithsdetection.com/technologies/millimetre-wave.html. [Accessed: 18-Jul-2014].
[72] “9/11 10 years on: Airport security still not as good as it could be - 9/6/2011 - Flight Global.” [Online]. Available: http://www.flightglobal.com/news/articles/911-10-years-on-airport-security-still-not-as-good-as-it-could-361393/. [Accessed: 07-Aug-2014].
[73] D. Novak, R. Waterhouse, and A. Farnham, “Millimeter-wave weapons detection system,” in *Applied Imagery and Pattern Recognition Workshop, 2005. Proceedings. 34th*, 2005, p. 6 pp.–20.
[74] “ProVision 2 | Advanced Imaging Technology.” [Online]. Available: http://www.sds.l-3com.com/advancedimaging/provision-2.htm. [Accessed: 06-Nov-2013].
[75] J. F. Federici, D. Gary, R. Barat, and D. Zimdars, “THz standoff detection and imaging of explosives and weapons (Invited Paper),” 2005, vol. 5781, pp. 75–84.
[76] “TERAHERTZ IMAGING:DEFENSE AGAINST TERROIST ACTIVITIES.” [Online]. Available: http://www.allvoices.com/contributed-news/1393975-terahertz-imaging. [Accessed: 08-Aug-2014].
[77] “ThruVision TS4 - Digital Barriers..” [Online]. Available: http://www.digitalbarriers.com/thruvision-ts4/. [Accessed: 09-Aug-2014].
[78] “ThruVision TS5 - Digital Barriers..” [Online]. Available: http://www.digitalbarriers.com/thruvision-ts5/. [Accessed: 09-Aug-2014].

[79] B. S. Alexandrov, V. Gelev, A. R. Bishop, A. Usheva, and K. ?. Rasmussen, “DNA Breathing Dynamics in the Presence of a Terahertz Field,” *Phys. Lett. A*, vol. 374, no. 10, p. 1214, Feb. 2010.

[80] P. W. Kruse, “Chapter 2 Principles of Uncooled Infrared Focal Plane Arrays,” in *Semiconductors and Semimetals*, vol. Volume 47, Paul W. Kruse and David D. Skatrud, Ed. Elsevier, 1997, pp. 17–42.

[81] “Iscon Imaging - Whole Body Imaging Solutions Without Radiation or Privacy Issues.” [Online]. Available: http://isconimaging.com/technology.htm. [Accessed: 07-Aug-2014].

[82] “Compton scattering - Wikipedia, the free encyclopedia.” [Online]. Available: http://en.wikipedia.org/wiki/Compton_scattering. [Accessed: 06-Aug-2014].

[83] H. Vogel, “Search by X-rays applied technology,” *Eur. J. Radiol.*, vol. 63, no. 2, pp. 227–236, Aug. 2007.

[84] “Image Gallery - American Science & Engineering.” [Online]. Available: http://www.as-e.com/resource-center/image-gallery/. [Accessed: 08-Aug-2014].

[85] X. J. at 9:38 am Fri, N. 19, and 2010, “Odds of cancer from TSA scanners about the same as terrorist blowing up your plane,” *Boing Boing*. .

[86] “Israel airports approve next-generation body scanner.” [Online]. Available: http://www.passengerterminaltoday.com/viewnews.php?NewsID=41772. [Accessed: 09-Aug-2014].

[87] O. of the Commissioner, “Consumer Updates - Very Low Health Risks from Full-Body X-ray Scanners.” [Online]. Available: http://www.fda.gov/ForConsumers/ConsumerUpdates/ucm231758.htm. [Accessed: 24-Apr-2013].

[88] “Tek84.” [Online]. Available: http://www.tek84.com/bodyscanner-more.html. [Accessed: 09-Aug-2014].

[89] M. G. ProPublica, N. 15, 2011, and 3:45 P.m, “Europe Bans X-Ray Body Scanners Used at U.S. Airports,” *ProPublica*. [Online]. Available: http://www.propublica.org/article/europe-bans-x-ray-body-scanners-used-at-u.s.-airports. [Accessed: 09-Aug-2014].

[90] “Scientists Question Safety Of New Airport Scanners,” *NPR.org*. [Online]. Available: http://www.npr.org/templates/story/story.php?storyId=126833083. [Accessed: 09-Aug-2014].

[91] *Handbook of Biological Effects of Electromagnetic Fields, Third Edition - 2 Volume Set*. .

[92] M. A. Stuchly, “Interaction of radiofrequency and microwave radiation with living systems,” *Radiat. Environ. Biophys.*, vol. 16, no. 1, pp. 1–14, Mar. 1979.

[93] K. R. Foster and H. P. Schwan, “Dielectric properties of tissues and biological materials: a critical review,” *Crit. Rev. Biomed. Eng.*, vol. 17, no. 1, pp. 25–104, 1989.

[94] A. Peyman, “Dielectric properties of tissues; variation with age and their relevance in exposure of children to electromagnetic fields; state of knowledge,” *Prog. Biophys. Mol. Biol.*, vol. 107, no. 3, pp. 434–438, Dec. 2011.

[95] M. R. Willis, “Dielectric and electronic properties of biological materials by R Pethig. pp 376. John Wiley & Sons, Chichester and New York. 1979. £15,” *Biochem. Educ.*, vol. 8, no. 1, pp. 31–31, Jan. 1980.

[96] R. Pethig and D. B. Kell, “The passive electrical properties of biological systems: their significance in physiology, biophysics and biotechnology,” *Phys. Med. Biol.*, vol. 32, no. 8, p. 933, Aug. 1987.

[97] H. P. Schwan and K. R. Foster, “RF-field interactions with biological systems: Electrical properties and biophysical mechanisms,” *Proc. IEEE*, vol. 68, no. 1, pp. 104–113, Jan. 1980.

[98] M. Zhang, E. G. Lim, Z. Wang, T. Tillo, K. L. Man, and J. C. Wang, “RF Characteristics of Wireless Capsule Endoscopy in Human Body,” in *Grid and Pervasive Computing*, J. J. (Jong H. Park, H. R. Arabnia, C. Kim, W. Shi, and J.-M. Gil, Eds. Springer Berlin Heidelberg, 2013, pp. 700–706.

[99] *Information systems design and intelligent applications*. New York, NY: Springer Berlin Heidelberg, 2015.

[100] X. Zhang, S. Zhu, and B. He, “Imaging Electric Properties of Biological Tissues by RF Field Mapping in MRI,” *IEEE Trans. Med. Imaging*, vol. 29, no. 2, pp. 474–481, Feb. 2010.

[101] “Polar molecules. By P. Debye, Ph.D., Pp. 172. New York: Chemical Catalog Co., Inc., 1929. $ 3.50,” *J. Soc. Chem. Ind.*, vol. 48, no. 43, pp. 1036–1037, Oct. 1929.

[102] W. Lai, T. Kind, and H. Wiggenhauser, “A Study of Concrete Hydration and Dielectric Relaxation Mechanism Using Ground Penetrating Radar and Short-Time Fourier Transform,” *EURASIP J. Adv. Signal Process.*, vol. 2010, no. 1, p. 317216, 2010.

[103] K. S. Cole and R. H. Cole, “Dispersion and Absorption in Dielectrics I. Alternating Current Characteristics,” *J. Chem. Phys.*, vol. 9, no. 4, pp. 341–351, Dec. 2004.

[104] “Cole-Cole-Diagramm – Wikipedia.” [Online]. Available: http://de.wikipedia.org/wiki/Cole-Cole-Diagramm. [Accessed: 24-Jul-2014].

[105] S. Gabriel, R. W. Lau, and C. Gabriel, “The dielectric properties of biological tissues: II. Measurements in the frequency range 10 Hz to 20 GHz,” *Phys. Med. Biol.*, vol. 41, no. 11, p. 2251, Nov. 1996.

[106] S. Y. Semenov, R. H. Svenson, A. E. Bulyshev, A. E. Souvorov, A. G. Nazarov, Y. E. Sizov, V. G. Posukh, A. V. Pavlovsky, P. N. Repin, and G. P. Tatsis, “Spatial resolution of microwave tomography for detection of myocardial ischemia and infarction-experimental study on two-dimensional models,” *IEEE Trans. Microw. Theory Tech.*, vol. 48, no. 4, pp. 538–544, 2000.

[107] “OET -- Radio Frequency Safety.” [Online]. Available: http://transition.fcc.gov/oet/rfsafety/dielectric.html. [Accessed: 19-Mar-2015].

[108] M. Kuzuoglu, K. Leblebicioglu, and Y. Z. Ider, “A fast image reconstruction algorithm for electrical impedance tomography,” *Physiol. Meas.*, vol. 15, no. 2A, p. A115, May 1994.

[109] “Dielectric Properties of Body Tissues: HTML clients.” [Online]. Available: http://niremf.ifac.cnr.it/tissprop/htmlclie/htmlclie.php. [Accessed: 04-Oct-2015].

[110] D. J. Daniels, *EM Detection of Concealed Targets*, 1 edition. Hoboken, N.J: Wiley-Blackwell, 2010.

[111] D. M. Pozar, *Microwave engineering*. Hoboken, NJ: Wiley, 2012.

[112] D. G. Watters, D. G. Falconer, K. J. Harker, R. Ueberschaer, and A. J. Bahr, “Microwave inspection of luggage for contraband materials using imaging and inverse-scattering algorithms,” *Res. Nondestruct. Eval.*, vol. 7, no. 2–3, pp. 153–168, 1995.

[113] S. Semenov, “Microwave tomography: review of the progress towards clinical applications,” *Philos. Trans. R. Soc. Math. Phys. Eng. Sci.*, vol. 367, no. 1900, pp. 3021–3042, Aug. 2009.

[114] A. M. Hassan and M. El-Shenawee, “Review of electromagnetic techniques for breast cancer detection,” *IEEE Rev. Biomed. Eng.*, vol. 4, pp. 103–118, 2011.
[115] R. Pethig, *Dielectric and electronic properties of biological materials*. Wiley, 1979.
[116] C. Polk and E. Postow, *Handbook of Biological Effects of Electromagnetic Fields, Third Edition - 2 Volume Set*. Taylor & Francis, 1995.
[117] “File:Tomographic fig1.png,” *Wikipedia, the free encyclopedia*. .
[118] “OET -- Radio Frequency Safety.” [Online]. Available: https://transition.fcc.gov/oet/rfsafety/dielectric.html. [Accessed: 13-Nov-2015].
[119] A. J. Devaney, E. A. Marengo, and F. K. Gruber, “Time-reversal-based imaging and inverse scattering of multiply scattering point targets,” *J. Acoust. Soc. Am.*, vol. 118, no. 5, pp. 3129–3138, 2005.
[120] A. J. Devaney, “Time reversal imaging of obscured targets from multistatic data,” *IEEE Trans. Antennas Propag.*, vol. 53, no. 5, pp. 1600 – 1610, May 2005.
[121] F. K. Gruber, E. A. Marengo, and A. J. Devaney, “Time-reversal imaging with multiple signal classification considering multiple scattering between the targets,” *J. Acoust. Soc. Am.*, vol. 115, no. 6, pp. 3042–3047, Jun. 2004.
[122] S. K. Lehman and A. J. Devaney, “Transmission mode time-reversal super-resolution imaging,” *J. Acoust. Soc. Am.*, vol. 113, no. 5, p. 2742, 2003.
[123] A. J. Devaney, “Twõ†¢ q¢† o_àw9A_í|¢ _ô† ooAí8 _m 4wà9Aqo9ë9Aô Gë9ë ZoAí8 èAU† á† B†¢ oëà ëíf 4ZTóz.”
[124] M. A. Stuchly, “Interaction of radiofrequency and microwave radiation with living systems,” *Radiat. Environ. Biophys.*, vol. 16, no. 1, pp. 1–14, Mar. 1979.
[125] M. Peichl, S. Dill, M. Jirousek, and H. Suess, “Near-field microwave imaging radiometers for security applications,” *Synth. Aperture Radar EUSAR 2008 7th Eur. Conf. On*, pp. 1 –4, Jun. 2008.
[126] T. Huang and A. S. Mohan, “A Microparticle Swarm Optimizer for the Reconstruction of Microwave Images,” *IEEE Trans. Antennas Propag.*, vol. 55, no. 3, pp. 568–576, 2007.
[127] S. K. Davis, H. Tandradinata, S. C. Hagness, and B. D. Van Veen, “Ultrawideband microwave breast cancer detection: A detection-theoretic approach using the generalized likelihood ratio test,” 2005. [Online]. Available: http://dx.doi.org/10.1109/TBME.2005.847528.
[128] R. Schmidt, “Multiple emitter location and signal parameter estimation,” *IEEE Trans. Antennas Propag.*, vol. 34, no. 3, pp. 276– 280, Mar. 1986.
[129] D. M. Sheen, D. L. McMakin, and T. E. Hall, “Near Field Imaging at Microwave and Millimeter Wave Frequencies,” in *Microwave Symposium, 2007. IEEE/MTT-S International*, 2007, pp. 1693–1696.
[130] J. Quintero, “Millimeter waves: How we got here, the physical challenges, and 5G opportunities,” *Nutaq*. .
[131] D. oleh DimAir, “Backscatter X-ray - X Ray Machines At Airports.” .
[132] “Madrid Train Station Blasts Kill 190,” *FoxNews.com*, 11-Mar-2004. [Online]. Available: http://www.foxnews.com/story/2004/03/11/madrid-train-station-blasts-kill-10. [Accessed: 28-Oct-2013].
[133] “Terror attacks at Russian transport double in 2010: official.” [Online]. Available: http://news.xinhuanet.com/english2010/world/2011-03/02/c_13756267.htm. [Accessed: 01-Aug-2013].
[134] “British airports on alert over fears that terrorists are plotting attack using ‘human bombs’ - Irish Mirror Online.” [Online]. Available:

http://www.irishmirror.ie/news/world-news/british-airports-alert-over-fears-3806303. [Accessed: 01-Aug-2014].
[135] "Domodedovo International Airport bombing," *Wikipedia, the free encyclopedia*. 20-Jul-2013.
[136] "Attempted assassination of Saudi Deputy Interior Minister fails," *Al-Shorfa*. [Online]. Available: http://al-shorfa.com/en_GB/articles/meii/features/2009/09/02/feature-02. [Accessed: 05-Aug-2014].
[137] "2012 Peshawar airport attack," *Wikipedia, the free encyclopedia*. 27-Jul-2013.
[138] "Taliban launch large attack on Kabul international airport | Reuters." [Online]. Available: http://www.reuters.com/article/2013/06/10/us-afghanistan-attack-airport-idUSBRE95900P20130610. [Accessed: 02-Aug-2013].
[139] "Westgate shopping mall attack," *Wikipedia, the free encyclopedia*. 25-Jul-2014.
[140] "Articles on Ideology | TRAC." [Online]. Available: http://www.trackingterrorism.org/ideology. [Accessed: 01-Aug-2013].
[141] "Global Agenda Council on Logistics & Supply Chain Systems 2013," *Global Agenda Council on Logistics & Supply Chain Systems 2013 | World Economic Forum*. [Online]. Available: http://www.weforum.org/content/global-agenda-council-logistics-supply-chain-systems-2013. [Accessed: 28-Oct-2013].
[142] "White House Commission on Aviation Safety and Security FEBRUARY 12, 1997." [Online]. Available: http://fas.org/irp/threat/212fin~1.html. [Accessed: 01-Aug-2014].
[143] D. Petersen and P. Polski, "International Aviation Security Research and Development," *J. Test. Eval.*, vol. 22, no. 3, p. 267, 1994.
[144] [Online]. Available: http://www.heathrowairport.com/static/HeathrowAboutUs/Downloads/PDF/Aviation_connectivity_and_economy.pdf. [Accessed: 01-Aug-2014].
[145] "wcms_208108.pdf." [Online]. Available: http://www.ilo.org/wcmsp5/groups/public/---ed_dialogue/---sector/documents/presentation/wcms_208108.pdf. [Accessed: 02-Aug-2013].
[146] K. Leone and R. Liu, "Measures of effectiveness for passenger-baggage security screening," *Transp. Res. Rec. J. Transp. Res. Board*, vol. 1822, no. 1, pp. 40–48, 2003.
[147] "http://eur-lex.europa.eu/LexUriServ/LexUriServ.do?uri=OJ:L:2008:097:0072:0084:EN:PDF." [Online]. Available: http://eur-lex.europa.eu/LexUriServ/LexUriServ.do?uri=OJ:L:2008:097:0072:0084:EN:PDF. [Accessed: 03-Aug-2014].
[148] B. . Klock, "Test and evaluation report for X-ray detection of threats using different X-ray functions," in *39th Annual 2005 International Carnahan Conference on Security Technology, 2005. CCST '05*, 2005, pp. 182–184.
[149] S. Michel, S. M. Koller, M. Ruh, and A. Schwaninger, "Do' Image Enhancement' Functions Really Enhance X-Ray Image Interpretation?," in *Proceedings of the 29th Annual Cognitive Science Society*, 2007, pp. 1301–1306.
[150] J. M. Wolfe, T. S. Horowitz, M. J. Van Wert, N. M. Kenner, S. S. Place, and N. Kibbi, "Low target prevalence is a stubborn source of errors in visual search tasks," *J. Exp. Psychol. Gen.*, vol. 136, no. 4, pp. 623–638, 2007.
[151] M. S. Fleck and S. R. Mitroff, "Rare Targets Are Rarely Missed in Correctable Search," *Psychol. Sci.*, vol. 18, no. 11, pp. 943–947, Nov. 2007.

[152] K. M. Ghylin, C. G. Drury, R. Batta, and L. Lin, “Temporal Effects in a Security Inspection Task: Breakdown of Performance Components,” *Proc. Hum. Factors Ergon. Soc. Annu. Meet.*, vol. 51, no. 2, pp. 93–97, Oct. 2007.
[153] N. H. Mackworth, “The breakdown of vigilance durning prolonged visual search,” *Q. J. Exp. Psychol.*, vol. 1, no. 1, pp. 6–21, Apr. 1948.
[154] M. Mendes, A. Schwaninger, N. Strebel, and S. Michel, “Why laptops should be screened separately when conventional x-ray screening is used,” in *2012 IEEE International Carnahan Conference on Security Technology (ICCST)*, 2012, pp. 267–273.
[155] P. Mehta and R. Smith-Bindman, “Airport full-body screening: what is the risk?,” *Arch. Intern. Med.*, vol. 171, no. 12, pp. 1112–1115, Jun. 2011.
[156] T. Orouji, S. M. H. Pooya, M. Jafarizadeh, H. R. Khosravi, and H. R. Mohammad, “Doses to the scanned individual and to the operator from an X-ray body scanner system,” *Radiat. Prot. Dosimetry*, vol. 147, no. 1–2, pp. 227–229, Sep. 2011.
[157] D. A. Schauer, “Does Security Screening with Backscatter X-Rays Do More Good than Harm?,” *Radiology*, vol. 259, no. 1, pp. 12–16, Apr. 2011.
[158] A. Frimpong, “Introduction of full body image scanners at the airports: a delicate balance of protecting privacy and ensuring national security,” *J. Transp. Secur.*, vol. 4, no. 3, pp. 221–229, Sep. 2011.
[159] F. Hofer and O. E. Wetter, “Operational and human factors issues of new airport security technology—two case studies,” *J. Transp. Secur.*, vol. 5, no. 4, pp. 277–291, Dec. 2012.
[160] A. Bolfing, T. Halbherr, and A. Schwaninger, “How Image Based Factors and Human Factors Contribute to Threat Detection Performance in X-Ray Aviation Security Screening,” in *HCI and Usability for Education and Work*, A. Holzinger, Ed. Springer Berlin Heidelberg, 2008, pp. 419–438.
[161] A. Schwaninger, F. Hofer, and O. E. Wetter, “Adaptive computer-based training increases on the job performance of x-ray screeners,” in *Security Technology, 2007 41st Annual IEEE International Carnahan Conference on*, 2007, pp. 117–124.
[162] S. Michel, S. M. Koller, J. C. de Ruiter, R. Moerland, M. Hogervorst, and A. Schwaninger, “Computer-based training increases efficiency in X-ray image interpretation by aviation security screeners,” in *Security Technology, 2007 41st Annual IEEE International Carnahan Conference on*, 2007, pp. 201–206.
[163] A. W. J. Wales, C. Anderson, K. L. Jones, A. Schwaninger, and J. A. Horne, “Evaluating the two-component inspection model in a simplified luggage search task,” *Behav. Res. Methods*, vol. 41, no. 3, pp. 937–943, Aug. 2009.
[164] D. Hardmeier, F. Hofer, and A. Schwaninger, “The X-ray object recognition test (X-ray ORT) - a reliable and valid instrument for measuring visual abilities needed in X-ray screening,” in *39th Annual 2005 International Carnahan Conference on Security Technology, 2005. CCST ’05*, 2005, pp. 189–192.
[165] A. Schwaninger, “Training of airport security screeners,” *AIRPORT*, vol. 2003, no. 5, pp. 11–13, 2003.
[166] S. M. Steiner-Koller, A. Bolfing, and A. Schwaninger, “Assessment of X-ray image interpretation competency of aviation security screeners,” in *Security Technology, 2009. 43rd Annual 2009 International Carnahan Conference on*, 2009, pp. 20–27.
[167] A. Schwaninger, “Increasing efficiency in airport security screening,” *WIT Trans. Built Environ.*, vol. 82, pp. 407–416, 2005.

[168] O. E. Wetter, D. Hardmeier, and F. Hofer, “Covert testing at airports: Exploring methodology and results,” in *42nd Annual IEEE International Carnahan Conference on Security Technology, 2008. ICCST 2008*, 2008, pp. 357–363.
[169] S. D. Warren and L. D. Brandeis, “Right to Privacy,” *Harv. Law Rev.*, vol. 4, p. 193, 1891 1890.
[170] O. Mironenko, “Body scanners versus privacy and data protection,” *Comput. Law Secur. Rev.*, vol. 27, no. 3, pp. 232–244, 2011.
[171] “The Universal Declaration of Human Rights.” [Online]. Available: http://www.un.org/en/documents/udhr/index.shtml#a13. [Accessed: 20-Mar-2014].
[172] C. Eze, “Africa: Now Showing at MMIA: Nude Images of Passengers,” *This Day (Lagos)*, 21-Sep-2010.
[173] “Full body scanners to be installed at nine more airports,” *Mail Online*. [Online]. Available: http://www.dailymail.co.uk/news/article-2512053/Full-body-scanners-installed-airports--passengers-FINALLY-allowed-opt-out.html. [Accessed: 20-Mar-2014].
[174] “TSA Pre✓™ Application Program,” *Transportation Security Administration*. [Online]. Available: /tsa-precheck/application-program. [Accessed: 21-Mar-2014].
[175] Q. Feng, H. Sahin, and K. C. Kapur, “Designing airport checked-baggage-screening strategies considering system capability and reliability,” *Reliab. Eng. Syst. Saf.*, vol. 94, no. 2, pp. 618–627, Feb. 2009.
[176] L. A. McLay, S. H. Jacobson, and J. E. Kobza, “Integer programming models and analysis for a multilevel passenger screening problem,” *IIE Trans.*, vol. 39, no. 1, pp. 73–81, 2007.
[177] A. J. Lee, L. A. McLay, and S. H. Jacobson, “Designing Aviation Security Passenger Screening Systems Using Nonlinear Control,” *SIAM J. Control Optim.*, vol. 48, no. 4, pp. 2085–2105, Jan. 2009.
[178] L. A. McLay, A. J. Lee, and S. H. Jacobson, “Risk-Based Policies for Airport Security Checkpoint Screening,” *Transp. Sci.*, vol. 44, no. 3, pp. 333–349, Jan. 2010.
[179] V. L. Lazar Babu, R. Batta, and L. Lin, “Passenger grouping under constant threat probability in an airport security system,” *Eur. J. Oper. Res.*, vol. 168, no. 2, pp. 633–644, Jan. 2006.
[180] X. Nie, R. Batta, C. G. Drury, and L. Lin, “Passenger grouping with risk levels in an airport security system,” *Eur. J. Oper. Res.*, vol. 194, no. 2, pp. 574–584, Apr. 2009.
[181] A. G. Nikolaev, S. H. Jacobson, and L. A. McLay, “A Sequential Stochastic Security System Design Problem for Aviation Security,” *Transp. Sci.*, vol. 41, no. 2, pp. 182–194, May 2007.
[182] J. Filipiak, “Dynamic Routing in a Queueing System with a Multiple Service Facility,” *Oper. Res.*, vol. 32, no. 5, pp. 1163–1180, Oct. 1984.
[183] F. P. Kelly and C. N. Laws, “Dynamic routing in open queueing networks: Brownian models, cut constraints and resource pooling,” *Queueing Syst.*, vol. 13, no. 1–3, pp. 47–86, Mar. 1993.
[184] M. Jain, “Finite capacity M/M/r queueing system with queue-dependent servers,” *Comput. Math. Appl.*, vol. 50, no. 1–2, pp. 187–199, Jul. 2005.
[185] P. R. Kumar and J. Walrand, “Individually Optimal Routing in Parallel Systems,” *J. Appl. Probab.*, vol. 22, no. 4, p. 989, Dec. 1985.
[186] W. Winston, “Optimality of the Shortest Line Discipline,” *J. Appl. Probab.*, vol. 14, no. 1, p. 181, Mar. 1977.

[187] S. Meyn, “Sequencing and Routing in Multiclass Queueing Networks Part I: Feedback Regulation,” *SIAM J. Control Optim.*, vol. 40, no. 3, pp. 741–776, Jan. 2001.
[188] J. M. Harrison and L. M. Wein, “Scheduling networks of queues: Heavy traffic analysis of a simple open network,” *Queueing Syst.*, vol. 5, no. 4, pp. 265–279, Dec. 1989.
[189] B. L. Schwartz, “Queuing Models with Lane Selection: A New Class of Problems,” *Oper. Res.*, vol. 22, no. 2, pp. 331–339, Apr. 1974.
[190] X. Nie, G. Parab, R. Batta, and L. Lin, “Simulation-based Selectee Lane queueing design for passenger checkpoint screening,” *Eur. J. Oper. Res.*, vol. 219, no. 1, pp. 146–155, May 2012.
[191] A. J. Lee and S. H. Jacobson, “The impact of aviation checkpoint queues on optimizing security screening effectiveness,” *Reliab. Eng. Syst. Saf.*, vol. 96, no. 8, pp. 900–911, Aug. 2011.
[192] International Commission on Non-Ionizing Radiation Protection, “ICNIRP statement on the ‘Guidelines for limiting exposure to time-varying electric, magnetic, and electromagnetic fields (up to 300 GHz),’” *Health Phys.*, vol. 97, no. 3, pp. 257–258, Sep. 2009.
[193] “IEEE Standard for Safety Levels With Respect to Human Exposure to Radio Frequency Electromagnetic Fields, 3 kHz to 300 GHz,” *IEEE Std C951-2005 Revis. IEEE Std C951-1991*, pp. 0_1–238, 2006.
[194] O. E. Wetter, J. Wegge, K. Jonas, and K.-H. Schmidt, “Dual Goals for Speed and Accuracy on the Same Performance Task,” *J. Pers. Psychol.*, vol. 11, no. 3, pp. 118–126, Jan. 2012.
[195] O. E. Wetter, H. Fuhrmann, M. Lipphardt, and F. Hofer, “Bringing adversaries together: The importance of a common management-level approach in complex work domains,” in *2011 IEEE International Carnahan Conference on Security Technology (ICCST)*, 2011, pp. 1–6.
[196] “Measuring and Improving Organizational Productivity: A Practical Guide - Robert D. Pritchard - Google Books.” [Online]. Available: http://books.google.co.uk/books/about/Measuring_and_Improving_Organizational_P.html?id=abIy-ewzrvMC&redir_esc=y. [Accessed: 05-Aug-2014].
[197] O. E. Wetter and M. Fuhrer, “A holistic approach for evaluating liquid explosive detection systems,” *J. Transp. Secur.*, vol. 6, no. 4, pp. 377–388, Dec. 2013.
[198] N. G. Cutmore, Y. Liu, and J. R. Tickner, “Development and commercialization of a fast-neutron/x-ray Cargo Scanner,” in *2010 IEEE International Conference on Technologies for Homeland Security (HST)*, 2010, pp. 330–336.
[199] “Transportation Security Administration,” *Transportation Security Administration*. [Online]. Available: /. [Accessed: 28-Aug-2013].
[200] “Most fake bombs missed by screeners - USATODAY.com.” [Online]. Available: http://usatoday30.usatoday.com/news/nation/2007-10-17-airport-security_N.htm. [Accessed: 28-Aug-2013].
[201] H. Chen, S. Lee, R. M. Rao, M.-A. Slamani, and P. K. Varshney, “Imaging for concealed weapon detection: a tutorial overview of development in imaging sensors and processing,” *IEEE Signal Process. Mag.*, vol. 22, no. 2, pp. 52–61, 2005.

Appendices

Appendix A

Script design of the simulated model in Lumerical FDTD solutions

```
Deleteall;


for(i=1:n){
addpower;
set("monitor type","point");
set("z",0);
set("y",dist*sin(2*pi*(i-1)/n));
set("x",dist*cos(2*pi*(i-1)/n));
set("name", "monitor_"+ num2str(i));

}


adddipole;

set("z",0);

set("y",0);set("y",dist*sin(2*pi*(Source-1)/n));
set("x",dist*cos(2*pi*(Source-1)/n));

setnamed("source","wavelength start",0.0000299792);
setnamed("source","wavelength stop",0.0000299792);
```

Appendix B

Simulation code in Lumerical FDTD solutions and data collections

```
monitor_Ex=matrix(40,40);
monitor_Ey=matrix(40,40);
monitor_Ez=matrix(40,40);

for(i=1:40){

filename="source"+num2str(i);
save(filename);
switchtolayout;

setnamed("analysis group", "Source",i);
run;
}
for(i=1:40){

filename="source"+num2str(i); # You can comment this line if you want to save the file for each simulation
load(filename); # You can comment this line if you want to save the file for each simulation


# I am using the getelectric command which returns the electric field intensity which is a positive real number
# If you want to return the complex field instead, change all of the following to :
# monitor(i,1)=sum(pinch(getresult("analysis group::monitor","E" ).E));
# monitor(i,2)=sum(pinch(getresult("analysis group::monitor_1","E" ).E));
# etc.
for( j=1:40){
monitor_dataset=getresult("analysis group::monitor_"+num2str(j),"E" );
monitor_Ex(i,j)=sum(pinch(monitor_dataset.Ex));
monitor_Ey(i,j)=sum(pinch(monitor_dataset.Ey));
monitor_Ez(i,j)=sum(pinch(monitor_dataset.Ez));
}
}


# the file named monitor_fields.txt will contain the information
write("monitor_fields_Ex.txt",num2str(monitor_Ex));
write("monitor_fields_Ey.txt",num2str(monitor_Ey));
write("monitor_fields_Ez.txt",num2str(monitor_Ez));
```

Appendix C

TR Music Code

```
function TRMUSIC_2D_Modified
%%%%%%%%%%%%%%%%%%%%%%%%%%%%%%%%%%%%set model
frequency=7e9;                    % frequency,unit:Herz
speed=3e8;                        % EM propagating speed in the
simulated media,unit:meter/second
lambda=speed/frequency;           % waveleng of EM wave,unit:meter
ImagingSizeX=0.30;                 % imaging reconstruction region in X
direction,unit:meter
ImagingSizeY=0.30;                 % imaging reconstruction region in Y
direction,unit:meter
%%%%%%%%%%%%%%%%%%%%%%%%%%%%%%%%%%%%get measurements
[filename pathname]=uigetfile('*.*','open Object data file');
str=[pathname,filename];

fid=fopen(str,'r');
if fid==-1
    output('open file fail')
end

Data_M=[];
i=1;
while (~feof(fid))

    data=fscanf(fid,'%s',1)
    if isempty(data)
        break
    end

    Data_M(i)=str2num(data);
    i=i+1;

end
Anum=length(Data_M)^0.5;
Data_Object=reshape(Data_M,Anum,Anum)';

%%%%%%%%%%%%%%%%%%%%%%%%%%%%%%%%%%%%%%get measurement of background
[filename pathname]=uigetfile('*.*','open Background data file');
str=[pathname,filename];

fid=fopen(str,'r');
if fid==-1
    output('open file fail')
end

Data_M=[];
i=1;
while (~feof(fid))

    data=fscanf(fid,'%s',1);
    if isempty(data)
        break
    end
```

```
    Data_M(i)=str2num(data);
    i=i+1;
end

Anum=length(Data_M)^0.5;
Data_Background=reshape(Data_M,Anum,Anum)';
Data=(Data_Object-Data_Background);
%%%%%%%%%%%%%%%%%%%%%%%%%%%%%%%%%%%%%%%%%%%%%%%%%%%%%%%%get antena axies
Angu=2*pi/Anum*(0:(Anum-1));        % angular positions of circle
array
R=0.2;                              % the radius of circle array,
unit:meter
Aposi=[R*cos(Angu);R*sin(Angu)];    % xy coordinats of antennas
%%%%%%%%%%%%%%%%%%%%%%%%%%%%%%%%%%%%%%%%%%%%%%%%%%%%%%%%%%%%%%%%%%%%%%%
%%%%%%%%%%%%%%%%%%%%%%%%%%%%%%%%%%%%%%%%%%%%%%%%%%%%%%%%%%%%%%%%%%%%%%%
noisefactor=0;
phasenoise=270;


energy=norm(Data,'fro')^2;
[U,D,V]=svd(Data);

svvector=diag(D);
weightofnoise=zeros(size(svvector));
totalenergy=norm(diag(D),'fro')^2;
for k=1:length(svvector)
    weightofnoise(k)=norm(svvector(1:k),'fro')^2/totalenergy;
end

Grid=100;                           % imaging reconstruction points
density
dx=ImagingSizeX/Grid;
dy=ImagingSizeY/Grid;
I=zeros(Grid+1);
boundary=1;
while boundary<Anum
    if weightofnoise(boundary)>0.7 && weightofnoise(boundary)<0.88
        boundary
        II=zeros(Grid+1);
        for jj=1:Grid+1%pixel
            for ii=1:Grid+1
                gx=illuminationvector([(ii-1-Grid/2)*dx;(jj-1-
Grid/2)*dy],Aposi,lambda);
                aa=0.0;
                for kk=boundary+1:Anum
                   aa=aa+(abs(U(:,kk).'*gx))^2+(abs(V(:,kk)'*gx))^2;
                end
                II(jj,ii)=1/aa;
            end
        end
        I=I+II;
    end
    boundary=boundary+1;
end

I=abs(I);
%save('N:\MyWork\ZhangPapers\result\image_metal_rec_4ge40.mat','I');
figure
```

```
[X,Y]=meshgrid(100*(-ImagingSizeX/2:dx:ImagingSizeX/2),100*(-
ImagingSizeY/2:dy:ImagingSizeY/2));
SVDVector=diag(D); SVDVector=10*log(SVDVector/max(SVDVector));

%save('N:\MyWork\ZhangPapers\result\metal_nonregular_4ge40_sv.txt','SV
DVector','-ascii');
%save('N:\MyWork\ZhangPapers\result\metal_nonregular_4ge40_er.txt','we
ightofnoise','-ascii');

subplot(2,2,1),plot(weightofnoise,'o-'),grid on;
subplot(2,2,3),plot(SVDVector,'o-'),grid
on,xlabel('N'),ylabel('Singular Value(d B)');axis square; xlim([1
length(SVDVector)]);ylim([min(SVDVector)-5 max(SVDVector)+5]);
%subplot(2,3,2),plot(diag(trEigValue),'*-'),grid
on,,xlabel('N'),ylabel('Eigen Value');
subplot(2,2,2),imagesc(100*(-ImagingSizeX/2:dx:ImagingSizeX/2),100*(-
ImagingSizeY/2:dy:ImagingSizeY/2),I); colorbar;axis xy
square,axis(100*([-ImagingSizeX/2 ImagingSizeX/2 -ImagingSizeY/2
ImagingSizeY/2])),xlabel('x(cm)'),ylabel('y(cm)');
%subplot(2,2,4),contour(X,Y,10*log(I),50); axis square,grid
on,axis(100*([-ImagingSizeX/2 ImagingSizeX/2 -ImagingSizeY/2
ImagingSizeY/2])),xlabel('x(cm)'),ylabel('y(cm)');
subplot(2,2,4),surf(X,Y,10*log(I)); shading interp; axis(100*([-
ImagingSizeX/2 ImagingSizeX/2 -ImagingSizeY/2 ImagingSizeY/2
min(min(10*log(I)))/100
max(max(10*log(I)))/100])),xlabel('x(cm)'),ylabel('y(cm)');
%subplot(2,3,5),surf(X,Y,10*log(abs(I2))),shading interp; axis(100*([-
ImagingSizeX/2 ImagingSizeX/2 -ImagingSizeY/2 ImagingSizeY/2 0
1])),xlabel('x(cm)'),ylabel('y(cm)');
%subplot(2,3,6),contour(X,Y,10*log(abs(I2)),50),axis square,grid
on,axis(100*[-ImagingSizeX/2 ImagingSizeX/2 -ImagingSizeY/2
ImagingSizeY/2]),xlabel('x(cm)'),ylabel('y(cm)');
% subplot(2,3,5),surf(X,Y,abs(psf)),shading interp,axis(100*([-
ImagingSizeX/2 ImagingSizeX/2 -ImagingSizeY/2 ImagingSizeY/2 0
max(max(abs(psf)))/100])),xlabel('x(cm)'),ylabel('y(cm)');
% subplot(2,3,6),contour(X,Y,abs(psf),50),axis square,grid
on,axis(100*[-ImagingSizeX/2 ImagingSizeX/2 -ImagingSizeY/2
ImagingSizeY/2]),xlabel('x(cm)'),ylabel('y(cm)');
figure,imagesc(100*(-ImagingSizeX/2:dx:ImagingSizeX/2),100*(-
ImagingSizeY/2:dy:ImagingSizeY/2),I); colorbar;axis xy
square,axis(100*([-ImagingSizeX/2 ImagingSizeX/2 -ImagingSizeY/2
ImagingSizeY/2])),xlabel('x(cm)'),ylabel('y(cm)');

% illumination vector generation function
function [IV]=illuminationvector(x1,x2,lambda)
    for ii=1:size(x2,2)
        for jj=1:size(x1,2)
            IV(ii,jj)=besselh(0,2,2*pi*norm(x1(:,jj)-
x2(:,ii),2)/lambda);
        end
    end
    IV=IV/norm(IV,2);

%%%%%%%%%%%%diagonal line equal to 0

%{
for i=1:length(Data)
    Data(i,i)=0;
end
```

Appendix D

Human body tissues dielectric properties from [118]

Frequency = 1000.00 MHz

Tissue	Epslon	Sigma
Bladder	18.849951	0.396606
Blood	61.065372	1.583073
Bone_Cancellous	20.584105	0.363929
Bone_Cortical	12.363424	0.155647
Bone_Marrow_Infiltrated	11.196044	0.239370
Bone_Marrow_Not_Infiltr	5.485393	0.042796
Breast_Fat	5.407877	0.052824
Cartilage	42.316879	0.828792
Cerebellum	48.857254	1.307865
Cerebro_Spinal_Fluid	68.438515	2.455200
Colon(Large_Intestine)	57.481392	1.127232
Cornea	54.834404	1.437892
Dura	44.200764	0.993314
Eye_Tissue(Sclera)	55.016594	1.205489
Fat	5.447024	0.053498
Fat(Mean)	11.294223	0.116371
Gall_Bladder	58.997078	1.288284
Gall_Blad_Bile	70.010414	1.875942
Grey_Matter	52.281815	0.985324
Heart	59.290333	1.283632
Kidney	57.939972	1.449651
Lens_Cortex	46.399349	0.824299
Lens_Nucleus	35.666695	0.511831
Liver	46.400772	0.897076
Lung(Inflated)	21.824909	0.474023
Lung(Deflated)	51.101418	0.896929
Muscle(Parallel_Fiber)	56.660660	1.034154
Muscle(Transverse_Fibr)	54.811028	0.978189
Nerve(Spinal_chord)	32.251652	0.599883
Ovary	49.781193	1.344658
Skin(Dry)	40.936264	0.899814
Skin(Wet)	45.710957	0.881826
Small_Intestine	58.870239	2.217532
Spleen	56.610710	1.322749
Stomach_Esop_Duodenum	64.797188	1.231625
Tendon	45.633930	0.759827
Testis_Prostate	60.258781	1.252566
Thyroid_Thymus	59.469212	1.078719
Tongue	55.016594	0.974955
Trachea	41.778152	0.802269
Uterus	60.776573	1.314722
Vitreous_Humour	68.875465	1.667309
White_Matter	38.577381	0.621925

Tissue	Permittivity	Conductivity	Density(app.)
Avg. Brain	45.429596	0.803625	1030.0
Avg. Skull	16.473764	0.259788	1850.0
Avg. Muscle	55.735844	1.006172	1040.0

Frequency = 2000.00 MHz

Tissue	Epslon	Sigma
Bladder	18.233961	0.577910
Blood	59.022324	2.186298
Bone_Cancellous	19.086840	0.652147
Bone_Cortical	11.653735	0.310047
Bone_Marrow_Infiltrated	10.560427	0.381228
Bone_Marrow_Not_Infiltr	5.347769	0.076143
Breast_Fat	5.232330	0.106125
Cartilage	39.759468	1.422889
Cerebellum	45.667870	1.822794
Cerebro_Spinal_Fluid	66.910255	3.074140
Colon(Large_Intestine)	54.728954	1.709016
Cornea	52.389404	1.983488
Dura	42.621681	1.419668
Eye_Tissue(Sclera)	53.270287	1.724382
Fat	5.327579	0.085915
Fat(Mean)	10.958710	0.212486
Gall_Bladder	58.039181	1.758431
Gall_Blad_Bile	68.848633	2.440050
Grey_Matter	49.691940	1.511044
Heart	55.816109	1.911761
Kidney	53.851925	2.089864
Lens_Cortex	45.125866	1.248484
Lens_Nucleus	34.436775	0.872733
Liver	43.821468	1.403848
Lung(Inflated)	20.790388	0.685185
Lung(Deflated)	49.058723	1.394516
Muscle(Parallel_Fiber)	55.048576	1.563861
Muscle(Transverse_Fibr)	53.290001	1.453851
Nerve(Spinal_chord)	30.626297	0.913736
Ovary	45.821945	1.948826
Skin(Dry)	38.567902	1.265463
Skin(Wet)	43.520454	1.335596
Small_Intestine	55.405083	2.833670
Spleen	53.378410	1.912456
Stomach_Esop_Duodenum	62.892017	1.843474
Tendon	43.908924	1.338648
Testis_Prostate	58.270180	1.826838
Thyroid_Thymus	57.849407	1.633252
Tongue	53.270287	1.493848
Trachea	40.262257	1.209725
Uterus	58.576450	1.901683
Vitreous_Humour	68.472313	2.155583
White_Matter	36.731686	1.001391

Tissue	Permittivity	Conductivity	Density(app.)
Avg. Brain	43.211815	1.256217	1030.0
Avg. Skull	15.370287	0.481097	1850.0
Avg. Muscle	54.169289	1.508856	1040.0

Frequency = 3000.00 MHz

Tissue	Epslon	Sigma
Bladder	17.720135	0.836041
Blood	57.353104	3.050023
Bone_Cancellous	17.943909	1.006083
Bone_Cortical	11.066273	0.506200
Bone_Marrow_Infiltrated	10.014117	0.561665
Bone_Marrow_Not_Infiltr	5.237837	0.120841
Breast_Fat	5.038583	0.178889
Cartilage	37.606441	2.204820
Cerebellum	43.895130	2.481987
Cerebro_Spinal_Fluid	65.390442	4.005437
Colon(Large_Intestine)	52.931404	2.494820
Cornea	50.741783	2.728974
Dura	41.340321	2.014976
Eye_Tissue(Sclera)	51.859085	2.468150
Fat	5.223881	0.130037
Fat(Mean)	10.655297	0.344170
Gall_Bladder	57.099659	2.496229
Gall_Blad_Bile	67.719376	3.325326
Grey_Matter	48.048622	2.218852
Heart	53.736992	2.728830
Kidney	51.587826	2.890790
Lens_Cortex	44.013100	1.865653
Lens_Nucleus	33.415573	1.387762
Liver	42.164696	2.075518
Lung(Inflated)	20.130270	0.968909
Lung(Deflated)	47.603607	2.084595
Muscle(Parallel_Fiber)	53.648708	2.331691
Muscle(Transverse_Fibr)	52.057980	2.142127
Nerve(Spinal_chord)	29.620144	1.329582
Ovary	43.519238	2.684416
Skin(Dry)	37.450352	1.740625
Skin(Wet)	42.112106	1.947430
Small_Intestine	53.372101	3.639210
Spleen	51.447182	2.686221
Stomach_Esop_Duodenum	61.267498	2.729206
Tendon	42.126114	2.166165
Testis_Prostate	56.694633	2.647093
Thyroid_Thymus	56.403088	2.441327
Tongue	51.859085	2.237616
Trachea	39.112415	1.784121
Uterus	56.921238	2.730568
Vitreous_Humour	67.816994	2.955925
White_Matter	35.541309	1.510638

Tissue	Permittivity	Conductivity	Density(app.)
Avg. Brain	41.794968	1.864745	1030.0
Avg. Skull	14.505091	0.756141	1850.0
Avg. Muscle	52.853344	2.236909	1040.0

Frequency = 4000.00 MHz

Tissue	Epslon	Sigma
Bladder	17.203909	1.158089
Blood	55.676739	4.133829
Bone_Cancellous	16.946363	1.398758
Bone_Cortical	10.531953	0.727466
Bone_Marrow_Infiltrated	9.513246	0.763736
Bone_Marrow_Not_Infiltr	5.135623	0.174125
Breast_Fat	4.839307	0.262300
Cartilage	35.568672	3.109459
Cerebellum	42.426952	3.279400
Cerebro_Spinal_Fluid	63.730064	5.195953
Colon(Large_Intestine)	51.309887	3.463443
Cornea	49.228466	3.651875
Dura	40.096230	2.745700
Eye_Tissue(Sclera)	50.448219	3.404340
Fat	5.124863	0.182898
Fat(Mean)	10.362132	0.502257
Gall_Bladder	56.005550	3.471673
Gall_Blad_Bile	66.405968	4.495789
Grey_Matter	46.579636	3.090741
Heart	51.960747	3.721706
Kidney	49.750916	3.849305
Lens_Cortex	42.866955	2.646292
Lens_Nucleus	32.387699	2.030912
Liver	40.688957	2.892883
Lung(Inflated)	19.540581	1.318113
Lung(Deflated)	46.231846	2.943226
Muscle(Parallel_Fiber)	52.215027	3.301380
Muscle(Transverse_Fibr)	50.820927	3.015586
Nerve(Spinal_chord)	28.739086	1.838678
Ovary	41.647400	3.536764
Skin(Dry)	36.587315	2.340467
Skin(Wet)	40.847412	2.701600
Small_Intestine	51.633865	4.621600
Spleen	49.784317	3.630427
Stomach_Esop_Duodenum	59.610611	3.847599
Tendon	40.238796	3.173510
Testis_Prostate	55.130844	3.678429
Thyroid_Thymus	54.906033	3.463722
Tongue	50.448219	3.173806
Trachea	37.996571	2.502838
Uterus	55.314041	3.768641
Vitreous_Humour	66.922874	4.049424
White_Matter	34.477913	2.136275

Tissue	Permittivity	Conductivity	Density(app.)
Avg. Brain	40.528774	2.613508	1030.0
Avg. Skull	13.739159	1.063112	1850.0
Avg. Muscle	51.517975	3.158483	1040.0